

---

# **LARGE-SCALE PROCESS-ORIENTED MODELLING OF SOIL EROSION BY WATER IN COMPLEX WATERSHEDS**

Daniel Waldmann

---



München 2010



---

# **LARGE-SCALE PROCESS-ORIENTED MODELLING OF SOIL EROSION BY WATER IN COMPLEX WATERSHEDS**

Daniel Waldmann

---

Dissertation  
an der Fakultät für Geowissenschaften  
der Ludwig–Maximilians–Universität  
München

vorgelegt von  
Daniel Waldmann  
aus München

München, den 08.02.2010

Erstgutachter: Prof. Dr. Wolfram Mauser  
Zweitgutachter: Prof. Dr. Karsten Schulz  
Tag der mündlichen Prüfung: 19.05.2010



## ACKNOWLEDGEMENTS

The compilation of this work would not have been possible with the aid of a number of people and organisations, which I would like to thank here.

First of all, I would like to thank my PhD supervisor Wolfram Mauser, not only for providing a PhD position to me, but also for having confidence in my skills. Furthermore he gave me the opportunity to learn lots about environmental modelling on a thematically, as well as technically sophisticated level. Besides the professional support he gave me, I would also like to thank him for his personal competence, mostly in amusing (extra-professional) conversations on the balcony.

This thesis was carried out within the project Global Change and the Hydrological Cycle (GLOWA)-Danube, therefore I would like to express my gratitude to the German Ministry of Research and Education (BMBF), which funded the project. Thanks to various organisations, lots of data have been provided, which supported this study. Data on suspended sediment was received from the GLOWA-Danube project partner Bavarian State Office for Environment (LfU) (prepared by Mario Knott). Meteorological data comes from the Bavarian State Office of Agriculture (LfL) (prepared by Jochen Weigand) and the *Berchtesgaden National Park*.

The teamwork at the Chair of Geography and Geographical Remote Sensing at the Department for Geography of the Ludwig-Maximilians University Munich (LMU) gave me the opportunity to learn many useful things from many colleagues, and the working atmosphere always was positive. So many thanks to *all* of my current and former colleagues.

Special thanks go to Markus Muerth for the critical reviews of my work and the aid in various scientific and technical problems (and also for the weather observations, in which Khaled Haider was also involved). Furthermore, I would like to thank a lot Tobias Hank, Thomas Marke, Matthias Bernhardt and Ulrich Strasser for all the informative discussions (especially those “after work”, but “in office”), Monika Prasch and Monika Tepfenhart for the good teamwork on the excursions, respectively in the programming course, Andrea Reiter and Ruth Weidinger for the data supply (Andrea also for the apples), Christoph Heinzeller for funny hours and interesting challenges in the “cold chamber“, Sara Stöber for the competent organisation of everything around GLOWA, and Ulrich Schäffler for his support in software development.

I appreciate Ralf Ludwig for introducing me into the project GLOWA-Danube and Karsten Schulz for his feedback from the reviews of this work.

I am indebted to all the people who reviewed this thesis, which was done (primarily) under linguistic aspects by all the (English, American and “Germglisch”) Barritts, and under scientific aspects by Markus Muerth.

Many thanks also to the GLOWA-Danube colleagues, especially to those from the *Agrarschlange*, and to the computer scientists. It was a great time in the project, scientifically, but also in the evenings after the conferences.

Finally I would like to thank all my friends and my family for supporting me all the time. I am particularly grateful of course to my parents and my brother for some special support. My

brother and Daniela Padula also deserve gratitude for board and lodging (and “WB”), which also applies to Markus Muerth and Monika Finken (after the visits in the pub; thanks to Markus for the good times). Many thanks go to all the Kalaghichi-Gandjineh family for their support during a long period of my work, especially to Schahrazad for her patience (and the lunch on the excursion). Philipp Haub also deserves my gratitude for accommodation, but in particular for his support and friendship. In the end I would like to thank Miranda Barritt, not only for suffering professional discussions (or maybe monologues) and correcting my English, but also for the good times and just being there.

## **ABSTRACT**

In recent years the global awareness of Climate Change led to an increased demand for scientific evaluations of potential impacts. The assessment of impacts is an important task in order to develop strategies for adaptation and mitigation. Climate research recognised global warming already more than 50 years ago, and since 1988 the Intergovernmental Panel on Climate Change (IPCC) provides the world with a scientific view on Climate Change and its impacts. This is important in particular on the regional scale, as global models cannot provide regional or local policymakers with adequate information on potential impacts. Therefore, in recent years, models have been developed to study the impacts of Climate Change and/or Global Change on the regional scale. The objective of the research project GLOWA-Danube is the development of an integrative Decision Support System (DSS) for investigation of the impacts of Global Change in the Upper Danube Basin and for evaluation of regional adaptation and mitigation strategies. In the coupled simulation system DANUBIA models from natural sciences interact with socioeconomic components. It is intended to predict, based on Global Change scenarios and human behaviour, the reactions of the water cycle and associated matter fluxes.

The main objective of this thesis is the integration of an erosion model into the framework of the GLOWA-Danube project within the boundaries of the Upper Danube Basin. The Upper Danube Basin is a very heterogenous watershed, therefore representing a challenge on modelling techniques, since a variety of processes has to be considered in the modelling approach. The erosion module to be developed is aimed to provide a basis for assessing environmental impacts of soil erosion by water resulting from Global Change conditions.

In early years of erosion research, models have been developed with the focus on providing guidelines for selection of appropriate control practices corresponding to the needs of individual farms. This resulted in empirical equations, which are applicable to the conditions they have been developed for. Recent developments accounted for a change of these conditions and a more universal applicability, which led to process-oriented or physically-based soil erosion models. The latter usually operate on a very small temporal and spatial scale, and thus are often difficult to parameterise and apply on larger catchments. Since GLOWA-Danube is intended to assess impacts on a regional scale, this work attempts to combine the coarse spatial resolution with physically-based process descriptions into an erosion module.

Since this erosion module is intended to represent a component within GLOWA-Danube, its development is strongly oriented to the modelling guidelines of the project. The latter are focused on the utilisation of physically-based process descriptions. This work presents an erosion module for mesoscale to large-scale erosion modelling. The module is strictly process-oriented, derived from a physically-based erosion model, and regarded to be capable of simulating the impacts of Global Change conditions on erosion processes. This is achieved by considering intra-annual variations of external variables influencing erosion, and preparing these within the erosion module to the appropriate base unit needed for the processing of

the physical equations of the erosion model. The modelling of detachment and transport of soil particles is based on momentum fluxes of rainfall and runoff, which exert forces on the soil. The magnitude of all of these opposing forces is modified dynamically over the whole simulation period by the mentioned external variables, such as canopy cover or soil freezing.

Due to the large number of processes influencing erosion, there is a strong dependency on inputs (respectively the quality of the inputs) from other sub-components of the modelling compound, as well as on parameters within the erosion module. The process-oriented structure of the model allows for identification of the most important parameters influencing soil erosion in the Upper Danube Basin. The application of the model shows, that explicit process descriptions are necessary for the correct reproduction of spatiotemporal patterns of soil loss, and therefore essential for Global Change assessment. Because of these strong feedbacks of the input variables on the modelled processes, this also leads to the conclusion, that correct model parameterisation is a crucial task and a deficient input parameter set inevitably leads to deficient results.

It is shown in this work, that the gap between seemingly coarse scale inputs and physically oriented process descriptions can be bridged for mesoscale to large-scale catchments. The erosion model could be scaled successfully to the temporal and spatial scale used within the DSS DANUBIA. The application of the erosion module shows adequate, plausible reactions on natural, as well as anthropogenic inputs.

The model integrates detailed physically-based process descriptions of the driving variables on the spatial scale applied and reacts sensitively on the temporal dynamics of external input variables. This allows for reliable assessment of potential Global and Climate Change impacts on soil erosion by water.

# CONTENTS

<b>Table of Contents</b>	<b>xii</b>
<b>List of Figures</b>	<b>xv</b>
<b>List of Tables</b>	<b>xviii</b>
<b>List of Acronyms and Abbreviations</b>	<b>xix</b>
<b>1 Introduction</b>	<b>1</b>
1.1 Background and Motivation . . . . .	1
1.1.1 GLOWA-Danube . . . . .	1
1.1.2 Impacts of Soil Erosion . . . . .	3
1.2 Objectives of this Study . . . . .	5
1.3 Structure of this Study . . . . .	5
<b>2 Study Area</b>	<b>7</b>
2.1 Overview . . . . .	7
2.2 Climate . . . . .	8
2.3 Geology and Soils . . . . .	12
2.4 Land Use . . . . .	15
2.5 Hydrology . . . . .	17
<b>3 Soil Erosion</b>	<b>19</b>
3.1 Basic Processes . . . . .	19
3.1.1 Impact of Raindrops . . . . .	20
3.1.2 Shallow Sheet Flow . . . . .	20
3.1.3 Rill Erosion . . . . .	21
3.2 Influencing Factors . . . . .	22
3.2.1 Precipitation . . . . .	23
3.2.1.1 Overview . . . . .	23
3.2.1.2 Regional Characterisation . . . . .	25
3.2.2 Soil . . . . .	27
3.2.2.1 Overview . . . . .	27
3.2.2.2 Regional Characterisation . . . . .	30
3.2.3 Land Use and Agricultural Management . . . . .	32
3.2.3.1 Overview . . . . .	32
3.2.3.2 Regional Characterisation . . . . .	34
3.2.4 Relief . . . . .	36
3.2.4.1 Overview . . . . .	36
3.2.4.2 Regional Characterisation . . . . .	38

3.3	Suspended Sediment Yield . . . . .	40
3.3.1	Overview . . . . .	40
3.3.2	Regional Characterisation . . . . .	42
<b>4</b>	<b>Methods and Models</b>	<b>47</b>
4.1	Aspects of Modelling Approaches . . . . .	47
4.2	The Hydrological Model PROMET . . . . .	48
4.2.1	Meteorology . . . . .	51
4.2.1.1	Temporal Interpolation . . . . .	53
4.2.1.2	Temporal Disaggregation . . . . .	53
4.2.1.3	Spatial Interpolation . . . . .	54
4.2.1.4	Computation of Radiation . . . . .	55
4.2.2	Soil . . . . .	57
4.2.2.1	Water Flux . . . . .	57
4.2.2.2	Heat Flux . . . . .	58
4.2.3	Vegetation and Agricultural Management . . . . .	59
4.2.4	Channel Flow . . . . .	61
4.3	Historical Development and State of the Art in Erosion Modelling . . . . .	62
4.4	Selection of the Approach for Erosion Modelling . . . . .	64
4.5	The Soil Erosion Module . . . . .	66
4.5.1	Basic Concept of EROSION 2D . . . . .	66
4.5.1.1	Particle Detachment . . . . .	66
4.5.1.2	Particle Transport . . . . .	70
4.5.1.3	Particle Size Distribution . . . . .	71
4.5.1.4	Erosion and Deposition . . . . .	71
4.5.1.5	Limitations and Simplifications of the Model . . . . .	72
4.5.2	Flow Concentration and Particle Detachment dependent on Scale . . . . .	72
4.5.2.1	Theoretical Considerations . . . . .	72
4.5.2.2	Implementation in the Erosion Module . . . . .	75
4.5.3	Particle Settling Velocity . . . . .	77
4.5.4	Reduction of Momentum Flux of Raindrops . . . . .	78
4.5.4.1	Interception and Throughfall . . . . .	78
4.5.4.2	Soil cover . . . . .	81
4.5.5	Critical Shear Stress . . . . .	81
4.5.5.1	Quantification of the Erosion Resistance . . . . .	82
4.5.5.2	Shear Strength . . . . .	84
4.5.5.3	Root Reinforcement . . . . .	85
4.5.5.4	Soil Freezing . . . . .	87
4.5.5.5	Relationship between Shear Strength and Critical Shear Stress . . . . .	88
4.5.6	Agricultural Management Practices . . . . .	89
4.5.6.1	Determination of Management States . . . . .	90
4.5.6.2	Impact of Management States . . . . .	91
4.6	Temporal Disaggregation of Precipitation . . . . .	91
4.6.1	Overview of Temporal Rainfall Disaggregation Approaches . . . . .	92

4.6.2	The Cascade Model after OLSSON . . . . .	94
4.6.2.1	Basic Concept . . . . .	94
4.6.2.2	Application of a Cascade Model . . . . .	96
4.6.3	Adaptation of the Cascade Model to <i>AtmoStations</i> . . . . .	97
4.6.3.1	Regionalisation . . . . .	97
4.6.3.2	Modifications . . . . .	99
<b>5</b>	<b>Parameterisation</b>	<b>103</b>
5.1	Calibration of the Cascade Model . . . . .	103
5.1.1	Available Data . . . . .	103
5.1.2	Verification of the Model Approach . . . . .	104
5.1.3	Model Parameterisation for the Study Area . . . . .	108
5.2	Parameterisation of the Erosion Module . . . . .	115
5.2.1	Critical Shear Stress . . . . .	116
5.2.2	Flow Concentration . . . . .	117
5.2.3	Canopy Interception . . . . .	118
5.2.4	Soil Cover and Decomposition . . . . .	120
5.2.5	Manning's Roughness Coefficient . . . . .	122
5.2.6	Parameterisation of Agricultural Management . . . . .	122
<b>6</b>	<b>Validation</b>	<b>125</b>
6.1	Validation of the Cascade Model . . . . .	125
6.1.1	Validation at the Point Scale . . . . .	125
6.1.2	Practical Application within <i>AtmoStations</i> . . . . .	126
6.2	Validation of the Erosion Model . . . . .	130
6.2.1	The Subcatchments of the <i>Große Laber</i> and <i>Ammer</i> . . . . .	131
6.2.2	Sensitivity Analysis . . . . .	134
6.2.2.1	Direct Parameter Variations . . . . .	135
6.2.2.2	Indirect Parameter Variations . . . . .	142
6.2.3	Plausibility Check . . . . .	149
6.2.3.1	Preliminary Considerations . . . . .	150
6.2.3.2	Event-based Inspection of Temporal Soil Loss Patterns . . . . .	153
6.2.3.3	Analysis of Long-term Temporal Soil Loss Patterns . . . . .	156
6.2.3.4	Assessment of Long-term Spatial Soil Loss Patterns . . . . .	159
6.2.3.5	Comparison to Various Other Sources . . . . .	162
<b>7</b>	<b>Summary</b>	<b>169</b>
7.1	Achievements . . . . .	169
7.2	Critical Review . . . . .	170
7.3	Outlook . . . . .	174
	<b>References</b>	<b>190</b>
	<b>Appendix</b>	<b>191</b>
A	Cascade parameterisation . . . . .	193
B	Disaggregation Performance . . . . .	199

---

C	Configuration of the Model Runs . . . . .	201
D	Mean Soil Losses per District . . . . .	202
E	Influence of Soil Parameterisation in the Naab Sub-catchment . . . . .	205



## LIST OF FIGURES

1.1	Core areas within the project GLOWA-Danube . . . . .	2
1.2	Components within the framework of the DSS DANUBIA . . . . .	2
1.3	Scenario representation in the DSS DANUBIA . . . . .	3
2.1	Overview of the Danube River Basin . . . . .	7
2.2	Overview of the Upper Danube Basin . . . . .	8
2.3	Climate of the Upper Danube Basin . . . . .	9
2.4	Annual cycle of air temperatures in the Upper Danube Basin . . . . .	10
2.5	Cross section of geological layers in the Upper Danube Basin . . . . .	13
2.6	Geology of the Upper Danube Basin . . . . .	14
2.7	Land cover map of the Upper Danube Basin . . . . .	16
2.8	Land cover percentages in the Upper Danube Basin . . . . .	16
3.1	Hjulstöm curve . . . . .	22
3.2	Kinetic energy of rainfall depending on intensity . . . . .	25
3.3	Precipitation regimes in the Upper Danube Basin . . . . .	26
3.4	Thunderstorm days in the Upper Danube Basin . . . . .	27
3.5	Erosivity in the Upper Danube Basin . . . . .	28
3.6	Soil type map of the Upper Danube Basin . . . . .	31
3.7	Erodibility in the Upper Danube Basin . . . . .	33
3.8	Percentages of crops to total arable land area . . . . .	35
3.9	Percentages of arable land in the Upper Danube Basin . . . . .	36
3.10	Protective influence of crops and cover in the Upper Danube Basin . . . . .	37
3.11	Slope length and slope steepness in the Upper Danube Basin . . . . .	39
3.12	Critical particle diameters for sediment suspension . . . . .	41
3.13	Confluence of the Inn and the Danube at Passau . . . . .	43
3.14	Comparative suspended sediment transport of the Danube . . . . .	43
4.1	Grid-based modelling scheme. . . . .	49
4.2	Schematic model structure of PROMET . . . . .	49
4.3	Land cover and land use classes modelled within PROMET . . . . .	50
4.4	Weather stations in <i>AtmoStations</i> . . . . .	52
4.5	Rainfall disaggregation in <i>AtmoStations</i> . . . . .	54
4.6	Spatial interpolation in <i>AtmoStations</i> . . . . .	56
4.7	Soil water fluxes simulated by the PROMET soil moisture module . . . . .	57
4.8	Flowchart of the biological subroutines . . . . .	59
4.9	Allocation of primary production to different plant parts . . . . .	61
4.10	Overview of the erosion module . . . . .	67
4.11	Subscale effects on flow concentration and particle detachment . . . . .	73

4.12 Geometrical structure of the EROSION 2D test plot . . . . .	75
4.13 Components generating canopy throughfall . . . . .	78
4.14 Fractional canopy cover and maximum intercepted water storage . . . . .	80
4.15 Schematics of the reduction of momentum flux . . . . .	82
4.16 Relative importance of vegetation cover and plant roots on erosion processes	86
4.17 Determination of the actual sowing and harvest dates . . . . .	90
4.18 Schematics of the disaggregation cascade . . . . .	95
4.19 $W_{x/x}$ -distribution of a cascade model . . . . .	96
4.20 Decision tree of precipitation regimes . . . . .	99
4.21 Spatial pattern of precipitation regimes . . . . .	100
5.1 Comparison of probabilities $P(1/0)$ , $P(0/1)$ and $P(x/x)$ for different stations .	110
5.2 $W_{x/x}$ -distributions of station <i>Osterseeon</i> for all volume and position classes .	111
5.3 Volume class thresholds for all position classes and regions . . . . .	112
5.4 Empirical $W_{x/x}$ -distributions of the generator . . . . .	114
5.5 Fractional canopy cover and maximum intercepted water storage for maize .	119
5.6 Fractional canopy cover and maximum intercepted water storage for wheat .	119
6.1 Seasonal mean precipitation intensities (ACD) . . . . .	129
6.2 Seasonal mean precipitation intensities (CD) . . . . .	130
6.3 Number of heavy precipitation days per year . . . . .	131
6.4 Location of the subcatchments <i>Große Laber</i> and <i>Ammer</i> . . . . .	132
6.5 Areal distribution of slope in the sub-catchments <i>Große Laber</i> and <i>Ammer</i> .	132
6.6 Sensitivity of the erosion model to variations concerning the grain size . . . .	137
6.7 Variations of the slope . . . . .	138
6.8 Variations of the flow concentration factor . . . . .	138
6.9 Variations of the soil cover . . . . .	139
6.10 Variations of Manning's roughness coefficient . . . . .	140
6.11 Influence of cohesion and angle of internal friction on soil loss . . . . .	141
6.12 Variations of the erosion resistance . . . . .	141
6.13 Sensitivity of all tested parameters . . . . .	142
6.14 Temporal course of rainfall and runoff formation induced by disaggregation methods . . . . .	143
6.15 Influence of soil freezing on runoff formation and soil loss . . . . .	144
6.16 Influence of momentum flux partitioning . . . . .	145
6.17 Influence of the particle settling velocity . . . . .	146
6.18 Influence of agricultural management . . . . .	146
6.19 Influence of land use types . . . . .	147
6.20 Influence of surface runoff . . . . .	148
6.21 Measured SSY and MQ at the gauges Schönach and Weilheim . . . . .	150
6.22 Measured specific sediment yield and discharge at the gauges Schönach and Weilheim (1995) . . . . .	150
6.23 Measured and modelled discharge for Schönach and Weilheim (1995) . . . .	151
6.24 Modelled precipitation and surface runoff for the watersheds of the Große Laber and Ammer (1995) . . . . .	152

6.25	Mean monthly precipitation amounts in the Große Laber and Ammer catchments	154
6.26	Measured SSY vs. modelled soil loss for the watersheds of the Große Laber and Ammer (1995)	155
6.27	Modelled monthly mean values of soil loss, precipitation and surface runoff of the Große Laber and Ammer watershed	156
6.28	Standardised monthly mean specific sediment yield (SSY) and soil loss for the Große Laber and Ammer watershed.	157
6.29	Standardised monthly mean measured and modelled discharge of the Große Laber watershed.	159
6.30	Modelled long-term monthly mean soil loss in the Upper Danube Basin	160
6.31	Mean annual soil loss in the Upper Danube Basin (erosion module)	160
6.32	Mean annual soil loss in the Upper Danube Basin (ABAG, PESERA)	163
6.33	Maps of mean annual soil loss for regions overlapping the Upper Danube Basin	164
6.34	Mean annual soil loss per district in the Upper Danube Basin	165
A1	Probabilities $P(1/0)$ , $P(0/1)$ and $P(x/x)$ of all levels for all position and volume classes	194
A2	$W_{x/x}$ -distributions of all levels for starting boxes	195
A3	$W_{x/x}$ -distributions of all levels for enclosed boxes	196
A4	$W_{x/x}$ -distributions of all levels for ending boxes	197
A5	$W_{x/x}$ -distributions of all levels for isolated boxes	198
E6	Qualitative comparison of soil losses by different parameterisations (Naab watershed)	205



## LIST OF TABLES

2.1	Major tributaries of the Danube . . . . .	17
2.2	Natural lakes in the Upper Danube Basin . . . . .	17
2.3	Reservoirs in the Upper Danube Basin . . . . .	18
2.4	Water transfers in the Upper Danube Basin . . . . .	18
3.1	Terminal velocities of raindrops depending on drop diameter . . . . .	24
3.2	Characteristics of the main breakdown mechanisms . . . . .	30
3.3	$K_b$ values for the soil type classes derived by MUERTH . . . . .	32
3.4	C-factors for all land uses . . . . .	35
3.5	Assignment table of mean effective slope length depending on slope inclination . . . . .	39
3.6	Mean flow velocities of the Danube . . . . .	42
3.7	Mean critical particle diameters . . . . .	42
3.8	Mean percentages of particle size classes transported as suspended sediment in the Danube . . . . .	44
4.1	Sowing and harvest dates for arable land . . . . .	60
4.2	Cutting periods for grassland . . . . .	60
4.3	Phenological stages modelled by the biological module. . . . .	61
4.4	Basic properties of selected erosion models . . . . .	63
4.5	Basic factors influencing soil erosion by water . . . . .	63
4.6	Root parameter exponents . . . . .	86
5.1	Attributes of the stations used for cascade calibration . . . . .	104
5.2	Mean disaggregation performances (precipitation sums of 1-hour time series) . . . . .	107
5.3	Mean disaggregation performances (kinetic energy of 1-hour time series) . . . . .	108
5.4	Empirical probabilities of the generator . . . . .	113
5.5	Values for effective cohesion $c'$ and angle of shearing resistance $\varphi'$ . . . . .	116
5.6	Flow concentration factors $f_{cf}$ for arable land . . . . .	117
5.7	Leaf angle distribution parameters $x$ and extinction coefficients $K_{be}$ . . . . .	118
5.8	Mean drip off heights for all modelled canopies. . . . .	120
5.9	Static soil cover values ( $f_{cs}$ ) for natural areas . . . . .	121
5.10	Coefficients for decomposition of organic material . . . . .	122
5.11	Maximum roughness values depending on land cover . . . . .	123
6.1	Mean disaggregation performances of all regions . . . . .	126
6.2	Mean modelled disaggregation performances (daily precipitation sums) . . . . .	127
6.3	Land use distribution of the sub-catchments <i>Große Laber</i> and <i>Ammer</i> . . . . .	133
6.4	Soil class distribution of the sub-catchments <i>Große Laber</i> and <i>Ammer</i> . . . . .	133
6.5	Slope statistics of the sub-catchments <i>Große Laber</i> and <i>Ammer</i> . . . . .	134

6.6	Characteristics and default values of the proxel selected for sensitivity analysis	134
6.7	Sensitivity of the erosion model to variations concerning the grain size . . . . .	136
6.8	Variations of the slope . . . . .	137
6.9	Variations of the flow concentration factor . . . . .	138
6.10	Variations of the soil cover . . . . .	139
6.11	Variations of Manning's roughness coefficient . . . . .	139
6.12	Sensitivity of the erosion model to variations concerning the detachability of the soil . . . . .	140
6.13	Variations of the erosion resistance . . . . .	141
6.14	Influence of disaggregation method on total soil loss . . . . .	143
6.15	Influence of soil freezing on total soil loss . . . . .	143
6.16	Influence of momentum flux partitioning . . . . .	144
6.17	Influence of the particle settling velocity on total soil loss . . . . .	145
6.18	Influence of agricultural management . . . . .	146
6.19	Influence of land use types . . . . .	147
6.20	Influence of surface runoff . . . . .	148
6.21	Attributes of the LfU gauges for measurement of suspended sediment . . . . .	149
6.22	Measured SSY and MQ at the gauges Schönach and Weilheim . . . . .	149
6.23	Modelled monthly mean values of soil loss of the Große Laber and Ammer watershed . . . . .	157
6.24	Statistical criteria of standardised mean monthly model results . . . . .	157
6.25	Ratios of soil loss depending on agricultural management practices . . . . .	158
6.26	Modelled discharge at the gauges Schönach and Weilheim . . . . .	159
6.27	Mean annual soil loss per land use in the Upper Danube Basin . . . . .	162
6.28	Mean annual soil losses calculated by different approaches . . . . .	166
A1	Parameters for the volume class threshold functions of the cascade . . . . .	193
A2	Empirical $W_{x/x}$ -distributions of the generator (rounded numerical values) . . . . .	193
B3	Mean modelled disaggregation performances (hourly values) . . . . .	199
D4	Mean long term annual soil losses per district . . . . .	202

## **LIST OF ACRONYMS AND ABBREVIATIONS**

**ABAG** Allgemeine Bodenabtragsgleichung

**ACD** advective-convective disaggregation

**ACRE** Agro-eConomic model for agricultural pRoduction on rEgional level

**ANSWERS** Areal Nonpoint Source Watershed Environment Response Simulation

**BMBF** German Ministry of Research and Education Bundesministerium für Bildung und Forschung

**CD** cascade disaggregation

**CET** Central European Time

**CLD** constant linear disaggregation

**ClimChAlp** Climate Change, Impacts and Adaptation Strategies in the Alpine Space

**CME** coefficient of model efficiency

**CREAMS** A Field Scale Model for Chemicals, Runoff, and Erosion for Agricultural Management Systems

**DSD** drop size distribution

**DSS** Decision Support System

**DTM** Digital Terrain Model

**DWA** German Association for Water, Wastewater and Waste (Deutsche Vereinigung für Wasserwirtschaft, Abwasser und Abfall)

**DWD** German Weather Service (Deutscher Wetterdienst)

**EPIC** Erosion Productivity Impact Calculator

**EUROSEM** European Soil Erosion Model

**FAO** Food and Agriculture Organization of the United Nations

**FT** freeze-thaw

**GIS** Geographical Information System

**GLOWA** Global Change and the Hydrological Cycle (Globaler Wandel des Wasserkreislaufes)

**IPCC** Intergovernmental Panel on Climate Change

- KINEROS** Kinematic Runoff and Soil Erosion Model
- LAI** leaf area index [ $\text{m}^2/\text{m}^2$ ]
- LfL** Bavarian State Office of Agriculture (Bayerische Landesanstalt für Landwirtschaft)
- LfU** Bavarian State Office for Environment (Bayerisches Landesamt für Umwelt)
- LMU** Ludwig-Maximilians University Munich
- LWD** Bavarian Avalanche Warning Service (Lawinenwarndienst Bayern)
- MONERIS** Modelling Nutrient Emissions in River Systems
- MQ** mean discharge
- P** phosphorus
- PESERA** Pan-European Soil Erosion Risk Assessment
- PP** particulate phosphorus
- PROMET** Processes of Radiation, Mass and Energy Transfer
- proxel** *process pixel*
- R<sup>2</sup>** coefficient of determination
- RCM** regional climate model
- RMSE** Root Mean Square Error
- RUSLE** Revised Universal Soil Loss Equation
- SHTM** Soil Heat Transfer Module
- SVAT** Soil Vegetation Atmosphere Transfer
- SCS** Soil Conservation Service
- SDR** sediment delivery ratio
- SSY** specific sediment yield
- TOA** top of atmosphere
- USDA** United States Department of Agriculture
- USLE** Universal Soil Loss Equation
- WEPP** Water Erosion Prediction Project
- WFD** EU Water Framework Directive
- WRB** World Reference Base for Soil Resources
- WSD** Austrian Waterway Authority (Wasserstraßendirektion)
- ZAMG** Central Institute for Meteorology and Geodynamics (Zentralanstalt für Meteorologie und Geodynamik)



# 1. INTRODUCTION

## 1.1. BACKGROUND AND MOTIVATION

Public interest in Climate Change is steadily growing. Global warming is induced, according to the IPCC with *very high confidence* (90%), by anthropogenic intensification of the natural green house effect. The main reasons are the emissions of carbon dioxide, methane and other trace gases (IPCC, 2007). But global warming is also induced and accompanied by other processes, such as land use changes, demographic development or globalisation, which is expressed in the term “Global Change”. The assessment of Global Change impacts is an important task in order to develop adaptation and mitigation strategies. This is important in particular on the regional scale, as global models cannot provide regional or local policymakers with adequate information on potential impacts. And because the adaptation process is different in different regions, in recent years models have been developed to study the impacts of Climate Change and/or Global Change on the regional scale.

This work evolved in the project GLOWA-Danube, which is intended to investigate the mentioned regional impacts, therefore the project is outlined in the following section.

### 1.1.1. GLOWA-DANUBE

The initiative GLOWA of the the German Ministry of Research and Education (BMBF), aims at investigating the “manifold consequences of Global Change on regional water resources in a variety of catchment areas with different natural and cultural characteristics” (LUDWIG ET AL., 2003). The project GLOWA-Danube within this initiative studies these impacts on the Upper Danube Basin. In order to achieve this task, an interdisciplinary, university-based network of experts developed the integrative Decision Support System (DSS) DANUBIA. The knowledge of a number of project groups, covering the fields of natural and social as well as computer sciences, is combined in the DSS DANUBIA. Fig. 1.1 represents the major issues of integrative Global Change research in alpine watersheds. Each depicted area of interest is treated by an expert project group, which develops a modelling component within DANUBIA. The components are coordinated by the core system and data is exchanged dynamically via interfaces (Fig. 1.2). This way DANUBIA simulates the water and energy fluxes in the natural environment, as well as the water use in energy production, farming, tourism, industry and households. The simulated model outputs are intended for stakeholders from politics, administration or economy, to support their decision-making regarding their interests, which may be influenced by future changes in the water cycle.

In order to predict future trends the DSS DANUBIA allows for simulation of Climate Change scenarios, either provided by a regional climate model (RCM) like REMO or MM5, or based on a stochastic weather generator (MAUSER ET AL., 2006). The natural components within DANUBIA are modelled on a physical basis, so that they directly react to meteorological changes. The environmental reactions are passed as altered matter and energy fluxes to the

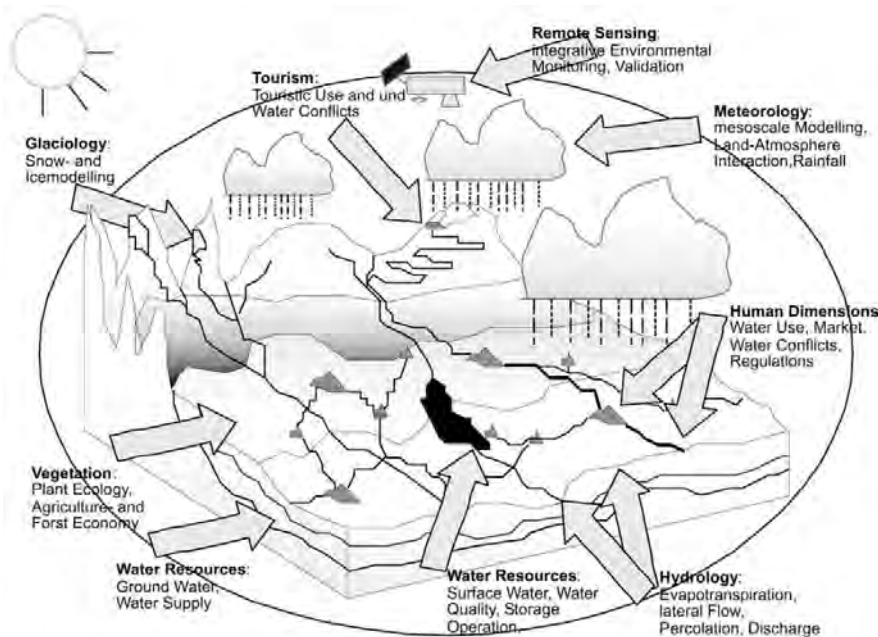


Fig. 1.1: Core areas within the GLOWA-Danube designating the involved expert project groups (LUDWIG ET AL., 2003).

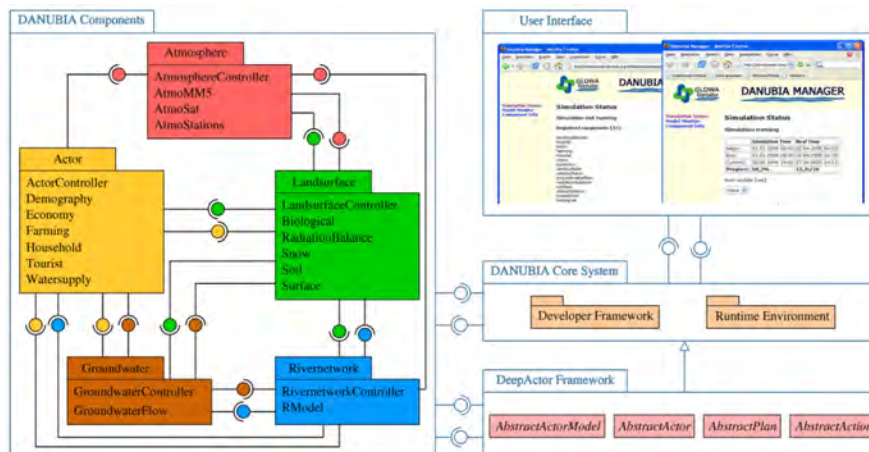


Fig. 1.2: Technical overview of the components within the framework of the DSS DANUBIA (MAUSER & MUERTH, 2008).

socioeconomic components, which in turn react on these, and eventually may change the natural processes (e.g. through land-use changes). Furthermore, the agent-based socioeconomic models also respond to externally defined political and economical conditions as well as demographic and sociological trends (Fig. 1.3). The socioeconomic models rely on the *DeepActor* framework of DANUBIA for representing human decision processes (BARTHEL ET AL., 2008). It allows each human actor within the Upper Danube Basin to react independently on changing conditions. A decision for a reaction is made by selecting and executing an appropriate plan, which consists of a predefined set of actions.

All of the modelled processes are abstracted to a basic spatial unit of 1 km x 1 km, which is termed a *process pixel* (proxel). The computation time step of the components varies from

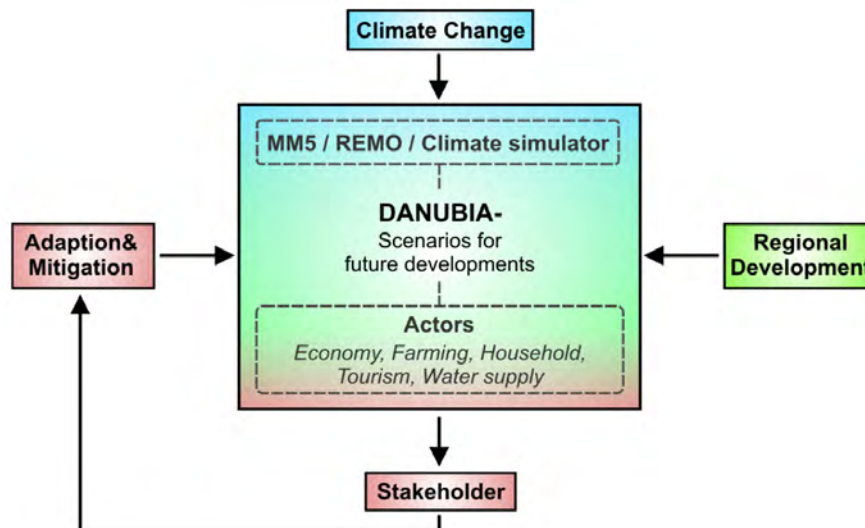


Fig. 1.3: Scenario representation in the DSS DANUBIA (MAUSER & MUERTH, 2008).

1 hour for the natural components up to 1 month for the agent-based actor models.

### 1.1.2. IMPACTS OF SOIL EROSION

SCHEFFER & SCHACHTSCHABEL (2002) define soil erosion as the detachment and transport of soil particles (primary particles or aggregates) along the soil surface. Depending on the transport medium it is differentiated between wind erosion or water erosion. Additionally there are special forms that do not involve a transport medium, as e.g. debris flow, land slides or solifluction. Solely anthropogenic forms of erosion are tillage erosion, which dislocates soil within an agricultural area, and transportation of soil sticking to root crops after harvest.

According to RICHTER (1998), soil erosion is not a recent problem, but reached a first climax in Europe in the early 14th century, when settlements and agriculture reduced forested areas. Records from the 17th and 18th century show complaints about deposition of soil, land degradation and spillage of cultivated land. Colonisation in North America and the following conversion of hitherto only extensively used land into intensively agriculturally used areas - often monocultures - lead to severe destruction of soil due to erosion at the end of the 18th century. Because of these problems, the USA founded the Soil Conservation Service (SCS) within the United States Department of Agriculture (USDA) in the 1920s and started the systematic research of soil erosion.

The damage associated with soil erosion is commonly classified into *on-site* and *off-site* effects. On-site effects refer to damage on the agricultural fields themselves and influence productivity and efficiency of the production. The off-site effects are those linked to transport and deposition of soil from production fields onto adjacent or downstream areas. The latter are often the most noticeable and mainly affect water quality. The following summary, compiled from LAL (2005), lists the causes and effects of both on-site and off-site damage:

- On-site effects:
  - Soil erosion removes the topsoil, which has the highest organic matter content and the most stable soil structure and provides optimal seedbed for germinating and

emerging plants. The removal reduces the water-holding capacity of the soil and the available rooting depth for the crop. This leads to reduced efficiency of water and nutrient use by the plant, and may also result in a shift in the types of plants that can be grown.

- Due to gullies or rills caused by soil erosion, agricultural operations may be disrupted, either through damage of machinery, or increased labour costs to restore original conditions.
- Transport and deposition of eroded soil and crop residue may bury emerging crops. Deposition of agricultural chemicals on adjacent fields can cause problems with plant growth, especially if crops are sensitive to the particular chemical.
- Off-site effects:
  - Economic impacts:
    - \* Deposited soil on road or residential areas causes costs for removal.
    - \* The latter applies also for sediments in lakes, rivers or reservoirs in order to maintain recreation, navigation and flow.
    - \* Contaminated sediment yield in rivers leads to additional costs for water treatment for residential and industrial water supply.
  - Environmental impacts: they usually take longer time to become noticeable and the main impacts are caused by effects of materials bound to the moving sediment, rather than by the sediment itself. Sediment deposition in streams, rivers and lakes may impact the biological health of an ecosystem through the following sediment-bound agents:
    - \* Nutrients, in particular phosphorus (P), can cause eutrophication and therefore reduction of water-quality.
    - \* Agricultural chemicals, such as herbicides or insecticides represent health hazards for both fish and humans, if toxic levels are exceeded.
    - \* Transport of pathogens from agricultural areas into adjacent waterbodies may harm fish, as well as human populations, if the water supply is contaminated.

Since the implementation of the EU Water Framework Directive (WFD) (WFD, 2000) in 2000, the interest in monitoring, modelling and evaluating off-site effects of soil erosion concerning water quality has grown. Eutrophication occurs through transport of P into aquatic ecosystems, as P is usually the limiting nutrient and thus also the main nutrient for eutrophication (e.g. ULÉN & KALISKY, 2005; MULQUEEN ET AL., 2004). In most soils, the quantity of soluble or readily desorbable P susceptible to transport is rather small, as P has a low solubility and clays have a high sorption capacity (e.g. PIERZYNSKI ET AL., 2005). This means, that P is bound to the particles and soil erosion plays a major role in the transport of diffuse, agriculturally derived particulate phosphorus (PP) into waterbodies.

## 1.2. OBJECTIVES OF THIS STUDY

The objective of this study is the development of an soil erosion module for the framework of the GLOWA-Danube project within the boundaries of the Upper Danube Basin. The soil erosion model to be integrated into this outline is intended to provide a basis for assessment of environmental impacts of soil erosion by water resulting from Global Change conditions. This involves the compliance of the following requirements:

- (a) Responsiveness on changing environmental conditions, as well as anthropogenic measures: Global Change implies not only Climate Change, but also involves anthropogenic interventions. A DSS, and thus the erosion model which shall be integrated into the latter, must be able to identify and show potential impacts of future adaptation and mitigation strategies. Therefore the model shall not be calibrated to present conditions, in order to guarantee reliability under different external conditions.
- (b) Reliable process representation: In order to assess possible future Climate Change scenarios, a physically-based model provides the capabilities of a reliable process representation (cf. Section 4.1). Explicit physical process representation also provides the feasibility of evaluation of mitigation strategies, as the reactions of involved processes on anthropogenic measures can be observed. Moreover, the understanding of processes may contribute to development of new mitigation measures, as the influence of individual processes can be quantitatively assessed.
- (c) Adequate process scaling: The Upper Danube Basin is a very large and heterogeneous region. Availability of input data and computational power still today limits the temporal and spatial resolution of environmental models. Therefore the erosion module shall be applicable efficiently on the meso- to large-scale, and represent the processes involved on this scale adequately.
- (d) Extensibility: As the erosion model shall act as a basis for assessment of erosion induced environmental impacts, it must be extensible within the DANUBIA framework, i.e. must not be constrained to (spatially and/or temporally) lumped output parameters, but must be able to interface to other model components on a proxel basis.

## 1.3. STRUCTURE OF THIS STUDY

Chapter 2 outlines the whole Danube catchment and the location of the Upper Danube Basin within the latter. The physical geography of the catchment is introduced with characterisations of the climate, geology and soils, the land use and hydrological aspects, in order to provide the reader with the necessary regional knowledge of the study area.

Chapter 3 first explains the basic processes involved in soil erosion, and then depicts the factors, which mainly influence soil erosion. These are described more detailed, and the introducing description given in Chapter 2 is extended by a regional characterisation of the factors, to emphasise their relevance for erosion modelling in the Upper Danube Basin. This chapter shows the minimum data requirements needed for implementing a soil erosion model according to the demands defined in Section 1.2.

As the erosion model shall be integrated into Processes of Radiation, Mass and Energy Transfer (PROMET), Chapter 4 briefly introduces this land surface model, with respect to the sub-components, which provide the data needed for modelling of soil erosion. With the knowledge of the data, which basically can be delivered by these sub-components, a suitable erosion model is selected for integration. The erosion model itself is described, and also the extensions, which are necessary for successful integration and adequate process representation.

Chapter 5 deals with the parameterisation of the models presented in Chapter 4.

The results from the parameterised models are validated in Chapter 6. The sensitivity of the erosion model within reasonable conditions is analysed and the plausibility is checked within the Upper Danube catchment.

Finally Chapter 7 summarises the achievements of this work and outlines the perspectives of future applications of the erosion model.

## 2. STUDY AREA

### 2.1. OVERVIEW

The Danube is the second largest river in Europe, having a length of 2,780 km. Its watershed ranges over 18 countries and covers an area of 801,463 km<sup>2</sup> (see Fig. 2.1). The Danube River Basin can be structured into three geologic and geographic divisions (ICPDR, 2005):

1. The Upper Danube Basin: here the Danube has its sources in the Black Forest. This area mainly covers parts of the Alps and their foothills in the south and low mountain ranges in the north and east. These regions show strong influence of Atlantic climate with high precipitation.
2. The Middle Danube Basin: the Pannonian Plain and the Transylvanian Uplands are surrounded by the Carpathians in the north and east, and the Dinaric Alps in the south-west. The south is influenced by Mediterranean climate.
3. The Lower Danube Basin covers the Bessarabian Upland in the north and the Romanian Plain in the south, where the Danube discharges into the Black Sea. It is characterised by Continental climate with lower precipitation and cold winters.



Fig. 2.1: Overview of the Danube River Basin and the location of the Upper Danube Basin, modified after ICPDR (2005)



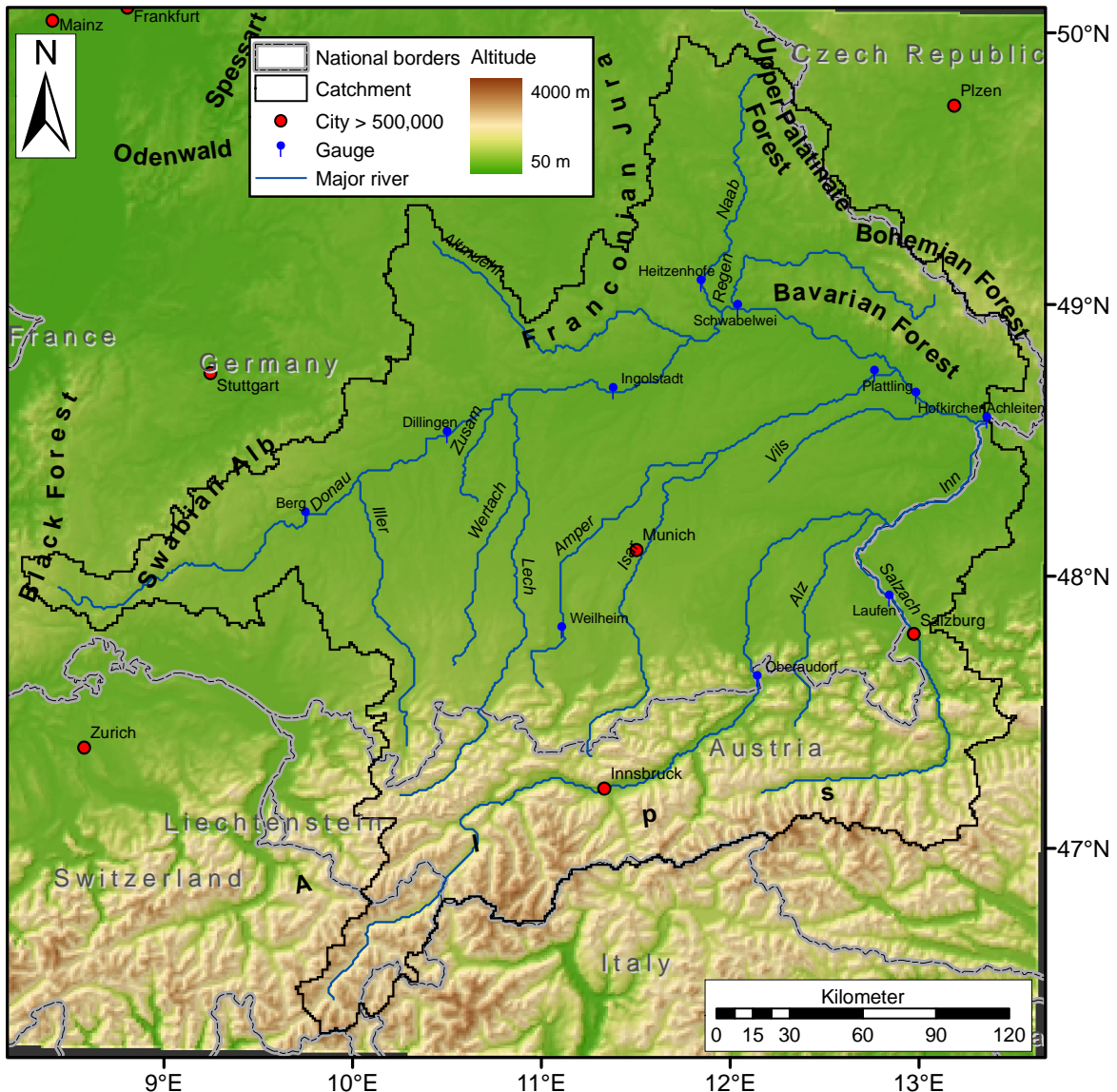


Fig. 2.2: Overview of the Upper Danube Basin

The different climatic conditions in the sub-basins distinctly influence the hydrological regime of the river. Largest discharge contribution is given by Austria (22.1%) followed by Romania (17.6%), which reflects the high precipitation amounts in the Alps and the Carpathian mountains. At its river mouth into the Black Sea, the Danube has an average discharge of about  $6,500 \text{ m}^3/\text{s}$ .

The project GLOWA-Danube focuses on the Upper Danube Basin with an area of  $76,653 \text{ km}^2$ . So the following sections are intended to characterise the geographical aspects of the upper region (see Fig. 2.2) of the Danube River Basin.

## 2.2. CLIMATE

Climate in Central Europe is governed by the large-scale atmospheric circulation, particularly by moist air masses transported by cyclones from south-westerly to northerly directions. The



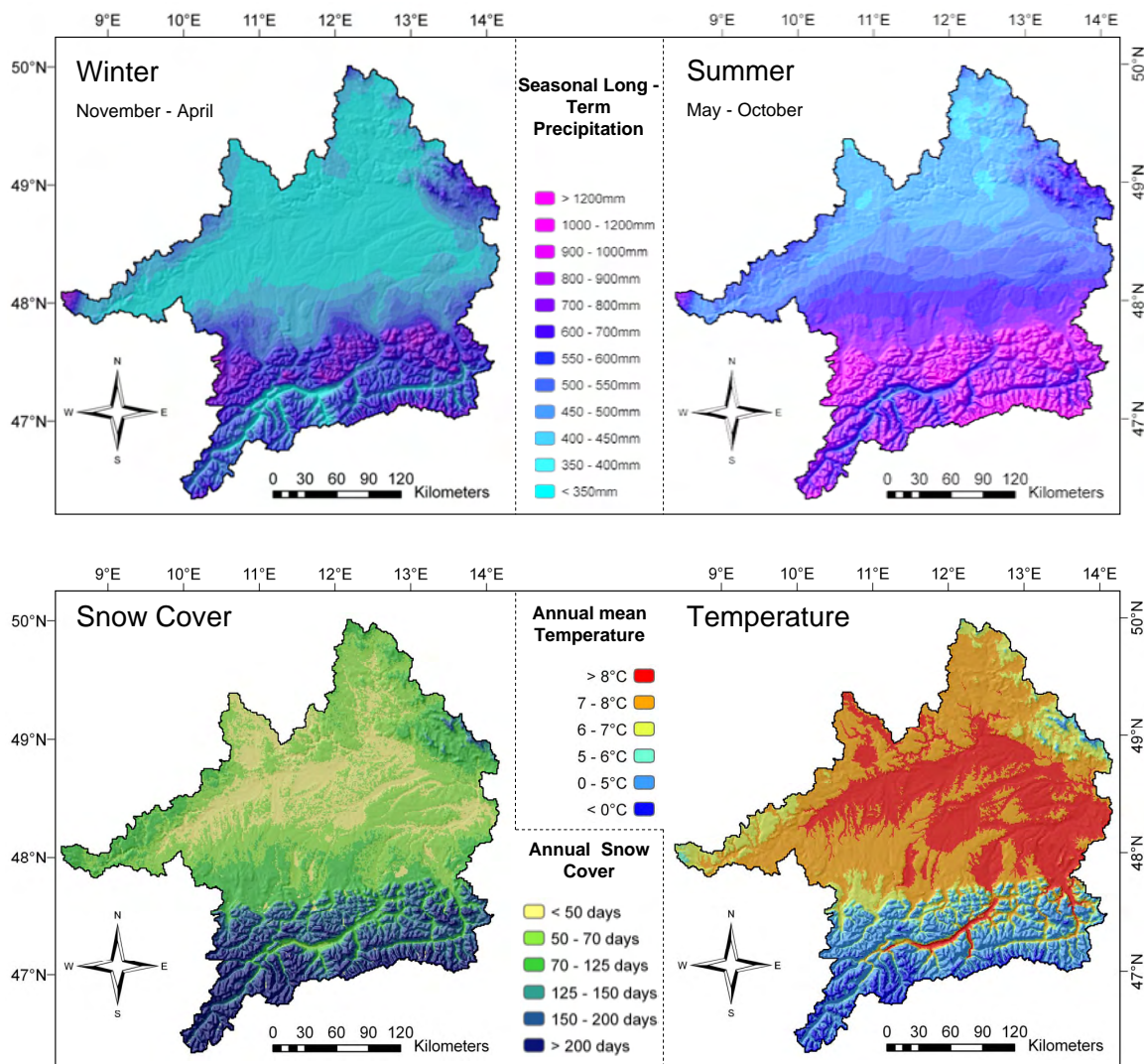


Fig. 2.3: Climate of the Upper Danube Basin, interpolated with PROMET for the years 1971–2000. Snow cover is defined as a day with a mean snow water equivalent  $\geq 1$  mm.

climate of the Upper Danube Basin can be identified according to the effective *Köppen-Geiger* classification system (KÖPPEN ET AL., 1936) as *Cfb*, meaning a warm temperate climate, fully humid with warm summers. Within this zone the basin is located in a transition area between the maritime climate of West Europe, characterised by mild winters and cool summers with high humidity, and the continental climate in the east, with cold winters, warm summers and low humidity.

Advective lift at warm and cold fronts of the cyclones leads to the formation of clouds and precipitation (BMU, 2001). Nevertheless the spatial distribution of rainfall in the study area is highly variable, as it is influenced by orography and continentality. Orography induces advective processes and influences the amount of rainfall in windward and leeward sides. Increasing continentality from west to east causes decreasing precipitation, but due to high

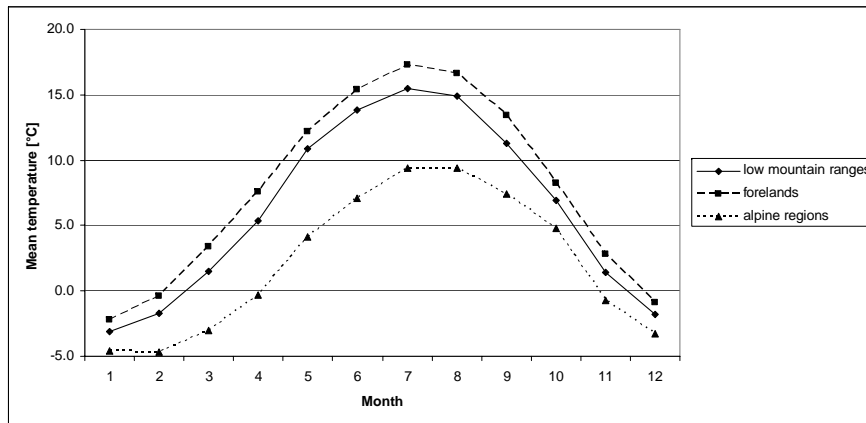


Fig. 2.4: Annual cycle of air temperatures from chosen climate stations representing different geographical areas (base data: DWD climatological station data from 1961 – 1990).

solar irradiation in the summer, convective processes frequently result in showers with high intensities. Within the annual cycle continentality leads to higher precipitation sums in summer and lower sums in winter. Mean annual precipitation in the Upper Danube Basin ranges from approximately 650 mm to over 2000 mm. A more detailed analysis on precipitation patterns is a subject in Section 3.2.1.2, as this is an important factor for soil erosion.

Due to continentality mean annual temperature amplitudes increase from west to east. Because of maritime influences the Upper Rhine Graben, which borders the catchment westward of the Black Forest, represents the warmest region, reaching annual mean temperatures between 9°C and 10°C. Annual mean temperatures in the low mountain ranges to the north of the Danube are lower due to higher altitudes: they range in the heights of the Spessart from 6°C to 10°C, average out below 7°C in the Swabian Alb and the Franconian Jura, and reach a minimum in the eastern Upper Palatinate Forest and Bavarian Forest with about 3°C to 7°C. For the lowlands south of the Danube a temperature increase towards the south would be expected, but this effect is superimposed by growing altitudes, resulting in mean temperatures of about 7 – 8°C. The temperature sinks to the south over the foothills of the Alps with about 6°C down to under -4°C at the peaks of the Alps. (BAYFORKLIM, 1996)

Fig. 2.4 shows the typical annual cycles of air temperatures of different geographical areas. All temperature curves show the same course, with a maximum in summer and a minimum in winter, as opposed to the course of precipitation which exhibits distinct patterns for these regions (see Section 3.2.1.2, Fig. 3.3). Temperatures mainly reflect the altitude above sea level, whereas temporal precipitation patterns follow orography and seasonal extended-range weather situations. Mean diurnal variations are more pronounced in the lowlands with approximately 5 – 6 K in contrast to mountain stations with amplitudes of 2 K. Depending on weather conditions, maximum temperature amplitudes in summer can reach up to 16 K or stay relatively constant on a cloudy day. Daily minimum temperatures are reached shortly before sunrise, highest values at 14:30 CET in winter and 16:00 CET in summer in the lowlands and about an hour earlier in the mountains, due to topographic effects. Absolute minimum temperatures range from approximately -24°C to -29°C virtually irrespective of altitude, as the cold air sinks down and concentrates at ground level, whereas air movements at the peaks of mountainous regions prevent further sinking of temperature. By contrast, the distribution of

maxima shows a considerable dependency of altitude, ranging from ca. 38°C in the lowlands to 18 °C at 3000 m a.s.l. in the Alps.

Local factors in the catchment area influencing mesoclimate are:

- some basins and valleys acting as heat reservoirs in spring and summer, or as pools of cold air in autumn and winter (e.g. the Inn valley)
- attenuating influence of surface water bodies (e.g. the Chiemsee)
- urban heat islands of the cities (e.g. Munich)
- evaporative heat loss in forested areas (e.g. the *Ebersberger Forst*)

Consequential mean temperature differences compared to the surrounding areas add up to about 1 K, but can be much higher under certain weather conditions.

A regional anomaly is the so-called *Föhn*, a warm and dry rain shadow wind, occurring at southerly directions of air flow. Moist air coming from the south, rises with a saturated adiabatic lapse rate upwards at the Alps, leading to precipitation. At the north side the air sinks down with a dry-adiabatic lapse rate, and thus has a higher temperature and lower moisture. Atmospheric conditions directing air from the north over the Alps invert this phenomenon. Important aspects concerning regions with frequent *Föhn* conditions are premature snowmelt in early spring and increased avalanche risk during winter. Regarding vegetation period and land use, the warm air masses can shift the beginning of spring in the southern Alps to an earlier date and permit cultivation of maize north of the Alps, or even wine in the area of Innsbruck (DWD, 2008).

Special periods, mostly concerning agroclimatological aspects, are characterized in the study area as follows:

- vegetation season: based on the definition, that the long-term daily mean air temperature does not fall below 5°C, this period lasts between 210 and 250 days in the lowlands, reduces to 150 to 200 days in the low mountain ranges<sup>1</sup>, and falls to zero in the high mountains above 2600 m a.s.l. For plant physiological reasons, some cultivations need a threshold of 10°C daily mean, which shortens the vegetation season by about 70 days.
- frost-free period: the number of days with a minimum air temperature above 0°C adds up to 180–190 in large stretches of the Upper Danube Basin. However there are local exceptions, like narrow valleys with pools of cold air, having less frost-free days, or warmer regions like urban heat islands and mild riparian areas, with longer frost-free periods.
- frost days: days with a maximum air temperature above 0°C constitute between less than 80 days in the lowlands, up to 140 days in the low mountain ranges and the higher alpine valleys, and exceed 200 days in locations above 200 m a.s.l. The number of frost days is influenced by local effects, analogous to the frost-free period.

---

<sup>1</sup>To avoid any misunderstanding: the term “low mountain ranges” refers to the German designation “Mittelgebirge” and denotes those low mountains ranges, which were formed before Alpine orogeny started

- summer days: maximum air temperatures above 25°C are closely related to altitude, but strongly influenced by continentality and a south-north gradient, caused by higher persistency of anticyclones in the south. Over 45 days can be counted at the lower Main, 40 to 45 days at Lake Constance, the lower Danube and the lower Inn. The Franconian Jura and Bavarian Forest records between 20 and 25 days, the foothills of the Alps and alpine valleys up to 30 days. Above 2000 m a.s.l. no summer days were ever registered.
- snow cover: influencing factors are altitude (temperature), orography (exposition, lee- and windward sides, pools of cold air), land cover (urban heat islands, forests) and wind induced transport. The resulting pattern is illustrated in Fig. 2.3 and corresponds well with the spatial distribution of air temperature and the relief.

### 2.3. GEOLOGY AND SOILS

Geologic stratification (see Fig. 2.5) of the Upper Danube Basin can be classified into four units (GLA, 1996):

- The Variscan North-Bavarian basement rock consists predominantly of granite and metamorphic rock, representing the fundament of the considerably younger overlying rock. Due to tectonic lift and erosion since the Cretaceous the bedrock appears at the surface in the northeastern parts of the catchment Fig. 2.6.
- The overlying rock north of the River Danube lies over the basement. The sedimentary rock originated during late Palaeozoic and Mesozoic ranges with a thickness of 300 m to 1500 m from the *Spessart* in the north down to the Danube into the molasse basin. South of the Danube the basement rock and the overlying cap-rock decline some thousand metres and are covered by molasse sediments.
- The Alpine orogeny began in early Mesozoic with deposition of sediments from the Tethys Ocean. Beginning convergent movement of the European and African plates in the Cretaceous led to folding and faulting of the sediment layers. The upper crust of the Apulian plate was thrust over the European crust. When in early Tertiary the subducting slab broke off, isostatic lift and further collision of the plates let the Alps rise with up to 5 mm per year.
- The molasse basin between the Danube and the forelands of the Alps is filled with a stratified sediment layer of up to 5000 m, which was eroded during the Alpine orogeny in Tertiary and deposited in the basin. It consists of limnic and fluvial sediments of various grain sizes and was influenced temporarily either by salt water or fresh water.

These four geological units are characterised by different hydrogeological properties (BARTHEL ET AL., 2005):

- Paleozoic basement: the gneiss and granite parent material of the Bavarian Forest, the Upper Palatinate Forest and the Black Forest shows basically low permeability. Merely a few granite deposits are weathered at their top layer, forming aquifers of only local relevance.

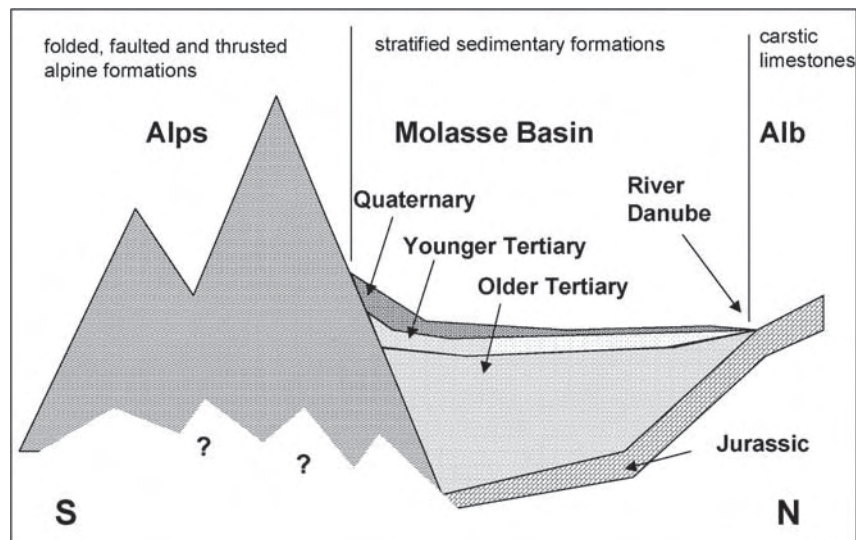


Fig. 2.5: Schematic cross section of the geological layers in the Upper Danube Basin (BARTHEL ET AL., 2005)

- (b) Jurassic karst: The low mountain ranges in the north of the Upper Danube Basin evolved during the Mesozoic. Vast parts of the Swabian and Franconian Alb are made up of *Malm* karst with very high permeabilities, contributing great amounts of water to the aquifer in the Danube valley. Some small areas are covered with non-alpine Cretaceous and Jurassic rock showing lower permeabilities. The breccias of the *Nördlinger Ries*, emerged from a meteorite impact, are also fairly impermeable.
- (c) The Alps: the Central Alps are consisting of alpine magmatic and metamorphic rocks from Triassic and Jurassic periods, representing an aquiclude. Sediments of the northern limestone Alps are mainly limestone, dolomite and marl, thus they are karstified resulting in medium to high permeabilities.
- (d) The molasse basin: The lowermost layer consists of tertiary marine and freshwater molasse sediments, acting altogether rather as an aquiclude. But in the regions surrounding the Pleistocene and Holocene drainage areas, quaternary alluvial sand and gravel deposits form the most important aquifer for the Upper Danube Basin. Unsorted moraine sediments, which can be found in areas near the foothills of the Alps, are very impermeable.

During the last period of the Quaternary, the Pleistocene, vast parts of Northern and Central Europe were glaciated. The glaciers spread from the Alps into the forelands, and some peaks of the low mountain ranges were marginally covered by ice. The last four glacial periods, called *Günz*, *Mindel*, *Riß* and *Würm*, reshaped the tertiary forms. Changes between glacials and interglacials led to advances and retreats of the glacier tongues, which formed moraines and cut in stream terraces by their drainage. The areas of Pleistocene glaciation have an above-average coverage with lakes and moor, compared to the ice free regions. Abrasion and plucking by the glacier tongue left depressions which were sealed with fine sediments and filled with water. This led to development of lakes and frequently through subsequent silting to moor. The glaciofluvial transport filled up the gravel plain around Munich (*Münchner*

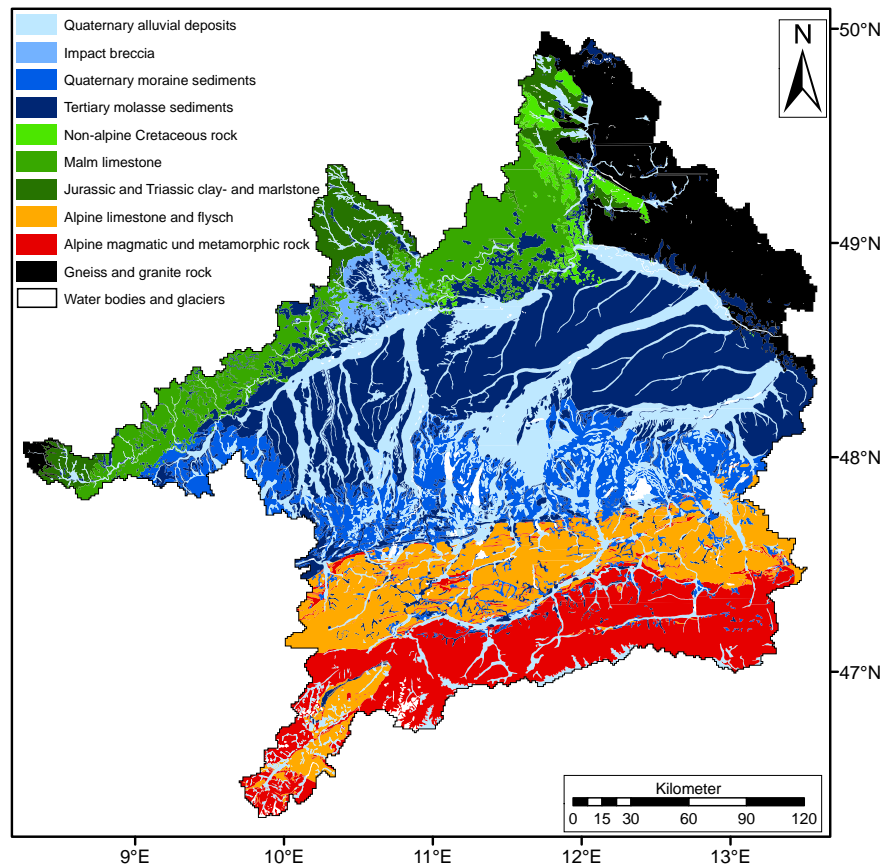


Fig. 2.6: Geology of the Upper Danube Basin, modified after BARTHEL ET AL. (2006). Red: Alps (a), blue: molasse basin (b), green: Jurassic karst (c), black: Palaeozoic basement (c), see text for detailed description.

*Schotterebene*), which forms the aquifer for the region. Transported rock is mainly composed of calcium carbonate, but also crystalline fractions can be found, which were transported via ice stream networks over transfluence passes from the Central Alps. To the north adjoins the *Tertiärhügelland*, which was formed during the Tertiary and remained free of ice in the Pleistocene. Aeolian transport from the glaciated areas deposited Loess sediments in the hilly terrain.

Due to the regional differences of bedrock, terrain, climate, vegetation and time of pedogenesis, the Upper Danube Basin is characterised by a variety of soil textures and soil types, which resemble the spatial pattern of the surface geology and geomorphology.

The Alps show distinct influences of the climatic altitudinal belt and parent material. The nival zone consists of very shallow, unconsolidated, extremely gravelly and stony material, designated by the World Reference Base for Soil Resources (WRB) (FAO, 2006) as Lithic Leptosols. These are followed further downhill – depending on the content of calcium carbonate in the parent material – by Dystric Leptosols in the northern Limestone Alps or by Rendzic Leptosols in the crystalline Central Alps.

The foothills of the Alps, made up of mainly unsorted moraine material, are dominated by Luvisols in the plain areas (e.g. the *Münchner Schotterebene*), with clay loam and sandy loam subsoils. At the steeper slopes of the moraines soil formation is disturbed, leading to rendzinic

influences. In the depressions accumulation of fine colluvial material induces frequent back-water conditions which explains development of gleyic Cambisols. High groundwater levels in river valleys form gleyic Fluvisols or Gleysols in hollows. Occasionally a transformation of Gleysols into eutric and distric Histosols can be found in depressions of various size. On the thick Loess sediments of the *Tertiärhügelland* fertile Cambisols with fine soil textures, ranging from silty loam to clay silt, developed.

In the Swabian and Franconian Alb loamy-clay soil textures prevail. As here the older bedrock was not covered by quaternary deposits, weathering is much more advanced as in the forelands of the Alps, and soil is more deficient in lime. On areas covered with upper Jurassic (*Malm*) limestone chromic Cambisols and rendzinic Leptosols can be found. In the older layers of the Jurassic (*Dogger* and *Lias*) Vertisols can be discovered, which partially merge into stagnic or gleyic Luvisols. The Upper Triassic sandstones naturally exhibit sandy soil textures, with dystric Leptosols, leptic Cambisols and Podzols.

The crystalline low mountain ranges of the Black Forest, Bavarian Forest, Bohemian Forest and Upper Palatinate Forest are dominated by dystric Leptosols and (leptic) Cambisols on granite bedrock, but tend to acidification and thus to podzolisation on gneissic parent material. (LUDWIG & MUERTH, 2006)

## 2.4. LAND USE

Fig. 2.7 shows the heterogeneous land cover in the Upper Danube Basin, which is a product of the above mentioned multifaceted climatic, geological and geomorphological conditions as well as anthropogenic interventions in natural ecosystems. The major land uses in the study area are various agricultural crops on arable land and grassland and forestry Fig. 2.8.

Cereal production takes place on over 50% of the total arable land, and is widespread over the whole catchment. Wheat is the most important type of crop as it is used for human consumption as well as for feeding livestock. On 27% of the arable area animal feed, such as maize silage and forage for cattle breeding, is planted. Rape cultivation amounts up to 6%, and is often used as a cover crop. On agriculturally favourable locations potatoes and sugar beets are grown (6%) and if the climate is particularly mild, specialised cultivations, like hop or fruit and vegetables (2%). (WIRSIG ET AL., 2006)

Land cover in alpine regions follows the climatic altitudinal belt. Due to high annual precipitation sums and low mean temperatures, the Alps and their forelands are dominated by grassland and mountain pastures for livestock farming of dairy cattle. Agriculture plays only a minor role with crop and forage cultivation. In the northern forelands better climatic conditions are the reason for an increase of arable land up to 60%, which is mainly made up of winter grain, root crops and maize. Also maize silage is planted for beef cattle breeding.

A high percentage of agricultural land use (80 – 90%) can be found in the *Tertiärhügelland* and the valley of the Danube, with its fertile soils. Apart from crops, large areas are covered with hop in the *Hallertau* and sugar beet in the *Gäuboden*.

The karstic underground of the Swabian and Franconian Alb offers unfavourable local characteristics for agricultural land use. Therefore the fraction of grassland adds up to 80 – 100%, though with less livestock farming than in the Alps.

As historically farming developed first on agriculturally usable areas, forests are largely lim-



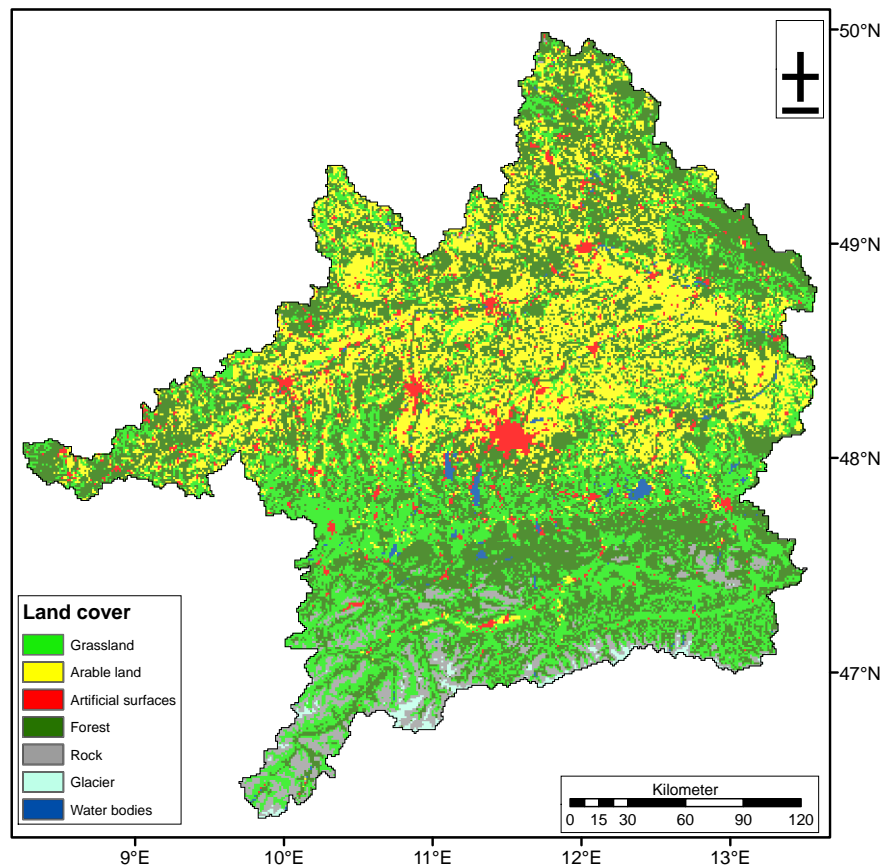


Fig. 2.7: Land cover map of the Upper Danube Basin (based on the CORINE Land Cover data and scaled up to resolution of 1 km<sup>2</sup>)

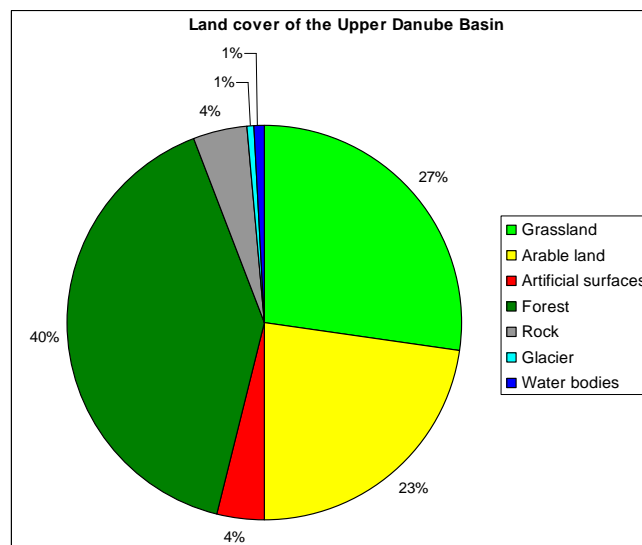


Fig. 2.8: Land cover percentages in the Upper Danube Basin (based on the CORINE Land Cover data and scaled up to a resolution of 1 km<sup>2</sup>)



ited to regions with adverse climatic conditions, steep relief or poor soils. Therefore extensive forested areas can be found in the low mountain ranges and Alps. Commercial forestry is practised intensively in the forelands of the Alps, which led to monocultures of coniferous forest. Larger appearances of deciduous and mixed forest can be found only in the Alps and the Swabian and Franconian Alb. (PROBECK ET AL., 2006)

## 2.5. HYDROLOGY

The heterogeneity of the Upper Danube Basin leads to a high temporal and spatial variability in runoff behaviour. In the sub-catchments discharge regimes from nival to pluvial can be observed. Greater areas with similar discharge behaviour therefore are the regions outlined above, i.e. the low mountain ranges, the flat forelands and the Alps and their foothills, where geology and soils (Section 2.3) and precipitation patterns (Section 3.2.1.2) resemble each other (BMU, 2001). So in alpine regions discharge maxima appear in late spring or early summer coinciding with the snowmelt and during summer runoff is influenced by the damping effect of glaciers. The low mountain regions show, additionally to the maximum in spring, a secondary peak in the winter months due to the precipitation regime. In the flat forelands a pluvial regime is emphasised, but the tributaries cause a transition between the regimes, resulting in a change from montane character at the headwaters to an alpine regime of the Danube at the catchment outlet. The main alpine tributaries from the south are the *Iller*, *Lech*, *Isar* and *Inn*. Inflows from the north with montane characteristics are the *Regen*, *Naab* and *Altmühl* (see Fig. 2.2 and Tab. 2.1).

Tab. 2.1: Major tributaries of the Danube (data source: LFW (2005))

Tributary	Gauge	Mean ann. discharge [m <sup>3</sup> /s]	Area [km <sup>2</sup> ]
Iller	Wiblingen	70.3	2,115
Lech	Augsburg u. Wertach	115	3,803
Isar	Plattling	176	8,839
Inn	Passau Ingling	741	26,063
Naab	Heitzenhofen	49.7	5,432
Altmühl	Beilngries o.d.Sulz	16.1	2,251
Regen	Marienthal	37.8	2,590
Danube (headwaters)	Neu-Ulm Bad Held	126	7,588

Most natural lakes can be found in the forelands of the Alps, developed through glacial abrasion in the Pleistocene. A selection of the largest lakes is given in Tab. 2.2. Reservoirs

Tab. 2.2: Natural lakes in the Upper Danube Basin (data source: DESTATIS (2007)).

Name	Area [km <sup>2</sup> ]	Mean depth [m]
Chiemsee	79.9	26
Starnberger See	56.4	53
Ammersee	46.6	38
Walchensee	16.1	81
Tegernsee	8.9	36

(see Tab. 2.3) are used for energy generation and flood control (e.g. the Forggensee) but also additionally for water management issues concerning low-flow (e.g. the *Sylvensteinsee* and the *Rottachsee*). Main waterways used for inland navigation are sections of the Danube with

*Tab. 2.3: Reservoirs in the Upper Danube Basin (data source: GLOWA-DANUBE (2007)).*

Reservoir	Volume [ $10^6 \text{ m}^3$ ]
Achensee	486
Kaprun reservoirs	170
Forggensee	168
Gepatschsee	139
Schlegeisspeicher	129
Sylvensteinsee	124.3

203 km length, and the Main-Danube Canal with 171 km length, which is also connected to the Rhine (DESTATIS, 2007). Via this connection water is abstracted (e.g. in times of low-flow conditions) and diverted into the Main, depending on the needs and discharge of the Danube up to  $125 \cdot 10^6 \text{ m}^3$  per year. Such changes in the hydrological cycle also occur by numerous water transfers into reservoirs (see Tab. 2.4), which virtually extend the size of the natural watershed. These anthropogenic interactions do not only modify the current discharge at the gauges, but also influence the discharge regime. (DESTATIS (2007), GLOWA-DANUBE (2007))

*Tab. 2.4: Water transfers in the Upper Danube Basin (data source: GLOWA-DANUBE (2007)).*

Transfer to	catchment extension [ $\text{km}^2$ ]
Stillup	328
Gepatsch	172
Kaprun	128
Sellrain	116
Achensee	112

### 3. SOIL EROSION

This chapter is intended to give an outline of the basic processes causing soil erosion by water and delineate the input parameters influencing the magnitude of particle detachment and transport. The processes involved can be abstracted and represented on many different temporal and spatial scales. Since modelling shall be performed within the project GLOWA-Danube, processes impacting on the mesoscale are emphasized, as opposed to microscale processes, which cannot be represented adequately. Thus, here merely an overview of microscale processes is given, for more detailed information concerning the physical processes on the microscale, the reader is referred to corresponding literature (e.g. CARSON (1971)). Impacts of soil erosion are not only the on-site effects, i.e. soil degradation on the concerned area, but also off-site effects, such as discharge of sediment-bound pollutants from agricultural areas into water bodies (cf. Section 1.1.2). A description of measurement techniques and the sediment yield situation in the Upper Danube Basin finally closes this chapter, as an established method for assessment of both on-site as well as off-site effects on the *regional scale* is the measurement of suspended sediment load at river gauges.

#### 3.1. BASIC PROCESSES

Soil erosion by water is commonly classified in *rill* and *interrill* erosion (e.g. AUERSWALD, 1993). If the prevailing detaching forces come from raindrop impact and transport occurs by an evenly distributed sheet flow, one speaks of interrill erosion (often also denoted *sheet* erosion). When runoff accumulates, its shear forces increase, and thus can detach more particles from the soil. Runoff follows its preferential flow path carving small rills along its way, which is called rill erosion. These small rivulets are separated by interrill areas, where rain-splash and diffuse overland flow dominate (as mentioned above), which is therefore termed interrill erosion.

Requirements for the occurrence of erosion are firstly the detachment of soil particles and secondly the transport of the detached particles. Detachment and transport can occur either by raindrop impact or by flowing water, or a combination of both. KINNELL (2005) identifies four processes:

- **Raindrop detachment with raindrop splash transport (RD-ST)**
- **Raindrop detachment with raindrop-induced flow transport (RD-RIFT)**
- **Raindrop detachment with flow transport (RD-FT)**
- **Flow detachment with flow transport (FD-FT)**

In the following sections (Section 3.1.1 – Section 3.1.3) the basic processes are described, which are responsible for the listed particle detachment and transport processes.

### 3.1.1. IMPACT OF RAINDROPS

According to BLUME (1990) the impact of raindrops transfers its kinetic energy to the soil. Because raindrops cannot infiltrate with their falling velocity, they exert shear forces parallel to the surface, catapulting particles out of the soil and also compacting and deforming the soil surface. If raindrop energy overcomes the bonds holding particles in the soil surface, transport may occur radially away from the site of detachment, which is called raindrop *splash* (RD-ST). The effect of raindrop detachment is greatest at the beginning of a storm, when overland flow is too thin to absorb the raindrop energy. (According to MUTCHLER & YOUNG (1975) as quoted in AUERSWALD (1993) the soil surface is completely protected from raindrop impact, if a sheet flow exists with a thickness of three times of the drop diameter.) Generally splash transport is rather insignificant and is the limiting factor for erosion caused by raindrop impact. On flat surfaces splash merely leads to a redistribution of soil (material splashed away from one point is replaced by material from the surrounding area). On sloped areas a net downward movement occurs, but even on steep slopes this only has a modest effect.

Usually the small soil particles are bound in greater aggregates, which need much more energy to be detached and transported. But the processes of slaking and dispersion disrupt the structure of the aggregates and break these down. Slaking mainly occurs during storm rainfall in summer on dry soils. Raindrop water penetrates the soil aggregates and compacts the entrapped air, causing overpressure within the aggregate. Differential swelling of clay particles may additionally stress the aggregates, finally fragmenting these into smaller parts. With additional wetting chemical bonds between the particles may be solved by the water, leading to dispersion of the aggregates. All these detached particles form a suspension which infiltrates the soil, whereby the pores of the soil become sealed (soil sealing). The sediment layer inhibits further infiltration and therefore promotes formation of shallow sheet flow on sloped surfaces. (SCHEFFER & SCHACHTSCHABEL, 2002)

### 3.1.2. SHALLOW SHEET FLOW

The formation of shallow sheet flow further increases soil moisture, which may lead to a destabilisation of soil aggregates and particles and thus facilitates particle detachment by raindrop impact. A thin film of water (approx. 1/10th to 3/10th of drop diameter) additionally promotes detachment and transport by raindrops, because the soil becomes particularly instable, if it is exposed to shear stresses. Since water is an incompressible medium, it transforms the energy of the raindrops into kinetic energy. This again forms waves parallel to the surface, which exert shear stress on the surface. Turbulent movement in the water film leads to particle suspension throughout the whole film of water (BLUME, 1990). Raindrops penetrate through the water film to detach soil particles that may then be splashed or lifted into the flow, which moves them downstream. Transport processes involved are raindrop impact and flowing water (RD-RIFT), which are more efficient than splash transport, and play a major role in moving material from interrill areas into rills. When the surface water flow increases, it can transport particles but its energy is not sufficient for particle detachment, which still may be done by raindrops (RD-FT). Its transport capacity is higher than RIFT and often both forms occur simultaneously in the same flows, with RIFT transporting coarse material, and FT the finer particles. An additional rise in surface flow finally provides the flow with the required

energy to detach particles (FD-FT). The *Hjulstöm curve* illustrated in Fig. 3.1 shows these basic dependencies between particle size and flow velocity (i.e. disregarding raindrops) in respect of particle detachment, transport and deposition.

Particle detachment in fluid media can be illustrated in a simplified way by considering the soil surface as one layer, and the laminar flow of water as a second, moving layer in distance  $x$ . The shear stress  $\tau$  acting on the particles can be written as (BLUME, 1990):

$$\tau = \eta \cdot \frac{\delta v}{\delta x} \quad (3.1)$$

where  $\eta$  is the viscosity of the fluid and  $\frac{\delta v}{\delta x}$  is the velocity gradient perpendicular to the layers. The shear stress leads to a shifting or rolling movement of the particles in the direction of flow. Particle exchange between the layers takes place after *Bernoulli's equation*:

$$p_0 = p + q \quad (3.2)$$

with  $p_0$ : total pressure,  $p$ : static pressure and  $q$ : dynamic pressure. This means essentially, that the sum of dynamic and static pressure is constant. So if dynamic pressure changes due to velocity variations in flow, static pressure changes, too. If e.g. dynamic pressure decreases at the location of an obstacle in the flow, the static pressure becomes higher and particles may be lifted into the flow. Moving particles may collide with other, stationary particles and push them into the flow by transferring fractions of their momentum to them. This leads to a chain reaction, which initially increases the amount of transported material with increasing flow distance until a balance is reached. Generally shear stress is less caused by runoff than by raindrops, because the velocity is lower, but as runoff reacts on a greater area and for a longer time, it can detach bigger particles (SCHEFFER & SCHACHTSCHABEL, 2002).

### 3.1.3. RILL EROSION

The sheet flow follows the micro relief in direction of the steepest slope, concentrating in small streams. In these rills the amount of water increases, leading to higher velocities and transport capacity (cf. Fig. 3.1). In those rilled areas where the runoff amount increases – especially in hollows, where flow paths converge – a change from rill erosion to *gully erosion* may occur. The concentrated water flow gains additional transport capacity and velocity, until it changes its flow regime from subcritical (flow velocity is smaller than wave velocity) to supercritical (flow velocity is greater than wave velocity). At small obstacles in the channel a hydraulic jump occurs, turning the flow back into sub-critical regime. This change results in a large energy loss which causes turbulences and erodes a small headcut which moves upwards gradually. The resulting channels are named *ephemeral gullies* when they can be tilled across, and thus can be removed. The classical term *gully* is used when the channels become too wide and deep for tilling, and represent a permanent form.

Generally sediment delivery (not erosion) into water bodies is higher through rill erosion, than through sheet erosion. Sheet erosion frequently redeposits eroded material in nearby depressions, whereas rill erosion transports material over greater distances. Through agricultural practices rills and furrows are often filled with fine material, which is quickly flushed away through the rills during the next storm event (BECKER & LAHMER, 2004).

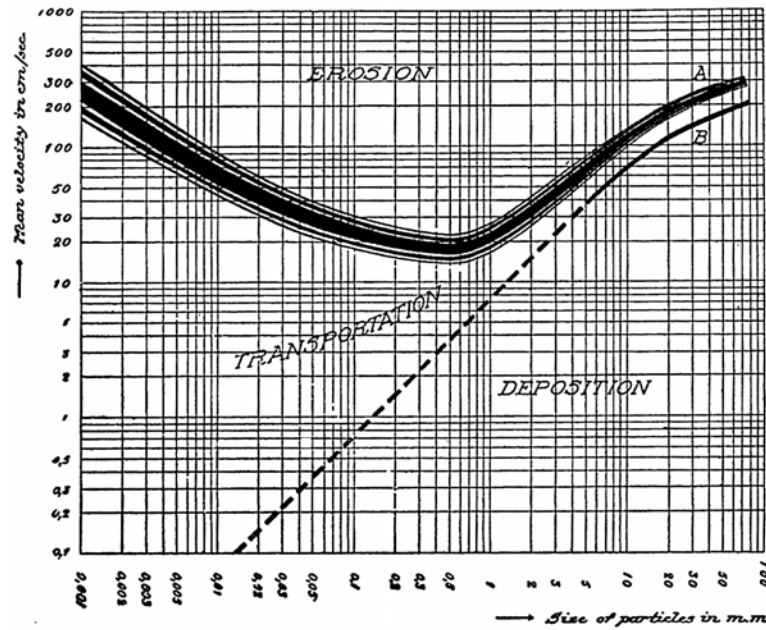


Fig. 3.1: The Hjulstöm curve (HJULSTRÖM (1939) found in SVERDRUP ET AL. (1942)) illustrates the basic dependencies between grain size and flow velocity. Higher flow velocities may transport bigger grains and small particle diameters require lower velocities to be eroded. The exception at approx. 0.5 mm, i.e. the increase of the curve at smaller grain sizes results from the higher cohesion of the clay particles.

### 3.2. INFLUENCING FACTORS

The following sections describe the parameters influencing soil erosion by water. For a better understanding of the involved processes, the most important factors are characterised for the Upper Danube Basin. In order to estimate their influence on soil erosion in the study area, additionally some comparative calculations are made, based on the Allgemeine Bodenabtragsgleichung (ABAG). One of the oldest and most used equations for estimation of soil erosion by water is the Universal Soil Loss Equation (USLE) (WISCHMEIER & SMITH, 1978). Since this is an empirical correlation developed in the United States, it was adapted by SCHWERTMANN (1981) for German environmental conditions under the name ABAG. It consists of six multiplicative factors, which allow for calculation of the long term average soil loss:

$$A = R \cdot K \cdot L \cdot S \cdot C \cdot P \quad (3.3)$$

where  $A$  is the soil loss in tons per hectare and year. The factors in Eq. (3.3) consider:

- $R$ : the impact of rainfall and runoff (erosivity); discussed in Section 3.2.1
- $K$ : the susceptibility of the soil to erosion (erodibility); discussed in Section 3.2.2
- $L$ : the influence of the effective slope length; discussed in Section 3.2.4
- $S$ : the influence of the slope inclination; discussed in Section 3.2.4
- $C$ : protecting effects of vegetation cover and crop rotation; discussed in Section 3.2.3
- $P$ : potential protective measures in agricultural practice; discussed in Section 3.2.3

The USLE respectively ABAG currently represents the most widely used soil erosion model in Europe KIRKBY ET AL. (2008). Nevertheless it is criticised increasingly due to its simplified concept of representation of soil erosion processes. The equation is used here anyway, for the presentation of the driving forces on soil erosion and to provide the reader with a basic impression of the soil erosion potential in the Upper Danube Basin. It has to be noted, that this does not serve as a validation basis for the soil erosion module presented in Section 4.5, since this would involve a validation of the ABAG itself in the Upper Danube Basin.

### **3.2.1. PRECIPITATION**

#### **3.2.1.1. OVERVIEW**

As already denoted in Section 3.1.1 and Section 3.1.2, the primary effect of precipitation on particle detachment and transport is raindrop impact. The processes involved can be subdivided in:

- shear stresses exerted on the soil, either directly on the dry soil, or on a thin film of water
- aggregate slaking upon rapid wetting causing stresses by entrapped air and differential swelling of particles
- dispersion of aggregates by continuously increasing wetting, which reduces the attractive forces between colloidal particles

The break-up of the particles leads to blocking of soil pores during infiltration of the suspension, causing soil sealing and thus inhibiting further infiltration. The intensity of these processes mainly depends on physical properties of the raindrops: the amount and size of the drops, as well as drop size distribution (DSD) and fall velocity affect the kinetic energy acting potentially on the soil. Naturally the actual impact of these processes on soil detachment and erosion depends on soil and vegetation parameters, which are described later on.

The erosive power of the rainfall is controlled by interactions between raindrop size, velocity and shape, the wind speed and the intensity of the precipitation event. With increasing raindrop size the terminal fall velocity increases, which leads to higher momentum of raindrops and therefore greater breakdown of aggregates. According to CERDÀ (1997) drop sizes vary from very small droplets to a maximum of approx. 6 mm. Because larger drops break into smaller droplets, drops with a diameter of more than 4 mm are extremely rare. Raindrops become unstable due to aerodynamic forces acting on the drop between a diameter of 4.6 and 5.4 mm (HUDSON (1981) as quoted in CERDÀ (1997)). Although laboratory studies indicate that isolated, individual water drops in free fall may reach diameters of approx. 10 mm before spontaneously breaking up, they usually break up earlier due to collisions with other drops (PRUPPACHER & PITTER (1971), LOW & LIST (1982) as quoted in HOBBS & RANGNO (2004)). CERDÀ (1997) appraised the results of various studies, whose findings were, that intensities between 50 and 100 mm/h and above 200 mm/h exhibit a larger proportion of drops with diameters above 4 mm due to coalescence of the drops. At intensities below 50 mm/h and between 100 and 200 mm/h the turbulence of the air more frequently causes break up of the drops, leading to generally smaller drop sizes.

Tab. 3.1: Terminal velocities of raindrops depending on drop diameter (compiled from SCHMIDT (1979) and BAUMGARTNER & LIEBSCHER (1996)).

Drop diameter [mm]	Terminal velocity [m/s]
0.002	0.00012
0.02	0.0012
0.2	0.72
1	4.0 – 4.1
2	6.3 – 6.5
3	7.6 – 8.1
4	8.5 – 8.8
5	8.8 – 9.1
6	9.0 – 9.3

Depending on drop size and drop mass, air drag limits the fall velocity of the raindrops. The resulting terminal velocities of raindrops with different diameters are illustrated in Tab. 3.1.

In order to be able to estimate the DSD, or at least the median drop diameter of a rainfall event, the relationship between raindrop size, fall velocity and rainfall intensity has been the subject in past studies. LAWS (1941) and LAWS & PARSONS (1943) empirically found correlations between rainfall intensity and fall velocity, which can be expressed by a simple potential relationship (see Eq. (4.10)).

As the momentum transferred by the drops is the interesting parameter for modelling of erosion, correlations between rainfall intensity and content of kinetic energy were derived based on studies mentioned above. WISCHMEIER & SMITH (1958) used measurements of DSD and terminal velocity to derive a logarithmic function of the form:

$$e_k = 11.9 + 8.76 \cdot \log R \quad (3.4)$$

with  $e_k$ : kinetic energy [ $\text{J}/\text{m}^2\text{m}$ ] and  $R$ : rainfall intensity [ $\text{mm}/\text{h}$ ].

Eq. (3.4) has been used for decades for the calculation of kinetic energy. Although the theoretical validity is questioned, it is still widely used, as it has proven to yield useful estimates of rainfall erosivity. Other researchers suggested (KINNELL (1980) as quoted in VAN DIJK ET AL. (2002)), that an exponential equation of the form

$$e_k = e_{max} \cdot (1 - a \cdot e^{-b \cdot R}) \quad (3.5)$$

describes the relationship between  $e_k$  and  $R$  better. Analysis in numerous studies led to specific coefficients  $e_{max}$ ,  $a$  and  $b$ , which consider regional characteristics of precipitation for various locations around the world. A list of over 20 pairs of coefficients can be found in VAN DIJK ET AL. (2002). Fig. 3.2 shows the content of kinetic energy depending on rainfall intensity, calculated after VAN DIJK ET AL. (2002). In order to relate the kinetic energy content to rainfall erosivity, total storm event erosivity is frequently calculated as the product of total event energy and a peak intensity (cf. e.g. WISCHMEIER & SMITH, 1978; SUKHANOVSKI ET AL., 2002). Therewith it is attempted to include the cumulative effects of many moderate-sized storms, as well as the effects of the occasional severe ones.

The above mentioned physical properties of the raindrops, as well as the studies empirically relating correlations between intensity and erosive power, show the relevance of rainfall



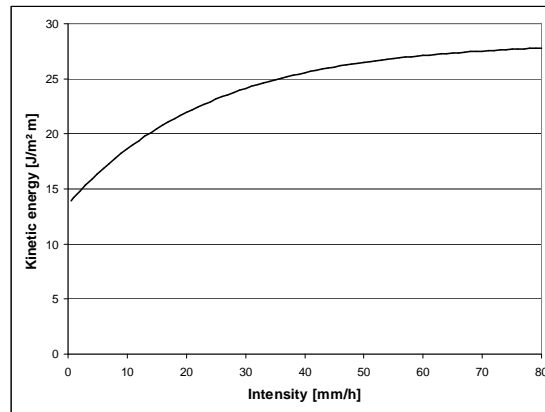


Fig. 3.2: Kinetic energy of rainfall depending on intensity, calculated with Eq. (3.5) and coefficients from VAN DIJK ET AL. (2002) ( $e_{max} = 38.3$ ,  $a = 0.52$ ,  $b = 0.042$ ).

intensity (and not necessarily the absolute rainfall volumes) for soil erosion. Since the intensity is largely governed by regional precipitation patterns, these are described for the Upper Danube Basin in the following section.

### 3.2.1.2. REGIONAL CHARACTERISATION

The distribution of precipitation in the Upper Danube Basin is not only influenced by the prevailing meteorological situation, but also modified by geographic and regional influences. According to BMU (2001) the annual course of precipitation in Germany can be divided into the following types:

- (a) Maritime type: The attenuating influence of the sea water delays the annual course of precipitation, resulting in a precipitation minimum in spring and a maximum in autumn.
- (b) Summer precipitation type: High irradiation leads to convective precipitation causing a distinctive maximum in the summer months.
- (c) Low mountain range type: Convective and advective processes together produce two maxima of approximately the same amplitude.
- (d) Winter precipitation type: The heights of the low mountain ranges have their maximum in winter.

As the Upper Danube Basin reveals precipitation types (b), (c) and (d) the regional climatological characteristics of the Upper Danube Basin concerning these types will be delineated in the following.

Maxima of mean annual precipitation sums are recorded at the peaks of the Alps with over 2000 mm, but vast parts of the Alps register about 1500 – 2000 mm. Comparable amounts are measured only in the Black Forest. Somewhat lesser amounts of 800 – 1200 mm can be found in higher parts of the alpine foothills and low mountain ranges. Causes for the high amounts of precipitation in the Alps and their foothills are orographic lift at northwesterly meteorological situations and frequent lapse conditions in summer. The low mountain ranges, which lie perpendicular to the prevailing winds, receive yielding rainfall at the windward side,

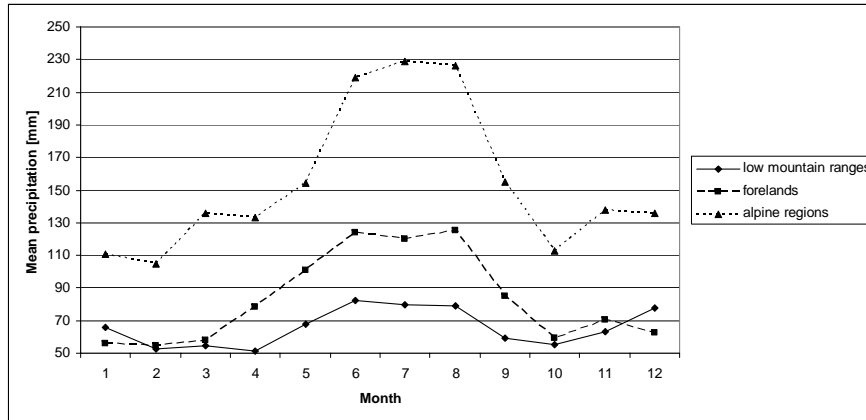


Fig. 3.3: Precipitation regimes in the Upper Danube Basin

even in low altitudes, whereas the leeward sides in the rain shadow are drier. (BAYFORKLIM, 1996)

Total precipitation amounts in the catchment are higher in summer. The higher air temperatures in summer permit a higher water vapour content in the atmosphere, which is fed by high evapotranspiration rates, thus summer precipitation is in most regions of the catchment higher than in winter (see Fig. 2.3). This is noticeable in Fig. 3.3, with a clear maximum in summer for alpine regions and forelands. In contrast, the low mountain ranges show a more balanced seasonal distribution, resulting from the increased influence of the westerlies in winter.

During hydrological winter (November to April) inversion conditions frequently emerge, thus precipitation structure is significantly influenced by passing cyclones and orographic lift. This becomes noticeable especially in the low mountain ranges, where cyclones in December often cause floods. Due to the low condensation level and higher wind velocities in winter, even low elevations experience precipitation. Autumn and late winter frequently exhibit anticyclonal situations from the east with dry conditions. The Alps, however, have a slightly accentuated maximum in early spring due to cyclonal activity from the north striking the mountains.

Hydrological summer (May to October) is the time of highest solar irradiation and prevailing lapse conditions, which facilitate thermal lift of air masses, thus often bringing thunderstorms with heavy rainfall. Fig. 3.4 shows the mean number of thunderstorm days in the study area, derived from remote sensing data by THIES ET AL. (2006). Thunderstorms originate preferentially in the area around mountainous regions, so the increased thunderstorm activity during summer concentrates on alpine regions, and the alpine foothills and lower areas surrounding the low mountain ranges, where the precipitation is released. A higher degree of continentality additionally promotes the regionally pronounced summer maximum in south Bavaria. Orographic lift only plays a role at higher elevations, as the condensation level lies higher than in winter.

As mentioned in Section 3.2.1.1, there is a variety of empirical correlations for evaluating the erosivity of rainfall. For German conditions, ROGLER & SCHWERTMANN (1981) developed a regression of summer rainfall (May – October)  $N_s$  [mm] to rainfall erosivity  $R$  [ $\text{kJ}/\text{m}^2 \cdot \text{mm}/\text{h}$ ]:

$$R = -1.48 + 0.141 \cdot N_s \quad (3.6)$$

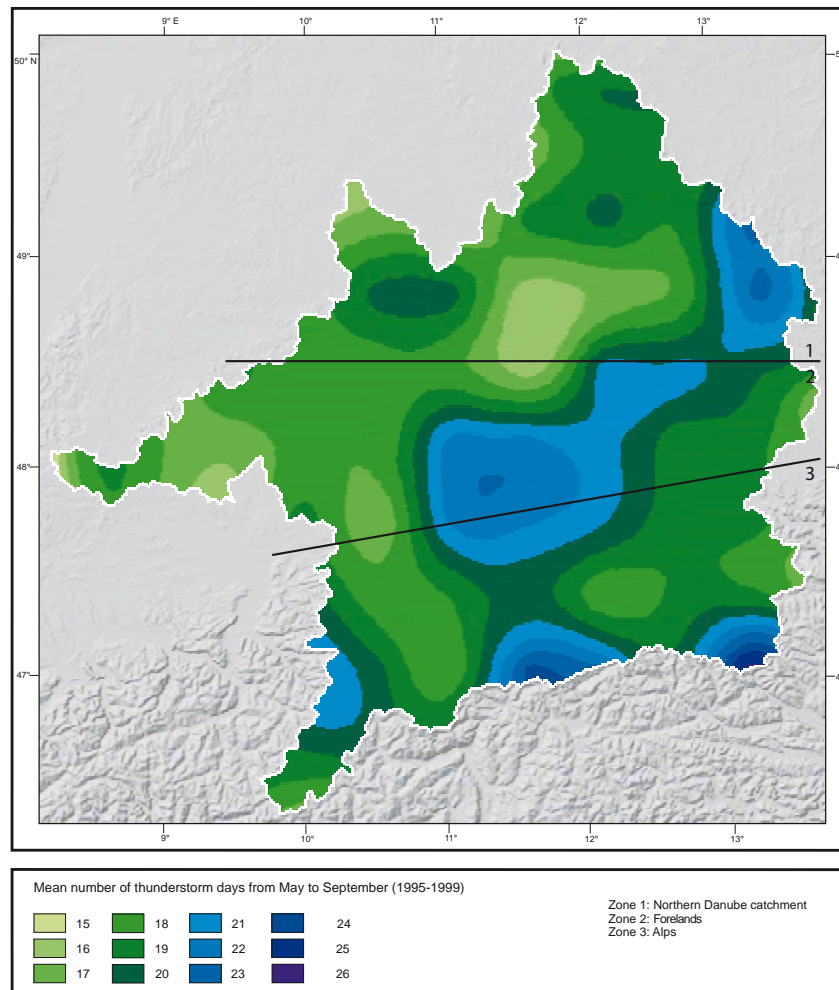


Fig. 3.4: Mean number of thunderstorm days in the Upper Danube Basin, modified after THIES ET AL. (2006)

Fig. 3.5 gives an impression of the spatial distribution of the rainfall erosivity in the Upper Danube Basin. The illustration is based on interpolated long term precipitation measurements (cf. Section 4.2.1) and computed with Eq. (3.6). It is obvious, that there is a similarity to the distribution of precipitation presented in Fig. 2.3. The reason is that Eq. (3.6) only takes into account the precipitation sum of the summer months. Nevertheless the pattern reflects erosivity very well, as a large amount of precipitation falls in the summer months during storms. These thunderstorms in turn are responsible for most of the erosive events in the course of the year.

### 3.2.2. SOIL

#### 3.2.2.1. OVERVIEW

The last section (Section 3.2.1) outlined the capability of precipitation to cause erosion, the rainfall *erosivity*. This section shows the susceptibility of the soil to these influences, or expressed reversely, the resistance of the soil to the erosive forces. After KAY & ANGERS (2002) soil *erodibility* is defined as the intrinsic susceptibility of soils to erosion, and therefore is

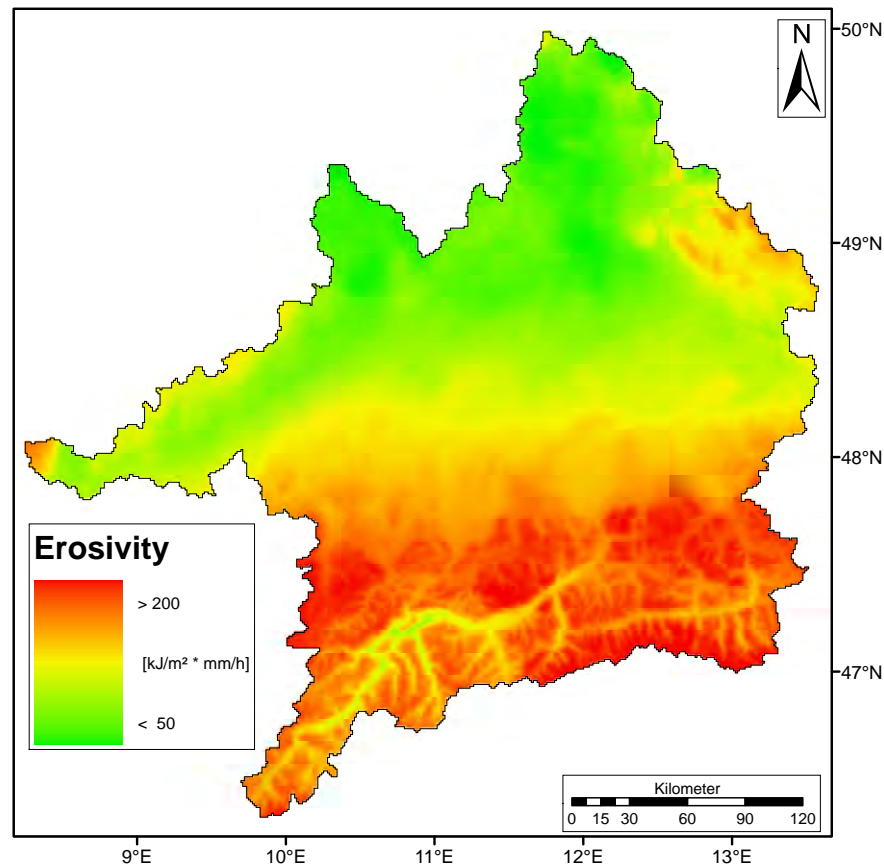


Fig. 3.5: Erosivity in the Upper Danube Basin ( $R$  factor). (base data: precipitation interpolated with PROMET for the years 1970 – 2003)

mainly determined by soil properties. The soil aggregate stability is a main factor controlling erodibility. Increased aggregate stability leads to a reduced detachability of particles and reduces the susceptibility to surface crusting, which both favour water erosion. The erodibility of soils is affected by a large number of factors which come together, and may be influenced by anthropogenic interaction, e.g. agricultural management practices (see Section 3.2.3). The following is a basic introduction to the most important determining factors in order to allow an estimate of their relevance at the mesoscale. More detailed information can be found in corresponding literature, e.g. AUERSWALD (1993), SCHEFFER & SCHACHTSCHABEL (2002) or SCHMIDT (1979).

Looking at the particle size distribution in the topsoil, one might think, that smaller particles might be eroded easier than bigger particles due to their smaller mass. But in fact this process is much more complex, as there are several properties depending on grain size. Small particles, such as clay form aggregates sooner and the higher aggregate stability impedes erosion. But their lower permeability facilitates formation of surface runoff, resulting in higher erosion potential. Bigger grain sizes such as sand show a reciprocal behaviour. Through weak aggregate formation and thus low aggregate stability they are more susceptible to erosion, but a high proportion of macropores leads to less surface runoff. SCHMIDT (1979) compared the evaluations of several authors regarding the erodibility of different soil types. Beside a somewhat heterogeneous rating for clay and sandy soils due to the complex-

ity of the involved processes, medium particle sizes (silt) are unanimously considered most vulnerable to erosion, especially Loess soils.

For erosion the soil structure in the upper horizon is most important. Although the lower horizons influence the whole process, e.g. by infiltration rates, the topsoil is the part which is eroded, and the effects of land use management practices on soil structure are most pronounced. "The term structural stability is used to describe the ability of the soil to retain its arrangement of solid and void space when exposed to different stresses" (KAY & ANGERS, 2002). Stresses may act on different scales, e.g. either on the primary particles of the aggregates or between the aggregates themselves or even on the stability of an entire slope. If the stress exceeds the internal soil strength, this results in deformation of the soil.

The forces acting on a stationary soil particle or aggregate can be summarised in a simplified way as:

- the weight of the particle itself,
- the cohesion and adhesion induced by particles themselves or by pore water, and
- the load caused by other particles.

Water may influence this equilibrium in three aspects (SCHEFFER & SCHACHTSCHABEL, 2002):

- It transfers the kinetic energy of its movement to the particles, which plays a major role on slopes.
- At fully saturated pore volume the buoyancy of water works on the particles.
- At partly saturated pore volume cohesive and adhesive forces develop.

Within the three-phase system of the soil each of the phases - solid (particles), liquid (water) and gaseous (air) - can transfer forces. The influence of air usually can be neglected, as air escapes quickly on compression in the soil. Thus the stresses working in the soil can be represented by:

$$\sigma = \sigma' + \chi \cdot u_w \quad (3.7)$$

where  $\sigma$ : total stress,  $\sigma'$ : effective stress acting on the soil particles,  $u$ : pore water pressure and  $\chi$ : factor depending on soil saturation (1 = saturated, 0 = dry).

For a given total stress the effective stress between soil particles thus depends only on pore water pressure. Saturated conditions with positive pore water pressure ( $\chi = 1$  and positive  $u_w$ ) mean a reduction of stability, whereas negative pore water pressure increases soil stability through the effect of water menisci. In unsaturated soil the effect of menisci only affects a part of the pore space, which is represented by the factor  $\chi$ . A stabilising effect through drying can only occur, if the decrease of  $\chi$  is smaller than the corresponding decrease of the pore water pressure. A typical example is the stability of sands, which reaches from an instable flowing condition ( $u \geq 0$ ) over stable ( $u < 0$ ) to an instable ripple if dry.

The destabilising effect of water also becomes apparent if soil is compressed, and the pore water pressure thereupon increases. Because of the incompressibility of water the soil system is temporarily stable, but as soon as shear stresses are exerted, it becomes instable.

Tab. 3.2: Characteristics of the main breakdown mechanisms (LE BISSONNAIS, 1996)

Mechanism	Type of forces involved	Soil properties controlling the mechanism	Resulting fragments	frag-	Intensity of the disaggregation
Slaking	Internal pressure by air entrapment during wetting	Porosity, wettability, internal cohesion	Microaggregates		Large
Breakdown by differential swelling	Internal pressure by clay differential swelling	Swelling potential, wetting conditions, cohesion	Macro- and microaggregates		Limited
Breakdown by rain-drop impact	External pressure by raindrop impact	Wet cohesion (clay, organic matter, oxides)	Elementary particles	parti-	Cumulative
Physico-chemical dispersion	Internal attractive forces between colloidal particles	Ionic status, clay mineralogy	Elementary particles	parti-	Total

The stability of the soil towards shear stress can be described by its shear strength  $\tau$  after the *Mohr-Coulomb* equation (ZHANG ET AL., 2001):

$$\tau = c' + (\sigma_n - u_w) \cdot \tan \varphi' \quad (3.8)$$

with  $\varphi'$ : effective angle of shearing resistance (or effective angle of internal friction),  $\sigma_n$ : total normal stress,  $c'$ : effective cohesion.

The shear strength is the force the soil can resist, before deformation or failure occurs. As Eq. (3.8) shows, the shear strength depends on water content and exerted stresses, but also on soil properties ( $\varphi'$ ,  $c'$ ). It is increased for soils with higher cohesion. Physico-chemical cohesion leads to formation of aggregates, which is mainly influenced by soil organic matter content, exchangeable sodium percentage and iron and aluminium oxides and oxyhydroxides (LE BISSONNAIS, 1996). Bonding forces increase shear strength between both the primary particles and between the aggregates. This bonding effect is important particularly in the topsoil, as particles or aggregates are easily detachable and transportable at the surface. LE BISSONNAIS (1996) compiled a list (Tab. 3.2) of the mechanisms dissolving the bonds and causing aggregate break-up (cf. Section 3.1.1). This leads to crust formation and surface sealing, which is a major cause of water erosion. As can be seen from Tab. 3.2 a variety of mechanisms controls aggregate stability and stability is strongly dependent on initial conditions of the soil (e.g. soil moisture, size of aggregates) Therefore empirical equations for describing soil erodibility have been developed, which are applied in the next section, in order to estimate the erodibility in the Upper Danube Basin.

### 3.2.2.2. REGIONAL CHARACTERISATION

In Section 2.3 a short introduction of the prevailing soils in the study area based on the WRB classification was presented. Unfortunately a homogeneous soil data set covering the whole study area is not available. The Soil Overview Map of Germany on a scale of 1:1,000,000 (Bodenübersichtskarte von Deutschland 1:1.000.000, BÜK1000) covers at least the German part of the basin based on the German soil taxonomy. For large parts of the Alps, especially

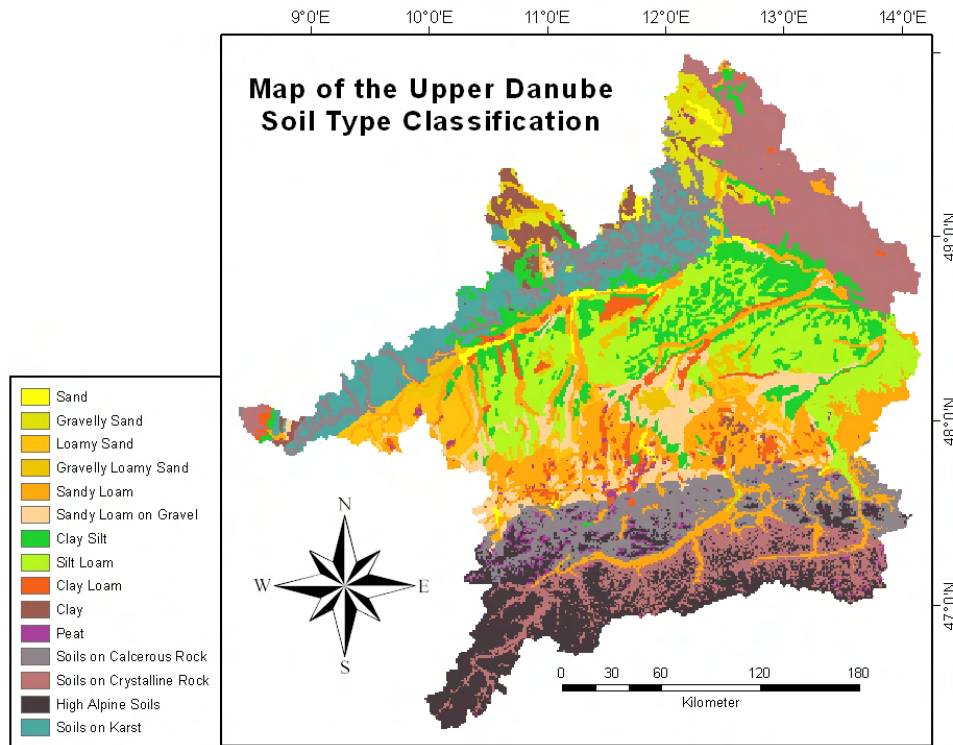


Fig. 3.6: Soil type map of the Upper Danube Basin (MUERTH, 2008). (For the taxonomy of the classification the reader is referred to the original work of the author).

for non-agricultural areas, no information is available. In order to provide the soil model (cf. Section 4.2.2) used within DANUBIA with input parameters, MUERTH (2008) compiled a basin-wide soil map (Fig. 3.6), which is used here to assess erodibility. The soil classes presented in this map do not refer to any national or international classification systems, but are based on the classes of the BÜK1000 and represent texture classes. A detailed description of the soil classification and parameterisation can be found in MUERTH (2008). For identification of erodible soils in the study area the erodibility factor of the ABAG ( $K$ -factor) was calculated for the Upper Danube Basin. The total  $K$  factor can be determined from factors for soil type  $K_b$ , organic matter content  $K_h$  and fraction of coarse material  $K_s$  (DIN19708, 2005; HENNINGS, 2000):

$$K = K_b + K_h + K_s \quad (3.9)$$

Tab. 3.3 lists the values of  $K_b$  which were assigned to the soil classes illustrated in Fig. 3.6. For a complete list of all available  $K_b$  values the reader is referred to HENNINGS (2000). The sub-factor for organic matter content is calculated as

$$K_h = 1.15 - 0.05 \cdot \text{OrganicMatterContent} [\%] \quad (3.10)$$

for contents up to 15%. The fraction of coarse material (> sand)  $SKE$  [%] allows for the calculation of

$$K_s = 0.973 - 0.0187 \cdot SKE + 0.0001 \cdot SKE^2 \quad (3.11)$$

The spatial distribution of the erodibility in the study area can be seen in Fig. 3.7. Soils with high erodibility can be found in the regions of Tertiary molasse sediments between the

Tab. 3.3:  $K_b$  values for the soil type classes derived by MUERTH (2008)

Soil type class	$K_b$	Soil type class	$K_b$
Sand	0.027244	Clay Loam	0.27244
Gravelly Sand	0.043785	Clay	0.075894
Loamy Sand	0.23352	Peat	n/a
Gravelly Loamy Sand	0.25298	Soils on Calcareous Rock	0.062272
Sandy Loam	0.210168	Soils on Crystalline Rock	0.048564
Sandy Loam on Gravel	0.099684	High Alpine Soils	0.116298
Clayey Silt	0.517636	Soils on Karst	0.143031
Silt Loam	0.376551		

*Münchner Schotterebene* and the Danube. The silty soils are susceptible to soil sealing and crusting, where erosion events do not only cause soil loss on agricultural fields, but also often pollute roadside ditches or sewage plants with sediments (AUERSWALD & SCHMIDT, 1986). Since these soils are covered with Loess, they represent fertile areas which are cultivated intensively, leading additionally to anthropogenic intensification of the erosion potential. Considerably lesser values of erodibility can be found in the more permeable moraine sediments and gravels which stretch across the forelands of the Alps and the glaciofluvial deposited gravel around the river valleys.

The Alps show small values of erodibility. They are covered with immature soils which have high permeabilities and a great fraction of coarse material and sand.

Around the Swabian and Franconian Alb the prevailing loamy-clay soil textures are classified as “soils on karst”. They have low erodibility in large parts due to bonding forces of the weathered loamy-clay soil, their relatively high fraction of coarse material and the high permeabilities.

Lowest erodibilities dominate clearly in the region of the Bavarian Forest. The soils are classified as “soils on crystalline rock”, like the central Alps. These soils show a very high fraction of sand and gravel in the upper layer, hindering detachment and transport by water.

### 3.2.3. LAND USE AND AGRICULTURAL MANAGEMENT

#### 3.2.3.1. OVERVIEW

Soil erosion by water, usually refers to erosion on agricultural areas, because in general only these are significantly affected by soil erosion. Soils of natural areas, such as forest grassland or marshes, are protected and consolidated by their vegetation cover (at least in the temperate zone). So if considering only the agricultural areas, man can influence soil erosion by changes of (agricultural) land use and by diverse management practices. This anthropogenic component is probably the most complex factor affecting soil erosion, as it is highly variable and causes direct feedback on soils and vegetation. This section gives an outline on some important aspects of the multitude of factors which are induced by agricultural land use and management practices.

Agricultural land use per se increases risk of soil erosion, as it removes the protecting natural vegetation cover and exposes the soil (at least to a certain degree) to the eroding



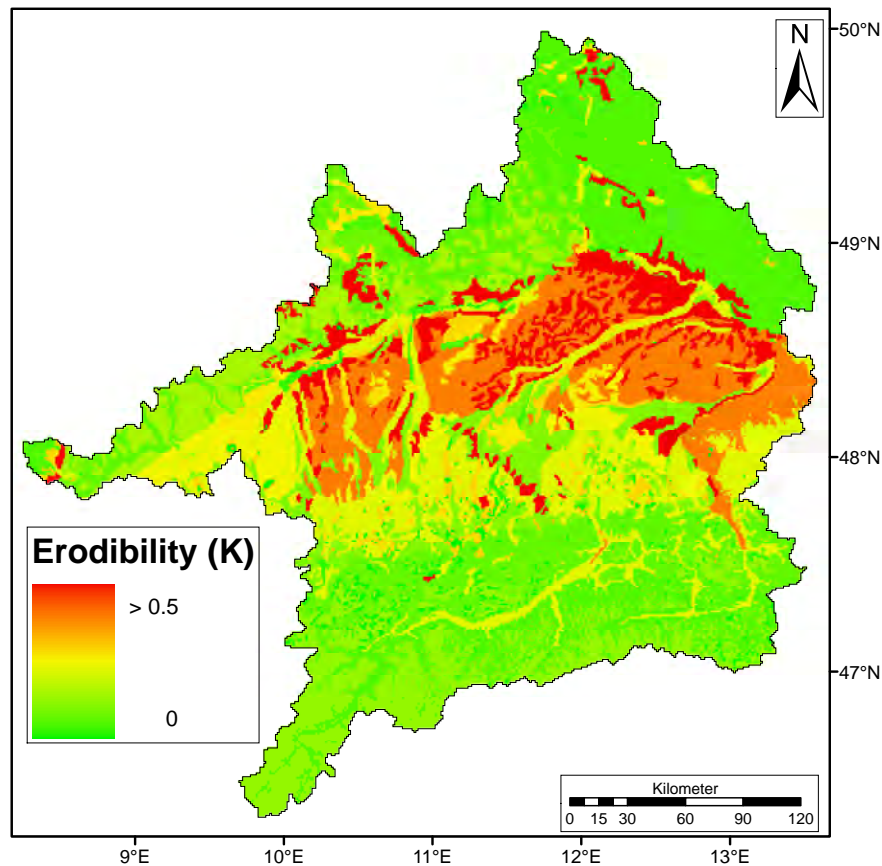


Fig. 3.7: Erodibility in the Upper Danube Basin (K factor) [ $t/ha \cdot a \cdot m^2/kJ \cdot h/mm$ ]

forces of rainfall and runoff. Natural vegetation, like forest or grassland, provides a good protection against the acting forces of erosion, but vegetation in agricultural areas does not necessarily lower these forces. It is true, that canopy interception absorbs a certain amount of the energy of rainfall depending on its coverage. But the intercepted water on the leaves accumulates and may drip off, forming relatively big drops which transfer their energy to the soil on impact (cf. Section 4.5.4.1). This effect increases with increasing height of the canopy, as drops accelerate during fall, so that rates of particle detachment can even exceed those of uncovered soil (SCHEFFER & SCHACHTSCHABEL, 2002). However, at rainfall events with high intensities, when surface runoff occurs, vegetation slows down the water flow and facilitates infiltration which decreases the erosive energy of the runoff. The roots of the plants consolidate soil structure and may form macropores. Organic matter content from plants raises biological activity, which stabilises soil aggregates (SCHMIDT, 1979). Organic matter is often added into the soil by mixing in crop residue during tillage.

Agricultural management practices may significantly influence the resistance of the soil to erosion. An important technique is crop rotation. In order to minimise the impacts of rainfall and runoff, the field should always be covered. For example forage like clover protects the soil well, as its cover is dense and lasts over a long period (usually up to several years). Maize, in contrast, covers the soil only sparsely during May to June, which is the time of strong erosive rainfall events. Since the soil is bare after harvest, the planting of cover crops afterwards, or leaving crop residue on the field is a method applied in conservation tillage. The Agriculture

and Consumer Protection Department of the Food and Agriculture Organization of the United Nations (FAO) characterises conservation agriculture by three principles (FAO, 2009):

- Continuous minimum mechanical soil disturbance
- Permanent organic soil cover
- Diversified crop rotations in the case of annual crops or plant associations in case of perennial crops

Soil disturbance is caused by ploughing, which is usually meant to increase fertility through mineralisation of soil nutrients. But in the long term this leads to a reduction of soil organic matter, decreasing soil stability. Using heavy machinery for tillage, soil structure is destroyed by compaction, infiltration capacity is shortened and the wheels leave rills where surface runoff concentrates. Due to the rills and plough furrows the direction of tillage should be parallel to the slope (contour tillage), as this influences the runoff pattern and slows down the water flows. Also the machinery used for tillage plays an important role (SCHMIDT, 1979):

- A plough leaves big clods and hollows, retaining water and facilitating infiltration. Soil displacement is only possible within the furrows.
- A harrow creates relatively good infiltration rates, but reduces stability by destroying aggregates.
- A roller has the most detrimental effect, as the soil is compacted, aggregates are destroyed and the surface becomes fairly impermeable, which is especially crucial in intensive showers.

Analogue to the furrows, which represent borderlines, the borders of agricultural plots also act limiting for runoff, as they are usually divided by vegetated strips. Therefore the size of the plots influences the severity of erosion, i.e. the smaller the plots, the more vegetated strips, which slow down runoff and thus impede concentration in rills. Naturally all above mentioned variables only apply to sloped surfaces, where detached soil particles can be washed off. Like the factors determining soil erodibility, land use and agricultural management practices, over such a large catchment area as the Upper Danube Basin, are difficult to register and quantify in terms of their influence on soil erosion. Hence these are often summarised in a single lumped parameter, e.g. the C- and P-factor of the ABAG.

### **3.2.3.2. REGIONAL CHARACTERISATION**

Fig. 3.8 summarises the description of land use in the Upper Danube Basin given in Section 2.4. Percentages may slightly deviate from the values given above, because Fig. 3.8 is based on the land cover classification on the CORINE Land Cover data sets. The illustration indicates the vulnerability of the crops to soil erosion. As it refers to arable land only, Fig. 3.9 shows the spatial distribution of arable land within the study area. As mentioned in Section 2.4, agriculture is not practiced in the Alps, and in their foothills only pastures and grassland are managed, but no crops cultivated. This can also be observed in the Bavarian Forest. Regions intensively used as arable land can be found south of the Danube in the

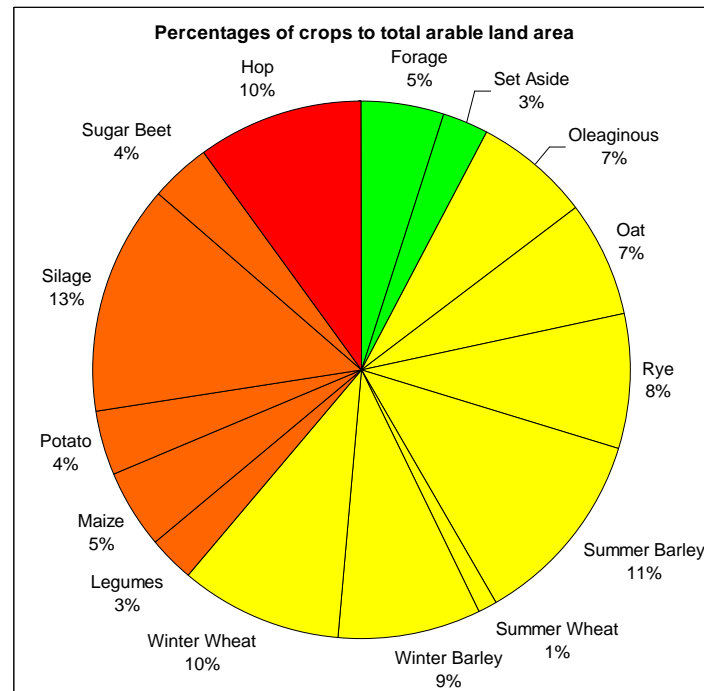


Fig. 3.8: Percentages of crops to total arable land area (based on the subscaled land use fraction of the crops to the land cover subtype Arable Land). The colors indicate the susceptibility of the cultivations to soil erosion due to soil exposure and agricultural management practices (green: good protection against erosive forces, red: vulnerable to erosion).

Tab. 3.4: C-factors for the ABAG for all land uses (taken from AUERSWALD & SCHMIDT (1986)).

Land use	C-factor
Forage	0.004
Forest	0.004
Grassland	0.004
Hop	0.67
Maize	0.40
Natural Vegetation	0.004
Root and tuber crops	0.40

*Tertiärhügelland* due to its fertile soils. In the lower part of the illustration the course of the Inn valley can be seen, where opportune climatic conditions favour agriculture. Depending on cultivated crop, the arable land areas are vulnerable to erosion in various degrees.

To estimate this influence, an evaluation of the ABAG C-factor was made. This factor expresses the protecting effects of different types of crops on the soil. The C-factors are taken from AUERSWALD & SCHMIDT (1986), who investigated the situation in Bavaria. The basis for the computation of the factors are Tab. 3.4 and the land cover map used within the project GLOWA-Danube, derived from Landsat TM and CORINE data sets. The map has a resolution of 1 km<sup>2</sup> and contains for each pixel a set of up to ten land uses and the corresponding area each land use covers. Comparing Fig. 3.9 and Fig. 3.10 it is obvious, that the patterns resemble each other closely, as the natural vegetation protects the soil well, in contrast

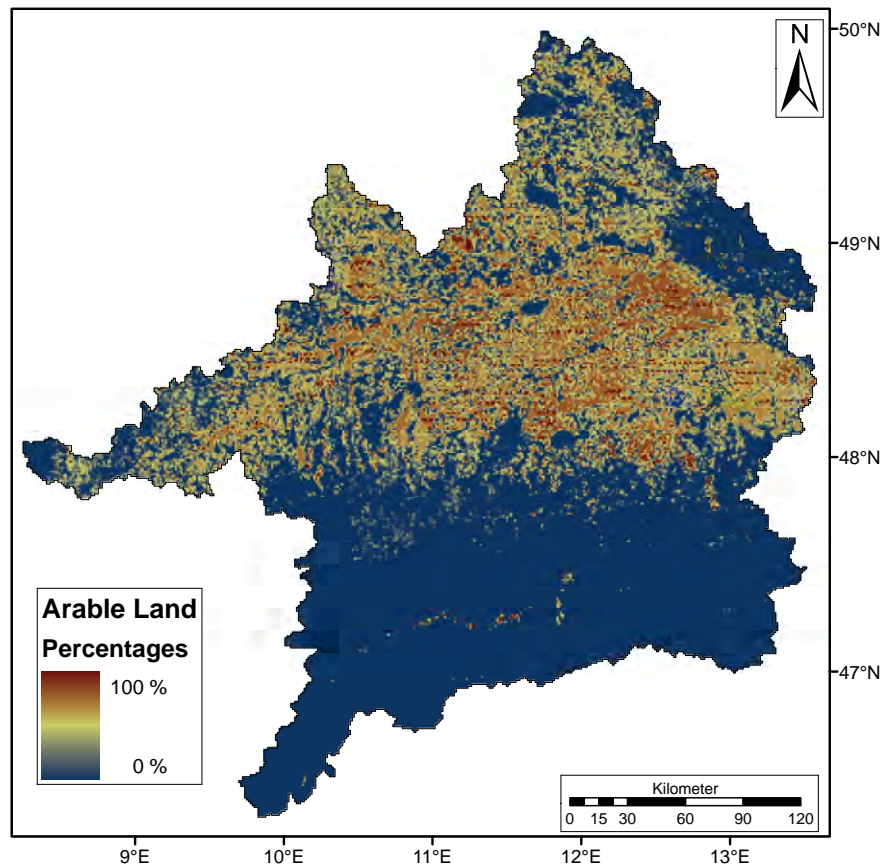


Fig. 3.9: Percentages of arable land in the Upper Danube Basin (based on the subscaled land cover fraction to the land cover subtype Arable Land).

to the agricultural areas in the northern two thirds of the study area. Particularly vulnerable regions are the *Hallertau* and the *Gäuboden*. The *Hallertau* is preferentially used for cultivation of hop, which has a low canopy cover and is usually grown on the same field over 15 years, intensifying the unfavourable conditions. Since cereals, which are more protective, are frequently grown on fields next to hop, the pattern in Fig. 3.10 is somewhat speckled. The *Gäuboden* is especially susceptible to erosion, because here mainly sugar beets, potatoes and maize besides some grain crops are planted.

### 3.2.4. RELIEF

#### 3.2.4.1. OVERVIEW

The slope steepness affects erosion, as on steeper relief surface runoff is accelerated. Due to the fact that the kinetic energy increases with the square of the velocity ( $E_{kin} = \frac{1}{2} \cdot m \cdot v^2$ ), the surface runoff is provided with more energy for particle detachment and transport on steeper slopes. According to SCHEFFER & SCHACHTSCHABEL (2002) a doubling of the slope angle increases the sediment yield by a factor of 2.9. The information regarding a critical slope angle, from which soil erosion is induced differ: SCHULTZE (1952) stated, that even on areas with 0° erosion may occur, whilst KURON (1948) considers slopes under 1° – 2° safe and DUBBER (1967) found movements of soil material on slopes of 1° (all as quoted in SCHMIDT

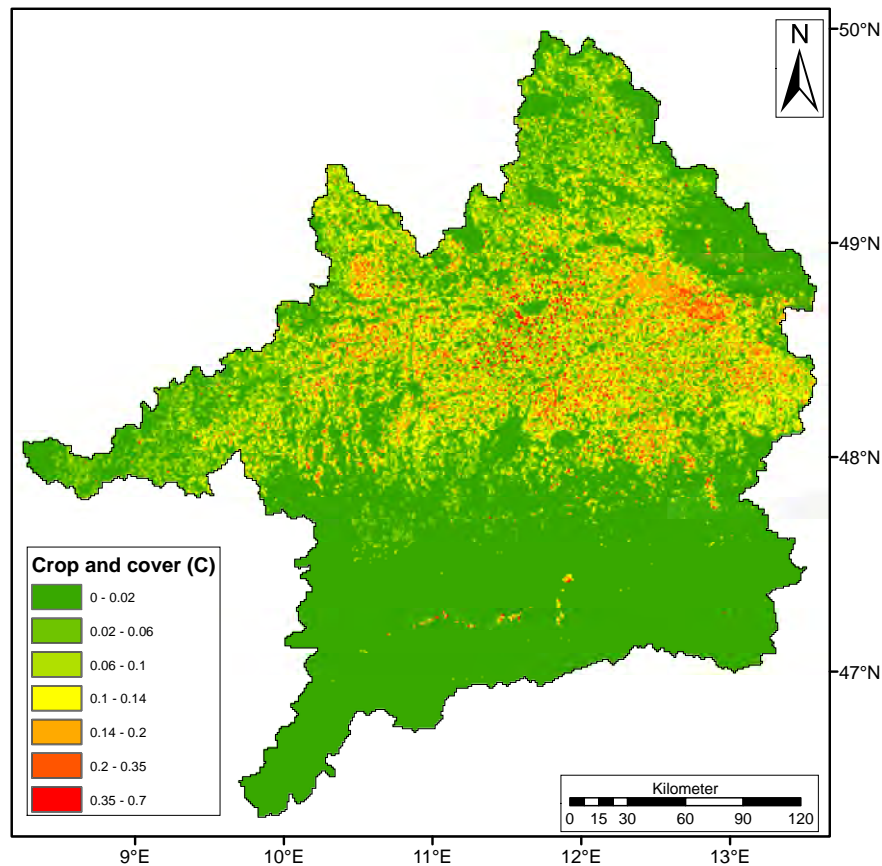


Fig. 3.10: Protective influence of crops and cover in the Upper Danube Basin (C factor)

(1979)). The relevant information from these statements is, that generally erosion may occur at very small angles. The deviations strongly depend on parameters as mentioned above, such as soil type or land use, but also on slope length and shape. Generally the impact of the slope length on erosion results from the fact, that with increasing slope length the contributing area grows, which in turn leads to an increase of the amount of surface runoff and a higher transport capacity. SCHEFFER & SCHACHTSCHABEL (2002) numeralise a decrease of soil erosion by about 30 % when slope length is halved. But this apparently logical conclusion need not always apply, and might even result in the opposite, i.e. runoff and sediment yield decline with increasing length, as the slope shape may superimpose this effect (SCHMIDT, 1979). Here the longitudinal profile as well as the cross profile of the slope play a role. The following longitudinal profile shapes have different effects:

- Concave slope: erosion is usually strongest in the steep upper third and decreases downwards, until in the lower part deposition prevails.
- Convex slope: the continuously increasing angle of the slope accelerates the flow, so that soil loss may be expected over the whole slope, but especially in the lower third.
- Straight slope: erosion dominates in the middle and lower areas, although net soil loss there may be smaller than in the upper area, as material may be re-deposited.

Regarding the cross-sectional profile one can say that concave profiles, which form a hollow, concentrate runoff in rills where detachment and transport is increased. Convex profiles lead to diverging runoff, i.e. lessen rill initiation and runoff energy. Depending on slope shape and thus runoff formation, a greater slope length also may act protecting. But this is usually only the case on gentle slopes with low runoff energy, where the water film of the flow absorbs the energy of the impacting raindrops. Slope length can be influenced particularly by anthropogenic interactions, as mentioned in Section 3.2.3.1. Measures such as terracing or drainage ditches between fields effectively reduce slope length by breaking up sheet and rill flow, which is therefore termed “effective slope length”. The importance of such techniques was already addressed in 1900 in the early years of the *Flurbereinigung*, which aimed at improving agricultural efficiency by restructuring agricultural estates (AUERSWALD & SCHMIDT, 1986).

### 3.2.4.2. REGIONAL CHARACTERISATION

As illustrated in Fig. 2.2 in Section 2.1 the highest altitudes in the Upper Danube Basin can be found in the Alps and in the low mountain regions. Here the relief is also steepest with high gradients, which results in a higher erosion risk. But, as stated in the last section, slope steepness alone does not necessarily mean a linear increase in erosion susceptibility in these areas. For estimation of the influence of slope steepness and effective slope length, the equations from the Revised Universal Soil Loss Equation (RUSLE) (RENARD ET AL., 1996) are used here to present the L and S factors:

$$L = \frac{\lambda}{22.13}^m \quad (3.12)$$

Here  $\lambda$  is the effective slope length and the slope-length exponent  $m$ , related to the ratio  $\beta$  of rill to interrill erosion, which can be calculated with:

$$m = \frac{\beta}{1 + \beta} \quad (3.13)$$

The ratio  $\beta$  is computed from:

$$\beta = \frac{\sin \theta / 0.0896}{3.0 \cdot (\sin \theta)^{0.8} + 0.56} \quad (3.14)$$

where  $\theta$  is the slope angle [°].

Equations for the slope steepness factor  $S$  are differentiated by slope:

$$S = \begin{cases} 10.8 \cdot \sin \theta + 0.03 & \text{for slopes} < 9 \% \\ 16.8 \cdot \sin \theta + 0.50 & \text{for slopes} \geq 9 \% \end{cases} \quad (3.15)$$

Eq. (3.12) requires the effective slope length  $\lambda$ , which would require field survey, to be determined exactly. Since this is virtually impossible over such a large area, AUERSWALD & SCHMIDT (1986) derived the latter from the *Bodenschätzungsübersichtskarte* of Bavaria. But the Upper Danube Basin extends over large parts of Austria and also Switzerland, where such information was not available for this study. Due to lack of data regarding the effective slope length other authors often assume a constant value for  $\lambda$ , e.g. ERHARD ET AL. (2002),



Tab. 3.5: Assignment table of mean effective slope length depending on slope inclination

Slope [%]	Length [m]	Slope [%]	Length [m]
0	175	- 19	140
- 1.5	250	- 23	125
- 4	200	- 29	75
- 13	150	> 29	50

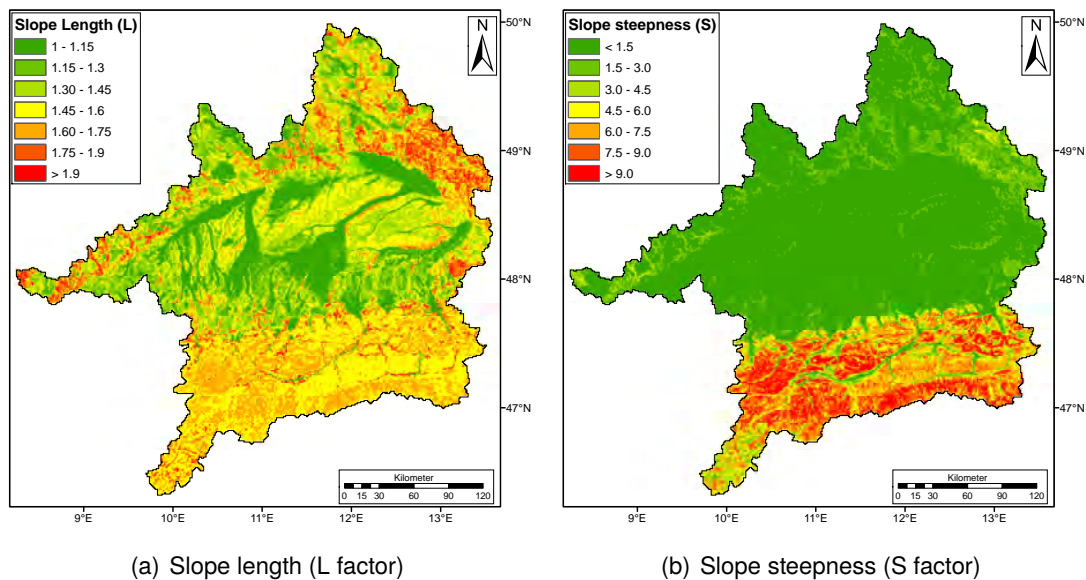


Fig. 3.11: Slope length and slope steepness in the Upper Danube Basin

who set it at a constant value of 250 m, what equals the spatial resolution of the input data sets they used. Since the resolution of the DTM used here is 1 km<sup>2</sup>, this would overestimate the L factors in the alpine regions. Therefore an estimation of the effective slope length based on the findings of AUERSWALD & SCHMIDT (1986) was carried out in this work. Tab. 3.5 lists the estimated mean slope lengths depending on the slope inclination. High slope lengths are favoured especially on arable land, as these are easier to manage with machinery. They can be found in areas with low relief and decrease strongly in steep relief, as application of machinery is not possible there to such an extent. The somewhat lower slope length of 175 m for plains derives from the fact, that condition there are more often too wet, as water drains better on sloped soils. This makes agricultural management more difficult, resulting in smaller field sizes.

The derivation of the slope based on the 1 km<sup>2</sup> DTM, results in underestimation of the slope, and thus leads to unrealistic values of the S factor. In order to gain a better representation of the slope, a 50 m DTM, based on data from the land surveying offices of Bavaria, Baden-Württemberg and Tyrol was used. Slopes were calculated from the high resolution data set and then aggregated by averaging to 1 km<sup>2</sup>.

The calculated results presented in Fig. 3.11 show, that the S factor strictly follows the relief. But for the L factor, one recognises a somewhat more differentiated pattern, as the L factor is influenced by rill initiation (cf.  $\beta$  in Eq. (3.14)) on steeper slopes and by the effective slope length. Comparing the patterns with illustrations of calculations from AUERSWALD & SCHMIDT

(1986) (no figure available here), the L factor calculated in this study is somewhat higher in Bavarian Forest, and a bit lower in the *Gäuboden* and the *Hallertau*. This probably results from the simplifying assignment of slope length depending on slope angle.

### 3.3. SUSPENDED SEDIMENT YIELD

#### 3.3.1. OVERVIEW

At the beginning of the 20th century utilisation of hydro-power and hydraulic engineering in the rivers of the Upper Danube Basin was intensified. Because such structures are affected by siltation, a more detailed knowledge of suspended sediment transport was required. The measuring method developed at that time is still applied today. Water is withdrawn from the rivers and filtered in order to quantify the amount of suspended sediment. (MANGELSDORF & SCHEURMANN, 1980)

The directive of the German Association for Water, Wastewater and Waste (DWA) for the measurement of suspended solids in water bodies defines these as solid matter which is in equilibrium with the water or is held in suspension by turbulences (DVWK, 1986). The most important aims of measurement are:

- evaluation of potential siltation of water bodies, hydraulic structures, flood plain areas, etc.
- estimation of abrasion on turbines
- assessment of ecological impacts on water quality (e.g. fish habitats which might be disturbed by suspended sediment or oxygen consumption of organic sediments through decay)
- survey of soil erosion in sub-catchments

The origin of suspended sediments is derived from a variety of different sources. Distinguishing between anthropogenic and natural sources, the human induced sources are for example urban wash-off in built up areas, industrial wastewater discharge, and sediment yield from building activities or special industries, like mining or gravel pits. Natural sources are e.g. physical weathering, streambank erosion and attrition of bed load, decomposition of organic material or chemical precipitation of solute minerals.

Measuring of suspended sediment in Bavaria began in 1924 and the directive of the DWA (DVWK, 1986) exactly defines the procedure for single point measurements, which is the established method used by the office for water management of the LfU. With a bucket of a defined volume (usually between 10 and 15 l) a sample is drawn from the channel line. The sample is filtered and the filter is dried and weighed under laboratory conditions. Common filters have a mean pore size of 6.1  $\mu\text{m}$ , but as pores get jammed during filtering, the effective diameter of particles which can be collected averages out to approx. 0.45  $\mu\text{m}$ . The sediment mass, multiplied with a correction factor depending on the sampling site, allows for calculation of the sediment concentration [ $\text{g}/\text{m}^3$ ] at the moment of measurement. Measurements are carried out 250 to 300 times per year, but the sampling interval is higher in exceptional cases



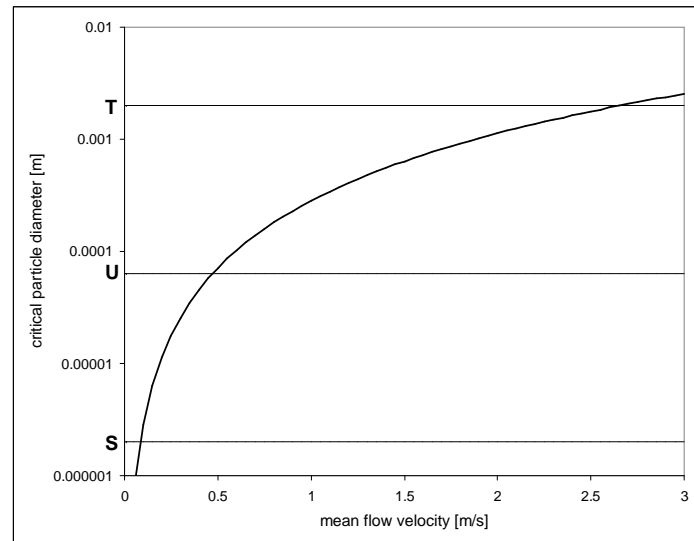


Fig. 3.12: Critical particle diameters for sediment suspension depending on mean flow velocity. The horizontal axes designate the aggregate classes sand (S), silt (U) and clay (T) according to the German classification system ( $2000 \mu\text{m} > S > 63 \mu\text{m} > U > 2 \mu\text{m} > T$ ).

like snowmelt or flood events. Through integration over this amount of samples a reliable value of annual sediment transport can be calculated.

NACHTNEBEL (1998) addresses the measuring accuracy of sediment concentration measurements carried out by the Austrian Waterway Authority (WSD), where sampling usually is executed with one litre buckets from the riverbank. Compared to sediment concentrations measured over the whole cross section of the river, the riverbank withdrawal may exhibit deviations of +/- 30%. The concentrations of a single measurement vary considerably over the cross section: the highest and lowest concentrations in the cross section may differ by a factor of 10 at low flow conditions, whereas at flood flow the factor reduces to 2 to 3, as increased turbulence causes better sediment mixing at riverbank zones. However, if the sediment concentrations are related to river discharge, the deviation between cross sectional measurements and single point measurements reduces to -10% to +3%, as for calculation of sediment concentrations based on cross sectional measurements the mean value is used.

Considering the particle sizes which can be measured, it is in many river segments not possible to collect the grain size class of sand, as it sinks down too fast. KRESSER (1964) (quoted in DVWK (1986)) found through measurements at several Austrian rivers, that the correlation between mean flow velocity  $v_m$  [m/s] and a critical particle diameter  $d_c$  [m] can be described by a constant Froude number  $Fr$ :

$$Fr^2 = \frac{v_m^2}{g \cdot d_c} = 360 \quad (3.16)$$

where  $g$  is the gravitational acceleration ( $9.81 \text{ m/s}^2$ ).

Fig. 3.12 gives a graphical representation of the correlation between flow velocity and grain size. Together with the mean flow velocities of the Danube in Tab. 3.6, this allows for calculation of the critical particle diameters which separate suspended load from bed load (see Tab. 3.7).

Tab. 3.6: Mean flow velocities of the Austrian section of the Danube in banked-up and free water levels (modified after NACHTNEBEL (1998)). Headwater and tailwater designate the river sections up- and downstream of hydro-power plants (MQ: mean discharge, HSQ: discharge at the highest navigable water level)

Discharge [ $\text{m}^3/\text{s}$ ]	Headwater [ $\text{m}/\text{s}$ ]	Tailwater [ $\text{m}/\text{s}$ ]	Free water level [ $\text{m}/\text{s}$ ]
MQ (1400 – 1900)	0.3 – 0.6	0.9 – 1.4	1.6 – 2.1
Q = 3000	0.5 – 0.9	1.2 – 2.5	1.9 – 2.7
HSQ (3700 – 5000)	0.8 – 1.3	1.5 – 3.0	2.1 – 3.3

Tab. 3.7: Mean critical particle diameters separating bed load and suspended load for the mean velocities of the Austrian sections of the Danube from Tab. 3.6

Discharge [ $\text{m}^3/\text{s}$ ]	Headwater [ $10^{-6}$ m]	Tailwater [ $10^{-6}$ m]	Free water level [ $10^{-6}$ m]
MQ (1400 – 1900)	26 – 102	229 – 555	725 – 1249
Q = 3000	71 – 229	408 – 1770	1022 – 2065
HSQ (3700 – 5000)	181 – 477	637 – 2549	1249 – 3084

So in undisturbed segments of the Danube, very coarse sand and coarse sand cannot be transported at mean discharge (MQ). Although the distribution of silt within the water is equally balanced over the vertical profile, this is not valid for the fraction of sand, as it accumulates in the lower regions near the riverbed.

So the amount of transported sediment, as well as the particle size distribution, depends strongly on flow velocities. This means, if measurements of suspended sediment shall be related to processes of erosion, one has to bear in mind, that the characteristics of the river strongly influence the transport process. For example small alpine rivers, like the Ammer, transport a multiple of the sediment amount of rivers in flat regions, like the Große Laber, although areal soil loss in the whole catchment of the latter is much higher. This can be explained with the lower transport capacity of flatland rivers, which causes bigger grain sizes to be deposited earlier. But even if energy suffices to transport those sediments as bedload, they could not be measured with the common methods, as they are located at the riverbed. On the other hand, a river in steep relief is able to transport bigger grain sizes in the suspended state, which then actually can be recorded with the measurement technique. Additionally processes in the river itself, such as bank erosion, riverbed erosion or remobilisation, are acting intensified in steeper riverbeds and affect the amount of collected sediment.

### 3.3.2. REGIONAL CHARACTERISATION

Fig. 3.13 shows the confluence of the river Inn and the Danube in Passau. Noticeable are the differences in colour, resulting from the lower concentrations of suspended sediment in the northern tributaries of the Danube, and higher concentrations in the southern tributaries, as schematically illustrated in Fig. 3.14. Whilst bed load in most rivers is only mobilised during discharge peaks, suspended sediment is transported over the whole year. Nevertheless major quantities of suspended sediment transport are bound to the months with above average runoff. These greater amounts of sediment transport are often limited to only a few



*Fig. 3.13: Confluence of the Inn and the Danube at Passau. (License: Creative Commons Attribution-Share Alike 2.0 Generic <http://creativecommons.org/licenses/by-sa/2.0/deed.en>)*

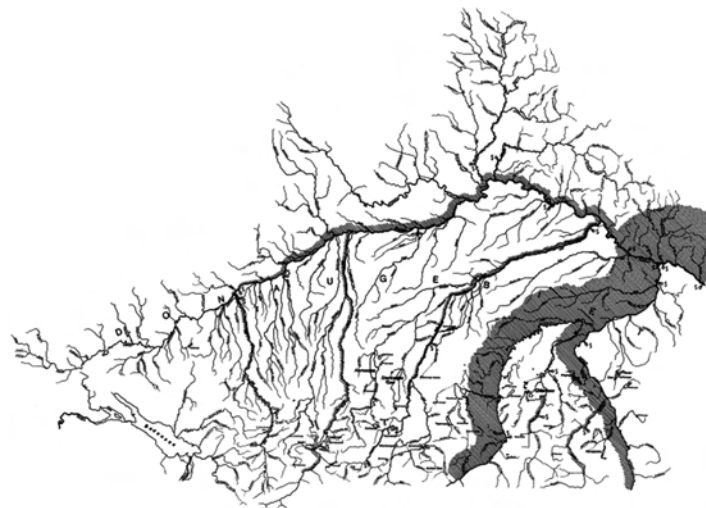


*Fig. 3.14: Comparative suspended sediment transport of the Danube and tributaries (modified after LFU (2009)).*

Tab. 3.8: Mean percentages of particle size classes transported as suspended sediment in the Danube (NACHTNEBEL, 1998).

Class	Diameter [ $\mu\text{m}$ ]	Percentage [%]
Sand (S)	< 2000	0.1
	< 630	0.3
	< 200	4.4
Silt (U)	< 63	16
	< 20	29
	< 6.3	24
Clay (T)	< 2	11
	< 0.6	15
	< 0.2	

short-term flood events in rivulets or small rivers, clearly noticeable as outstanding sediment peaks. The confluence of small tributaries in the major rivers forms a complex hydrological regime, and thus attenuates the influence of the regimes of the tributaries or of single events in sub-catchments. This altogether leads to a more steady distribution of sediment load in the major rivers over the course of the year with less pronounced peaks (MANGELSDORF & SCHEURMANN, 1980).

Considering single events, the correlation of suspended sediment transport to heavy precipitation events is greater than its link to discharge (NACHTNEBEL, 1998). The amount of transported material during flood events depends primarily on sediment yield washed into waterbodies by rainfall and seems to be greater than the amount of re-mobilised material. 70 – 80% of the annual suspended sediment charge is transported in only 10% of the time. The amount of transported sediment during rare flood events, in which the vast majority of the sediment originates from soil erosion, may even exceed mean annual amounts. Nevertheless two thirds of long-term sediment transport occurs during slightly increased discharge (between MQ and HSQ), so that the observation of flood events alone is not sufficient, i.e. a continuous measurement is necessary.

According to NACHTNEBEL (1998), who investigated the origin and composition of sediments in the Danube and its tributaries, soil erosion contributes an essential part to sediment delivery into surface waters. But particularly in steep alpine catchments other forms of erosion like debris flow are important, whose relative ratio to sediment delivery can not be specified. Additionally, particles sedimented in the upstream area of reservoirs may become re-mobilised during the passage of a flood wave, which may represent a major fraction of the total annual sediment charge in some rivers. A reliable differentiation of the ratio of re-mobilised and recent sediment is not possible. The influence of hydro structures on remobilisation cannot be quantified, but probably leads to a higher frequency of high concentrations of suspended sediment (due to remobilisation).

Altogether, the suspended sediment distribution in the Danube itself is relatively homogeneous, the mean percentages (for measurements near the surface) are 25% clay, 70% silt and 5% sand (Tab. 3.8). The mineralogical composition of sediment from tributaries naturally differs depending on the bedrock of the respective sub-catchment. But, surprisingly the fractions of the transported grain sizes vary only slightly in the tributaries, and along the lon-

itudinal section of the Danube the influence of the tributaries on the grain size distribution in the Danube diminishes. NACHTNEBEL (1998) even could not find noticeable differences in sediment composition caused by hydro structures, but assumes, that this might be due to the measurement conditions, as in his study the samples have been taken during increased discharge.



## 4. METHODS AND MODELS

### 4.1. ASPECTS OF MODELLING APPROACHES

A crucial aspect for simulating potential impacts of Climate Change is the selection of an adequate modelling approach. Generally these can be divided into empirical and physically-based models. Empirical models do not consider the governing physical laws of the processes involved, and reflect only the relations between input and output data for the local basin characteristics and the climate conditions during the time period they were developed. Thus it is questionable if they are suitable for modelling the impacts of future Climate Change (LEAVESLEY, 1994). They “generally simplify the set of processes operating, so that they may not be appropriate under particular local circumstances”, and the USLE-approach does not properly distinguish between soil and climatic conditions in the infiltration process. Process models in contrast have the potential to respond explicitly to changes in climate or land use and so have great promise for developing scenarios of change (KIRKBY ET AL., 2008). They are considered to be invariant in space and time and allow a physical interpretation of the results they produce. Nevertheless physically-based models are often criticised, that their extensive use of parameters cannot be linked anymore to the actual processes, and thus they are often not parameterised but calibrated to measured data (LEAVESLEY, 1994).

The strategy of the project GLOWA-Danube for the simulation of natural components is strongly focused on physically-based process descriptions. Since this work was developed within the project GLOWA-Danube, whose basic principles comply with the requirements postulated in Section 1.2, the latter are picked up again and addressed here more detailed.

The usage of a physically-based model intrinsically allows for an explicit process representation (to a certain degree), since physics is intended to describe processes, respectively calculate these and the magnitude of resulting impacts. Purely mathematical or statistical (black box) models in contrast do not consider the processes, but rather correlate observed data sets to the desired output parameter(s). Nevertheless, irrespective whether a process-oriented or whether an empirical model is developed, the governing equations or variables which are utilised, have to be derived on, respectively for an adequate scale. This means, that for example the inclusion of a factor describing microtopography into an empirical model computing on a scale of  $1 \text{ km}^2$  is not reasonable, since the variability of microtopography cannot be represented on  $1 \text{ km}^2$ . Considering a physically-based model for the same purpose, it would not make sense to include equations for calculation of flow paths on a scale of centimetres. In both cases this process or parameter of the model has to be abstracted. The degree of abstraction should be related to the relative impact of the different input parameters. For example a highly detailed calculation of raindrop impact on the soil is useless, if runoff represents the driving force (and maybe is even left unconsidered). It is the task of the developer to evaluate which processes or input data are relevant, respectively significantly influence the (final) result on the scale considered, and therefore should be included into the model.

The issues of adequate process scaling addressed above are closely related to a reliable process representation. Only if the processes are represented on an adequate scale, the model may reliably be used for simulating impacts of Climate Change scenarios. For example the R-factor of the USLE, used in Section 3.2.1, which is based on the sum of the precipitation volume in summer only, should be regarded critically for the calculation of scenarios. Assuming e.g. - according to the IPCC (CHRISTENSEN ET AL., 2007) - an increase in winter precipitation amounts with a coincident decrease of summer volumes, the R-factor according to Eq. (3.6) would compute lower soil loss values for future conditions. But in spite of lower summer precipitation volumes, the IPCC mentions a possible increase in extreme events in summer (in Central Europe). This in turn leads to the expectation, that erosion risk in summer might increase, since the majority of erosive events occurs in only a few thunderstorms in summer ((cf. e.g. NEARING ET AL., 2005)). Additionally the increased winter precipitation volumes may increase soil losses in winter, which is not considered by the empirical equation at all.

Altogether, this means not only that there is a need of adequate process representation, but also that it is necessary to include the relevant processes into the model. If these requirements are fulfilled, the model should be able to respond to changing external conditions. However, as mentioned above, physically-based models often use an extensive set of parameters, and thus are often calibrated due to a lack of the latter during model parameterisation for the study site. Depending on the degree of calibration, the model configuration thus may only be valid for the calibration conditions, and even may be completely invalid for Climate Change conditions, where impacts on the model are uncertain.

The considerations of this section serve as a guideline for the integration of an erosion module into the DSS DANUBIA. For modelling the land surface processes in this study, the hydrological model PROMET (MAUSER & BACH, 2009) is applied, which is used within the modelling framework DANUBIA of the GLOWA-Danube project (LUDWIG ET AL., 2003). The development of PROMET is guided by maximising physical process descriptions and simultaneously minimising model calibration by parameterising with literature sources and/or measurements. Since this model compound provides the basis for the erosion model, the next chapter delineates PROMET, which then is followed by a description of the erosion model.

## 4.2. THE HYDROLOGICAL MODEL PROMET

The distributed hydrological model PROMET evolved from a Soil Vegetation Atmosphere Transfer (SVAT)-scheme originally developed by MAUSER & SCHÄDLICH (1998). It was continuously extended during the project GLOWA-Danube (see Chapter 1), and its latest developments include a coupling of energy and water fluxes of the land surface with biophysical processes. All modelled processes are calculated for an input grid (Fig. 4.1(a)), which represents the whole catchment. On the basis of each grid cell, all processes considered by the model are computed (therefore a grid cell is called a *proxel*, as shown in Fig. 4.1(b)). The processes which currently can be simulated by PROMET, respectively its sub-components, are illustrated in Fig. 4.2. For realistic computation of mass and energy fluxes PROMET distinguishes between 27 land cover and land use classes (see Fig. 4.3). The input parameters each sub-component requires, are provided either as simple lists, or as GIS-layers, if they



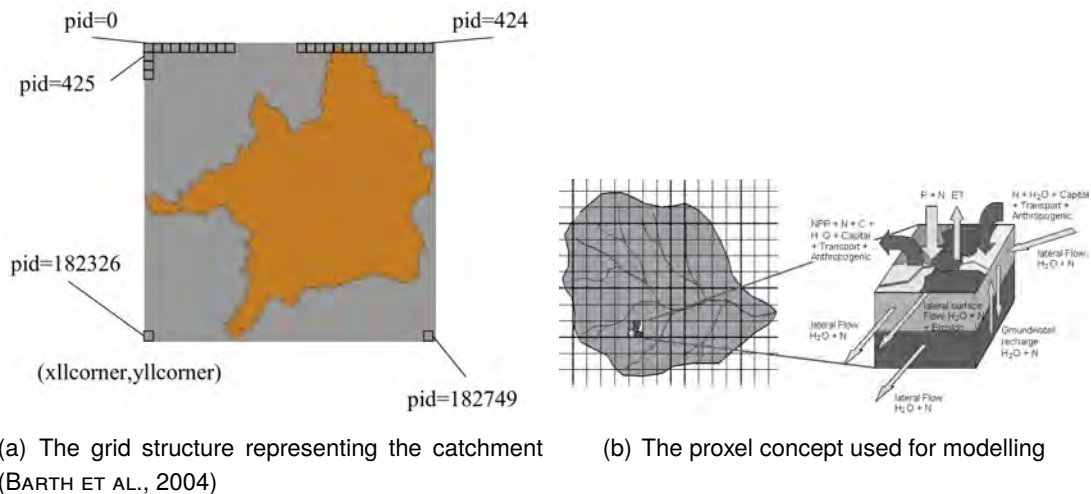


Fig. 4.1: Grid based modelling based on the proxel concept, as used for modelling within PROMET

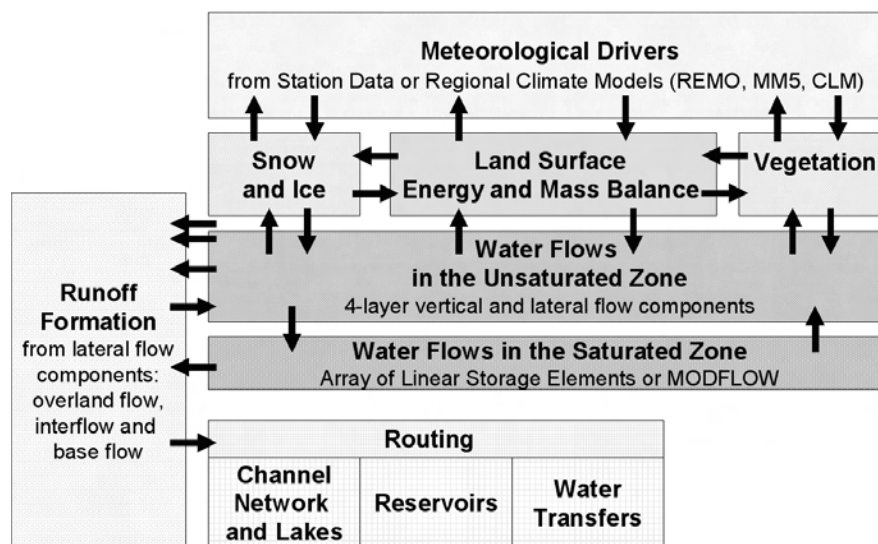


Fig. 4.2: Schematic model structure of PROMET with its interacting sub-components (MAUSER & BACH, 2009)

have a spatial context. The default resolution of PROMET within DANUBIA, is a spatial extent of one proxel of 1000 m x 1000 m, and a temporal computation time step of 1 hour.

The following list briefly summarises the component descriptions given in MAUSER & BACH (2009):

- Meteorology: this component is made up of two sub-components providing meteorological drivers to the land surface model. The first sub-component interpolates and disaggregates measured station data, whereas the second sub-component allows coupling to regional climate models.
- Land surface energy and mass balance: for closing the energy balance on the land surface, the exchange of water and energy between the land surface and the atmosphere is modelled. The energy balance is iteratively solved by exchanging fluxes of incoming and outgoing shortwave and longwave radiation, latent and sensible heat fluxes and the

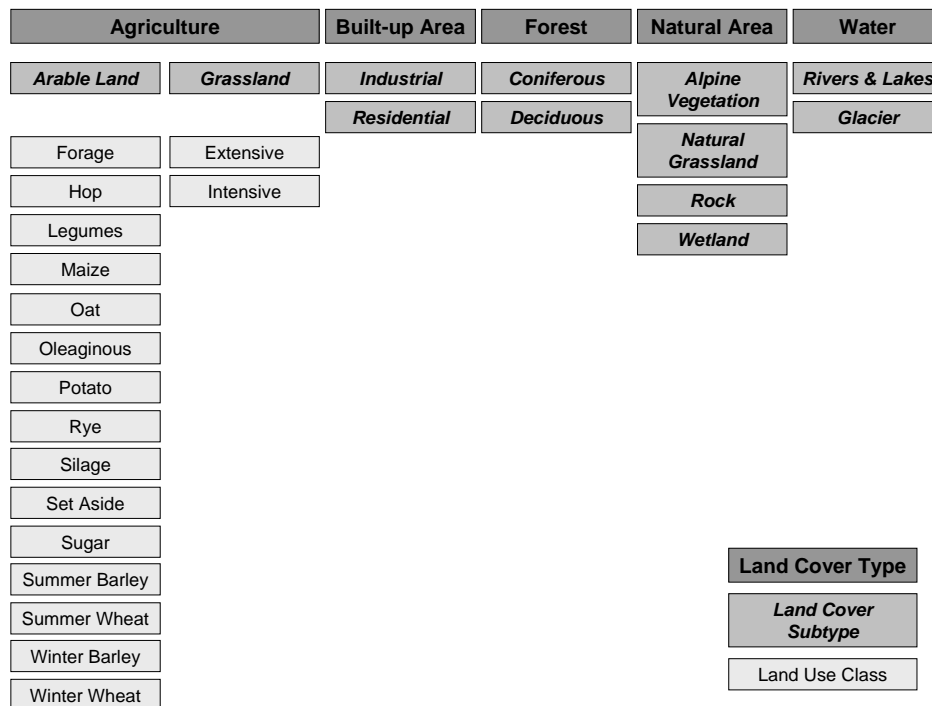


Fig. 4.3: Land cover and land use classes modelled within PROMET

ground heat flux within the soil, vegetation and snow components.

- (c) Vegetation: two sub-components can be used to simulate plant water and energy fluxes. The first one calculates evapotranspiration based on the *Penman-Monteith* (MONTEITH, 1965) approach. The other one uses the physiological model of FARQUHAR ET AL. (1980), which additionally simulates plant CO<sub>2</sub> exchange and growth dynamically.
- (d) Snow and ice: this component models energy balance, water equivalent and melt rate of the snow and ice cover. At first the state of aggregation of precipitation is calculated using a wet bulb temperature threshold. Potential melting conditions are calculated depending on air temperature and available energy. If necessary the liquid water storage of the snow pack is filled or released.
- (e) Soil hydraulics and soil temperature: the soil model computes soil water content and soil temperature and related vertical and lateral flows of water in and on the unsaturated zone. Excess water is either transported laterally to neighbouring proxels, or contributes to groundwater recharge. Under dry conditions capillary rise may occur.
- (f) Groundwater: the groundwater component is responsible for water flows in the saturated zone and exchanges water with the unsaturated zone and the channel network. It consists of two sub-components. Sub-component 1 comprises a simple linear storage element for each proxel. A time constant between one hour and one year, depending on the distance of the proxel to the next main channel, controls the flow into this channel. Subcomponent 2 interfaces to the groundwater model MODFLOW (USGS, 2008) transferring flows to and from the soil and the channel network.

- (g) Channel flow: the purpose of this component is the routing of lateral water flows on (i.e. surface runoff) and in (i.e. interflow) the soil according to the topographic conditions. This process also involves the formation of the channel network and the calculation of flow velocities and changes of water storage in the channel based on the Muskingum-Cunge-Todini method (CUNGE, 1969; TODINI, 2007). Runoff retention by lakes is also implemented.
- (h) Man-made hydraulic structures: this module simulates the hydraulic behaviour of water transfers and reservoirs within the channel network. Reservoirs are technically treated as lakes and individual monthly lookup-tables provide a translation of storage volumes into discharge. A second collection of lookup-tables is used to model the anthropogenic water transfers between proxels, which are not naturally connected. All lookup tables can be adapted during runtime to different management strategies.

PROMET calculates a large amount of parameters, which are linked directly or indirectly to erosion processes. Therefore the following subsections explain only the approaches of the sub-components, which provide data needed for modelling of erosion, and thus affect model outputs directly.

#### 4.2.1. METEOROLOGY

Meteorological input is the driving force for a physically based hydrological model. The information must cover the whole modelling area and must be available for every spatial computation unit. Methods to provide distributed meteorological input data are either coupling the model with a regional climate model or interpolating measured data from weather stations.

PROMET offers the possibility to couple with regional climate models (MARKE & MAUSER, 2008). This interface downscales fluxes of energy and mass from climate models and provides them to PROMET. A detailed description can be found in MARKE (2008).

Common techniques for the spatial interpolation of meteorological variables are Thiessen polygons, Kriging, inverse-distance weighting, splining or artificial neural networks. A comparison of popular interpolation methods can be found e.g. in VICENTE-SERRANO ET AL. (2003). Interpolation of measured data is a (computationally) efficient and practical way to gain spatially distributed variables. Within the project GLOWA-Danube a time series of over 40 years is available for model validation runs. Additionally, as the main focus of the project is the assessment of future trends in the water cycle due to Climate Change, PROMET is equipped with a stochastic weather generator (MAUSER ET AL., 2006), which generates future climate data based on the historical time series. Therefore, in this study the sub-component for disaggregation and interpolation of station data is used, instead of coupling with regional climate models, and the approach of *AtmoStations* is delineated in the following.

Meteorological input data for PROMET is provided by weather stations of the German Weather Service (DWD) in Germany and the Central Institute for Meteorology and Geodynamics (ZAMG) in Austria. Measurements are made three times per day at 7:00, 14:00 and 21:00 CET (the so-called *Mannheimer Stunden*). Fig. 4.4 shows all available stations in the study area, passing recorded data to the meteorological interpolation and disaggregation model *AtmoStations*. Disregarding some measurement gaps, the 277 stations theoretically

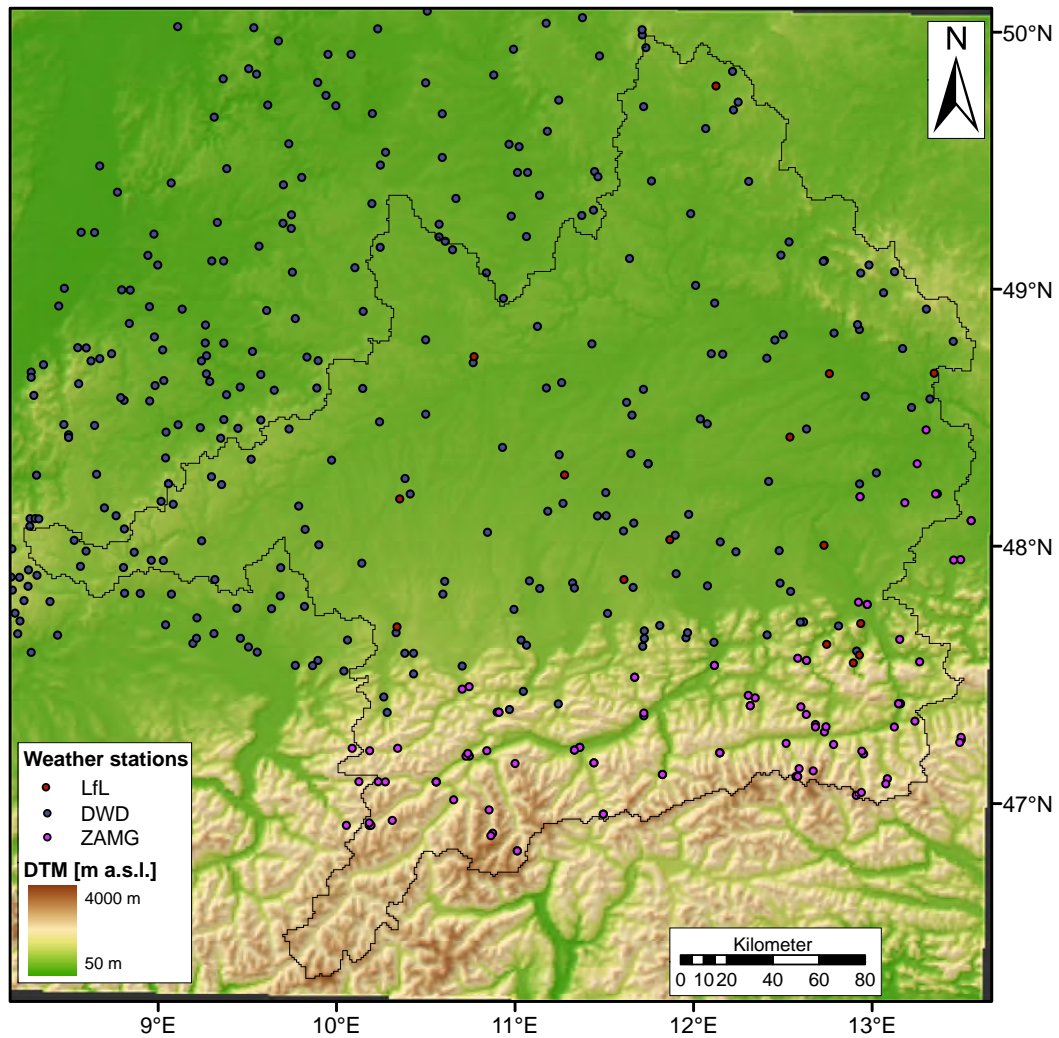


Fig. 4.4: Available weather stations used in AtmoStations

provide data from 1960 – 2006. Based on measured values, *AtmoStations* models the following variables:

- air temperature
- relative air humidity
- wind speed
- rainfall intensity
- incoming direct shortwave radiation (via cloudiness)
- incoming diffuse shortwave radiation (via cloudiness)
- incoming longwave radiation (via cloudiness)
- CO<sub>2</sub> partial pressure

These values represent discrete, punctual values, as they are only available at the *Mannheimer Stunden* on proxels owning a weather station. Thus they have to be interpolated spatiotemporally to provide meteorological input parameters for each simulation time step on each proxel.

The basic approach of *AtmoStations* consists of temporal interpolation and disaggregation, spatial interpolation and finally computation of incoming radiation. The following sections summarize this approach as described in MAUSER (2002), with emphasis on disaggregation and interpolation of rainfall, because rainfall intensity has a direct impact on erosion processes. The other modelled variables only indirectly influence erosion (see Chapter 3), thus they are only briefly mentioned to complete the description of the approach.

#### 4.2.1.1. TEMPORAL INTERPOLATION

Air temperature, air humidity, fractional clear sky (from cloudiness) and wind speed are interpolated temporally using a cubic spline. Temporal interpolation for gaining values for each arbitrary point in time is a valid procedure for these variables, as they are continua. Further information on this processing step can be found in MAUSER (2002).

#### 4.2.1.2. TEMPORAL DISAGGREGATION

As precipitation occurs in form of events and thus is a discrete variable, measured values cannot be interpolated temporally. Instead they have to be disaggregated temporally to retrieve values for each simulation time step. Measured values of rainfall represent the accumulated precipitation volume collected since the last measurement. Rainfall measurements take place at the *Mannheimer Stunden*, respectively at 7:00 and 19:00 local mean time for ZAMG stations. These differences of the measurement intervals are taken into account by *AtmoStations* as far as possible to minimize the degree of inhomogeneity in the datasets (COLGAN & WEIDINGER, 2006). The basic procedure of disaggregation is described here exemplarily (see Fig. 4.5) for the case of measurements based on the *Mannheimer Stunden*.

Events are classified in two different types:

- (a) advective events with long duration and low intensity (prevailing in spring and autumn).  
An event is considered advective, if precipitation occurs on two or more succeeding time stamps.
- (b) convective events of short duration and high intensity (dominating in the summer months).  
An event is considered convective, if precipitation occurs only at one time stamp.

Depending on the type of rainfall a defined procedure disaggregates the rainfall into hourly values (see Fig. 4.5):

- (a) advective type: the rainfall volume is distributed evenly over the preceding hours.
- (b) convective type: multiplication factors divide rainfall in a bell-shaped form with a maximum equal to the half of the precipitation sum.

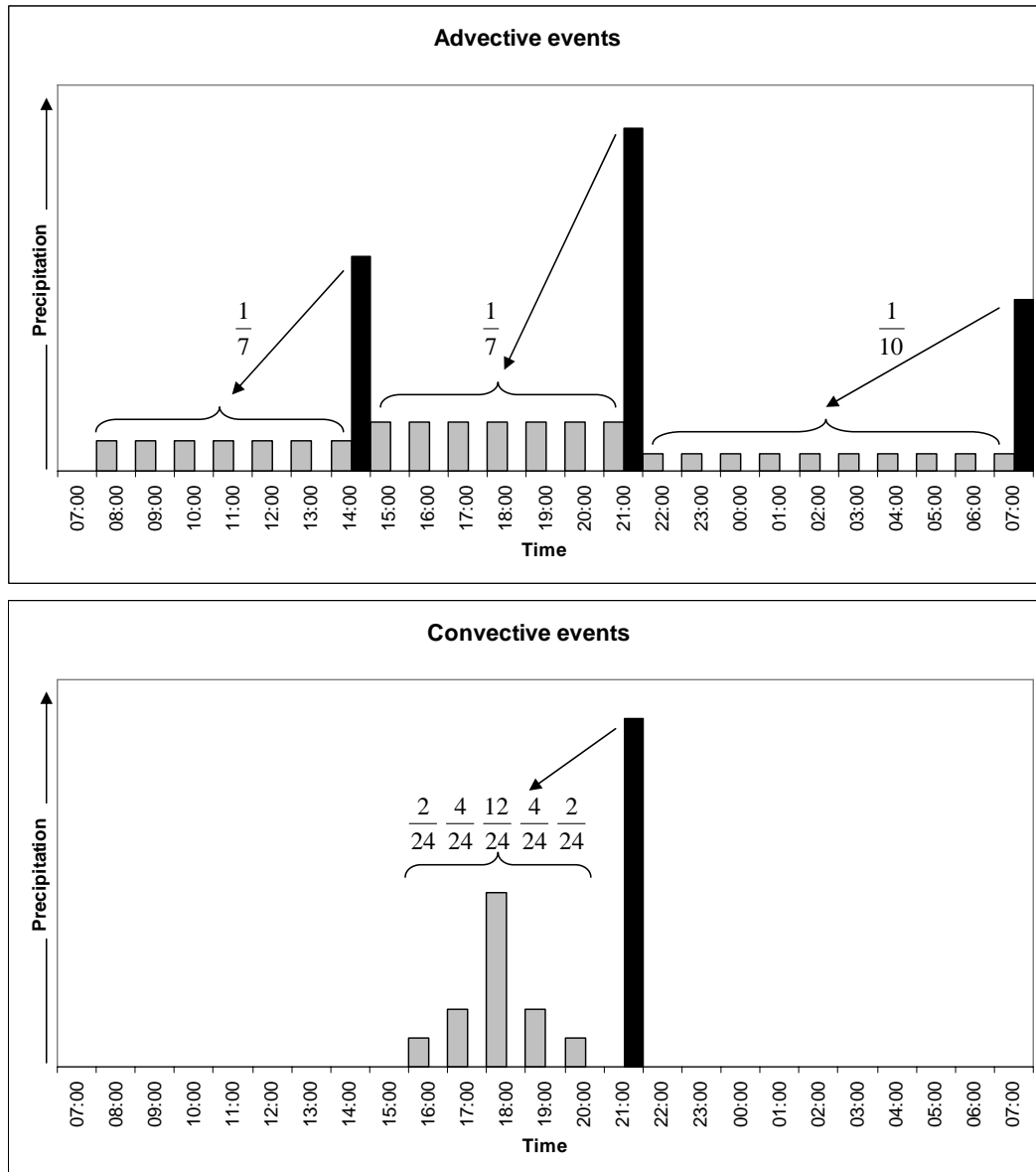


Fig. 4.5: Scheme of disaggregation methods used in AtmoStations. (black: measured values at the Mannheimer Stunden, grey: disaggregated hourly values)

#### 4.2.1.3. SPATIAL INTERPOLATION

After temporal interpolation and disaggregation, hourly values are available only for proxels with a weather station. In order to derive meteorological input parameters for all other proxels spatial interpolation is needed, which is implemented in the following manner:

1. The temporally interpolated values are used to calculate the altitudinal gradient. For that purpose a linear regression is fitted through the values of all stations regarding their elevation (see Fig. 4.6(a)). The regression equation represents the average behaviour of the respective parameter at the current model time as a function of altitude.
2. By subtraction of the measured values from the calculated values with the regression equations, the residuals are formed. This step leads to residuals for each proxel with a

weather station (see Fig. 4.6(b)).

3. It is assumed, that these residuals are independent of altitude, and thus can be interpolated in vertical directions, to achieve values for surrounding proxels with different elevation. To interpolate a value for each non-station proxel, six neighbouring stations are selected, as illustrated in Fig. 4.6(c). From the four quadrants the four nearest stations are selected, and the two stations closest to the proxel (excluding the latter four). For each of these six stations the relative Euclidean distance to the proxel (optionally either linear, quadratic or cubic) is determined. The relative distances are used as a weighting for the station values, to calculate the interpolated residual for the proxel.
4. With the regression equation from step 1 and the elevation of the proxel the average value of the corresponding meteorological parameter is calculated. Addition of the previously interpolated residual finally leads to the spatially interpolated value for the processed proxel.

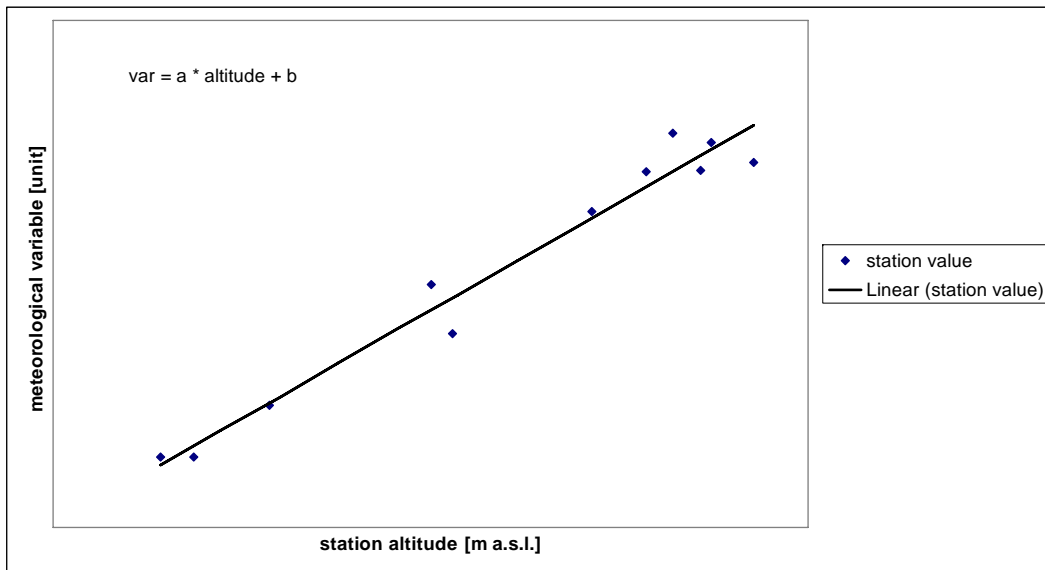
As relative air humidity shows a nonlinear dependency of temperature and therewith the altitude, it cannot directly be interpolated spatially. Therefore it is first converted to absolute humidity, then interpolated and converted back to relative humidity.

The interpolation using the described method produces good results for fields with a continuous spatial distribution, which also show a strong dependency on altitude. But the discrete parameter rainfall - especially in alpine regions - shows a high spatial variability and is strongly influenced by orographic lift resulting from the atmospheric circulation. Therefore the residuals of the linear regression cannot be applied for rainfall interpolation, and *AtmoStations* uses an adapted approach of FRÜH ET AL. (2006) to adjust interpolated rainfall intensities. They analysed monthly rainfall records of 10 years from over 2000 stations, taking into account the complex catchment orography. This results in monthly correction factors for each proxel, which are applied to the spatially interpolated rainfall intensities (in this case *not* the residuals). The resulting redistribution accounts for small-scale patterns especially in the Alps, but also in the low mountain ranges.

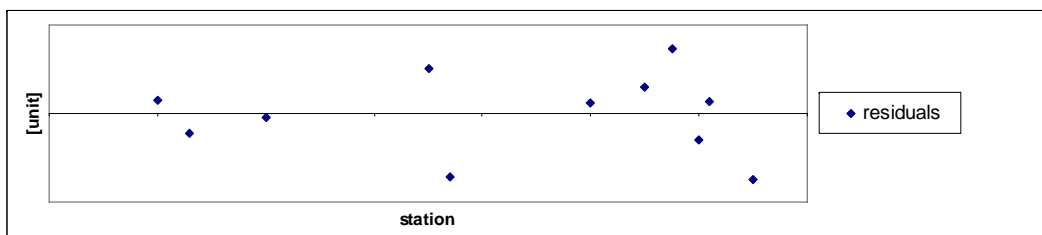
#### 4.2.1.4. COMPUTATION OF RADIATION

As incoming radiation is not measured by the climate stations, it has to be derived indirectly. *AtmoStations* calculates direct and diffuse shortwave radiation (0.3 – 3  $\mu\text{m}$ ) and longwave radiation (3 – 100  $\mu\text{m}$ ), using the following procedure:

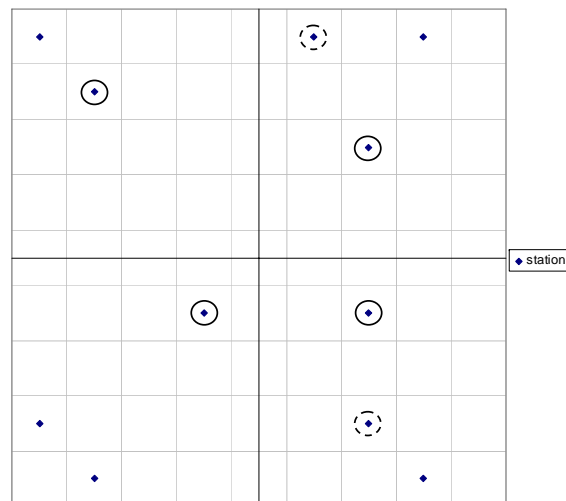
1. computation of top of atmosphere (TOA) solar irradiation from solar geometry: the current model time together with the geographic coordinates of the proxel is used to calculate sun elevation, sun azimuth and the solar constant (seasonally modified by the eccentricity of the earth's orbit)
2. calculation of atmospheric transmissivity with the topography of the proxel and a standard atmosphere profile
3. determination of the proportion of incoming direct and diffuse shortwave radiation (of the transmitted total shortwave radiation) with previously interpolated fractional clear sky



(a) Linear regression of altitudinal gradient



(b) Residuals of station values from (a)



(c) Selection of stations for interpolation (solid: nearest stations from the four quadrants, dashed: nearest remaining two stations)

Fig. 4.6: Spatial interpolation in Atmosstations (edited after MAUSER (2002))



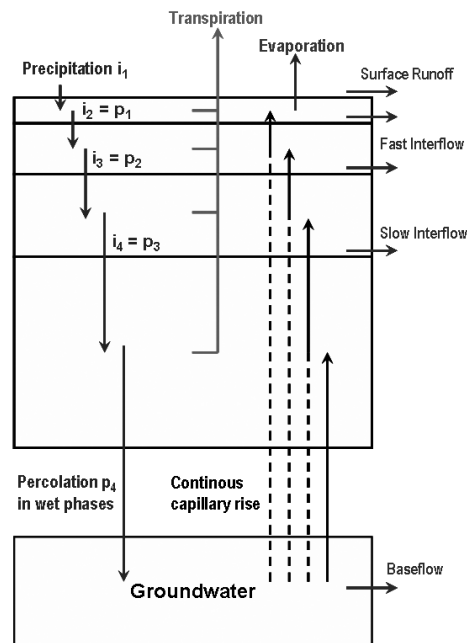


Fig. 4.7: Soil water fluxes simulated by the PROMET soil moisture module (MUERTH, 2008)

- interpolated air temperature and fractional clear sky are used to compute the incoming longwave radiation

For further information on this approach, the reader is referred to MAUSER (2002) and MAUSER & BACH (2009).

## 4.2.2. SOIL

### 4.2.2.1. WATER FLUX

The soil component consists of a soil hydraulic module for simulating vertical and horizontal water fluxes in the unsaturated soil and a soil heat transfer and storage module for modelling distributed soil temperature fields. The soil moisture module uses an approach of EAGLESON (1978) to simulate water fluxes in the soil column, which was modified (MAUSER & SCHÄDLICH, 1998) and extended by MAUSER & BACH (2009) to compute up to four soil layers. This section outlines the model descriptions given in MUERTH (2008). For a more detailed view the reader is referred to the original works. Fig. 4.7 shows the basic processes simulated in the approach. Basically water fluxes are calculated for each of the four layers, whereas every layer is characterized by its own static properties and dynamic state. Water sources into a layer can be either infiltration from above (by effective precipitation  $i_1$  or by percolation from overlying layers  $p_1$ ,  $p_2$ ,  $p_3$ ) or capillary rise from below (groundwater table or subjacent layer). Water withdrawal occurs by evaporation (from the uppermost layer), by root water uptake (from every rooted layer) or gravitational drain (every layer). Capillary rise and gravitational drain are summed up, forming the net percolation of a layer. If the net percolation from a layer exceeds the infiltration capacity of the lower layer, the excess water is discharged laterally as fast or slow interflow, or as surface runoff if it is the uppermost layer. The underlying concept of EAGLESON (1978) is the representation of the soil as a single homogeneous column, whose

water content is defined by infiltration and exfiltration. This balance is calculated by solving the *Philip* equation (PHILIP, 1957) and for validity of its solution EAGLESON (1978) claimed compliance to the following conditions:

- The groundwater table lies much deeper than the modelled soil layer. This is considered by the soil moisture module via the bubbling pressure head of the lowest soil layer (MUERTH, 2008).
- The soil moisture is uniformly distributed over the whole modelled soil compartment. Every layer modelled within PROMET is considered homogeneous, exchange occurs only at the boundaries.
- The distribution of roots must be homogeneous. This is regarded by the four layer module by allowing only different root distributions between layers, but not within a single layer.

If these requirements are fulfilled, EAGLESON (1978) assumes the following cases for in- and exfiltration:

- $i_p < f_i^*$ : if the precipitation intensity  $i_p$  is lower than the infiltration rate  $f_i^*$ , the soil is unsaturated and the water infiltrates into the column
- $i_p \geq f_i^*$ : if the precipitation intensity exceeds the infiltration rate, the soil gets saturated and water cannot infiltrate, i.e. runs off laterally at the layer surface
- $E_p < f_e^*$ : if the evaporative demand  $E_p$  is lower than the exfiltration capacity  $f_e^*$ , the demanded water can evaporate and the soil does not run dry
- $E_p \geq f_e^*$ : if the evaporation demand exceeds the exfiltration capacity, the soil runs dry and  $f_e^*$  defines the amount of evaporated water

In order to calculate the fluxes leading to the described states, EAGLESON (1978) uses an analytical solution of the *Philip* equation, which is approximated by the *Brooks-Corey* equation (BROOKS & COREY, 1964). Solving the *Brooks-Corey* equation requires knowledge of the following static soil properties:

- saturated hydraulic conductivity  $k_s$
- bubbling pressure head  $\Psi(1)$
- pore-size distribution index  $m$
- effective porosity  $n$

#### 4.2.2.2. HEAT FLUX

As PROMET offers a module for iteratively computing the surface energy balance, it is also possible, to calculate heat fluxes between the four soil layers and the atmospheric boundary layer, which occurs in the Soil Heat Transfer Module (SHTM) developed by MUERTH (2008), which is described in the following lines. The basis are one-dimensional, conductive heat

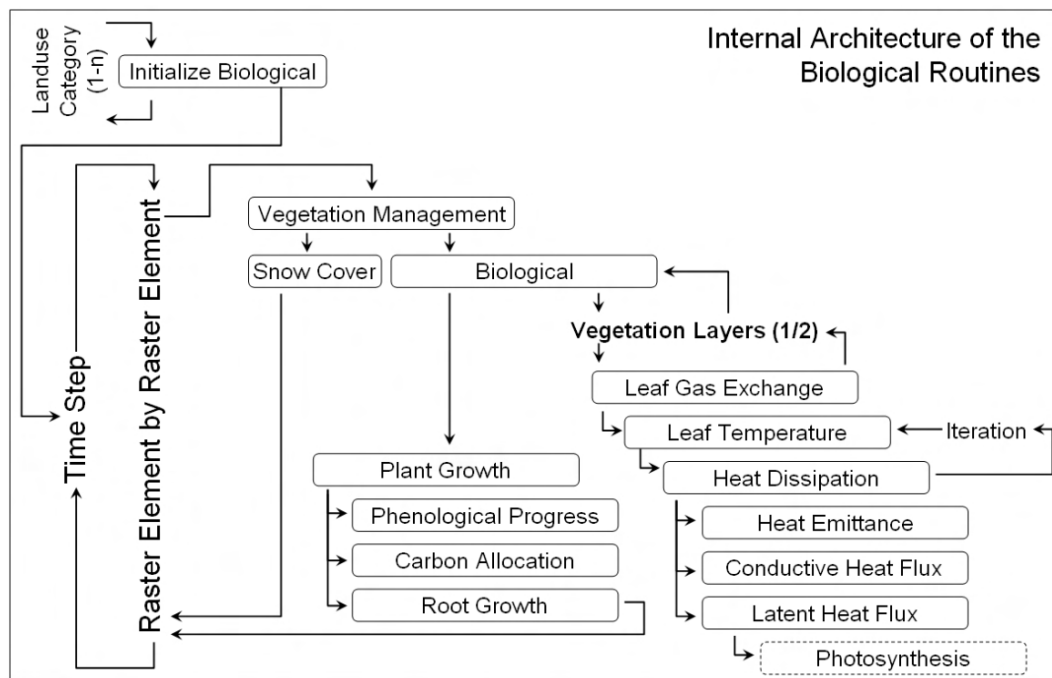


Fig. 4.8: Flowchart of the biological subroutines (HANK, 2008)

transfer equations, which are solved for each layer, thus commencing the heat flux downwards. The upper boundary condition is the soil surface temperature from the land surface energy and mass balance component. The lower boundary condition is given by an analytical solution of the virtual layer, which lies below the lowermost soil layer, depending on annual characteristics of the air temperature. The latter is dynamically updated at the end of the hydrological year from input weather data to account for annual differences in air temperature. The resulting soil temperatures of each layer also allow for simulation of soil freezing. If the layer temperature drops below the freezing point, the potentially releasable latent energy of the soil water is stored. This energy within a layer acts as a buffer, before the temperature further diminishes. When the soil finally freezes, the amount of liquid and frozen water in the soil is determined with an empirical relationship between soil temperature and freezing point temperature. Frozen soil impedes vertical water movement by a reduction of hydraulic conductivity or may even lead to ice blocking, thus increasing (surface) runoff.

#### 4.2.3. VEGETATION AND AGRICULTURAL MANAGEMENT

As already mentioned, PROMET offers two sub-components for modelling vegetation. The first one is based on the *Penman-Monteith* equation (MONTEITH, 1965) for calculation of evapotranspiration. Stomatal inhibition is described through environmental factors following approaches from JARVIS & MORISON (1981) and BALDOCCHI ET AL. (1987). Since this sub-component can not dynamically model the annual course of LAI, plant height and albedo, this section only describes the sub-component based on the approach by FARQUHAR ET AL. (1980), which models plants fully physiological and dynamically. An extensive description of the PROMET biological model can be found in HANK (2008).

As shown in Fig. 4.8, the mechanism controlling plant growth in each time step is the vege-

Tab. 4.1: Sowing and harvest dates for arable land (DOY: day of year).

Crop	Sowing [DOY]	Harvest [DOY]	Crop	Sowing [DOY]	Harvest [DOY]
Forage	67	221	Rye	283	232
Hop	114	308	Sugar beet	91	293
Legumes	114	308	Silage	114	288
Maize	114	278	Summer barley	75	221
Oat	74	237	Summer wheat	67	221
Oleaginous	232	201	Winter barley	263	201
Potato	100	263	Winter wheat	288	231

Tab. 4.2: Cutting periods for grassland. Period 1 starts with the beginning of active plant growth. For extensive grassland only two cuts per season are possible.

Grassland type	Period 1	Period 2	Period 3
Intensive	begin – 20.6.	20.7. – 15.8.	20.9. – 20.10.
Extensive	begin – 15.6.	n/a	20.9. – 20.10.

tation management routine. It particularly regulates the growth of the agricultural vegetation types (see Fig. 4.3).

All arable crops are sowed at their cultivar specific sowing date (see Tab. 4.1). This planting process enables the respective biological submodels for crop growth. After planting these subroutines decide on actual growth. Since natural vegetation and perennial crops have no sowing date, they basically start growing when the snow cover is melted. Deciduous forest is an exception, because it starts active growth with the emergence of leaves, which is controlled by the phenology submodel.

The growth period ends for all agricultural crops, when they are harvested. This is represented by the cultivar specific harvest day (see Tab. 4.1), which disables plant growth and sets the corresponding plant parameters like leaf area index [ $\text{m}^2/\text{m}^2$ ] (LAI) or plant height to zero. An exception is made for agricultural grassland, which is cut instead of harvested.

Cutting is coupled to empirically determined cutting periods and LAI values. If the begin of the cutting period is reached and the LAI exceeds a value of four, cutting is initialised. If the LAI did not reach the threshold during the period, the meadow is cut anyway. The periods for intensive and extensive grassland are shown in Tab. 4.2.

When a vegetation type enters the period of active growing the actual biological model is computed. The basis of the biological module is the leaf energy balance. It is solved through an iterative process, which approximates an equilibrium between the absorbed radiation of the leaf on the one hand, and the longwave emission, latent energy flux and conductive heat dissipation on the other. Computation of the energy balance also considers leaf gas exchange and photosynthesis of the plant, which account for primary production. The resulting fixed carbon is then distributed to the different parts of the plant. This development of the plant is controlled by its phenological stage (cf. Tab. 4.3), whose progress is modelled in dependence of the air temperature. According to the current phenological stage, carbon is distributed in different ratios to root, leaf, stem or grain of the plant (see Fig. 4.9). This means, that during the first phenological stages most of the production is used for growth of the root system.

Tab. 4.3: Phenological stages modelled by the biological module of PROMET, as defined in HANK (2008)

Name	BBCH	Name	BBCH
Pregermination	00 – 03	Harvestable vegetative parts	40 – 49
Germination	05	Inflorescence	50 – 59
Emergence	09	Flowering	60 – 69
Leaf Development	10 – 19	Fruit development	70 – 77
Side-shoot development	20 – 29	Maturity	83 – 99
Stem elongation	30 – 39		

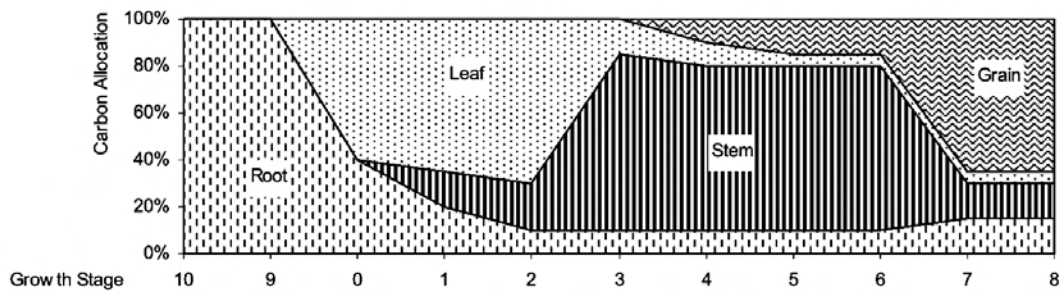


Fig. 4.9: Allocation of primary production to different plant parts depending on phenological stage. Exemplary parameters for winter wheat. (HANK, 2008)

With emergence, leaf development gains most of the productivity and the stem slowly grows. When stem elongation begins, this ratio is reversed until the beginning of fruit development, where the fruit assimilates 60% of the total carbon. This is also the point, when leaf and stem biomass start to decrease, accounting for the loss of leaves turning brown during the ripening. This reducing process continues for the roots in the maturity stadium, simulating senescence.

#### 4.2.4. CHANNEL FLOW

For routing of flow, it is assumed, that each proxel in the watershed is part of the channel network. Each proxel contains a channel and the proxels are hydraulically interconnected through topography. These assumptions mean, that for correct routing of runoff, each proxel has a lower limit to its possible area. It has empirically been validated, that the limit is well below  $200 \text{ m} \cdot 200 \text{ m}$  for the Upper Danube Basin, i.e. a proxel of  $1 \text{ km}^2$  definitely contains a channel (MAUSER & BACH, 2009). The complete amount of overland flow produced by the soil component (Section 4.2.2) is directly delivered into these channels. The interflow of each soil layer is routed according to topography from each proxel to proxel until a major tributary is encountered. The network of major tributaries is determined by a geology-dependent threshold of the upland-area (critical source area). The routing through the network occurs in a self-organising process by transferring channel flow from each proxel to its hydraulic neighbour. In order to avoid instabilities in the calculation of routing, the component uses the kinematic wave approach of the Muskingum-Cunge method as modified by TODINI (2007), which is over-clocked to a time step of 2 minutes. Channel flow, which enters a lake, is added to the water volume of the lake, and the discharge of lakes is calculated with an empirical relationship

determined by regular measurements of the discharge and the area of each lake.

### 4.3. HISTORICAL DEVELOPMENT AND STATE OF THE ART IN EROSION MODELLING

The severe problems due to soil erosion in the USA at the beginning of the 20th century (cf. Section 1.1.2) initiated the development of erosion models. According to RICHTER (1998), the first practically usable approach is represented by the USLE (WISCHMEIER & SMITH, 1965). The USLE is an empirical equation, derived from extensive measured data sets. It calculates the mean annual soil loss based on factors comprising rainfall, soil erodibility, slope length, slope gradient, cropping management and erosion control practice. In recent decades the interest in off-site effects has grown and as the USLE is not capable of modelling transport and deposition, numerous derivatives and advancements for the equation have been developed. These models are based on process-oriented, physically-based approaches, but often rely on some components from the USLE. As recently as in the 1990s another generation of models evolved, also on a physical basis, but intentionally avoiding the inclusion of any components of the USLE. Tab. 4.4 summarises some of the established models and their basic properties. For a more extensive overview of erosion models the reader is referred to MERRITT ET AL. (2003).

Tab. 4.5 shows the most important factors influencing soil erosion. Soil erosion models consider these factors to various degrees.

Empirical models usually calculate soil loss with only a few of the factors, by statistically correlating those, which are considered by the developer to be the most important ones, to soil loss. This requires extensive field measurements and hence is limited to the regional conditions where it was developed. The most popular example is the USLE, which was developed in the USA over 20 years, but in order to be applicable in other regions, it was comprehensively adapted (e.g. for Germany by SCHWERTMANN (1981), West Africa, or India (both stated in KLISCH (2003))). The advantage of such an approach, once it is adapted, is the user-friendly applicability, which often even allows for calculation in situ by the farmer himself, i.e. without extensive hard- and software requirements (e.g. an LfL-booklet (LfL, 2005)). A drawback is, that only a long-term annual mean value can be calculated, i.e. simulation of single events is not possible, and further on, temporal and spatial variability of input parameters is not considered. This basically renders e.g. the USLE unsuitable for Global Change assessment, respectively requires further adaptations, as e.g. incorporated in the RUSLE.

Physically based models in contrast, make use of many more input parameters, often even more than those listed in Tab. 4.5, and link these with physical equations to calculate erosion processes. The vast number of input parameters they require (which in contrast are implicitly included in empirical equations in their lumped parameter set), usually demands a lot of work until they can be operated on the desired plot or catchment. The physical basis of such models generally provides them with spatial and temporal independence, making them universally applicable in theoretically any arbitrary region. Nevertheless they often rely on or incorporate empirical components, as the processes involved are too complex to model them on a truly physical basis. But process orientation and the usage of physical base units makes sub-components of the models more exchangeable and extensible.

As mentioned, the temporal representation of erosion models is either based on a sin-

Tab. 4.4: Basic properties of selected erosion models (compiled from RICHTER (1998); KLISCH (2003); DEINLEIN & BÖHM (2000) and quoted literature, pb: physically based).

Model	Approach (detach- ment/transport)	Spatial represen- tation	Temporal basis	Developer
USLE	empirical (n/a)	plot/field	long-term annual mean	WISCHMEIER & SMITH (1965)
ABAG	USLE adaptation	plot/field	long-term annual mean	SCHWERTMANN (1981)
RUSLE	revised eqs. of USLE, pb	plot/field	long-term annual mean	RENARD ET AL. (1996)
CREAMS	USLE- based/transport capacity, pb	plot/field, pb	single event	KINSEL (1980)
EPIC	USLE and deriva- tives, pb	plot/field	continuous	WILLIAMS ET AL. (1983)
EUROSEM	transport capac- ity/sediment con- centration, pb	plot/field & catch- ment	single event	MORGAN ET AL. (1998)
EROSION 2D	momentum flux/transport capacity, pb	plot/field	single event	SCHMIDT (1996)
WEPP	shear stress/transport capacity, pb	plot/field & catch- ment	continuous	FLANAGAN & NEARING (1995)
KINEROS	transport capac- ity/sediment con- centration, pb	watershed	single event	WOOLHISER ET AL. (1990)

Tab. 4.5: Basic factors influencing soil erosion by water (KLISCH, 2003).

Climate	Relief	Soil	Vegetation	Management
rainfall intensity	slope length	particle size dis- tribution	land use	date of tillage
rainfall duration	slope gradient	bulk density	canopy cover	type of tillage
rainfall frequency	slope shape catchment area	soil structure water content  organic matter content permeability cation exchange capacity shear strength sealing plant litter roughness	vegetation height rooting depth	depth of tillage protection mea- sures

gle long-term annual mean value (empirical models), or on a single event (physically based models). Some models are also capable of a continuous simulation, as they include sub-components for dynamic computation of plant growth, soil consolidation, etc. Concerning the spatial representation, models deal with input parameters and process calculations either in a lumped or a distributed way. Lumped models treat the input parameters as lumped over the whole area of analysis, e.g. the USLE describes a plot or a field with a single parameter set and calculates the output for this unit. Distributed models reflect the spatial variability by sub-dividing the whole area into smaller units, which are calculated (and parameterised) separately. This distribution may consist of homogeneous irregular-sized units, or a regular grid.

In the early years of development of erosion models, these have been kept simple, because extensive use of computer aided calculation was not available. But also nowadays these early models are often used for assessment of soil erosion or incorporated in other models, especially when considering large areas (e.g. the USLE used in Modelling Nutrient Emissions in River Systems (MONERIS) (BEHRENDT ET AL., 2007)). Application of physically based models above the watershed/catchment scale is rarely executed, on the one hand due to the extensive parameterisation, and on the other hand these models usually need calibration data to work properly, which is not available at larger scales. So generally only for modelling on the catchment scale or at smaller scales, there is a clear trend to physically based modelling, as they respond to single events and allow for physical interpretation of modelling results.

#### 4.4. SELECTION OF THE APPROACH FOR EROSION MODELLING

This chapter is intended to select the appropriate modelling approach for implementation within PROMET. Since modelling of erosion is performed within a land surface model, it is only necessary to identify the approach, i.e. the governing equations for modelling of the erosion processes. A complete modelling framework which is capable of simulating runoff routing, plant growth, etc. is not required, as such sub-models are already available in PROMET (cf. Section 4.2).

Due to the considerable amount of soil erosion models, a list of requirements was compiled, in order to filter out the appropriate model approaches. Some erosion models are essentially based on the same governing equations, they merely differ in sub-components, such as computation of infiltration, or connection of spatial computation units to a whole catchment. Since this study is only interested in the governing equations regarding erosion processes, only the most important existing models are mentioned here. For more detailed reading and summaries of the models, the reader is referred to reviews of e.g. MERRITT ET AL. (2003) or SAAVEDRA (2005).

The following requirements are considered to be *necessarily* fulfilled for successful adaptation into PROMET within the Upper Danube catchment:

- The model must be freely available, respectively at least the governing equations must be published and documented.
- The model must be physically based, as it shall be used for simulating Climate Change scenarios. Even if empirical or semi-empirical models are able to react adequately on



changing external conditions, it is hardly or not at all possible to physically interpret the reactions and the model behaviour.

- The model must not rely on intensive calibration to measured data, as this cannot be performed for the large extent of the Upper Danube Basin. Calibration may also lose its validity when climate conditions change in the future.
- The model must be able to simulate single events. It may not produce temporally lumped outputs only (e.g. monthly or annual).

Further on the following requirements *should* be fulfilled for a straightforward adaptation:

- The applicable scale of the model should range in the correct dimension. This needs not to be fulfilled for the whole model, as only the governing equations will be used. But the internal process representation of the governing equations needs to be valid for the considered scale.
- The input parameters should be directly acquirable for the Upper Danube Basin, i.e. the effort of extensive regionalisation of parameters should be avoided.

Regarding the first two requirements - free availability and a physical basis - the list of models reduces to the following: Areal Nonpoint Source Watershed Environment Response Simulation (ANSWERS), European Soil Erosion Model (EUROSEM), EROSION 2D, Water Erosion Prediction Project (WEPP), A Field Scale Model for Chemicals, Runoff, and Erosion for Agricultural Management Systems (CREAMS) and Erosion Productivity Impact Calculator (EPIC).

Although the models ANSWERS, CREAMS and EPIC represent processes on a physical base, particle detachment is modelled with empirical factors of the USLE, which cannot be physically quantified. Therefore they were considered to be inappropriate for the purpose of this work.

The basis of the modelling approach of the WEPP model, which was intended to replace the USLE, sounds promising as it models detailed processes on a physical base. This is the reason, why WEPP needs a very high amount of input parameters, which are difficult to gain. According to MERRITT ET AL. (2003) many of the model parameters may need to be calibrated against observed data, which causes problems with the physical interpretability of the model.

The approaches of the two remaining models - EUROSEM and EROSION 2D - are compared in the following:

- Particle detachment
  - EUROSEM: Detachment by raindrops is calculated with the kinetic energy of the drops and the detachability of the soil. For computation of detachment by runoff, the transport capacity of the flow and the detachability determine the amount of detached material.
  - EROSION 2D: The momentum flux of rainfall and runoff is calculated, which is compared to the resistance the soil can bring up. The ratio between these forces determines the amount of detached material.
- Particle transport

- EUROSEM: The transport of detached particles is modelled as a function of unit stream power in rills, and a modified function for interrill flow transport.
- EROSION 2D: The momentum fluxes of rainfall and runoff act opposed to the sinking velocity of the soil particles. The ratio between the opposing forces determines the amount of material, which can be transported.

Finally it was decided to adapt the model EROSION 2D for this study, for the main reason, that it apparently does not require extensive calibration. A comparison of physically based erosion models in the same catchment with identical conditions (JETTEN ET AL., 1999) yielded similar good result for both models, but EUROSEM required more effort in calibration than EROSION 3D<sup>1</sup>. In the same catchment, FOLLY ET AL. (1999) calibrated three parameters for the runoff sub-model and three parameters for the erosion model itself, before running the model. SCHMIDT ET AL. (1997) on the other hand, calibrated only one parameter for the runoff sub-model. Other reasons for the selection of EROSION 2D are:

- It requires considerably less input parameters than EUROSEM,
- it is better documented (e.g. SCHMIDT (1996); SCHMIDT ET AL. (1996)),
- a catalogue of input parameters is readily available (SCHMIDT ET AL., 1996), and
- it is in operational use in Saxony by environmental and agricultural offices (BLA-GEO, 2003).

## 4.5. THE SOIL EROSION MODULE

This section describes the erosion module for PROMET developed during this study. Fig. 4.10 shows an overview of the model, including the modifications and extensions which have been made to the original EROSION 2D model.

### 4.5.1. BASIC CONCEPT OF EROSION 2D

The basic concept of the model EROSION 2D developed by SCHMIDT (1996) essentially consists of two parts: particle detachment on the one hand, and particle transport on the other hand. Particle detachment is induced by the impacts of rainfall and runoff, which exert forces on the soil particles. If these exceed the forces holding the soil particles, detachment occurs. Detached particles then are transported, if the flow force of the surface runoff compensates the sinking movement of the detached particles within the flow.

#### 4.5.1.1. PARTICLE DETACHMENT

For particle detachment the mobilising forces of the fluid acting on the soil – given by rainfall and runoff – have to be greater than the forces holding the soil particles – mainly gravity and cohesion between the soil particles. The mobilising forces depend on the velocity and mass of rainfall and runoff, quantified by the respective momentum fluxes.

<sup>1</sup>EROSION 3D is based on the same equations as EROSION 2D, but it extends the approach for three-dimensional, lateral mass fluxes, whereas EROSION 2D is only capable of modelling a two-dimensional plot.

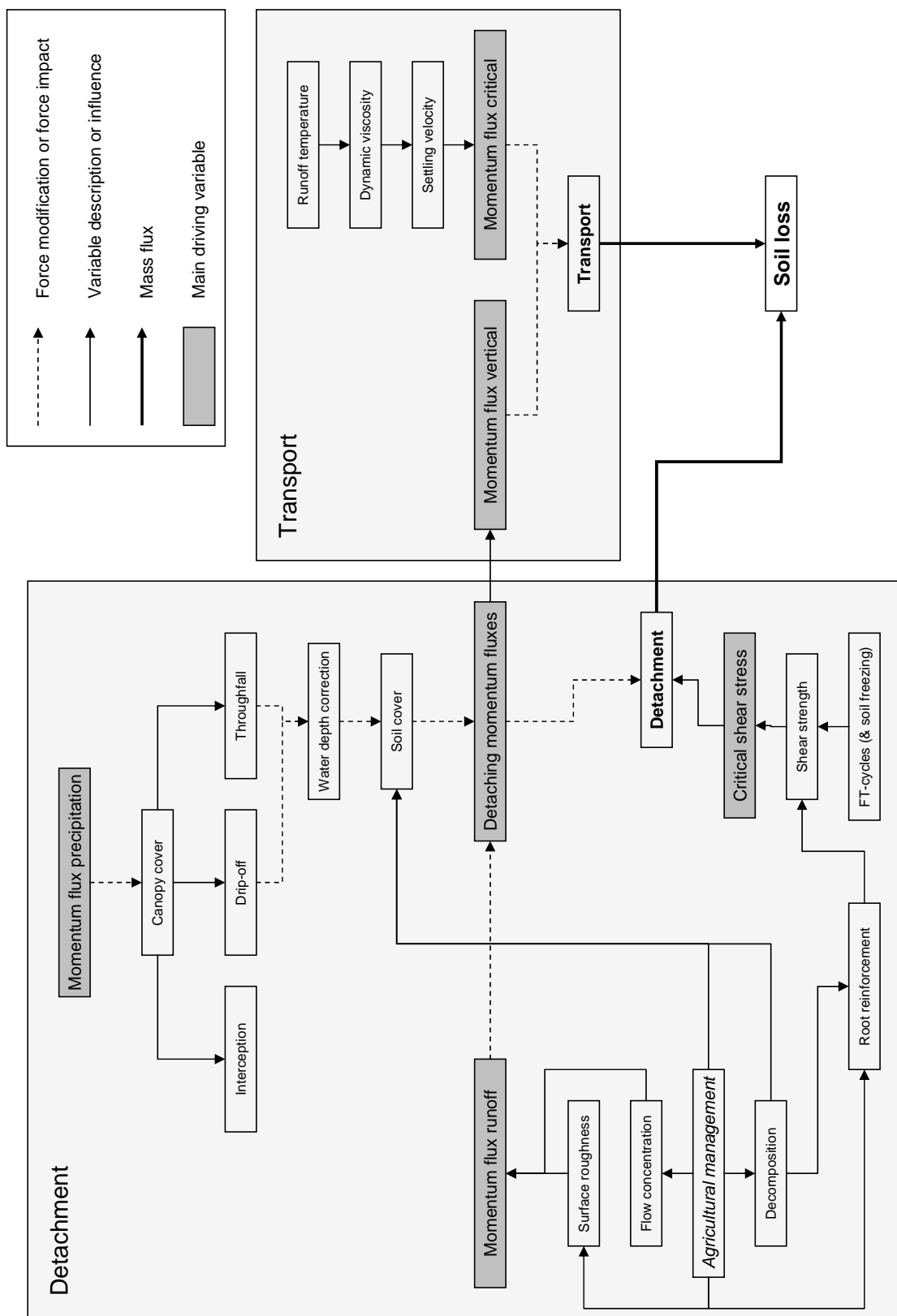


Fig. 4.10: Simplified overview of the erosion module developed in this study. Only dynamic components are included in this illustration, static input parameters are omitted for reasons of clarity.

SCHMIDT (1996) intentionally simplifies the actual runoff behaviour in his approach, as flow paths cannot be defined for the scale applied, due to the heterogeneous surface conditions and its strong temporal variability.

The momentum flux of the surface runoff is defined as

$$\varphi_q = \frac{w_q \cdot v_q}{\Delta x} \quad (4.1)$$

with  $\varphi_q$ : momentum flux of surface runoff [ $\text{N}/\text{m}^2$ ],  $w_q$ : mass flux of surface runoff [ $\text{kg}/\text{ms}$ ],  $v_q$ : mean velocity of surface runoff [ $\text{m}/\text{s}$ ] and  $\Delta x$ : length of slope segment [ $\text{m}$ ].

Mass flux  $w_q$  and discharge rate  $q$  are calculated with

$$w_q = q \cdot \rho_q \quad (4.2)$$

$$q = (r_\alpha - i) \cdot \Delta x + q_{in} \quad (4.3)$$

with  $q$ : discharge rate [ $\text{m}^3/\text{ms}$ ],  $\rho_q$ : density of surface runoff [ $\text{kg}/\text{m}^3$ ],  $r_\alpha$ : precipitation intensity [ $\text{m}/\text{s}$ ],  $i$ : infiltration rate [ $\text{m}/\text{s}$ ] and  $q_{in}$ : inflow from above [ $\text{m}^3/\text{ms}$ ].

Runoff velocity is calculated with the established *Manning* formula:

$$v_q = \frac{1}{n} \cdot \delta^{\frac{2}{3}} \cdot S^{\frac{1}{2}} \quad (4.4)$$

with  $n$ : Manning's friction coefficient [ $\text{s}/\text{m}^{\frac{1}{3}}$ ],  $\delta$ : depth of flow [ $\text{m}$ ] and  $S$ : slope [ $\text{m}/\text{m}$ ].

Actually the variable  $\delta$  represents the hydraulic radius in the original formula. But assuming, that runoff occurs as thin sheet flow only, the hydraulic radius can be replaced with the depth of flow  $\delta$ , calculated by

$$\delta = \left( \frac{q \cdot n}{S^{\frac{1}{2}}} \right)^{\frac{2}{3}} \quad (4.5)$$

The momentum flux of the raindrops exerted on the soil surface is defined analogue to the momentum flux of the runoff:

$$\varphi_r = w_r \cdot v_r \quad (4.6)$$

with  $\varphi_r$ : momentum flux of raindrops [ $\text{N}/\text{m}^2$ ],  $w_r$ : mass flux of raindrops [ $\text{kg}/\text{m}^2\text{s}$ ] and  $v_r$ : mean fall velocity of raindrops [ $\text{m}/\text{s}$ ].

The mass flux of the raindrops is represented by

$$w_r = r_\alpha \cdot \rho_r \quad (4.7)$$

with  $r_\alpha$ : rainfall intensity related to the slope [ $\text{m}/\text{s}$ ] and  $\rho_r$ : density of raindrops [ $\text{kg}/\text{m}^3$ ].

The slope influences the effect of the raindrops in two ways. Firstly, the impact of the raindrops is attenuated with increasing slope (Eq. (4.8)), as the projected area gets larger. And secondly, only the component of the momentum flux directed downwards the slope contributes to splash erosion. Therefore  $\varphi_r$  is corrected with the sine of the slope (Eq. (4.9)), thus becoming zero on plain surfaces.

$$r_\alpha = r \cdot \cos \alpha \quad (4.8)$$

$$\varphi_{r,\alpha} = w_r \cdot v_r \cdot \sin \alpha \quad (4.9)$$

with  $r$ : rainfall intensity [ $\text{m}/\text{s}$ ] and  $\alpha$ : slope [ $^\circ$ ].

Raindrop fall velocity is calculated with an empirically derived correlation between rainfall intensity and fall velocity. LAWS (1941) related fall velocity of raindrops to mean drop size and this in turn to intensity (LAWS & PARSONS, 1943), leading to:

$$v_r = 4.5 \cdot r^{0.12} \quad (4.10)$$

with  $v_r$ : mean fall velocity of raindrops [m/s] and  $r$ : rainfall intensity [mm/h].

As vegetation protects soil particles from direct detachment by raindrops, the attenuating influence of canopy cover is considered with:

$$c_c = \frac{A_{leaf}}{A} \quad (4.11)$$

with  $c_c$ : fractional canopy cover [-],  $A_{leaf}$ : projected leaf area [m] and  $A$ : total projected area [m].

Applying Eq. (4.7) – Eq. (4.11) on Eq. (4.6) finally results in

$$\varphi_{r,\alpha} = r_\alpha \cdot \rho_r \cdot v_r \cdot \sin \alpha \cdot (1 - c_c) \quad (4.12)$$

The above equations allow for calculation of the mobilising forces, i.e. the sum of the momentum flux of raindrops and runoff. In order to determine the actual detachment of the soil, one needs to know the resisting forces of the soil. In order to define this erosion resistance, SCHMIDT (1996) uses the fact, that emergence of measurable sediment deposition requires a critical minimum discharge  $q_{crit}$ . The size of  $q_{crit}$  depends on specific properties of the inundated surface and is a measure of the resistance, which the soil matrix opposes the forces of the acting fluid forces. Substituting  $q_{crit}$  into Eq. (4.2) respectively Eq. (4.1) leads to the critical momentum flux

$$\varphi_{crit} = \frac{q_{crit} \cdot \rho_q \cdot v_q}{\Delta x} \quad (4.13)$$

which characterises the specific erodibility of the soil analogue to the previously defined equations for computation of momentum flux (Eq. (4.1) and Eq. (4.6)). The critical discharge  $q_{crit}$  in Eq. (4.13) which initiates erosion, was determined by SCHMIDT (1996) in flume experiments for various setups. The formal conformity of the momentum fluxes of rainfall and runoff with the critical momentum flux  $\varphi_{crit}$  allows for combination of these into the dimensionless erosion coefficient  $E$ :

$$E = \frac{\varphi_q + \varphi_{r,\alpha}}{\varphi_{crit}} \quad (4.14)$$

$\varphi_{crit}$  designates the force of rainfall and runoff required to detach soil particles. Its opposing force, the resistance of the soil against detachment, is therefore called erosion resistance. The erosion coefficient  $E$  then indicates the ability of the current conditions to cause soil erosion. For derivation of a quantitative correlation SCHMIDT (1996) experimentally analysed the relation between the sediment mass flux  $q_{s,pot}$  and the erosion coefficient  $E$ , which resulted in the following formula:

$$q_{s,pot} = (1.75 \cdot E - 1.75) \cdot 10^{-4} \quad (4.15)$$

where  $q_{s,pot}$  [kg/ms] represents the potential amount of detachable particles per unit of area and unit of time, if the transport capacity of the flow is sufficiently high. If  $E > 1$  the forces released by raindrop impact and overland flow exceed the erosion resistance of the soil. Values of  $E \leq 1$  represent flow conditions without particle detachment.

#### 4.5.1.2. PARTICLE TRANSPORT

For particle transport the forces holding particles in suspension, i.e. vertical turbulences, have to be greater than the forces dragging the particles down, i.e. gravity.

Downward movement of soil particles is modelled after *Stokes' law*:

$$v_p = \frac{D^2 \cdot (\rho_p - \rho_q) \cdot g}{18 \cdot \eta} \quad (4.16)$$

with  $v_p$ : settling velocity of the particles [m/s],  $D$ : particle diameter [m],  $\rho_p$ : particle density [kg/m<sup>3</sup>],  $\rho_q$ : density of the fluid (runoff) [kg/m<sup>3</sup>],  $g$ : gravitational acceleration [m/s<sup>2</sup>] and  $\eta$ : dynamic viscosity of the fluid (runoff) [kg/ms].

Actually Stokes' law is only valid for spherical objects with very small *Reynolds numbers*, i.e. when inertia of the fluid is negligible. But as the main concern is the relative behaviour of the particles depending on their grain size, rather than absolute values of the settling velocity, SCHMIDT (1996) represents these processes simplified with Eq. (4.16). In this way the number of particles in the fluid, which influences the settling velocity, is also neglected.

Analogue to the critical momentum flux detaching particles, a critical momentum flux of the particles can be defined (Eq. (4.18)), indicating the downward movement of the particles. If  $\varphi_{p,crit}$  is undercut, particles begin to settle.

$$\varphi_{p,crit} = w_p \cdot v_p \quad (4.17)$$

where the mass flux of the settling particles  $w_p$  [kg/m<sup>2</sup>s] can be expressed as:

$$w_p = c \cdot \rho_p \cdot v_p \quad (4.18)$$

with  $c$ : concentration of suspended particles.

A vertical component of the momentum flux of the sheet flow  $\varphi_{q,vert}$  opposes the critical momentum flux of the particles  $\varphi_{p,crit}$ . It is assumed, that  $\varphi_{q,vert}$  is a part of the total momentum flux, which is composed of the surface runoff and the raindrop impact:

$$\varphi_{q,vert} = \frac{1}{\kappa} \cdot (\varphi_q + \varphi_{r,\alpha}) \quad (4.19)$$

where  $\kappa$  represents a dimensionless deposition coefficient, affecting the relative ratio of  $\varphi_{q,vert}$  to the total momentum flux. Analysis of experimental data led, according to SCHMIDT (1996), to a value of  $\kappa$  in the order of approx. 1000.

After reaching transport capacity the vertical component of the momentum flux equals the critical momentum flux of the particles in suspension:

$$\varphi_{q,vert} = \varphi_{p,crit} \quad (4.20)$$

Substituting Eq. (4.17) – Eq. (4.19) into Eq. (4.20) and solving the equation for  $c$  leads to:

$$c_{max} = \frac{1}{\kappa} \cdot \frac{\varphi_q + \varphi_{r,\alpha}}{\rho_p \cdot v_p^2} \quad (4.21)$$

with  $c_{max}$ : concentration of particles at transport capacity [m<sup>3</sup>/m<sup>3</sup>].

The maximum sediment mass flux which can be transported  $q_{s,max}$  [kg/ms] can then be calculated as:

$$q_{s,max} = c_{max} \cdot \rho_p \cdot q \quad (4.22)$$

### 4.5.1.3. PARTICLE SIZE DISTRIBUTION

As the transport capacity (Eq. (4.22)) is calculated depending on particle size, EROSION 2D is capable of modelling particle size distributions in the transported sediment. Simplifying assumptions by SCHMIDT (1996) concerning sediment transport are:

- Particle detachment always occurs in the ratio, in which the particles exist in the soil of the observed segment. This means, that particle size distribution initially resembles the distribution of parent substrate.
- Particle detachment always occurs in the same fractions, which the soil is composed of. This means, that particle size distribution initially resembles the distribution of parent substrate.
- Transport capacity is calculated separately for each particle diameter of the respective particle class to be modelled. Within each particle class the detachment of soil particles per unit of area and unit of time is limited by this particle specific transport capacity.
- the *potential* mass flux of detached sediment  $q_{s,pot}$  at location  $x$  can only be greater or equal than  $q_{s,pot}$  at location  $x - 1$ , as firstly all sediment is routed downwards, and afterwards the transport capacity is determined.

Based on these assumptions the following cases of sediment transport can be distinguished:

1.  $q_{s,pot} \geq q_{s,max}$  in all particle classes: particle specific transport capacity limits the actual transport of detached sediment in every particle class. Actual sediment mass flux  $q_{s,i}$  for each particle class  $i$  then corresponds to the transport capacity of the particle class:  $q_{s,i} = q_{s,max,i}$
2.  $q_{s,pot} < q_{s,max}$  in all particle classes: if transport capacity in each particle class is higher than the actually detached sediment, sediment mass flux is set to the quantity of detached material:  $q_{s,i} = q_{s,pot,i}$
3. a combination of the latter two in some particle classes: i.e.  $q_{s,pot} < q_{s,max}$  in some particle classes; for these classes  $q_{s,i} = q_{s,pot,i}$  holds, and for the rest  $q_{s,i}$  is set to  $q_{s,max,i}$ .

### 4.5.1.4. EROSION AND DEPOSITION

Applying above equations on each unit of area and unit of time, net deposition can be calculated as:

$$\gamma = \left( \frac{q_{s,in} - q_{s,out}}{\Delta x} \right) \quad (4.23)$$

with  $q_{s,in}$ : sediment delivery from segment above [kg/ms],  $q_{s,out}$ : sediment delivery out of the segment [kg/ms] and  $\gamma$ : net deposition [kg/m<sup>2</sup>s] (i.e. erosion if  $\gamma < 0$  and deposition if  $\gamma > 0$ ).

#### 4.5.1.5. LIMITATIONS AND SIMPLIFICATIONS OF THE MODEL

In order to represent the erosion processes in a physically based mathematical model, simplifications and limitations regarding the process descriptions have to be made. This section deals with these assumptions made by SCHMIDT (1996) during the development of EROSION 2D. In the following sections some changes and extensions to the original model, which have been made in the context of this work, are explained. The following list summarises the major simplifications (for a detailed list of intrinsic limitations the reader is referred to SCHMIDT (1996)):

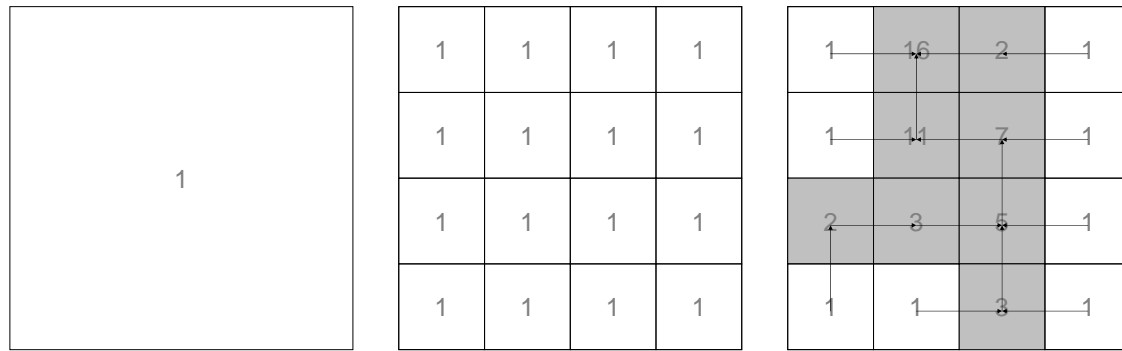
- The influence of suspended sediment on runoff behaviour is neglected.
- The model applies only for transport of primary particles in suspension. These are moved by forces of turbulent flow. The transport of larger particles ( $> 1 \text{ mm}$ ) and aggregates as bedload cannot be represented.
- Precipitation is distributed uniformly over the considered area. The angle of incidence of the rain drops and the influence of wind on the behaviour of the drops is not considered.
- The model is valid predominantly for sheet erosion, as it does not contain an approach to describe flow paths (in contrast to the three-dimensional version EROSION 3D (VON WERNER, 1995)). In the present study an approach to implicitly take rill erosion and flow paths into account was introduced (Section 4.5.2).
- The effects on soil detachment through water dripping from leaves is neglected, as well as canopy interception. The representation of interception and leaf drip is included in the soil erosion module of PROMET and is discussed in Section 4.5.4.1.
- The infiltration component of EROSION 2D simplifies some processes, but as PROMET has its own soil module, these are not relevant for the context of this study, and therefore not mentioned here.

#### 4.5.2. FLOW CONCENTRATION AND PARTICLE DETACHMENT DEPENDENT ON SCALE

##### 4.5.2.1. THEORETICAL CONSIDERATIONS

Most physically based erosion models compute on a high spatial and temporal resolution. EROSION 2D uses time step of  $10 \text{ min}$ , and an internal spatial resolution of  $1 \text{ m}$ . Adapting this model to a coarser resolution, i.e. to  $1 \text{ km}^2$  as used in this study, means an information loss concerning flow paths and runoff accumulation. Fig. 4.11 illustrates this problem. The modelled surface runoff, which is passed from the soil component of PROMET to the erosion model, merely represents an areal mean value of the whole proxel (Fig. 4.11(a)). This could be e.g.  $1 \text{ mm}$  and quantifies, if multiplied with the unit area, the total surface runoff leaving this unit (in an arbitrary time step). So calculating the erosion routines on this unit area means converting the given input surface runoff value to the internal computation unit of the erosion module. This leads theoretically (if other subscale factors, such as slope, are neglected) to the same result, as calculating the same routines repeatedly on a higher spatial resolution (see Fig. 4.11(b)), because the input parameters (based on another resolution)

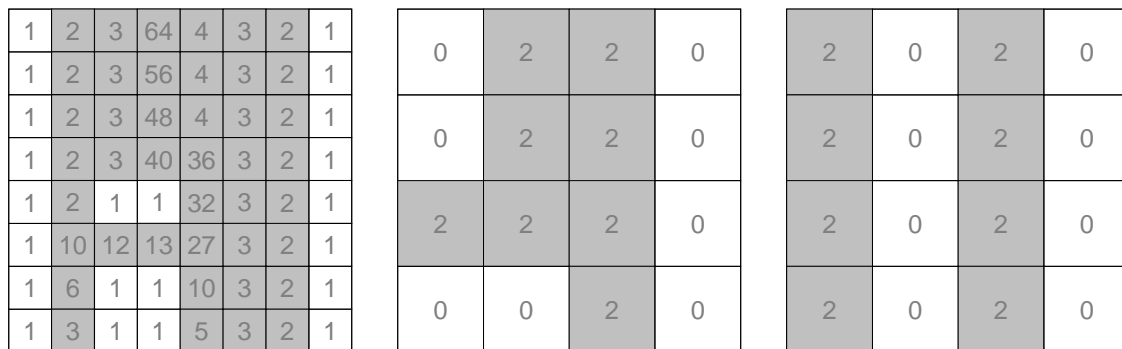




(a) Representation of a single spatial computation unit, i.e. a whole proxel as illustrated in (a). Each sub-unit has a surface runoff of 1 mm, distributed equally over the proxel.

(b) subscale representation of the proxel in (a), but with subscale information on the flow paths and directions. Since no subscale information is available, the surface runoff is distributed evenly.

(c) subscale representation of the proxel in (a), but with subscale information on the flow paths and directions.



(d) Illustration of (c) with doubled spatial resolution. (The arrows indicating the flow direction have been omitted for the purpose of clarity).

(e) Same representation of the proxel in (c), but with no subscale information on the flow directions.

(f) Abstract representation of the proxel in (c), but with no subscale information on the flow directions. Fig. 4.12

*Fig. 4.11: Subscale effects on flow concentration and particle detachment. The arrows indicate the flow paths of surface runoff. Gray colour denotes the areas where runoff concentrates.*

are likewise converted to the same internal resolution. But calculating the erosion routines either based on a whole proxel, or on a multiple of sub-proxels, means neglecting any flow concentration. Fig. 4.11(c) shows the flow paths of the proxel, if subscale information was available. The difference to the previous illustrations is, that the sub-proxels do no longer contain the mean values, but runoff concentrates along the relief. The total discharge leaving the proxel accumulates in a single sub-proxel, which represents the outlet. It is obvious, that along the flow path the amount of collected runoff is much higher and therefore has much more energy to detach (and transport) particles, but the total amount leaving the proxel is the same. It is just the sum of the runoff discharging on a small outlet. This leads to the crucial question, which spatial resolution is required to adequately represent runoff behaviour and resultant particle detachment.

Among various other studies, VON WERNER (1995) already dealt with this question during

the development and evaluation of the three dimensional version of EROSION 2D, which is able to simulate flow paths. He tested the model EROSION 3D with identical input data sets, varying only the spatial resolution from 2.5 m to 100 m. The test site had an area of 0.78 km<sup>2</sup> and the net erosion for the simulated event varied from 0.14 (at 100 m) to 0.73 (at 2.5 m) tons per hectare, with a measured net erosion of approx. 0.3 tons per hectare. He concludes, that the optimum resolution for his test site constitutes between 10 and 20 m, as very high resolution overestimates (inadequate process representation by the model) and very low resolution underestimates (inadequate representation of input parameters) net erosion. The main reason for the above mentioned overestimation of erosion, is the accumulation of surface runoff in flow paths. On a coarser resolution, runoff would be distributed over a larger area, whereas at fine resolution, the concentration leads to high discharge amounts and detachment rates. Such concentrated flow paths would have to be treated as drainage channel by the model EROSION 3D, in order to avoid further accumulation and particle detachment.

This can be demonstrated with some theoretical considerations based on Fig. 4.11. As already noted, the the total runoff amount from Fig. 4.11(b) equals Fig. 4.11(c), but the forces acting on the subscale units increase. So if a grid with yet a higher resolution is assumed (see Fig. 4.11(d)), the flow concentration would once more increase, resulting in higher detachment rates. The important question then is, if this grid represents processes better, or if there are processes on this scale, which cannot be comprised (as e.g. sediment transport in channels), thus leading to simulation errors.

Another problem, irrespective of spatial resolution, is the availability of subscale information on measures, like pipeworks, drainage channels or vegetation strips, disturbing the drainage network. Imagining a vertical drainage channel in Fig. 4.11(c) separating the upper half from the lower half of the proxel, the channel would discharge all of the runoff from the lower part out of the proxel. It would be lost for the upper half, and the three affected, gray coloured proxels would only gain 2, 4 and 8 (instead of 7, 11 and 16) units of surface runoff along the flow path. VON WERNER (1995) actually encountered such problems on a catchment size of 0.78 km<sup>2</sup>, which is less than the area of a single proxel of 1 km<sup>2</sup>, as used in this study. It is virtually impossible to gain subscale information about drainage networks (or structures like vegetation strips with similar effects) on such an areal extent as the Upper Danube Basin.

Therefore an approximation of subscale flow concentration is introduced here, which is illustrated in Fig. 4.11(e). The basic assumption is, that the whole runoff volume concentrates on a certain definable area of the proxel. But as no subscale information on flow paths is available and the outlet of the proxel is unknown, a redistribution of the whole runoff volume of the proxel is carried out, where the *sum* of the subscale unit runoff must equal the total proxel volume. Thus the runoff is accumulated along its flow path, whereas the other subproxels do not receive any runoff in order to conserve the total outflow volume. Note, that there are no arrows drawn in Fig. 4.11(e) indicating the flow direction (like in Fig. 4.11(b)), as the flow direction essentially is irrelevant. The important aspect is, that usually a certain threshold of force acting on the soil, has to be exceeded to initiate particle detachment (as discussed below). Assuming, this threshold is overcome at a runoff volume above 1 unit, it can be seen, that the situation in Fig. 4.11(b), does not produce an detachment of soil. A comparison between Fig. 4.11(c) and Fig. 4.11(e), shows that detachment occurs on the same area, but to a different extent. The sum of total detached sediment in Fig. 4.11(c)

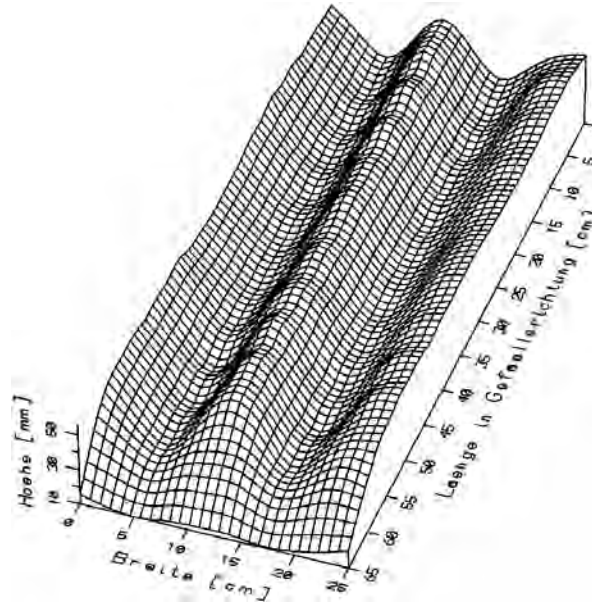


Fig. 4.12: Geometrical structure of the EROSION 2D test plot, which SCHMIDT (1996) used for derivation of the sediment mass flux equation.

would be much greater, even if detachment was a linear process, which it is definitely not. It is arguable, which of the two approaches delivers the “more correct” result, as this is again the scaling question mentioned above. Therefore this concept is further abstracted to a smaller scale.

Fig. 4.12 shows the set up SCHMIDT (1996) used for determining the sediment mass flux equation (Eq. (4.15) in Section 4.5.1.1). He performed experiments with surface runoff only, and experiments with both runoff and rainfall simulation. For all experiments he found a threshold of approx.  $3 \cdot 10^{-5} \text{ m}^3/\text{m} \cdot \text{s}$ , which has to be exceeded for initiation of sediment mass flux. The sowing furrows can clearly be recognised, which implies, that runoff concentrates there. EROSION 2D does not explicitly model rill erosion (Section 4.5.1.5) but the experimental set up and thus the derivation of the empirical equation implicitly include a kind of rill erosion due to the flow concentration. This means, that the flow concentration as presented above, theoretically should be considered on the scale of this plot, too. Since the course of the furrows or rills on a larger scale can only be estimated, the abstracted concept of flow concentration without directional information (Fig. 4.11(e)) is used to describe this behaviour on the micro scale. Fig. 4.11(f) shows the abstracted representation of the plot from Fig. 4.12.

#### 4.5.2.2. IMPLEMENTATION IN THE EROSION MODULE

In order to implement the presented abstract, scale-invariant concept of flow concentration in the erosion module, a flow concentration factor ( $f_{cf}$ ) is introduced. It is defined as the width of flow concentration  $w_f$  [m] to the total width of the considered unit area  $w_a$  [m]:

$$f_{cf} = \frac{w_f}{w_a} \quad (4.24)$$

The  $f_{cf}$  is dimensionless and ranges theoretically from values above 0 to 1, where 1 can be visualised e.g. as sheet flow or a totally plane proxel surface, and very low values indicate e.g. an area trenched by many small rills. So the  $f_{cf}$  defines two fractions of a proxel, which are treated differently by the erosion module. For the sake of simplicity the fractions will be termed rill and interrill area in the following. The technical implementation in the erosion module uses the factor to concentrate the flow on the given fraction, and computes the detachment and transport equations based on rill and interrill area. The calculation of the momentum flux of the runoff is limited to rill areas, but the momentum flux of the raindrops can act on the whole area. It is assumed, that particles detached by raindrops on the interrill areas (indicated by zero runoff units in Fig. 4.11(e) and Fig. 4.11(f)) are transported by splash into the rills, where they can be transported further on by concentrated flow.

So the processes of detachment and transport can be computed as described in the following list:

1. The available amount of runoff is scaled with the given  $f_{cf}$ , i.e. is concentrated on a virtual area.
2. With the concentrated runoff volume, velocity and momentum flux of the flow are calculated.
3. Momentum flux of rainfall is calculated and the rill and interrill areas are taken into account (as described below).
4. The total momentum flux is used to calculate the particle detachment. The resulting detachment is reduced with the  $f_{cf}$  to the actual rill area for the case of rill erosion, whereas detachment by raindrops may act on the whole area.
5. The transport capacity of the concentrated flow is determined. For calculation of the maximum particle concentration only the momentum flux of the drops on the rill areas is considered (instead of  $\varphi_{r,\alpha}$  in Eq. (4.21)). Based on the total available amount of runoff ( $q$  in Eq. (4.22)) on this proxel, the amount of sediment actually leaving the proxel is computed.

For computation of the momentum flux of the raindrops, rill and interrill area are considered, but additionally also the partitions of direct throughfall and leaf drip as described in Section 4.5.4.1. Momentum flux for each partition is calculated separately after the following scheme:

1. Momentum flux depending on drop size and velocity is calculated.
2. Only in case of rill areas: raindrop diameter is compared to flow depth, and if necessary, momentum flux is reduced according to Eq. (4.25).
3. Rill and interrill areas are considered by multiplying the corresponding calculated momentum fluxes with their fractional area (given by  $f_{cf}$ ).
4. The momentum fluxes of rill and interrill areas are added up.

The reduction of the momentum flux of the raindrops, depending on flow depth in the rill areas is expressed by (WICKS & BATHURST, 1996):

$$f_{fd} = e^{1 - \frac{h}{D_d}} \quad (4.25)$$

where  $f_{fd}$  is the water depth correction factor,  $h$  is the flow depth [m] and  $D_d$  is the median drop diameter [m]. The median drop diameter is either set to the leaf drip diameter, if drip off occurs (see Section 4.5.4.1), or approximated for direct throughfall after LAWS & PARSONS (1943) with:

$$D_d = 0.00124 \cdot I^{0.182} \quad (4.26)$$

where  $I$  is the rainfall intensity [mm/h].

#### 4.5.3. PARTICLE SETTLING VELOCITY

SCHMIDT (1996) calculates the particle settling velocity based on Eq. (4.16), which actually is valid only for very small Reynolds numbers ( $Re \leq 1$ , CHENG (1997)). However, as the modified model now implicitly takes rills into account (Section 4.5.2), higher flow velocities are modelled and therefore Reynolds numbers of flow increase. Thus it is reasonable to replace Eq. (4.16) with an approach by CHENG (1997), which holds for a wide range of Reynolds numbers from the Stokes flow to the turbulent regime:

$$v_p = \frac{\nu}{D} \cdot \left( \sqrt{25 + 1.2 \cdot D^2} \right)^{1.5} \quad (4.27)$$

where  $\nu$  is the kinematic viscosity of the fluid [Pa·s] and  $D$  is a dimensionless particle diameter.

The dimensionless particle diameter can be calculated with:

$$D = \left( \frac{\rho_p - \rho_q \cdot g}{\rho_q \nu^2} \right)^{\frac{1}{3}} \cdot D \quad (4.28)$$

and the kinematic viscosity is:

$$\nu = \frac{\eta}{\rho_q} \quad (4.29)$$

As the dynamic viscosity  $\eta$  depends on temperature, it is computed with the following equation (GORDON ET AL., 2004):

$$\eta = \frac{0.0018}{1 + 0.0337 \cdot T + 0.00022 \cdot T^2} \quad (4.30)$$

where  $T$  is the fluid temperature [°C].

The fluid temperature  $T$ , i.e. the temperature of the surface runoff is estimated for this study as the mean value of the soil temperature  $T_s$  [°C] and the temperature of the raindrops  $T_r$  [°C]:

$$T = \frac{T_s + T_r}{2} \quad (4.31)$$

For estimation of  $T_r$ , here it is assumed, that the drops have the same temperature as the cloud, where they originated, and do not dissipate heat during falling through the drag. Furthermore the altitude of the cloud is set to 1000 m above ground, which leads with a mean saturated adiabatic lapse rate of 6.5 K/km to an estimate for the drop temperature of:

$$T_r = T_a - 6.5 \quad (4.32)$$

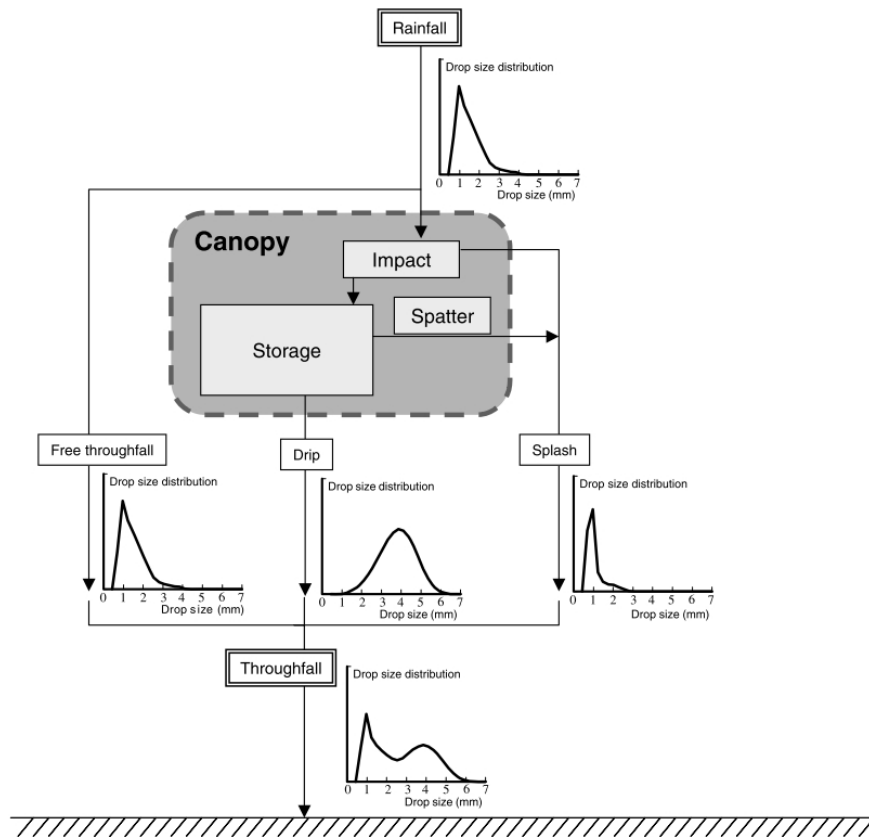


Fig. 4.13: Schematic illustration of the components generating throughfall (NANKO ET AL., 2006). The modelled components in the present study are “Free throughfall” and “Drip”.

where  $T_a$  is the air temperature [ $^{\circ}\text{C}$ ] in 2 m above ground.

With the aid of Eq. (4.28) – Eq. (4.32), Eq. (4.27) can be solved for each particle class, and particle transport is calculated as described above in Section 4.5.1.2.

#### 4.5.4. REDUCTION OF MOMENTUM FLUX OF RAINDROPS

##### 4.5.4.1. INTERCEPTION AND THROUGHFALL

Canopy cover protects the soil against raindrop impact and splash effects. The drops are intercepted by the leaves and only dripping may pass kinetic energy to the soil. The equations of the model EROSION 2D consider canopy cover as the fraction of projected leaf area to total projected area (Eq. (4.11)). Momentum flux of raindrops is only exerted by the fraction of direct throughfall. But, as mentioned in Section 3.2.3, the effect of drips from leaves can have a significant effect on soil detachment, hence the intercepted throughfall is considered additionally to the direct throughfall in the modelling approach of this study (see Fig. 4.13). For estimation of fractional canopy cover, SCHMIDT ET AL. (1996) provide simple methods for visual estimation in situ or a look-up table with monthly mean values for common types of vegetation and land cover. Since the erosion module within GLOWA-Danube shall be used to investigate future trends in soil erosion, a dynamic approach is required, because the annual course of phenology and leaf development are very likely to shift in the future.

A common method used in modelling of light transmission through canopy is calculation of

fractional cover from the LAI. PROMET computes plant growth dynamically and takes conditions of a changing climate into account (Section 4.2.3). For calculation of intercepted water and radiation the fractional cover  $c_{fp}$  is determined with (after HANK (2008)):

$$c_{fp} = 1 - e^{-LAI} \quad (4.33)$$

Eq. (4.33) is only dependent of the LAI. In order to take the canopy structure into account, calculation of canopy cover was replaced with a more sophisticated approach from CAMPBELL & NORMAN (1998):

$$c_{fb}(\psi) = 1 - e^{-K_{be}(\psi) \cdot LAI} \quad (4.34)$$

where  $c_{fb}(\psi)$  is the fraction of incident beam radiation from zenith angle  $\psi$  penetrating the canopy. The extinction coefficient of a canopy of black leaves with an ellipsoidal leaf angle distribution  $K_{be}(\psi)$  is:

$$K_{be}(\psi) = \frac{\sqrt{x^2 + \tan^2 \psi}}{x + 1.774 \cdot (x + 1.182)^{-0.733}} \quad (4.35)$$

The parameter  $x$  is the ratio of average projected areas of canopy elements on horizontal and vertical surfaces. For vertical leaf angle distributions  $x = 0$ , spherical distributions have  $x = 1$  and for horizontal leaf canopies  $x$  approaches infinity. Parameter values  $x$  for canopies modelled within this study can be found in Section 5.2.3. By using a vertical incident angle  $\psi$ , Eq. (4.34) and Eq. (4.35) can also be used for computation of throughfall and intercepted water.

The maximum intercepted water storage  $\Delta I_{max}$  [mm] is then calculated as (after HANK (2008)):

$$\Delta I_{max} = c_{fb} \cdot (0.935 + 0.498 \cdot LAI - 0.00575 \cdot LAI^2) \quad (4.36)$$

with a minimum interception capacity  $\Delta I_{max}$  of 0.935 mm for defoliated canopies ( $LAI = 0$ ). Fig. 4.14 shows the differences between the two approaches for computation of fractional cover and the effect on maximum intercepted water storage.

The filling and drainage of intercepted water storage follows a concept of GASH (1979), assuming that no drip off from leaves occurs until storage is filled completely. Subsequent precipitation then may lead to draining of the storage, which is represented by adding this portion to the effective precipitation (HANK, 2008). For rainfall erosivity this means:

- Throughfall always transfers its momentum flux to the uncovered soil according to the fractional canopy cover represented by the term  $(1 - c_c)$  in Eq. (4.12).
- For calculation of the momentum flux of raindrops the empirical formula of LAWS & PARSONS (1943) (Eq. (4.10)) is used, which gives the terminal velocity, i.e. the constant speed, when gravitational and frictional forces are in equilibrium. This is not valid for drops dripping down from leaves in a height ranging from several centimetres to metres (whereby kinetic energy is much lower).

Therefore the velocity of the dripping raindrops from intercepted water storage has to be calculated separately. This can be achieved with *Newton's second law of motion*

$$F = m \cdot a \quad (4.37)$$

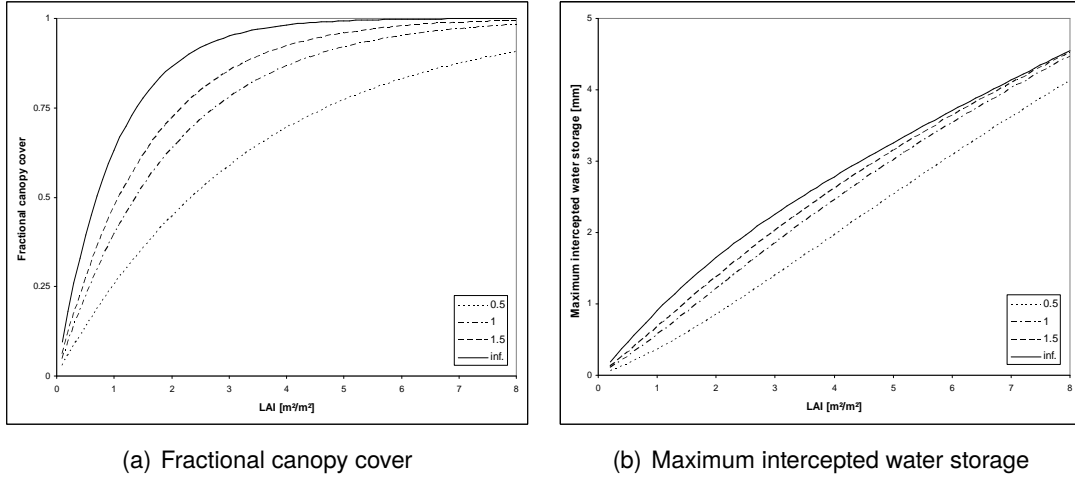


Fig. 4.14: Fractional canopy cover and maximum intercepted water storage calculated for different leaf angle distribution parameters  $x$ . The incident angle for precipitation is set to zero. The graph marked with "inf." represents a horizontal leaf distribution respectively the constant extinction coefficient of -1, as used in Eq. (4.33).

which says that the net force on an object is equal to the mass of the object multiplied by its acceleration. The force  $F$  [N] acting on the raindrop equals the product of its mass  $m$  [kg] and acceleration (here the gravitational acceleration  $g$  with  $9.81 \text{ m/s}^2$ ). In the opposite direction of  $F$  acts the drag force  $F_D$ :

$$F_D = \frac{1}{2} \cdot \rho \cdot v^2 \cdot C_D \cdot A \quad (4.38)$$

where  $\rho$ : density of the fluid (air),  $v$ : velocity of the object (raindrop),  $C_D$ : drag coefficient and  $A$ : reference area. This equilibrium can be expressed with:

$$m \cdot g - F_D = m \cdot \frac{\delta v}{\delta t} \quad (4.39)$$

with the acceleration  $a$  written as  $\frac{\delta v}{\delta t}$ . Substituting and solving Eq. (4.39) for  $\delta v$  leads to:

$$\delta v = \left( g - \frac{C_D \cdot \rho \cdot A \cdot v^2}{2 \cdot m} \right) \cdot \delta t \quad (4.40)$$

which allows for computation of the raindrop velocity at each desired time step, if the variables  $C_D$ ,  $\rho$ ,  $A$ , and  $m$  are known. The drag coefficient actually changes with velocity, as it depends on the Reynolds number, but for spherical objects it can be estimated as 0.41. The density of air at  $20^\circ\text{C}$  is  $1.2041 \text{ kg/m}^3$ . The reference area  $A$ , in this context for raindrops, is the projected area of a sphere ( $A = r^2 \cdot \pi$ ). The mass of a raindrop is calculated from its volume times the density of water ( $1000 \text{ kg/m}^3$ ). So the only missing variable is the radius or diameter of the raindrop.

BRANDT (1989) found, that intercepted throughfall drop sizes are sensitive neither to rainfall intensity nor to the canopy structure or leaf characteristics. Leaf shape, size and texture do not influence the drop size distribution, provided that individual leaves are grouped into a canopy. Results showed, that the distributions of throughfall under plants are unimodal and normal with a median drop diameter between 4.91 and 5.28 mm, which corresponds to the findings of other studies which the author compared. By analysis of regression BRANDT (1989) found a



function for the median drop size (diameter)  $D_{50}$  [mm] depending on rainfall intensity  $I$  [mm/h] (Eq. (4.41)), where the parameter 0.03 emphasises the insensitivity to rainfall intensity.

$$D_{50} = 4.71 \cdot I^{0.03} \quad (4.41)$$

Finally BRANDT (1989) suggests for simulation of intercepted throughfall a normal distribution with a mean of between 4.52 and 4.95 mm and a standard deviation ranging from 0.79 to 1.3 mm. So for calculation of drip off from leaves within PROMET a constant value for the drop diameter  $D_d$  of 4.6 mm is used.

In order to find the velocity of raindrop hitting the soil a numerical approximation of  $\delta v$  is calculated for sufficiently small time steps  $\delta t$ . The mean fall height  $h$  [m] of the raindrop is estimated as:

$$h = \kappa \cdot h_c \quad (4.42)$$

where  $h_c$  is the canopy height [m] and  $\kappa$  is a plant specific factor accounting for the relative drip off height. Since all variables for solution of Eq. (4.40) are known, a look-up table can be precomputed to save computation time. The momentum flux of the raindrops is finally computed once for direct throughfall after Eq. (4.12), and once for intercepted throughfall from the excess of intercepted water storage  $I_t$  [mm] after

$$I_t = I - \Delta I_{max} \quad (4.43)$$

with numerical approximation of  $\delta v$  in Eq. (4.40).

#### 4.5.4.2. SOIL COVER

The separation of drip off and throughfall allows for a realistic description of the momentum fluxes reaching the soil. But nevertheless often an additional protecting layer exists directly on top of the soil surface. This may be e.g. straw or litter in forests, crop residue or mulch on agricultural areas, or even a high coarse material content of the soil itself. This cover layer absorbs the energy of the raindrops, irrespective if they result from leaf drip, or from direct throughfall. The energy of the drops hitting the cover layer is no more available for detachment of soil particles, it merely may contribute to surface runoff. For this reason, the additional fractional soil cover layer  $f_{cs}$  was introduced into the model ((c) in Fig. 4.15). It designates the unit area of soil cover  $A_c$  [m<sup>2</sup>] to the unit area of soil  $A_s$  [m<sup>2</sup>] and therefore can be expressed as a fraction ranging from 0 (no cover material) to 1 (complete cover):

$$f_{cs} = \frac{A_c}{A_s} \quad (4.44)$$

In the context of the model, the cover layer is located between the vegetation and the soil, and it is assumed, that the cover is distributed uniformly. Technically, this means, that the total momentum flux of the raindrops, resulting from drip off and throughfall, which already may be reduced by flow depth, is reduced by the fractional soil cover layer  $f_{cs}$ .

#### 4.5.5. CRITICAL SHEAR STRESS

*Note: Actually the erosion resistance is merely a parameter for the erosion model, and therefore its derivation should appear in the chapter for model parameterisation (Chapter 5). But*

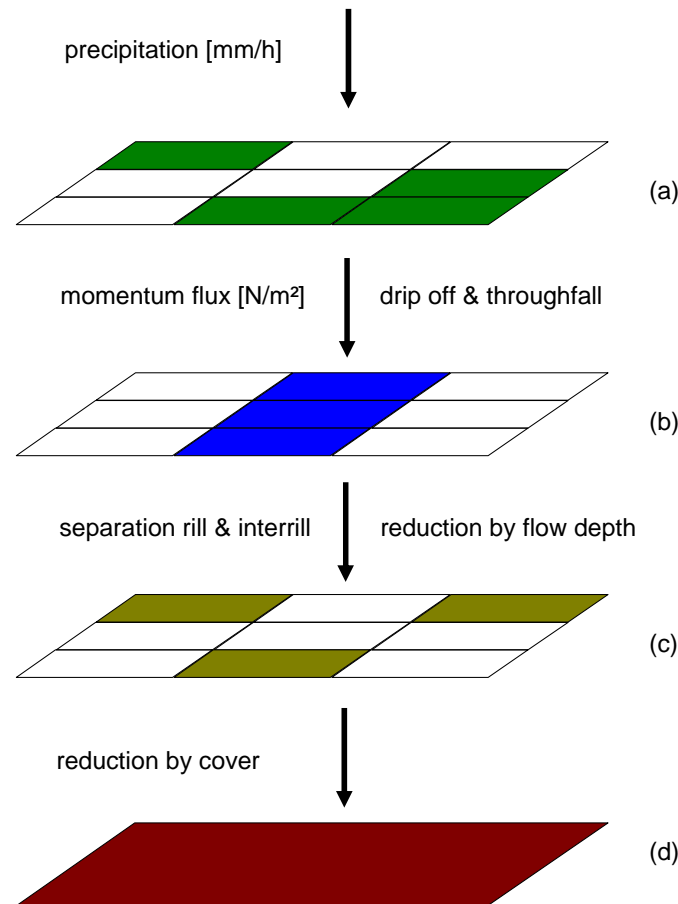


Fig. 4.15: Schematics of the reduction of momentum flux by interception, throughfall, flow depth and soil cover. Explanations: (a) The precipitation received from the atmosphere is split up into direct throughfall and leaf drip. (b) The resulting momentum flux is split up into a rill and an interrill component. If necessary, the rill component is reduced by flow depth. (c) Soil cover reduces the total momentum flux by its fraction. (d) The resulting total momentum flux is available for detachment of soil particles. (The colored areas in (a), (b) and (c) mark obstacles for raindrops, i.e. modify momentum flux.)

as in this study an approach for dynamic calculation of the erosion resistance via the critical shear stress was developed, and due to its complexity, this approach is described here in the following sections.

#### 4.5.5.1. QUANTIFICATION OF THE EROSION RESISTANCE

The erosion coefficient  $E$  in Eq. (4.15) represents the central parameter for the detachment of soil particles, respectively for the magnitude of the potential sediment mass flux  $q_{s,pot}$ . The critical momentum flux  $\varphi_{crit}$  in Eq. (4.14) indicates the detachability of a soil, depending on its properties, such as soil texture and structure, aggregate stability, content of organic matter, root penetration, etc.

For derivation of  $\varphi_{crit}$  for diverse soil types and conditions, SCHMIDT (1996) set up a number of experiments on different plots, where all input parameters were measured. An adjustment of  $\varphi_{crit}$ , until the values of modelled erosion matched the measured values, lead to a param-

eter set of erosion resistances for different agricultural management techniques, soil types, types of land use and phenological stages. This parameter catalogue, published in SCHMIDT ET AL. (1996), allows for selection of erosion resistances for a variety of different conditions. But the listed value of the erosion resistance for a given condition implicitly summarises the contributing effect of each single variable to the final value. So if values for certain conditions are not listed in the catalogue, a value has to be extrapolated or estimated. Therefore it seems reasonable to try to derive this parameter in a way of considering physically measurable factors influencing the stability of the soil. SCHMIDT (1996) tried to correlate the erosion resistance with the shear strength of the soil, measured with a pocket shearmeter at saturation. He concluded, that there probably exists a log-linear correlation, but due to the small amount of measurements, no empirical equation could be found.

Further effort to quantify the spatial and temporal variability of the erosion resistance was attempted by GERLINGER (1996). Somewhat contradictory to the mentioned parameter catalogue, he found, that temporal variability during the growing season is only small. As also interannual variability is small, it should be possible to determine the erosion resistance at any arbitrary date before the soil is completely covered with vegetation. However variations within a single event could be observed, in the way, that the erosion resistance increases with increasing soil moisture. In GERLINGER (2000), a flow chart of regression equations is given, relating soil properties to the erosion resistance. Most significant influence was found for the content of clay, organic matter and initial soil moisture, but not for the shear strength of the soil. From a physico-chemical point of view the content of clay and organic matter clearly has a stabilising effect (see Section 3.2.2.1), but the shear strength should also correlate with the erosion resistance. TENGBEH (1993) measured an increase of the shear strength of cohesive soils with decreasing moisture content. This effect might be compensated for dry soils by slaking to a certain degree, but in the study of DE BAETS ET AL. (2008), cohesion values nevertheless were larger for dry topsoils than for wet samples.

Parameterisation of the erosion resistance has been a subject in various other studies (e.g. SIEGRIST (2004), VON WERNER (1995)), and frequently could only be derived by calibrating the model to measured sediment yields. Because for the present study calibration is neither desirable, nor possible due to the large areal extent, and the correlations between soil moisture and erosion resistance mentioned above seem to be somewhat contradictory<sup>2</sup>, an approach for derivation of the erosion resistance based on cohesion, soil moisture and root reinforcement was developed. Furthermore the approach presented below (Section 4.5.5.2), seems to be more universally applicable, as its input parameters can easier be determined,

---

<sup>2</sup>A possible explanation for the increase of the erosion resistance with increasing initial soil moisture, as found e.g. in GERLINGER (2000) might be as follows:

SCHMIDT (1996) identified in a sensitivity analysis during model development the initial soil moisture as the most sensitive input parameter, which might explain overestimations of surface runoff, if this input parameter is not set correctly. For example in the study of FUCHS ET AL. (2004) the discharge was overestimated by EROSION 3D ranging from approx. 200% to 800% of the measured discharge. This increases the momentum flux of the runoff, which naturally in turn intensifies detachment and transport of soil. Since in some studies (e.g. SIEGRIST (2004) and GERLINGER (2000)) the erosion resistance was calculated back from measured data, the erosion resistance must increase (i.e. is manually adjusted) to allow the model to calculate correct results. Therefore it might be possible that the erosion resistance is used in some studies as a calibration parameter for correcting model deficiencies or shortcomings in parameterisation of a completely different origin.

than the “original” erosion resistance.

#### 4.5.5.2. SHEAR STRENGTH

In geotechnical engineering equations based on the Mohr-Coulomb theory have been used over the last decades for the prediction of the shear strength of saturated soils (FREDLUND ET AL., 1996). Even though soils are often unsaturated, slope stability analyses are usually based on saturated shear strength parameters (VANAPALLI ET AL., 1996). FREDLUND & RAHARDJO (1993) (as quoted in FREDLUND ET AL. (1996)) showed in laboratory studies, that there is a relationship between the soil-water characteristic curve and the unsaturated soil properties. Based on the *Mohr-Coulomb* equation (Eq. (3.8) in Section 3.2.2.1) FREDLUND ET AL. (1978) (as quoted in VANAPALLI ET AL. (1996)) proposed the following equation for the shear strength  $\tau$  of unsaturated soils:

$$\tau = c' + (\sigma_n - u_a) \cdot \tan \varphi' + (u_a - u_w) \cdot \tan \varphi^b \quad (4.45)$$

with  $c'$  effective cohesion of saturated soil,  $\varphi^b$ : the angle of shearing resistance with respect to matric suction,  $\varphi'$ : effective angle of shearing resistance for a saturated soil,  $(\sigma_n - u_a)$ : net normal stress on the plane of failure at failure and  $(u_a - u_w)$ : matric suction of the soil on the plane of failure (here  $u_a$  is pore-air pressure).

VANAPALLI ET AL. (1996) assume, that the contribution of matric suction to shear strength is proportional to the product of matric suction  $(u_a - u_w)$  and the normalised area of water  $a_w$ , which can be expressed as:

$$\tau = a_w \cdot (u_a - u_w) \cdot \tan \varphi' \quad (4.46)$$

The dimensionless normalised area of water is the ratio of the area of water corresponding to any degree of saturation to the total area of water at 100% saturation, i.e. varies from unity at saturation to zero when the soil is completely dry. It can be visualised as representing the amount of water in the soil. At high values of saturation the pore-water pressure directly affects the effective stress in contributing to the shear strength. But this applies only until the soil begins to desaturate. So the rate at which suction contributes to shear strength can be related to the normalised area of water. Since the normalised area of water in turn is assumed to be in direct proportion to the normalised volumetric water content  $\Theta$ , this relation can be written as:

$$a_w = \Theta^\kappa \quad (4.47)$$

where  $\kappa$  is a fitting parameter.

These considerations finally lead VANAPALLI ET AL. (1996) to the following equation for the shear strength of an unsaturated soil at any given suction:

$$\tau = c' + (\sigma_n - u_a) \cdot \tan \varphi' + (u_a - u_w) \cdot \Theta^\kappa \cdot \tan \varphi' \quad (4.48)$$

The first part in Eq. (4.48) represents the saturated shear strength. The second part is the shear strength contribution due to suction, which can be predicted using the soil-water characteristic curve. Using Eq. (4.48), it has to be considered, that the angle of shearing resistance is influenced by the suction. Various studies presented in VANAPALLI ET AL. (1996) reported an independence of  $\varphi'$  for different soils within a range of suctions between 0 – 500 kPa.

Therefore this range is proposed as a valid range for using constant values of  $\varphi'$  in practical purposes.

For modelling of soil erosion, only the soil shear strength of the upper soil layer needs to be known. Since neither heavy loads on the topsoil, nor lower (compressed) subsoil layers shall be modelled, the net normal stress can be neglected. Further assuming, that the soil air is nearly at atmospheric pressure (ZHANG ET AL., 2001) and does not transmit considerable stresses within the soil (SCHEFFER & SCHACHTSCHABEL, 2002), Eq. (4.48) can be simplified to:

$$\tau = c' + \Theta^\kappa \cdot \Psi \cdot \tan \varphi' \quad (4.49)$$

with  $c'$ : effective cohesion [Pa],  $\Theta$ : normalized volumetric water content (effective saturation) [0-1],  $\kappa$ : fitting parameter [-],  $\Psi$ : matric suction [Pa] and  $\varphi'$ : angle of shearing resistance at saturation [°].

#### 4.5.5.3. ROOT REINFORCEMENT

As mentioned above in Section 4.5.5.1, the erosion resistance depends on a variety of influencing factors. One of these, which is neglected in Eq. (4.49), is the soil reinforcement of plant roots. Although the shear strength of a soil has only recently been recognised as a determinant of its resistance to erosion, slope stability research acknowledges the substantial importance of vegetation roots for soil reinforcement since its beginning (GYSSELS ET AL., 2005). Because shear strength is strongly influenced by root effects, these should be considered for calculation of erosion resistance, especially because root density is highest in topsoils and decreases exponentially with soil depth. Species with a shallow but dense network (e.g. meadows) therefore have a more protective influence to soil erosion as deep rooted species (e.g. deciduous forest). According to GYSSELS ET AL. (2005), roots and rhizomes contribute to soil strength by binding the soil and introducing extra cohesion over any intrinsic cohesion that the soil had without these. They increase the effective cohesion of the soil, but not the angle of effective shearing resistance, which can be expressed in a modified version of Eq. (3.8) (GRAY & LEISER (1982) as quoted in GYSSELS ET AL. (2005)):

$$\tau = (c' + c_r) + (\sigma_n - u_w) \cdot \tan \varphi' \quad (4.50)$$

$c_r$  in Eq. (4.50) is the additional cohesion due to roots (WU ET AL. (1979) as quoted in GYSSELS ET AL. (2005)):

$$c_r = T_r \cdot \frac{A_r}{A} \cdot (\cos \beta \cdot \tan \varphi' + \sin \beta) \quad (4.51)$$

with  $T_r$ : total tensile strength of roots accounted for different diameters [Pa],  $A_r$ : area of shear surface occupied by roots [m<sup>2</sup>],  $A$ : total area considered [m<sup>2</sup>] and  $\beta$ : shear distortion from vertical [°].

According to WU ET AL. (1979) the term  $(\cos \beta \tan \varphi' + \sin \beta)$  in Eq. (4.51) is relatively insensitive to changes in  $\beta$  and is close to 1.2 for a large range of angles of shearing resistance, which allows to write:

$$c_r = 1.2 \cdot T_r \cdot \frac{A_r}{A} \quad (4.52)$$

Root tensile strength is highly variable with a nonlinear inverse relationship between root diameter and strength. The type of the relationship between diverse root parameters and soil

Tab. 4.6: Root parameter exponents for Eq. (4.53).

Erosion process	Root density [ $\text{kg}/\text{m}^3$ ]	Root length density [ $\text{km}/\text{m}^3$ ]
Splash detachment	0.0	0.0
Interrill erosion	0.084 – 0.168	0.0 – 0.004
Rill erosion	0.330 – 0.855	0.002 – 0.114

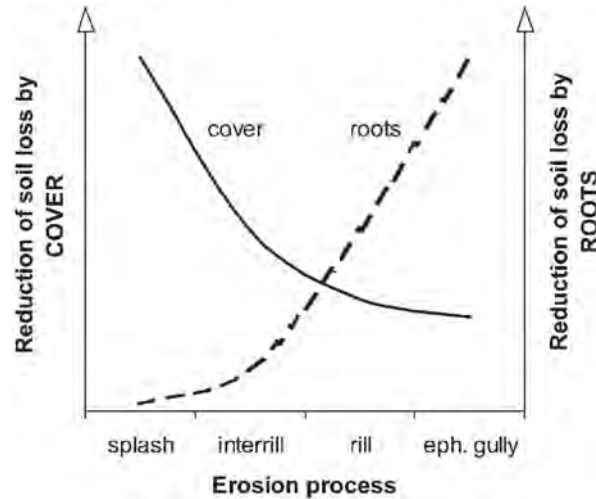


Fig. 4.16: Relative importance of vegetation cover and plant roots on the intensity of several water erosion processes (GYSSELS ET AL., 2005).

cohesion still is a field of research. However a literature review by GYSSELS ET AL. (2005) of a number of comparable studies, revealed an exponential decrease of soil erodibility and detachment with root length density. The influence of roots was already acknowledged in early erosion modelling via simple correction factors and is actually incorporated in modern physically based models via an exponential decline of erodibility. This exponential relationship can be summarised for the majority of models and studies with:

$$SEP = e^{-b \cdot RP} \quad (4.53)$$

where  $SEP$  is a soil erosion parameter (e.g. rill or interrill erodibility),  $b$  is a constant and  $RP$  is a root parameter (e.g. root density or root length density).

Ranges for the constant  $b$  in Eq. (4.53) are given in Tab. 4.6. As one can see, values for  $b$  are gradually increasing from splash detachment over interrill erosion to rill erosion. These increments originate from the distinct influence of the roots on the respective process. The strongest effect can be observed for rill erosion, as the concentrated flow in the rills directly acts *within* the top soil layer, which is permeated and stabilised by roots. Whereas during interrill erosion, where usually only a thin sheet flow occurs, the influence is limited to the surface of the soil only. Finally, for splash detachment, the root effect is not significant, and neglected in the works examined by GYSSELS ET AL. (2005). Nevertheless he concludes, that the total effect of root reinforcement on soil erosion is at least as important as the protecting effect of vegetation cover (see Fig. 4.16).

In order to consider the influence of root reinforcement in the calculation of shear strength (Eq. (4.49)), the cohesion due to roots has to be added to the cohesion of the soil, according

to Eq. (4.50). The additional cohesion by roots is calculated with Eq. (4.53) and as the main input root parameter, the root length density (received from the PROMET biological module, cf. Section 4.2.3) is chosen. But as Eq. (4.53) refers to an exponential decline in erodibility with the root parameter, whereas cohesion actually grows with the root parameter, the equation is inverted:

$$c'_t = c' + \left( c' \cdot (1 - e^{-b \cdot RLD}) \right) \quad (4.54)$$

where  $c'_t$  is the total effective cohesion of the soil, including root cohesion and  $RLD$  is the root length density [ $\text{km}/\text{m}^3$ ].

During the growing season the root length density is calculated dynamically by the PROMET biological module. But, considering agricultural crops, if plants are harvested, the  $RLD$  is naturally set to zero. Thus, in order to take into account the stabilising effect of crop residue and dead roots, for calculation of  $c'_t$  the  $RLD$  value of the time step *before* harvest is used. This applies until sowing, when tillage practices heavily disturb the soil structure.

#### 4.5.5.4. SOIL FREEZING

Soil freezing (as described in Section 4.2.2) not only influences hydraulic properties of the soil and (surface) runoff behaviour within PROMET (MUERTH & MAUSER, 2008; MUERTH, 2008), but also soil erodibility. If ice forms in soil pores, it pushes soil grains apart, reducing their degree of interlocking and the soil density. The amount of this soil expansion depends on various factors, such as (GATTO ET AL., 2002):

- the soil-water content when freezing starts,
- the volume of water drawn to the freezing zone,
- soil texture,
- the depth of the frost line,
- the rate of frost penetration,
- and the number of freeze-thaw (FT) cycles.

A frozen soil, which is newly thawed, can be more erodible than at any other time of the year, and this weakened state persists until the excess water drains and cohesion is re-established. A literature review of GATTO ET AL. (2002) summarises the most important effects of the dynamic process of FT cycling:

- Soil water is redistributed: the difference between the upper soil temperature and the air temperature in winter leads to energy losses from the soil, i.e. soil starts freezing in the top layer and the frost line commences downwards. The suction resulting from soil freezing initiates capillary rise from the lower layers to the upper layers. Soil strength is high when a soil is frozen, is weakest when it has recently thawed, and recovers its strength when soil drains (see also Section 4.5.5.2), particles resettle and cohesion re-establishes.

- Soil density and strength is reduced in undisturbed, as well as in compacted surface soils. The reduction of the soil density is most effective when the volumetric water content approaches the volume of soil pores. Mechanical compaction in ruts often persists in the soil layer below the frost line, which has important implications for erosion, because subsurface conditions affect runoff.
- The reduced soil density resulting from FT cycles, increases infiltration rates in both compacted and uncompacted soils. FT cycling even may loosen compacted soils, so that the infiltration rate after FT often returns to or near its previously uncompacted values.
- The geometry of the soil surface and the cross-sectional geometry of rills and ruts is changed. Formation of ice lenses in the soil can heave the soil upward more than the thickness of the lenses. A high temperature gradient during freezing favours needle-ice growth, which results in a “fluffed” surface with low cohesion. Observations showed, that this leads to high erosion rates during early runoff, but erosion rates are quickly reduced, as soon as the supply of loosened soil is exhausted.

The soil erosion module handles FT cycles borrowed from the WEPP (FLANAGAN & NEARING, 1995) model, where FT cycles influence erodibility as follows:

- If the soil has undergone one or more FT cycles, adjustments to interrill and rill erodibility and to the critical shear stress are made.
- For each FT cycle the soil becomes more unstable, dependent also on soil matric potential, until a maximum of 10 cycles has been reached.
- The adjustments are discarded, if the soil dries to less than 33.3 kPa.

As these adjustments are based on non-linear empirical equations, the absolute values cannot be used in the context of this study. Therefore the decrease of soil stability is approximated in the following way: As the influence of matric suction is already considered (Section 4.5.5.2), only an adjustment for soil cohesion is needed. Various studies (e.g. OZTAS & FAYETORBAY (2003), LEHRSCHE ET AL. (1991)) showed that initial wet aggregate stability decreases with FT cycles, depending on conditions, by about 20% to 80%. But the effect of the number of FT cycles seems to be somewhat inconsistent, i.e. stability increases over the first few cycles, but then decreases again. Therefore the number of cycles is neglected in this study, and a constant decrease of soil cohesion is assumed (modelled as a simple freeze-thaw multiplication factor  $f_{ft}$ ), as soon as the first FT cycle passed through. Like in WEPP, the factor acts only, if at least one FT cycle occurred (i.e. the soil freezes then thaws again), and the soil matric suction did not exceed 33.3 kPa. If the soil is frozen, soil cohesion is set to an infinitely high value, to prevent detachment.

#### **4.5.5.5. RELATIONSHIP BETWEEN SHEAR STRENGTH AND CRITICAL SHEAR STRESS**

As mentioned in Section 4.5.5.1, SCHMIDT (1996) supposed a relationship between the shear strength of the soil and the erosion resistance. A similar relationship has been found in many other studies, and represents the basis for detachment in various erosion models (e.g. WEPP



(FLANAGAN & NEARING, 1995), SHESED (WICKS & BATHURST, 1996) or EUROSEM (MORGAN ET AL., 1998)). For modelling, usually not the shear strength is used, but the critical shear stress, the soil can resist, before detachment initiates. LÉONARD & RICHARD (2004) compared experimental data from 10 studies combining soil shear strength  $\sigma_s$  [Pa] and critical shear stress  $\tau_c$  [Pa] and proposed a linear relationship:

$$\tau_c = \beta \cdot \sigma_s \quad (4.55)$$

where  $\beta$  is estimated as  $2.6 \cdot 10^{-4}$  with a coefficient of determination  $R^2 = 0.93$ , valid for shear strength ranging from 0 to 20 kPa.

Finally Eq. (4.55) is used in this study to convert the computed shear strength to values of critical shear stress.

#### 4.5.6. AGRICULTURAL MANAGEMENT PRACTICES

As the state of the soil - and thus its erodibility - on agricultural areas is dominated by anthropogenic measures, a reasonable representation of the latter is essential. Their influences have a high intra-annual variability, which makes them important particularly for long-term simulations, where in situ conditions cannot be fed into the model (in contrast to single event-based models, where in situ conditions are usually determined before simulation). In order to approximate the influence of agricultural management practices on soil erosion, some modifications and extensions to the original agricultural management routines (Section 4.2.3) of PROMET had to be carried out, which are described in the next sections.

As data about the application of exact management practices, such as conservation tillage, contour ploughing, etc., over the whole extent of the Upper Danube are not available, merely a differentiation of the status of a field is made. Furthermore, for parameterisation (Section 5.2), it is assumed that conventional tillage systems dominate in the study area. The following states have been considered as the most important anthropogenic influences:

- *sowed*: This status means, that the cultivation has been sowed. This is important, because the seedbed preparation alters the soil surface roughness and structure and usually destroys aggregates.
- *emerged*: The emergence of the plants introduces additional surface roughness to the soil. With increasing plant growth the surface runoff is slowed down.
- *harvested*: After harvest, the vegetation cover is removed. But usually a fraction of the yield stays on the field as crop residue, protecting the bare field to a certain degree from erosion.
- *ploughed*: Conventional ploughing leads to a strong increase of surface roughness. Additionally crop residue is buried in the soil.
- *toSow*: This status was introduced to take account of different, dynamic sowing dates.
- *toHarvest*: This status was introduced to take account of different, dynamic harvest dates.

These states are stored in variables, which can be queried by subroutines of the erosion model, in order to describe various changes in soil structure.

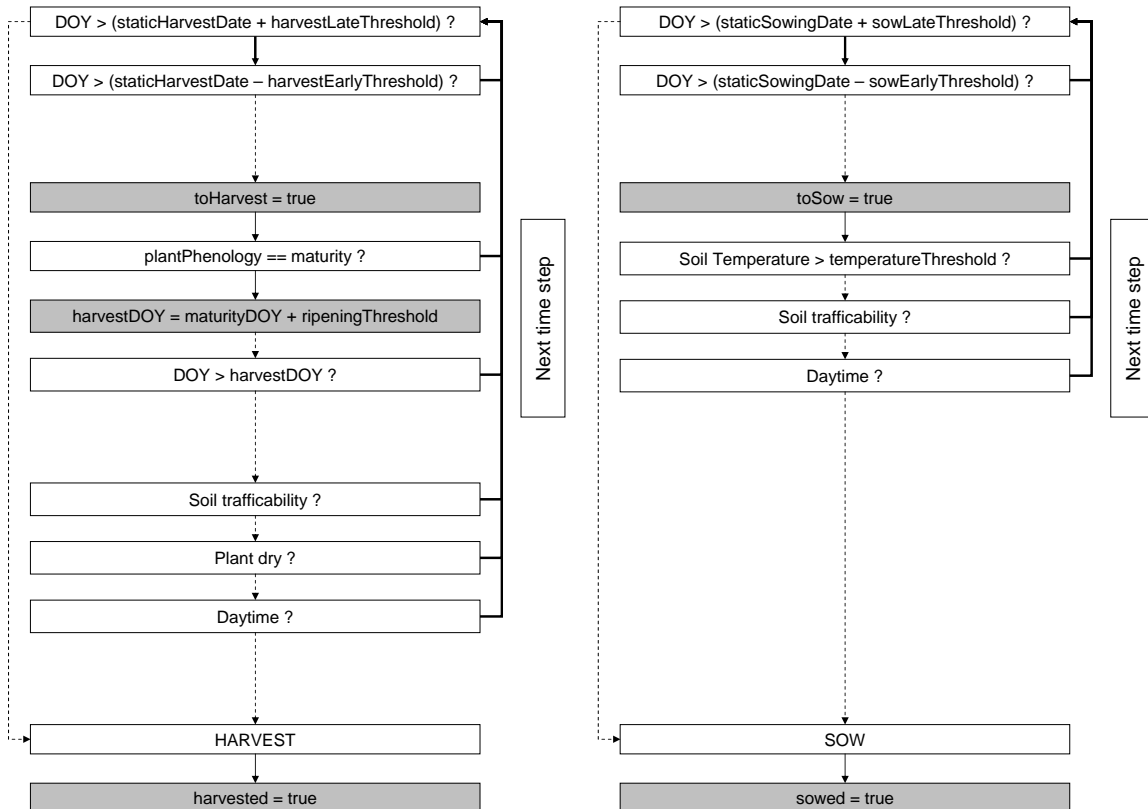


Fig. 4.17: Determination of the actual sowing and harvest dates, as implemented in the agricultural management routine. (Conditions are followed by a question mark. If the condition is evaluated as true, the dotted arrows indicate the next step. If it is false, the bold arrow is followed. Grey background means state transitions. Further explanations in text.)

#### 4.5.6.1. DETERMINATION OF MANAGEMENT STATES

Harvest, ploughing and sowing have severe impacts on soil erosion, as they change the vegetation cover and disturb the soil. Not only the action itself is important for modelling soil erosion, but also the date, when the measure occurs. In the Upper Danube Basin the date of harvest (of some cultivars) coincides with a period of frequent heavy precipitation events in summer. So the date of harvest may strongly distort the simulation or prediction of erosion events, if e.g. the model “harvests” too early and thus removes protecting vegetation cover. Modelling the correct date of harvest for the whole Upper Danube Basin is virtually impossible (especially for climate scenario runs), so errors are very likely to occur. This is especially important when modelling Climate Change scenarios, in which the dates of sowing and harvest are very likely to shift. But as the vegetation component of PROMET is capable of simulating plant physiology, the usage of the static sowing and harvest dates, listed in Tab. 4.1, has been replaced by a dynamic approach (Fig. 4.17).

Depending on the phenological stage of the plant, provided by the biological module, and environmental conditions needed for harvesting, the actual date of harvest is determined. For this purpose, the flowchart in Fig. 4.17 is processed, and if a condition is evaluated as false, the flowchart is repeatedly processed for the next time step. The two variables *harvestEarlyThreshold* and *harvestLateThreshold* define an interval around the mentioned

static harvest dates, within which harvest occurs. If *harvestLateThreshold* is passed, harvest is *forced*. If *harvestEarlyThreshold* reached, harvest is *allowed*. Then the phenology of the plant is checked for maturity, whereupon, if maturity is reached, a plant dependent addend (*ripeningThreshold*) is added to the day of maturity (*maturityDOY*). The resulting *harvestDOY* thus designates the date, when the plant has passed the actual process of ripening (or drying out). From here on only external conditions have to be fulfilled for harvest to occur. The soil module of PROMET, passes a status flag depending on matric suction, which signs the trafficability. If the matric suction increases to a pF-value greater than 3.0 (or 0.1 MPa), the soil is considered to be dry enough to be trafficed. The condition, if the plant is dry, is evaluated with the aid of the intercepted water storage, which has to be empty. Finally harvest is restricted to model times between 04:00 and 22:00 CET.

After a cultivation has been harvested, a land use dependent addition (analogous to the maturity addend) is used to calculate the date of ploughing. The process of ploughing sets the status variable *ploughed* to true.

The process of sowing, as illustrated in Tab. 4.1, is very similar to harvest and is oriented at an interval around the static sowing dates. Within the interval a land use dependent temperature threshold is used to determine if sowing occurs. The threshold is compared to the currently modelled soil temperature of the uppermost soil layer, and if it is exceeded, sowing is allowed. If the conditions for soil trafficability and daytime are fulfilled additionally, sowing is initiated and the status variable *sowed* is set to true.

#### 4.5.6.2. IMPACT OF MANAGEMENT STATES

The impact of the management states is considered in the erosion module for the following purposes:

- Surface roughness: The surface roughness is taken into account with Manning's  $n$ , which influences runoff velocity (described in Section 5.2.5).
- Flow concentration: The flow concentration factor, as described in Section 4.5.2, is influenced by the states *sowed* and *ploughed*. For sowed conditions,  $f_{cf}$  takes low values, thus simulating the furrows of the seedbed, in which the flow concentrates. For ploughed conditions, it has high values, as any regular structures or rills are eliminated.
- Crop residue: After harvest, it is assumed, that crop residue stays on the surface of the field (cf. Section 4.5.4.2). After ploughing the crop residue is buried by the tillage action. For the period between harvest and sowing decomposition of crop residue is modelled (see Section 5.2.4).
- Roots: After harvest, roots remaining in the soil are decomposed similar to crop residue (cf. Section 4.5.5.3).

## 4.6. TEMPORAL DISAGGREGATION OF PRECIPITATION

In hydrological modelling, precipitation data is the most important driving input parameter. The temporal resolution of the input data needed, ranges as far as from the monthly scale,

e.g. in long-term ecological modelling of lakes, over hours (e.g. in water balance modelling), down to event-based modelling with a resolution of minutes, for example in flood forecasting or urban drainage systems analysis. While primarily small study areas are equipped with a high resolution observational network, bigger catchments often only have gauges recording on a daily base. Moreover, historical precipitation records, which are frequently used for model validation, usually are available in much lower temporal resolution than modern measurements. All these reasons argue for the temporal disaggregation of precipitation.

As illustrated in Section 3.2.1.2, rainfall intensities in the Upper Danube Basin show a strong spatio-temporal variability. The simplified method used for disaggregation in PROMET, leads to an underestimation of rainfall intensities, especially for convective events, as maximum values are limited to the half of the measured input value (see Fig. 4.5). Since particularly convective events in summer trigger soil erosion, an alternative approach for temporal disaggregation is demanded.

Various scientific areas of interest have different demands on the quality and resolution of disaggregated data, so that a variety of methods exists to deal with this issue, which are subject of the next section.

#### 4.6.1. OVERVIEW OF TEMPORAL RAINFALL DISAGGREGATION APPROACHES

Literature reviews on available models can be found e.g. in GÜNTNER ET AL. (2001), HERSHENHORN & WOOLHISER (1987) or FLANAGAN & NEARING (1995). The following list briefly describes the approaches of the most common techniques:

- Theoretical probability distribution functions: This approach uses theoretical probability distribution functions to describe the characteristics of rainfall. A mathematical function, which best describes the properties of regional rainfall characteristics, is chosen and fitted to empirical data. According to individual requirements, variables can be e.g. number of events per day, starting times or event volume. Common practices represent the occurrence of rainfall events with a Poisson form and the event amount and duration with skewed normal, exponential, beta or gamma, or diverse joint distributions (see CONNOLLY ET AL., 1998). The number of parameters describing the probability distribution functions ranges in dimensions of 5000–6000 (SRIKANTHAN & McMAHON (1985), after HERSHENHORN & WOOLHISER (1987)) to approximately 10 or less (e.g. CONNOLLY ET AL. (1998)), depending on purpose. ECONOPOULY ET AL. (1990) achieved spatial transferability of the model parameters within climatologically homogeneous regions.
- Rectangular pulses models: According to (KHALIQ & CUNNANE, 1996), these cluster-based models represent the rainfall events as clusters of rain cells, considering the rain cells as pulses with a random duration and random intensity which is constant throughout the cell duration. The cluster process is based on an initial Poisson process of storm origins, which is associated with a random number of cells. The temporal distribution of the cells is carried out according to the Neyman-Scott or Bartlett-Lewis cluster process, using five main parameters in their original form of (RODRIGUEZ-ITURBE ET AL., 1987) (OLSSON & BURLANDO, 2002). They have been extended by COWPERTWAIT (1991) and regionalised by COWPERTWAIT ET AL. (1996a,b), and are considered to represent a very

robust and practical approach disaggregation of continuous rainfall time-series (OLSSON & BURLANDO, 2002).

- Random cascade models: Cascade models evolved from fractal theory, based on the assumption, that characteristic scales exist in an arbitrary system, within which statistical properties marginally change. Many natural systems show similar or self-similar behaviour over different spatial or temporal resolutions. If the observed statistical properties of a process are governed by the same relationship at different scales or resolutions, these can be used for disaggregating or downscaling the process. Early models were originally used in statistical turbulence (e.g. MANDELBROT, 1974) and proposed by SCHERTZER & LOVEJOY (1987) for constructing physically based stochastic models. Cascade processes are suitable for spatial downscaling (see e.g. FERRARIS ET AL., 2003) as well as for temporal disaggregation (see Section 4.6.2). OLSSON (1998) was the first who used these models for rainfall disaggregation by repeatedly redistributing the available rainfall into smaller temporal units, according to empirically determined rules.

The findings of the studies of GÜNTNER ET AL. (2001), HINGRAY & BEN HABA (2005), and MOLNAR & BURLANDO (2005) generally showed good overall performance of cascade models, in spite of the simplistic and applied model design, which allows simple parameter estimation. Therefore these are examined for their applicability within GLOWA-Danube. The requirements at least to be fulfilled for successful integration into PROMET are:

- (a) Conservation of mass, as this is one of the basic principles claimed by MAUSER & BACH (2009) for the physically based model PROMET. Canonical cascades only preserve mass on average, whereas microcanonical cascades exactly conserve mass.
- (b) The ability to be easily adapted to different climate regions, as the Upper Danube Basin is a very heterogeneous watershed (see Section 3.2.1.2). GÜNTNER ET AL. (2001) applied a cascade model in two different regions with a semi-arid tropical, and a temperate climate. Results showed an overall high accuracy, indicating applicability for hydrological modelling in differing climate regions. As an example for successful hydrological application, the work of GÜNTNER (2002) is to be mentioned.
- (c) The ability to disaggregate time-series of several hours to at least one hour or less, as input data ranges from 7 to 10 hours and the standard modelling time step in PROMET is one hour (see Section 4.2.1). Various studies successfully used cascade models in different temporal resolutions, e.g. HINGRAY & BEN HABA (2005) generated 10-minute time step series from hourly data, whereas OLSSON (1998) disaggregated rainfall from 17 hours to one hour.

Concluding this section, a microcanonical random cascade seems to represent a well-balanced solution for rainfall disaggregation, regarding the aims of this study and its implementation in PROMET.

#### 4.6.2. THE CASCADE MODEL AFTER OLSSON

The basic concept of cascade models, is a process of repeatedly dividing a given dimension into successively smaller units. Each division step redistributes a given magnitude following previously defined parameters. The underlying idea is self-similarity over a certain range of scales. In order to apply cascade processes on temporal rainfall disaggregation, a number of studies was conducted (e.g. OLSSON ET AL., 1993; OLSSON, 1995), leading to the result, that rainfall is characterised by multifractal behaviour over a range of scales. “Scaling implies that statistical properties of the process observed at different scales, i.e., resolutions, are governed by the same relationship [...]” (OLSSON, 1998). One way to preserve these scaling properties at each resolution, is to use a so-called bounded random cascade. The term “bounded” means a fitting of the scale-dependent behaviour of the cascade parameters with a power function depending on scale (see e.g. MOLNAR & BURLANDO, 2005). This is usually achieved by deriving a log-log linear relationship between the cascade parameters and the timescale applied. Another approach is represented by unbounded random cascades, where parameters are independent of scale. Such a model was applied by OLSSON (1998), who assessed the scaling behaviour of rainfall time series, and found a range, where statistical properties are *scale-invariant*, i.e. do not change significantly. In his study area, he verified the existence of scale-invariant conditions between approximately 1 hour and 1 week.

##### 4.6.2.1. BASIC CONCEPT

The model used for temporal disaggregation of precipitation is a multiplicative microcanonical random cascade with branching number 2, defined after OLSSON (1998) and extended by GÜNTNER ET AL. (2001), which is briefly described in this section. It is characterised by exact conservation of mass as opposed to canonical cascades.

Fig. 4.18 visualizes exemplarily the basic scheme. In order to disaggregate the rainfall data, at first statistics have to be calculated from empirical data to form the so-called *generator*, which controls the disaggregation process. The cascade *level* denotes the time series at a certain temporal resolution, which is doubled or halved at the transition (called *modulation*) to a higher, respectively lower level. A time interval at an arbitrary level is called a *box*, which can be *dry* or *wet*, depending on its rainfall volume  $V$ . The volumes of the boxes are classified as

- *above mean volume* or
- *below mean volume*.

A split-up of a box during a modulation, a *branching*, results in two equally sized boxes in the higher level at the adjacent time intervals  $t_1$  and  $t_2$ . The original volume is redistributed with two multiplicative *weights*  $W_1$  and  $W_2$ , with  $W_1 + W_2 = 1$ . Three weighting possibilities are available at a modulation to a higher level:

- *1/0-division*: the whole rainfall volume  $V$  occurred during  $t_1$ , then  $V_1 = 1$  and  $V_2 = 0$  on the higher level
- *0/1-division*: occurs if  $W_1 = 0$  and  $W_2 = 1$ , leading to  $V_1 = 0$  and  $V_2 = 1$

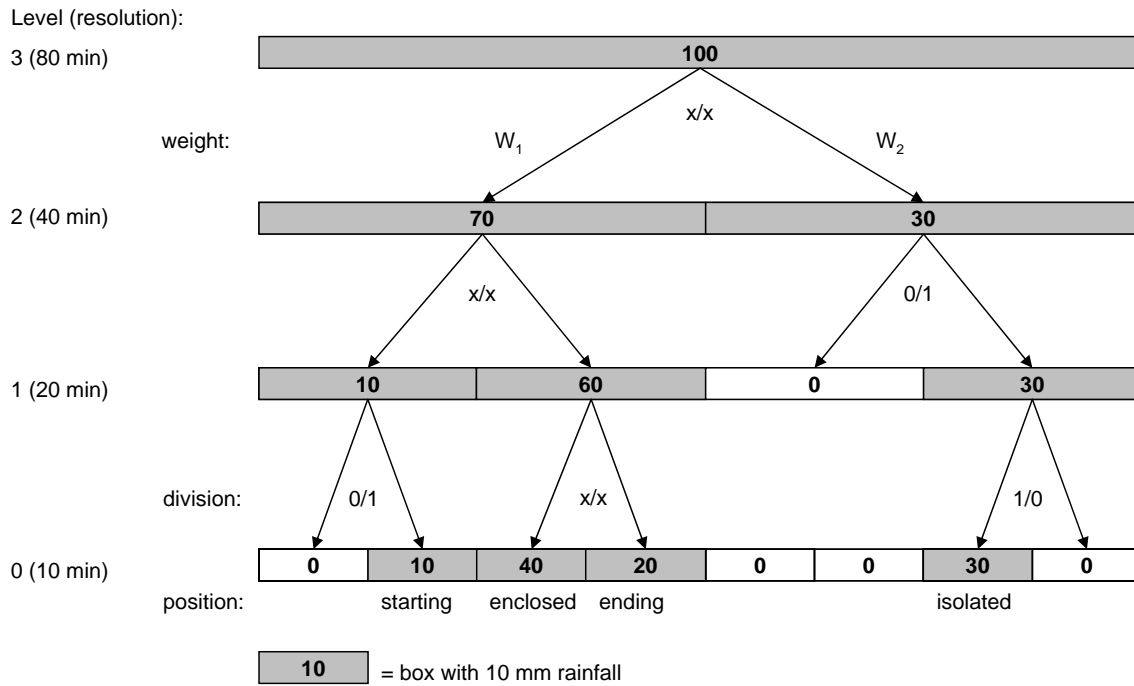


Fig. 4.18: Schematics of the cascade process as defined by OLSSON (1998)

- *x/x-division*: if rainfall is divided to  $t_1$  and  $t_2$  with  $V_1 > 0$  and  $V_2 > 0$

To improve model performance, the *position* of the box is taken into account, which is referred as:

- *starting*: if a precipitation event is beginning, i.e. the preceding box is dry and the succeeding box is wet
- *enclosed*: if the box observed is enclosed by wet boxes
- *ending*: an ending precipitation event, inverse to the starting case
- *isolated*: the box is surrounded by dry boxes

For construction of the generator of the model, a successive aggregation of data at the highest level available has to be done, until the desired resolution, for which disaggregation shall be carried out, is reached. During these aggregation steps statistics regarding volume, position and division are collected, resulting in frequencies for each combination at each level. These frequencies are converted to probabilities  $P$  which define the generator. In this way the generator defined by Eq. (4.56) has 24 parameters, derived from the combination of 2 volume classes, 4 position classes and 3 division classes.

$$W_1, W_2 = \begin{cases} 1 \text{ and } 0 & \text{with } P(1/0) \\ 0 \text{ and } 1 & \text{with } P(0/1) \\ W_{x/x} \text{ and } 1 - W_{x/x} & \text{with } P(x/x) \end{cases} \quad (4.56)$$

where  $0 < W_{x/x} < 1$  and  $P(0/1) + P(1/0) + P(x/x) = 1$ .

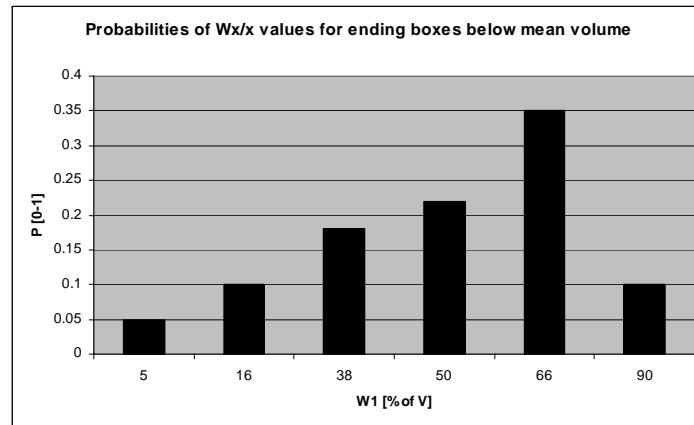


Fig. 4.19: Exemplary  $W_{x/x}$ -distribution for ending boxes below mean volume of a the generator of a cascade model

Additionally for the case of a  $x/x$ -division, a probability distribution for the volume fractions is calculated, called a  $W_{x/x}$ -distribution. The  $W_{x/x}$ -distribution consists of a number of classes for the weights  $W$ , with their associated probabilities, for each volume and position class, as exemplarily shown in Fig. 4.19.

#### 4.6.2.2. APPLICATION OF A CASCADE MODEL

The steps from preparing the generator to applying the model for disaggregation are illustrated in this section, to provide an understanding for the modifications made in this study to adapt the model to *AtmoStations*, which is subject in Section 4.6.3.

As already mentioned, in order to use a cascade model, its generator first has to be calculated and calibrated using high resolution empirical data. The properties of the generator then are used to disaggregate the desired low resolution datasets. The following listing summarises the required steps:

1. Aggregation: Aggregation starts at the level with the highest temporal resolution (e.g. level 0 in Fig. 4.18). For calculation of the generator, statistics accounting for rainfall properties are collected the following way:
  - a) The volumes of two adjacent boxes are added up into a box in the upper level. The temporal resolution of the boxes in the upper level is doubled.
  - b) The type of division is determined from the two aggregated boxes in the lower level. In case of a  $x/x$ -division, the ratio of the weights  $W_1$  and  $W_2$  forming the upper box, is calculated. The classes for volume and position are defined by the new, resulting box.
  - c) All boxes of the current level are evaluated this way and the information gained, concerning volume, position and division for this level, is stored.

This aggregation procedure (steps 1a–1c) is repeated until the desired temporal resolution (e.g. level 3 in Fig. 4.18) is reached.



2. Generator calculation: After the aggregation from step 1 frequencies for each modulation are available, which are used to form the generator:
  - a) In order to form a valid generator, the degree of scale invariance has to be assessed. This can be done by analysing the distribution of the probabilities  $P(1/0)$ ,  $P(0/1)$  and  $P(x/x)$  and the distribution of  $W_{x/x}$  over the aggregated levels. Scale invariance can be assumed, if the distributions basically show the same shape.
  - b) When scale-invariant levels are defined, the probabilities and weights can be averaged over these levels. The generator is only applicable within these levels.
3. Disaggregation: Now the previously built generator, as well as a low resolution time series for disaggregation is available. The process is carried out beginning with the first box at the given temporal resolution of the time series (e.g. 80 minutes at level 3 in Fig. 4.18) in these steps:
  - a) The position and volume class of the box is determined.
  - b) A uniformly distributed random number is drawn, and from it the type of division is determined using the probabilities for the given volume and position class.
  - c) The box is split up according to the type of division. In case of a x/x-division a second random number is generated, which is used to determine the volumes  $W_1$  and  $W_2$  with the help of the corresponding  $W_{x/x}$ -distribution of the box. The division occurs by multiplying the original volume with the weights and setting the resolution of the lower level to the half.
  - d) Division is repeated this way for all boxes of the level, thus forming the next lower level.

Steps 3a – 3d are repeated until the desired resolution (e.g. 10 minutes in Fig. 4.18) is reached.

### 4.6.3. ADAPTATION OF THE CASCADE MODEL TO *AtmoStations*

In order to provide high resolution precipitation data within PROMET, the above illustrated cascade model was implemented and adapted for the sub-component *AtmoStations*. An evaluation of the model approach and the parameterisation can be found in Section 5.1. Model validation is treated in Section 6.1. This section describes the implemented changes which had to be made for the adaptation of the cascade model to the requirements of this study.

#### 4.6.3.1. REGIONALISATION

GÜNTNER ET AL. (2001) compared parameters and performance of a cascade model in two climates with different rainfall generating mechanisms for three stations each. They found, that scale-invariance from daily time series down to hourly resolution is fulfilled well for both climates. But the model parameters differed noticeably, due to convective processes in the semi-arid tropical region (Brazil) and advective processes with frontal passages in the temperate area (United Kingdom). The main differences were a substantially lower value for

$P(x/x)$  in the semi-arid climate and higher probabilities  $P(0/1)$  and  $P(1/0)$  for starting, respectively ending boxes in the temperate climate. These observations can be attributed to frequent advective events with long durations in Britain, leading to prevalent  $x/x$ -divisions for enclosed boxes surrounded by  $0/1$ -divisions and  $1/0$ -divisions at the starting and ending boxes of the events. For convective events in Brazil, the lower  $P(x/x)$  values can be explained by higher probabilities, that an enclosed box belongs to an independent short-term rainfall and thus is more often split by a  $0/1$ - or  $1/0$ -division. Spatial parameter transferability for the Brazilian stations was given, whereas the British stations showed more pronounced regional differences.

These findings encourage a successful regionalisation of the model parameters, although the Upper Danube Basin shows a high spatial precipitation variability, caused by different processes (see Section 3.2.1.2). GÜNTNER ET AL. (2001) consider mean annual rainfall as a potential measure for parameter variations within the temperate climate. Indeed mean annual precipitation varies strongly within the Upper Danube Basin, but at the GLOWA-Danube test site it seems to be more reasonable to incorporate the different rainfall forming processes for distinguishing model parameter variations.

Based on the regional precipitation characteristics described in Section 3.2.1.2, precipitation regimes for the Upper Danube Basin are defined, which are used as a basis for parameterisation of the cascade model. Following precipitation regimes are considered to represent the characteristics of the study area adequately:

- (a) Low mountain ranges and surrounding areas: two nearly equal maxima in summer and winter, caused by convection respectively advection
- (b) Forelands: maximum of precipitation in summer, induced by convective processes
- (c) Alpine regions: very high maximum in summer, but also influenced by orographic lift

Typical annual variations for these regimes are presented in Fig. 3.3.

In order to perform disaggregation with a cascade model in *AtmoStations*, at first generators for each of the defined regimes have to be built. For the derivation of the parameters, high resolution precipitation data provided by the agrometeorological network Bavaria, as listed in Section 5.1 Tab. 5.1, is available.

During runtime *AtmoStations* has up to 377 proxels with weather stations available for interpolation, where exact precipitation amounts are known. In order to minimise computational effort and interpolation errors, disaggregation is done only on station proxels. Thus, when applying a regionalised generator, a mapping of the station proxels to their corresponding precipitation regimes is needed. The most significant differences between the regimes are the annual variations of precipitation, which are used as the primary decision criterion. The secondary criterion is the altitude of the proxel. FRÜH ET AL. (2006) found that mesoscale dynamical processes, as e.g. valley breezes are more important for precipitation distribution than orographic features. This confirms a classification of the regions not only by altitude, but also by rainfall regime. For assignment of the proxels to the regimes, the following rules are used:

1. *JJA/DJF*: if the ratio of the precipitation sums of the summer months (June, July, August) to the winter months (December, January, February) is less than 1.6, the proxel

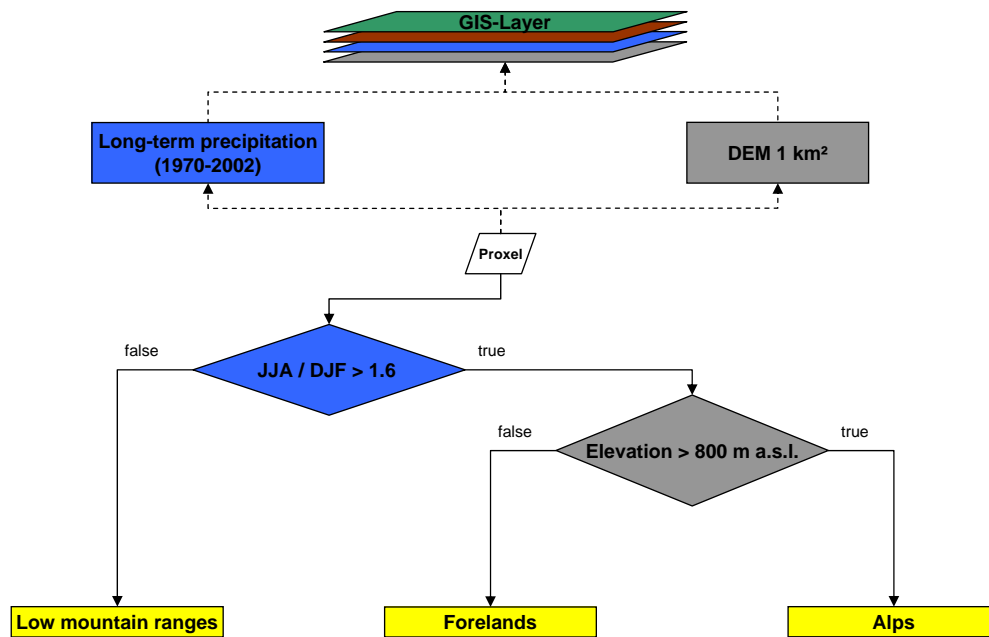


Fig. 4.20: Decision tree of precipitation regimes

is assigned to the low mountain ranges

2. Elevation: if the elevation of the proxel is less than 800 m, it belongs to the forelands regime, else it is alpine.

For automatic assignment of a regime to each proxel, the decision tree illustrated in Fig. 4.20 is applied. From long-term precipitation data (1970–2002) interpolated by PROMET, the ratio of the precipitation sums is calculated, and a second GIS-layer provides elevation data. With these input data sets, the decision tree is applied on each proxel, resulting in the pattern presented in Fig. 4.21. This spatial pattern serves as an input layer for *AtmoStations*. Each station proxel is looked up in this layer, to determine the precipitation regime and thus the generator, which will be used for disaggregation of rainfall data.

#### 4.6.3.2. MODIFICATIONS

For the purpose of this study some modifications to the model illustrated above are made, which are listed in the following:

- (a) GÜNTNER ET AL. (2001) introduced a weighting for the calculation of the generator probabilities of a generator. When averaging over the scale-invariant levels, the higher resolution levels contribute a larger amount of boxes to the statistics. Therefore they should have greater influence on the resulting properties of a generator to increase the accuracy of the estimated P values. The actual implementation considers this concept by calculating a weighting factor for each level in dependency of its number of wet boxes. When the properties of a generator are calculated, the statistics of each level are multiplied with the factor. This results in weighted probabilities  $P(1/0)$ ,  $P(0/1)$ ,  $P(x/x)$  and weighted probabilities of the  $W_{x/x}$ -distributions.

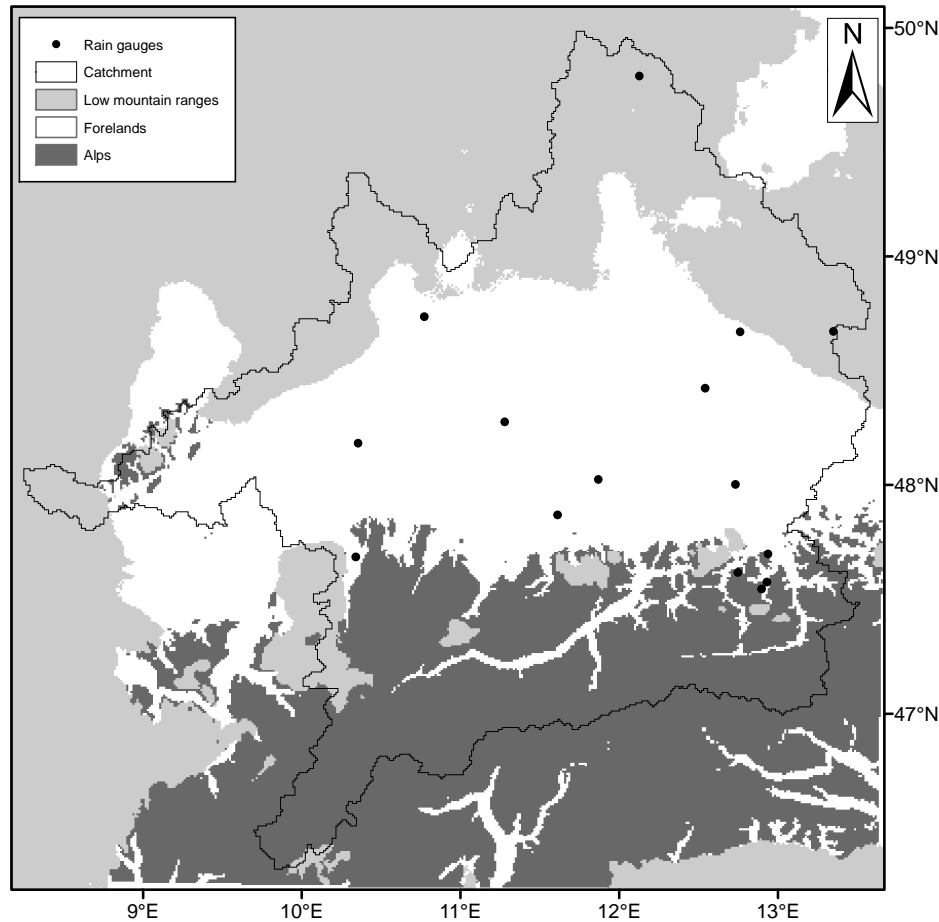


Fig. 4.21: Spatial pattern of precipitation regimes

Furthermore the definition of OLSSON (1998) for  $W_{x/x}$ -distributions leads to symmetrical distributions. GÜNTNER ET AL. (2001) defines the distribution as  $W_2 = 1 - W_1$ , allowing to reproduce internal event asymmetries. This way e.g. storm events may be represented better, as asymmetrical distributions can redistribute large parts of the volume to the beginning of the event.

- (b) The boundary between the volume classes was set by OLSSON (1998) to the mean volume of all boxes in a level. GÜNTNER ET AL. (2001) compared various values (upper and lower quartile, median and mean) to distinguish between small and large volumes. They found, that the mean suits best for the generation of the parameters of their model. But for application within this study, which focuses on heavy precipitation events, it seems to be reasonable to introduce a more significant threshold. The mean value does not contain information about the event structure, it just divides absolute values. It has long been recognised, that absolute rainfall amount not necessarily influences runoff and erosion, but its intensity and temporal distribution (see e.g. DIKAU, 1986). Heavy precipitation events lead to destruction of the soil aggregates at the surface, causing splash erosion as well as reduction of infiltration rates by soil sealing. Advective persistent precipitation may also have high volumes, but over longer time intervals, which induces surface runoff and erosion by overflow of the soil water storage. Therefore a separation of advective

and convective events is considered important. Assuming that convective precipitation has higher dynamics and variability than the usually more static advective events, rainfall intensity can be used to define a threshold for the generator. The gradient of the rainfall intensity between two consecutive boxes quantifies the relative dynamics of the precipitation event, irrespective of the absolute amount. Seasonal differences in precipitation patterns are governed either by convective processes, i.e. higher dynamics in summer, or advective processes in winter. However advective precipitation may also occur in summer, thus the generator must be capable of recognising these. In order to separate the events, the 90th percentiles are used instead of the mean, to differentiate more clearly between the rainfall characteristics. The evaluation of the generators properties in Section 5.1.3 shows, that probabilities and  $W_{x/x}$ -distributions of all regions are very similar, and thus regionalisation of the generator shall be achieved by fitting the volume threshold to the regions. Additionally the volume thresholds are calculated for each position class, as the latter contains implicit information about the dynamics in the event structure of the different regions.

- (c) To determinate the number of histogram intervals  $k$  for  $n$  values, OLSSON (1998) suggests the formula  $k = 1 + 3.3 \log n$ . A problem of this definition is, that for higher cascade levels too few values  $n$  exist, resulting in too few classes and thus a coarse probability distribution. If otherwise too many classes are formed, the number of members assigned to each class becomes very small. Therefore the number of classes is fixed in this study to seven, resulting in clear patterns of the histogram.
- (d) As the desired temporal resolution in AtmoStations is 1 h, a re-aggregation of the disaggregated boxes has to be made. The input resolution of precipitation data is 10, respectively 7 hours, which results after disaggregation over 7 levels in an output resolution of 9.375 min, respectively 6.5625 min. As a re-aggregation to 60 min does not result in integer numbers, the excess boxes are added to the re-aggregated volumes in a regular pattern.



## 5. PARAMETERISATION

*Note: As described in Section 4.2, the land surface model PROMET consists of a number of sub-models, which all have to be parameterised, and therefore need a huge amount of input data. It is beyond the scope of this work, to describe the exact parameterisation of the sub-models used within this study. Thus, merely the model parameters, which are most important for the results of the erosion module, are briefly addressed in appendix C.*

### 5.1. CALIBRATION OF THE CASCADE MODEL

This section covers not only the calibration and configuration of the cascade model. Because the study area is a very heterogeneous region, some preliminary testing has to be executed, in order to verify the applicability of the cascade model for the different geographic regions. Also the correct setup of the cascade configuration must be found and evaluated.

#### 5.1.1. AVAILABLE DATA

For calibration and validation of the cascade model, high resolution precipitation data, as presented in Tab. 5.1, is available. The datasets are provided by four different organisations:

- German Weather Service (DWD): the DWD not only provides long-term measurements from climate stations three times per day, but also has a meteorological station (*Schönanau*), recording with a temporal resolution of 10 min.
- Central Institute for Meteorology and Geodynamics (ZAMG): the ZAMG of the Austrian Federal Ministry of Science and Research operates station *Untersberg* with a measuring interval of 30 min.
- Bavarian Avalanche Warning Service (LWD): the LWD operates the stations *Reiteralm* and *Kühroint* of the *Berchtesgaden National Park* in a 10 min interval.
- Bavarian State Office of Agriculture (LfL): all other stations in Tab. 5.1, which were not mentioned above, belong to the agrometeorological network Bavaria, which measures in a 10 min cycle.

Stations from the DWD, ZAMG and LfL have to fulfill high quality standards, and data is corrected before delivery. LWD stations are located in high mountain areas and therefore measurements are more influenced by incidents as e.g. wind drift or snow packs falling down into the devices. The records received were post-processed at the Department for Geography, LMU, and measurement errors have been corrected.

This data is used to derive a cascade parameterisation for disaggregation over a time scale ranging from 10 min to 640 min.

Tab. 5.1: Attributes of the stations used for calibration of the generators of the cascade model. The temporal resolution of the stations is 10 min, except for Untersberg (30 min) and Jenner (15 min). The regimes are denoted with (a): Low mountain ranges, (b): Forelands and (c): Alps. (\*): no data of 1997.

Name	Latitude	Longitude	Altitude [m a.s.l.]	Mean annual precipitation [mm]	Time period	Regime
Engersdorf	48°27'08" N	12°38'04" E	460	800–900	'95–'05 (*)	(b)
Großberghofen	48°19'21" N	11°18'44" E	345	800–850	'95–'05	(b)
Jenner	47°35'45" N	12°59'50" E	660	n/a	'04–'05	(b)
Konnersreuth	49°49'36" N	12°15'01" E	540	700–800	'95–'05	(a)
Kringell	48°40'52" N	13°29'35" E	450	900–1000	'00–'05	(a)
Kühroint	47°33'57" N	12°57'39" E	1407	n/a	'04–'05	(c)
Neuhof	48°47'09" N	10°47'10" E	518	700–800	'95–'05	(b)
Neusling	48°41'40" N	12°52'36" E	345	750–800	'95–'05	(b)
Nilling	48°01'40" N	12°48'45" E	390	1000–1400	'95–'05 (*)	(b)
Osterseeon	48°03'54" N	11°55'08" E	560	1000–1400	'95–'05	(b)
Reiteralms	47°38'32" N	12°48'40" E	1615	n/a	'04–'05	(c)
Reschenberg	48°13'58" N	10°21'01" E	560	800–950	'95–'05	(b)
Schönau	47°36'38" N	12°59'02" E	617	n/a	'02–'05	(b)
Spitalhof	47°44'03" N	10°20'11" E	720	1100–1400	'95–'05	(b)
Untersberg	47°43'07" N	13°03'08" E	1776	approx. 1900	'98–'04	(c)
Wettlkam	47°54'46" N	11°38'55" E	675	1100–1400	'95–'05 (*)	(b)

### 5.1.2. VERIFICATION OF THE MODEL APPROACH

Picking up the requirements on a disaggregation model postulated in 4.6.1, some preliminary considerations have to be made, in order to verify the concept of the model for usage within PROMET. Prior to applying the model in *AtmoStations* the impacts of a different disaggregation method on possibly affected components of PROMET have to be considered, as temporal precipitation patterns not only influence the erosion model:

- The conventional disaggregation method is not able to produce hourly rainfall intensities greater than the half of the rainfall amount within one *Mannheimer Stunde*. Theoretically, the cascade model may redistribute the entire volume of one *Mannheimer Stunde* to a single time step, as it includes *1/0-divisions* and *0/1-divisions*. But since the divisions are based on an empirical probability distribution, such a redistribution is virtually impossible. Nevertheless, higher rainfall intensities compared to the conventional disaggregation may be expected. Although PROMET does not include a module for soil surface sealing, formation of surface runoff might be influenced by higher precipitation intensities. The soil water module in PROMET uses the infiltration capacity after EAGLESON (1978), which is derived from the well-known *Philip* equation (cf. Section 4.2.2). Hence, if the precipitation intensity exceeds the infiltration capacity, surface runoff is generated. Therefore potential impacts of modified rainfall intensities on runoff formation should be considered.
- Disaggregation in *AtmoStations* currently occurs over the whole interval between two



*Mannheimer Stunden*. Thus it is most likely, that the generated number of wet intervals is overestimated by trend. In contrast, the *1/0-divisions* and *0/1-divisions* of the cascade model may lead to a higher amount of dry periods, possibly even to erroneous separation of events. Since this influences evapotranspiration, a preliminary inspection of changes in the dry periods shall be made.

- The stochastic redistribution of precipitation leads to different realisations, dependent of the random seed used during disaggregation. For model validation this means, that an averaging of model runs over a sufficient number of simulations with different seeds has to be executed. On the other hand model simulations with PROMET should be fully reproducible, which can be achieved by using the same seeds for model runs. Thus validation of the cascade model will be made with an ensemble of disaggregation simulations, and impacts on PROMET will be assessed with a fixed random seed.
- A temporal shift of disaggregated events alters runoff formation. In both disaggregation models a temporal shift of the disaggregated events is very likely to occur. The conventional disaggregation method disaggregates precipitation with a constant pattern, and thus cannot reproduce the actual time of occurrence of the event. The cascade model distributes precipitation randomly and may reproduce the actual time of the event only with a certain probability. But as this shift sums up to a maximum of 10 hours and the focus of PROMET lies on long-term modelling of global change impacts, this issue can be considered insignificant.
- A temporal shift of disaggregated events alters runoff formation. In both disaggregation models a temporal shift of the disaggregated events is very likely to occur. The conventional disaggregation method redistributes precipitation schematically between two *Mannheimer Stunden*, irrespective, when the event actually occurred, whereas the cascade model rearranges rainfall randomly. But as this shift sums up to a maximum of 10 hours and the focus of PROMET lies on long-term modelling of global change impacts, this issue can be considered insignificant.

For evaluation of possible influences on other model components and comparison of the two methods, a series of model runs was executed and analysed. As the common time step used in PROMET is one hour, and thus the disaggregation routine of *AtmoStations* also works on this interval, analysis is done on an hourly basis. Three different disaggregation methods are tested and compared to measured data with the following setup:

1. constant linear disaggregation (CLD): a constant rainfall intensity is assumed for the whole sampling interval, i.e. the measured precipitation sum is distributed linearly over the preceding hours, resulting in equal hourly values of one 7th respectively one 10th of the sum. This model is only used as a benchmark for the other models tested and to stress differences between them.
2. simple advective-convective disaggregation (ACD): This is the conventional method implemented in *AtmoStations* and described in Section 4.2.1.2. The only difference to the CLD is the altered disaggregation of convective events.

3. cascade disaggregation (CD): This is the model after OLSSON, as delineated in Section 4.6.2. For evaluation, one generator for each station was calculated by successively aggregating the data over 7 levels to 640 minutes. This target resolution of approximately 10 hours was chosen, as it is the maximum time step between two *Mannheimer Stunden*, which subsequently shall be disaggregated. For these preliminary tests scale invariance of the cascade was assumed, and the properties of the generators were calculated from all available levels. Disaggregation was done from the aggregated 640 min down to 10 min and then sequentially re-aggregated to 1 hour to provide the common base for evaluation of the models.

Because CLD and ACD are of deterministic behaviour, one model run for each time series is sufficient for calculating statistics, whereas for CD 100 ensemble runs with different random seeds are used to obtain mean model performances. As already mentioned in Section 4.6.1, the study area is made up of different climate regions, therefore the following three datasets from representative meteorological stations were chosen for analysis:

- (a) *Konnernsreuth*: with a total number of datasets  $n = 96422$  and a total precipitation sum of 7350 mm. The percentiles of the recorded precipitation volumes [mm/ $\delta$  t] are:  $P_{25} = 0.1$ ,  $P_{50} = 0.3$ ,  $P_{75} = 0.8$ ,  $P_{90} = 1.6$ .
- (b) *Osterseeon*: with a total number of datasets  $n = 96422$  and a total precipitation sum of 11580 mm. The percentiles of the recorded precipitation volumes [mm/ $\delta$  t] are:  $P_{25} = 0.1$ ,  $P_{50} = 0.4$ ,  $P_{75} = 1.0$ ,  $P_{90} = 2.0$ .
- (c) *Reiteralm*: with a total number of datasets  $n = 8325$  and a total precipitation sum of 1459 mm. The percentiles of the recorded precipitation volumes [mm/ $\delta$  t] are:  $P_{25} = 0.2$ ,  $P_{50} = 0.5$ ,  $P_{75} = 1.1$ ,  $P_{90} = 2.4$ .

The resulting statistics of the disaggregation experiments are listed in Tab. 5.2. For calculation of the number of events greater than the 25th, 50th 75th and 90th percentiles the values of the measured data as specified above have been used. Since the measured time series naturally contain a high amount of intervals with zero rainfall, zero values have been omitted for calculation of the percentiles, the mean and the standard deviation.

As expected, a comparison of the results of the performance of the different methods shows, that CD leads to a higher variability and stronger extreme values, than the CLD and ACD. This is true for all regions and results from the conceptual design of the models. The number of intervals with precipitation is largely overestimated by CLD, as every *Mannheimer Stunde* with recorded precipitation leads to a preceding wet interval of at least 7 hours (which also results in the low mean value). But also ACD overestimates the number of wet intervals, as it uses nearly the same redistribution of wet intervals as CLD. This redistribution additionally causes lower standard deviations (i.e. lower temporal variability) and mean values than found in the measured datasets. Differences between the two techniques can be found in the better reproduction of maxima and percentiles of ACD, because of the consideration of convective events. Nevertheless, these are too low, compared to the measured values, and the frequencies of storm events are reduced, whereas precipitation intervals with lower volumes are overestimated. This is, as already mentioned, due to the limitation of maxima to the half of the measured volume, and the cutback in the percentiles very likely derives from the extent

Tab. 5.2: Mean performances of the different disaggregation methods compared to measured values. Listed are statistics of hourly precipitation sums [mm] for the stations Konnersreuth (a), Osterseeon (b) and Reiteralm(c). (no > 0: number of intervals with precipitation > 0, %-zero: percentage of zero rainfall intervals, max: absolute maximum,  $\sigma$ : standard deviation, no >  $P_{XX}$ : number of intervals > XXth percentile of measured data)

Station	Method	no > 0	%-zero	mean	$\sigma$	max	no > $P_{25}$	no > $P_{50}$	no > $P_{75}$	no > $P_{90}$
(a)	meas.	10769	88.8	0.68	1.19	39.00	7511	5021	2594	1045
	CLD	28782	84.2	0.26	0.42	7.53	14574	7396	2267	494
	ACD	26747	84.8	0.27	0.47	20.05	14065	7237	2307	547
	CD	12044	88.0	0.61	1.00	35.81	9157	6351	2767	882
(b)	meas.	13589	85.9	0.85	1.44	31.70	10144	6325	3178	1314
	CLD	31316	79.8	0.37	0.56	6.11	18725	8810	2890	731
	ACD	29739	80.3	0.39	0.59	12.40	18298	8749	2944	779
	CD	14942	85.2	0.77	1.22	27.17	11733	7742	3581	1185
(c)	meas.	1284	84.6	1.14	2.40	29.70	930	620	320	125
	CLD	2226	79.5	0.66	1.41	19.07	1412	769	350	99
	ACD	2152	79.9	0.68	1.47	19.07	1387	755	345	93
	CD	1005	87.7	1.45	2.27	21.83	800	629	397	149

of convective events over two *Mannheimer Stunden*. Since events in summer mostly occur in evening hours, they are recorded in two succeeding measuring intervals (21:00 CET and 07:00 CET), and thus disaggregated as an advective event.

By contrast all of the statistical values of CD are considerably more closely to the values of the measured datasets. Concerns about too high rainfall intensities can be rejected, as confirmed by the values of absolute maxima and particularly by the number of intervals exceeding the percentiles  $P_{75}$  and  $P_{90}$ . By means of the statistical values assessed an erroneous event separation cannot be rejected, but as the total number of wet events is represented adequately by the model, merely the mentioned shift of up to 10 hours can occur.

Concerning the statistical differences between the regions, these can derive in the case of the deterministic techniques only from the characteristics of regional rainfall patterns, whereas CD should be able to reproduce the patterns in all regions with similarly good results. But by comparing the regional CD results it can be noticed, that the number of intervals > 0 is lower and the mean and upper percentile values are higher as in regions (a) and (b). This may indicate an overestimation of extreme values in the Alpine region.

Additionally Tab. 5.3 lists the statistics of the kinetic energy content of the 1 hour intervals from the time series. Kinetic energy content is calculated with the following equation, which is commonly used in derivatives of the USLE (see e.g. MORGAN, 2001):

$$e_k = 8.95 + 8.44 \log I \quad (5.1)$$

with  $e_k$ : kinetic energy [J/m<sup>2</sup>mm] and  $I$ : rainfall intensity [mm/h].

The calculation of the kinetic energy for CD is based on high resolution 10 min disaggregated data. Although the results of CD thereby cannot be compared directly with the deterministic methods, they are presented here, to demonstrate the impacts and potential usefulness of high resolution rainfall on hydrologic and erosion modelling.

Tab. 5.3: Mean performances of the different disaggregation methods compared to measured values. Listed are statistics of hourly kinetic energy [ $\text{J}/\text{m}^2\text{mm}$ ] for the stations Konnersreuth (a), Osterseeon (b) and Reiteralm(c). Note, that the values for “CD” and “measured” are based on 10 min intervals, whereas “ACD” and “CLD” are based on 1 h, i.e. they are not comparable. ( $\text{no} > 0$ : number of intervals with kinetic energy  $> 0$ ,  $\text{max}$ : absolute maximum,  $\sigma$ : standard deviation,  $\text{no} > P_{XX}$ : number of intervals  $> XX$ th percentile of measured data)

Station	Method	no $> 0$	mean	$\sigma$	max	no $> P_{25}$	no $> P_{50}$	no $> P_{75}$	no $> P_{90}$
(a)	meas.	10769	25.32	19.83	114.95	7511	5359	2679	1076
	CLD	15187	4.73	2.96	16.35	3346	0	0	0
	ACD	14643	4.80	3.02	19.94	3327	1	0	0
	CD	11546	20.83	16.79	116.47	9295	4839	1861	589
(b)	meas.	13589	29.05	21.49	124.73	10144	6789	3397	1352
	CLD	19433	5.40	3.24	15.59	6186	0	0	0
	ACD	18981	5.46	3.28	18.18	6166	0	0	0
	CD	14298	24.13	19.25	126.98	11802	5809	2356	817
(c)	meas.	1284	31.52	22.33	127.62	907	637	320	128
	CLD	1710	6.33	3.44	19.76	31	0	0	0
	ACD	1674	6.37	3.46	19.76	37	0	0	0
	CD	1021	27.60	22.71	118.15	651	389	205	85

The results in Tab. 5.3 altogether show the same tendencies as those in Tab. 5.2, though differences between the disaggregation methods are more accentuated, which basically comes from the higher temporal resolution, but also from generally higher rainfall intensities. Maxima and all percentile values of the two deterministic methods are considerably lower, whereas CD reproduces the values calculated from the measured data relatively well. Reviewing these results in conjunction with those from Tab. 5.2 the better performance derives from the characteristics of a cascade model: the utilisation of  $0/1$ - and  $1/0$ -divisions leads to a large amount of dry intervals and the empirically calculated weights  $W_1$  and  $W_2$  frequently distribute rainfall in variable sized volumes.

Summarising the outcomes of this section, the cascade approach provides reasonable results in rainfall disaggregation, and therefore shall be parametrised in the next section.

### 5.1.3. MODEL PARAMETERISATION FOR THE STUDY AREA

In order to find the appropriate cascade configurations for the different regions defined in Section 4.6.3.1, three representative stations have been chosen for assessment of the generator properties. As a result, different probabilities  $P(1/0)$ ,  $P(0/1)$ ,  $P(x/x)$  and  $W_{x/x}$ -distributions for each region, which reflect the different rainfall generating mechanisms of the distinguished precipitation regimes, may be expected, which is tested in the following.

Following the definitions in Section 4.6.2, for each station weighted empirical properties are calculated over 7 levels, irrespective of potential non-scale-invariance. Examining the results presented in Fig. 5.1, one notices that all probabilities of all stations range in the same magnitude. The only discrepancy can be observed for the probabilities of isolated boxes with volumes above mean. The break at station (c) might indicate the stronger influence of heavy convective summer precipitation. But as the total number of records in this dataset is rela-

tively small, this is probably caused by insufficient occurrences of  $W_{x/x}$ -distributions for this position and volume class in the lower levels<sup>1</sup>. This cannot be found in datasets from other stations of the same region, and therefore can be neglected. So the similarity of the probabilities of the three stations leads to the assumption, that the usage of multiple generators (one for each region) is redundant.

One can see a strong dependency of the probabilities from the position class, i.e. high values of  $P(0/1)$ ,  $P(1/0)$  at starting respectively ending boxes, and frequent  $x/x$ -divisions for enclosed boxes. For all volumes above mean the probability of  $x/x$ -divisions increases substantially, so  $W_{x/x}$ -distributions have considerable influence on higher event volumes. Therefore, before confirming the assumption, that using only one generator for all regimes is enough, the histograms of the  $W_{x/x}$ -distributions should be analysed.

A visual comparison of  $W_{x/x}$ -distributions of stations from the different regions shows, that they do not differ significantly. Fig. 5.2 illustrates an typical example, what the  $W_{x/x}$ -distributions generally look like. As expected, they exhibit similar shapes as the histograms of stations in temperate climate, as presented by GÜNTNER ET AL. (2001). The position classes form the most accentuated patterns, reproducing the typical structure of precipitation events: starting and ending classes are left respectively right skewed, forming ascending and descending patterns, which assign the bulk of the volume to the event. Distributions for enclosed boxes are bell-shaped, as precipitation is mostly distributed equally within the event. Noticeable are the peaks at  $W_1$  volumes of 50% in all position classes below mean volume. These lead to an altogether more even distribution in lower precipitation events. In classes above mean value the peaks disappear in favour of a shift into the “direction” of the event. That means for starting boxes, that the probability of higher  $W_2$  volumes increases, distributing a larger part of the volume to the event, instead of dividing it into halves (as likely for volumes below mean). This applies analogously to the ending boxes. For isolated boxes above mean the distribution is rather evenly distributed with a slight ascend to higher  $W_1$  volumes. Thus it follows, that events with higher volumes are disaggregated more often into a large and a small part, conserving rainfall intensity peaks.

Altogether, the properties of the generator, especially the differences between the volume classes below and above mean, reflect the advective as well as convective processes of the regions. Basically the governing processes are the same in all regions, their influence is merely of different intensity within the seasonal course (see Section 3.2.1.2), which obviously are depicted implicitly by the generators properties. Therefore only one generator will be used, under the premise that seasonal influences can be represented correctly. This can be achieved by using seasonal generators, but as various studies (see e.g. OLSSON, 1998; GÜNTNER ET AL., 2001; HINGRAY & BEN HAH, 2005) showed that this brings only insignificant improvements, a redefinition of the volume class threshold is used for this purpose. For each region all records of the corresponding stations were used to calculate the 90th percentiles of the gradients of the rainfall intensity between two consecutive boxes (as described in Section 4.6.3.2) for all position classes. This results in the thresholds dividing the volume classes “above” and “below”.

<sup>1</sup>Each transition to a lower level, i.e. a doubling of the temporal resolution, reduces the number of available boxes by 50%. Thus, at the lower levels less boxes are available for the calculation of statistics, which may distort the results.

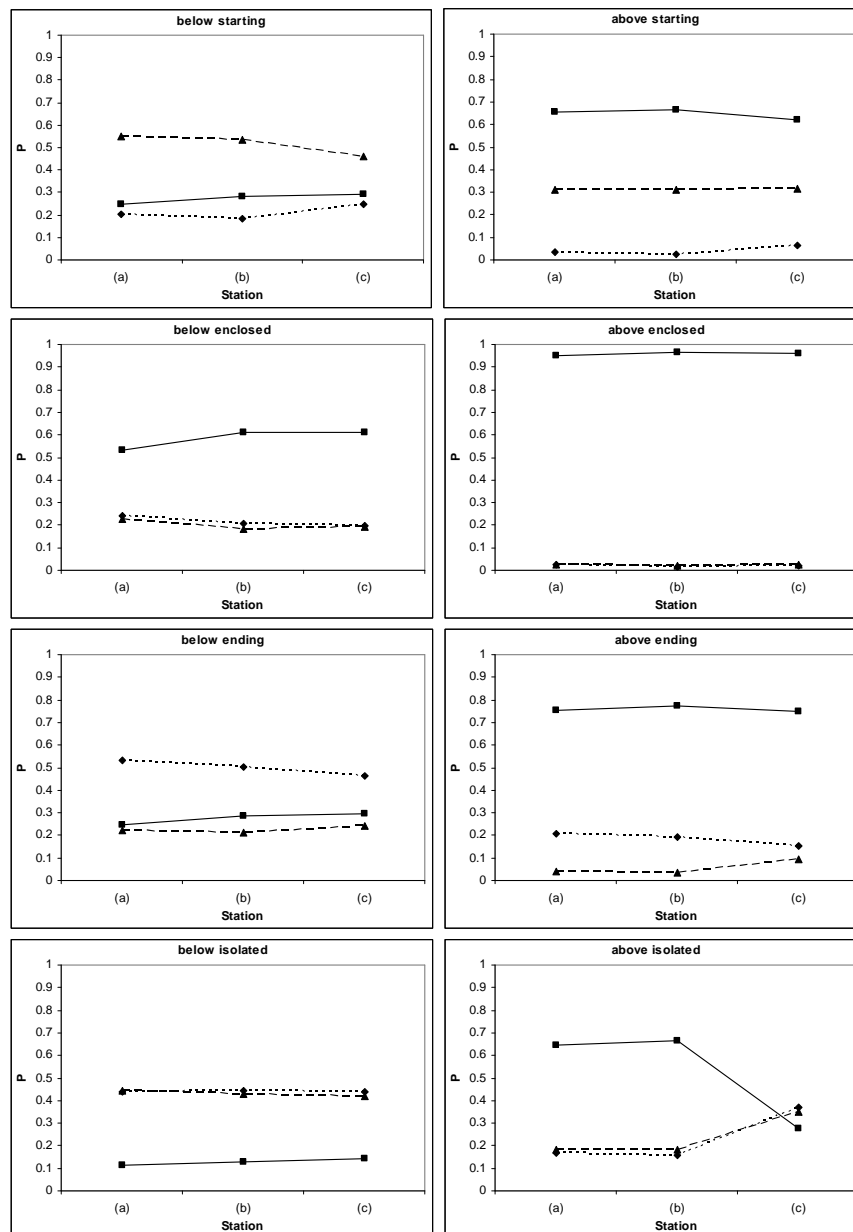


Fig. 5.1: Comparison of the empirical probabilities  $P(1/0)$ ,  $P(0/1)$  and  $P(x/x)$ , derived from the stations Konnersreuth (a), Osterseeon (b) and Reiteralm (c). (dashed: 0/1-division, solid: x/x-division, dotted: 1/0-division)

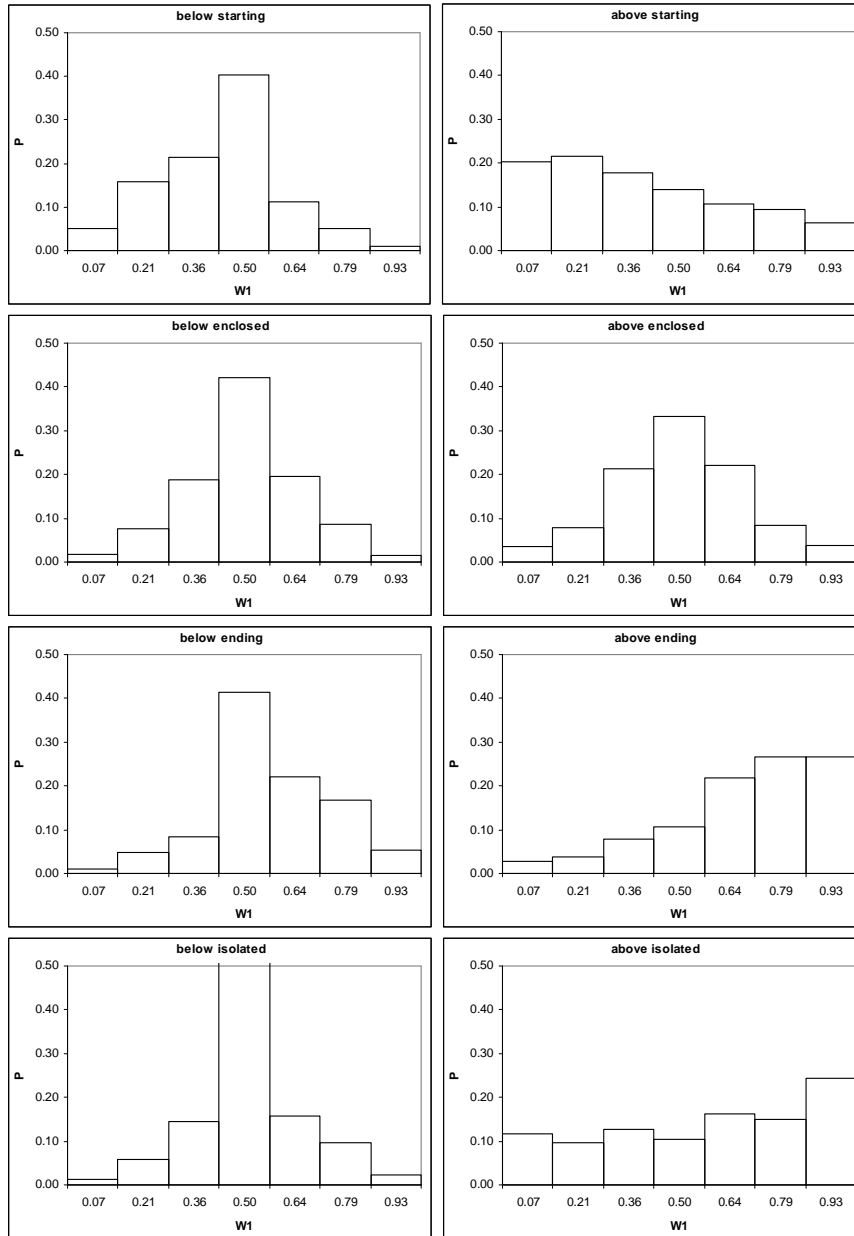


Fig. 5.2: Exemplary  $W_{x/x}$ -distributions for all volume and position classes, empirically derived from station Osterseen. (Further explanations in the text.)

Fig. 5.3 shows the averaged thresholds for timescales between 10 min and 640 min. But as disaggregation shall be done down from 10 respectively 7 hours, there is a slight temporal shift to the aggregated cascade levels (10.6 respectively 5.3 hours), and thus the empirically determined thresholds are not applicable for disaggregation of the resolutions available in *AtmoStations*. Therefore a power function of the form

$$y = ax^b \quad (5.2)$$

with  $y$ : gradient [mm/h] and  $x$ : resolution [h]

was fitted to the empirical thresholds. Eq. (5.2) in combination with the coefficients  $a$  and  $b$ , listed in Tab. A1 in appendix A, allows for calculation of the volume threshold at the desired

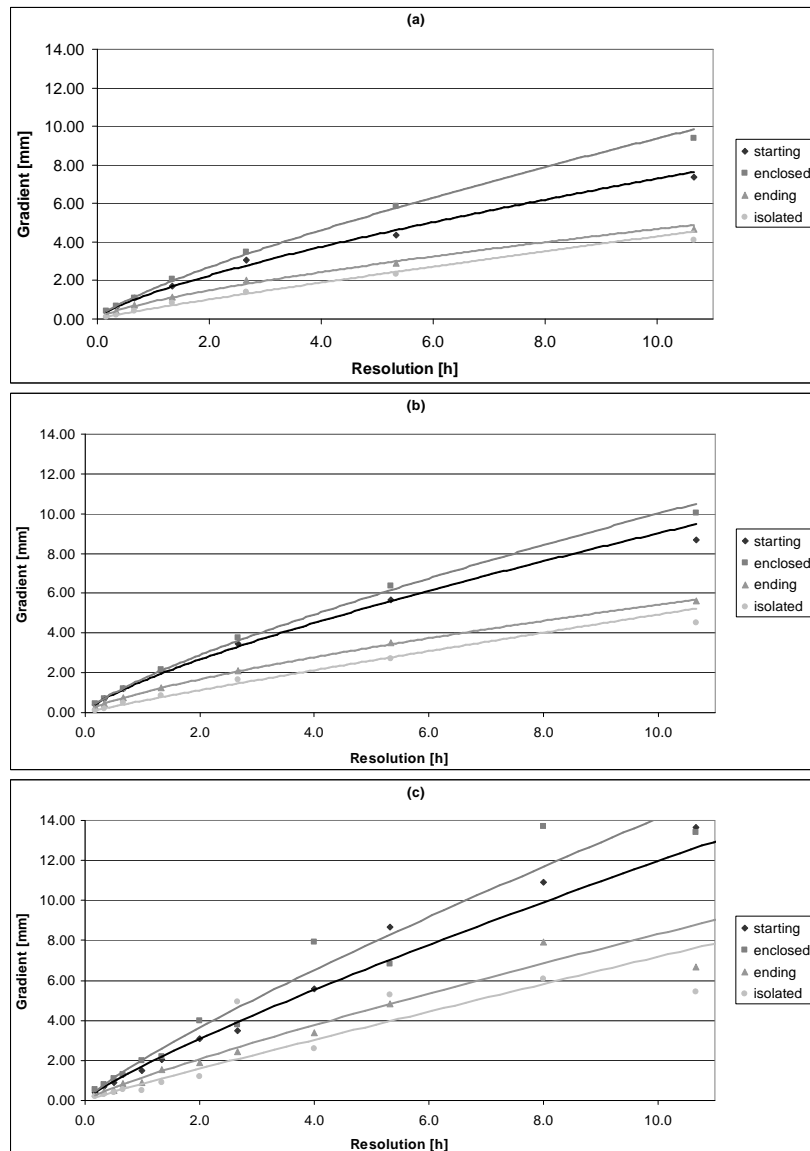


Fig. 5.3: Mean volume class thresholds (90th percentiles of the gradients) for all position classes of regions (a): Low mountain ranges, (b): Forelands and (c): Alps. Lines are fitted power functions, dots are empirical mean values.

resolutions. Comparing the diagrams in Fig. 5.3, it is noticeable, that the thresholds tend to increase from region (a) to (c), indicating higher dynamics in the Forelands and Alps. This fits reasonably to the higher precipitation amounts in summer in these regions, caused by higher convective activity, and more frequent storm events with high intra-storm variability. The diagram for region (c) has a somewhat higher scatter than the other, probably caused by some minor errors in measurement for stations *Kühroint* and *Reiteralm*, which are difficult to locate. On such potential outliers, the regression equation has a smoothing effect.

Based on the findings above, a single generator for all regions is calculated from the data available (except for *Untersberg*, as its resolution amounts to 30 min). For the calculation of the generator, the volume thresholds of the respective regions are used, and all modifications described in Section 4.6.3.2 are applied. Since the generator may only be applied over



Tab. 5.4: Empirically determined probabilities  $P(1/0)$ ,  $P(0/1)$  and  $P(x/x)$  of the generator.

Volume	Position	Division		
		0/1	x/x	1/0
below	starting	0.51	0.32	0.17
	enclosed	0.12	0.74	0.14
	ending	0.20	0.29	0.51
	isolated	0.44	0.11	0.45
above	starting	0.28	0.70	0.02
	enclosed	0.09	0.86	0.05
	ending	0.03	0.79	0.18
	isolated	0.19	0.64	0.17

a time scale, for which scale-invariance is given (cf. Section 4.6.2.1), this condition has to be checked, prior to calculating the generator. For assessment of scale-invariance, the properties of the cascade generator are plotted over all levels (see appendix A). These plots are *not* weighted, as they indicate the degree of scale-invariance. They are used for evaluation of scale-invariance, and if scale-invariance can be assumed, weighted averages of the properties over all (scale-invariant) levels may be calculated. The probability plots in Fig. A1 show a generally smooth distribution with no clearly recognisable trend. The break between 0/1- and 1/0-divisions at the lowest resolution for isolated boxes above threshold, is supposed to result from station *Reiteralm*, similar to the irregularity noted above in Fig. 5.1. This issue again can be neglected, as a weighting of the probabilities over all levels will compensate potential measurement errors. A comparison of the  $W_{x/x}$ -distributions of all position classes (see appendix A) shows, that the distribution over all levels has the same tendencies, also over both volume classes. Starting and ending boxes show nearly the same shapes for all levels, naturally mirrored at  $W_1 = 0.5$ . At this point higher resolutions with volume below threshold show a pronounced peak, resulting from a more even distribution in advective events. This is also true for the other position classes. With increasing interval duration the pattern smoothens, i.e. a distribution in two uneven volumes becomes more probable, produced by the general shape of precipitation events. After averaging over the scale-invariant levels this variation of the  $W_{x/x}$ -distributions with increasing modulations will be implicitly included in the generator, as

- the shape of distributions above volume threshold resemble those of the volumes below threshold at lower temporal resolution and
- the volume threshold function is not defined linearly over all levels, i.e. is capable of recognising event structure in dependence of temporal resolution.

Overall, the properties of the generator exhibit sufficient consistency over all levels, therefore scale-invariance is considered to be fulfilled and the weighted averages of the properties were calculated. In order to merge the generators of the three regions, they were weighted depending on the quantity of their contributed input data. Resulting probabilities are illustrated in Tab. 5.4 and  $W_{x/x}$ -distributions in Fig. 5.4.

The properties of the generator reasonably reflect the event structure in the study area.

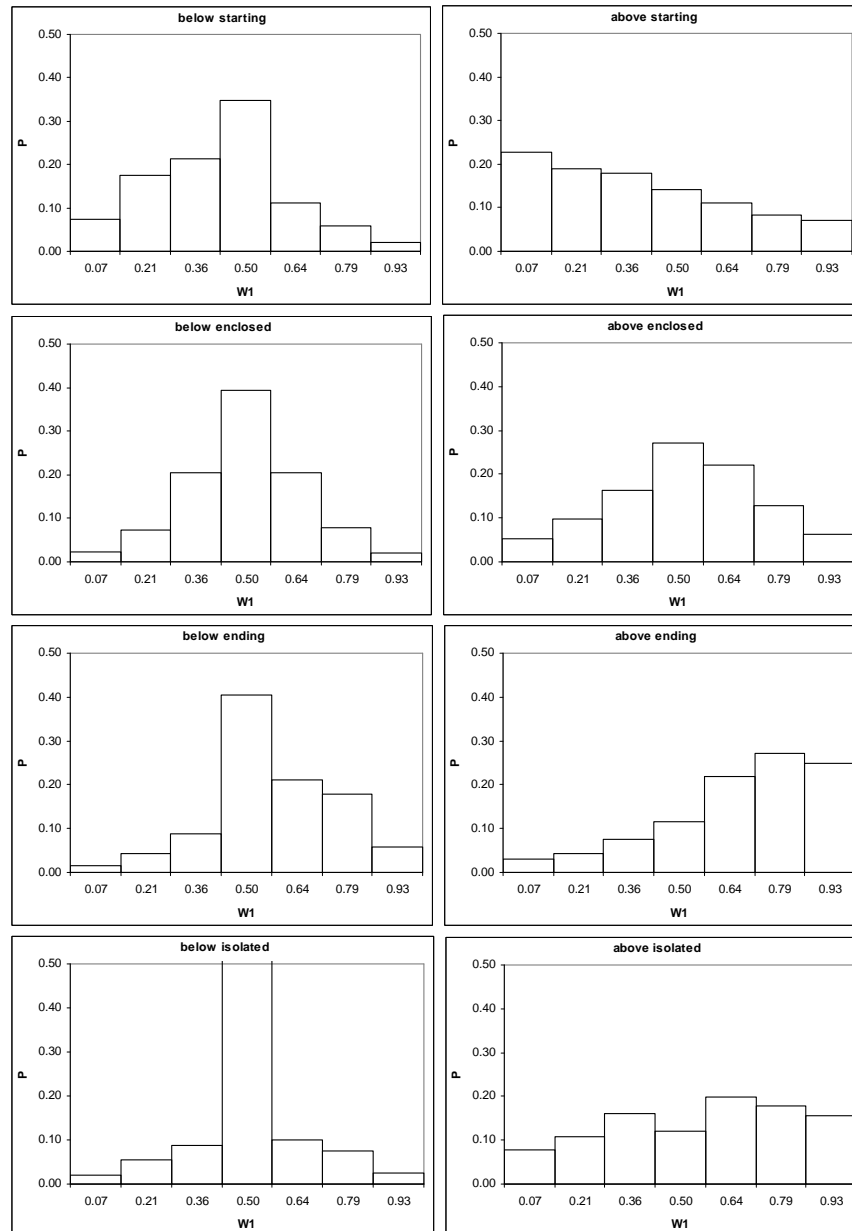


Fig. 5.4: Empirically determined  $W_{x/x}$ -distributions of the generator (for numerical values see Tab. A2).

For advective events with low volumes, the high values of  $P(0/1)$  respectively  $P(1/0)$  induce a distinct delineation of the beginning and ending of the event. Within the event (i.e. enclosed boxes), the probability of a  $x/x$ -distribution is highest, and the high probability of  $W_1$  and  $W_2$  receiving 50% of the volume, distributes precipitation evenly.  $W_{x/x}$ -distributions for starting and ending boxes show the tendency to distribute precipitation rather moderate to the event. Altogether this results in a gradually beginning and ending, steady event. By contrast, convective events are disaggregated with higher variability. For all position classes the probabilities  $P(x/x)$  are dominating, i.e. the  $W_{x/x}$ -distributions gain in importance. Starting and ending  $W_{x/x}$ -distributions more often cause a split-up in uneven parts, compared to volumes below threshold, thus conserving peaks better. Inside the events distributions of 50% of the volume prevail, but not as strong as for volumes below threshold, leading to the more

irregular structure of storm events.

The comparison of the generators properties has shown, that a differentiation of the regions via multiple generators is not necessary, as the rainfall generating mechanisms in the study area are basically the same. Obviously, climatic differences have to be more distinct, as e.g. in the study of GÜNTNER ET AL. (2001). They found greater differences in the properties of a generator in a temperate climate with frequent advective events, and a semi-arid climate with dominating short-term convective rainfall. Problems in performance arose especially for the frontal-dominated temperate climate, with an overestimation of rainfall extremes with increasing temporal resolution. In this study this problem shall be overcome with a discrimination of advective and convective events with a resolution-dependent gradient. With increasing regional convective activity this threshold increases, and thus should be capable of separating the different rainfall dynamics of the regions.

## 5.2. PARAMETERISATION OF THE EROSION MODULE

“Since future conditions are necessarily unknown, calibration is particularly undesirable for global change studies” (FAVIS-MORTLOCK ET AL. (1996) as quoted in (JETTEN ET AL., 1999)). Just for this reason the erosion module shall not be calibrated, and furthermore, this is virtually impossible at the current state of art in erosion modelling. Usually all physically based erosion models have one or more central parameters, which are either intended for calibration<sup>2</sup>, or are at least adjusted by the user, even if not intended for this purpose<sup>3</sup>, in order to fit the model results to measured data. To overcome this dilemma between the need to calibrate, and the intention not to calibrate, a suggestion of JETTEN ET AL. (1999), who examined the performance of six erosion models under the same conditions, is followed. They recommend a visual calibration by means of comparing observed and simulated erosion *patterns*, instead of focusing on sediment leaving the study area. Thus the following procedure was applied for the determination and optimisation of the parameters:

1. Eliminate as much static calibration parameters as possible, by fixing them to a constant value. So e.g. the deposition coefficient is fixed.
2. Eliminate as much variable parameters as possible, by making them dependent on influencing parameters. (This step was already dealt with in model adaptation, Section 4.5). So e.g. the critical momentum flux of the soil is bound to soil and plant properties.
3. Set all well-known parameters, which are used in equations of step 2, to reasonable values from literature sources. If a parameter is not known well, make a best guess.
4. Compare model outputs to observed data, especially for temporal patterns (e.g. like response of soil loss to FT cycles), rather than for absolute values. If the model outputs does not deliver satisfying results, go to the previous step.

---

<sup>2</sup>E.g. EUROSEM provides guidelines (MORGAN ET AL., 1998) for parameter calibration and EROSION 2D offers a deposition coefficient, which is suggested for calibration.)

<sup>3</sup>E.g. the erosion resistance in EROSION 2D is a physically based parameter, but as no suitable method for its measurement has been found yet, it can be experimentally determined by adjusting it in simulation runs, until modelled sediment output matches measured sediment output.

Tab. 5.5: Values for effective cohesion  $c'$  and angle of shearing resistance  $\varphi'$  for all soil type classes.

Soil type class	$c'$	$\varphi'$	Soil type class	$c'$	$\varphi'$
Sand	0.5	30.0	Clay Loam	8.0	22.3
Gravelly Sand	0.5	30.0	Clay	10.5	20.5
Loamy Sand	1.0	25.9	Peat	n/a	n/a
Gravelly Loamy Sand	1.3	24.1	Soils on Calcareous Rock	6.0	23.7
Sandy Loam	1.3	25.9	Soils on Crystalline Rock	2.0	26.3
Sandy Loam on Gravel	1.4	26.5	High Alpine Soils	8.0	22.3
Clayey Silt	1.5	20.0	Soils on Karst	9.0	21.0
Silt Loam	1.5	21.2			

### 5.2.1. CRITICAL SHEAR STRESS

As mentioned in Section 4.5.5.1, the correct parameterisation of the erosion resistance is a crucial task, therefore it is determined with a dynamic calculation, depending on soil cohesion, root reinforcement and FT cycles.

The basic value for the critical shear stress is the soil cohesion, which has been estimated for the soil types in the Upper Danube Basin from literature sources (MORGAN ET AL., 1998; LIU ET AL., 2003). Guidelines for the angle of shearing resistance are listed in DVWK (1995), LFULG (2005) or LEBERT (2008). The selected values for the effective cohesion  $c'$  and the angle of shearing resistance  $\varphi'$  are listed in Tab. 5.5. As the depicted values for the angle of shearing resistance are only valid for matric suctions from 0 – 500 kPa (approx. a pF-value of 3.7), the calculation of shear strength is limited to a pF-value of 3.7 (or 500 kPa), i.e. is set to a maximum at this value and does not increase, even if the matric suction increases.

Literature values for calculation of root reinforcement via the root length density (Eq. (4.53)) range up to  $0.004 \text{ km/m}^3$  for interrill erosion, but as rill erosion is taken into account (Section 4.5.5.3), this parameter is set to a somewhat higher value of  $0.056 \text{ km/m}^3$  (this is the mean value for rill erosion, given in GYSSELS ET AL. (2005)).

Due to a lack of knowledge concerning the exact behaviour of soil cohesion during FT cycles (as discussed in Section 4.5.5.4), the freeze-thaw multiplication factor  $f_{ft}$  was set to a constant value of 0.65.

The fitting parameter  $\kappa$  in Eq. (4.49) for calculation of the shear strength, was set to a constant value of 2.0 (FREDLUND ET AL. (1996) and VANAPALLI ET AL. (1996) used a range of 1.0 to 4.8).

Finally, for the conversion of the shear strength to the critical shear stress, Eq. (4.55) is applied, with a value of  $2.6 \cdot 10^{-4}$  for  $\beta$  (according to LÉONARD & RICHARD (2004); cf. Section 4.5.5.5). The resulting shear stress then ranges up to dimensions of approx. 50 Pa. But the values of the erosion resistance, as derived by SCHMIDT ET AL. (1996), differ in magnitude by a factor of about  $10^{-3}$  to  $10^{-4}$ , therefore  $\tau_c$  is multiplied by 0.0005, in order to bring the shear stress into the dimension of the erosion resistance. Due to the limited range of Eq. (4.55), values of shear strength are limited to a maximum of 20 kPa, before converting them to critical shear stress.

Tab. 5.6: Flow concentration factors  $f_{cf}$  for arable land at state "sowed".

Land use	$f_{cf}$	Land use	$f_{cf}$
Forage	1.00	Rye	0.10
Hop	0.05	Silage	0.07
Legumes	0.05	Sugar	0.05
Maize	0.07	Summer Barley	0.10
Oat	0.10	Summer Wheat	0.10
Oleaginous	0.10	Winter Barley	0.10
Potato	0.05	Winter Wheat	0.10

### 5.2.2. FLOW CONCENTRATION

The parameterisation of the flow concentration factor  $f_{cf}$  is twofold. Flow concentration on agricultural (arable) areas is assumed to be dominated by agricultural management practices, whereas on natural areas it is controlled predominantly by the slope. The reasons for these assumptions are:

- Steep slopes strongly favour formation of rill systems due to higher flow velocities, greater upslope contributing area and other slope geometry than on gentle slopes (cf. e.g. DESMET ET AL. (1999), YAO ET AL. (2008)). In the Upper Danube Basin the land on steeper areas is usually used for forestry, pasture, or it exists in its original, natural state. This means, that there are no anthropogenic measures, which change soil surface structure, thus they are assumed to form solely naturally by flow paths, depending on slope.
- Agricultural areas in the Upper Danube Basin are usually located on relatively smooth slopes. The slope plays a minor role, but the surface structure is heavily modified by the operations of ploughing and seedbed preparation. Therefore it is assumed, that surface runoff concentrates in structures predefined by these actions, and very unlikely incises or overruns the structures (e.g. conventional plough furrows have a depth between approx. 10 cm and 30 cm).

So on arable land, the value of the  $f_{cf}$  is estimated depending on agricultural management practices, respectively the state of the field (cf. Section 4.5.6) for the corresponding crops:

- harvested*:  $f_{cf} = 1.0$ , due to remaining crop residue after harvest,
- ploughed*:  $f_{cf} = 0.5$ , as conventional ploughing strongly increases surface roughness, and water flow may channel between the furrow slices.
- sowed*: after conventional seedbed preparation the surface roughness is very low, and the flow concentrates in clearly distinguishable rows (cf. e.g. the sample plot of SCHMIDT (1996), illustrated in Fig. 4.12, Section 4.5.2). Depending on the cultivated plant, the seedbed preparation differs. Tab. 5.6 shows the estimated values for arable crops.

For parameterisation of flow concentration on natural areas and agricultural grassland, the ratio  $\beta$  of rill to interrill erosion from the RUSLE is used:

$$\beta = \frac{\frac{\sin \alpha}{0.0896}}{3.0 \cdot (\sin \alpha)^{0.8} + 0.56} \quad (5.3)$$

Tab. 5.7: Leaf angle distribution parameters  $x$  for all types of vegetation and their corresponding extinction coefficients  $K_{be}$  for a vertical incident angle.

Crop	$x$	$K_{be}$	Crop	$x$	$K_{be}$
Alpine Vegetation	2.10	0.74	Oleaginous	1.92	0.72
Coniferous Forest	3.30	0.83	Potato	2.00	0.73
Deciduous Forest	3.00	0.83	Rye	1.20	0.57
Extensive Grassland	1.20	0.57	Set Aside	1.20	0.57
Forage	2.60	0.80	Silage	1.37	0.61
Hop	0.70	0.39	Summer Barley	1.20	0.57
Intensive Grassland	1.20	0.57	Sugar	1.68	0.68
Legumes	2.17	0.75	Summer Wheat	0.96	0.49
Maize	1.37	0.61	Wet Land	1.40	0.62
Natural Grassland	1.20	0.57	Winter Barley	1.20	0.57
Oat	1.27	0.58	Winter Wheat	0.96	0.49

where  $\alpha$  is the slope angle [ $^{\circ}$ ]. In order to scale  $\beta$  to the correct dimension of the  $f_{cf}$ , the reciprocal  $\frac{1}{\beta}$  is used, and values of above 1.0 are restricted. The resulting values of the  $f_{cf}$  then range from 1.0 at an angle of approx.  $5^{\circ}$  to approx. 0.32 at an angle of  $90^{\circ}$ .

### 5.2.3. CANOPY INTERCEPTION

For calculation of interception and throughfall, as described in Section 4.5.4.1, the vegetation dependent leaf angle distribution parameter  $x$  is needed. Tab. 5.7 lists the values of  $x$  used for computation of the fractional canopy cover within PROMET. They are derived from CAMPBELL & NORMAN (1998) and estimated for canopies where no parameterisation is available.

Fig. 5.5 and Fig. 5.6 show the effects of a vegetation dependent extinction coefficient on fractional canopy cover  $f_c$  and maximum intercepted water storage  $\Delta I_{max}$ . Illustrated are typical courses of the LAI during a growth period, measured in situ by the Department for Geography of the *Ludwig-Maximilians University* Munich. Both figures basically show the same behaviour: the values of  $f_c$  and  $\Delta I_{max}$  are somewhat lower for the vegetation dependent coefficient. The graph of the fractional canopy cover for the constant coefficient approaches a closure of nearly 100% early in the vegetation period, whilst the vegetation dependent coefficient never exceeds values of approx. 90%. The latter seems to be more realistic when comparing both these courses to values given in SCHMIDT ET AL. (1996).

As illustrated in Fig. 4.14, differences in the leaf angle distribution parameter  $x$  become more obvious with decreasing values of  $x$ , i.e. a more erect shape of canopy, which leads to a considerably lower canopy coverage. So for cultivations like hop, utilisation of Eq. (4.34) can significantly improve the calculated canopy cover, while the higher values for  $x$  in Tab. 5.7, e.g. for forest, do not have such a distinctive influence on resulting canopy closure.

The mean drip off height ( $\kappa$  in Eq. (4.42)) for all modelled canopies is estimated visually from photographs. The results are presented in Tab. 5.8.

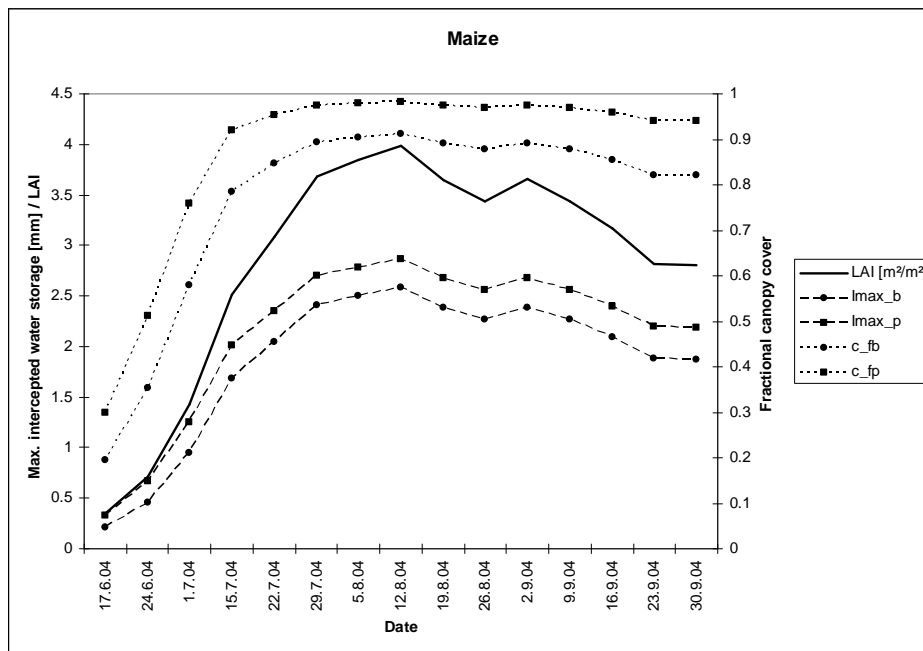


Fig. 5.5: Fractional canopy cover and maximum intercepted water storage for maize, derived exemplarily from LAI measurements. (dashed: maximum intercepted water storage, dotted: fractional canopy cover; circles: calculated with variable extinction coefficient  $K_{be}$  from Eq. (4.34), squares: calculated with constant extinction coefficient from Eq. (4.33))

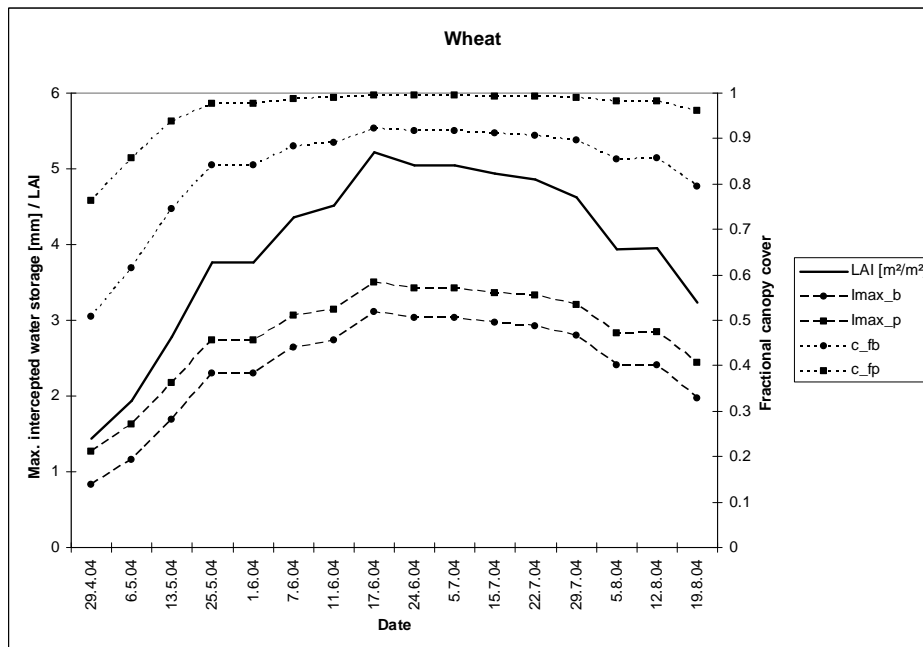


Fig. 5.6: Fractional canopy cover and maximum intercepted water storage for maize, derived exemplarily from LAI measurements. (dashed: maximum intercepted water storage, dotted: fractional canopy cover; circles: calculated with variable extinction coefficient  $K_{be}$  from Eq. (4.34), squares: calculated with constant extinction coefficient from Eq. (4.33))

Tab. 5.8: Mean drip off heights for all modelled canopies.

Crop	$\kappa$	Crop	$\kappa$
Alpine Vegetation	0.05	Oleaginous	0.40
Coniferous Forest	0.20	Potato	0.45
Deciduous Forest	0.30	Rye	0.55
Extensive Grassland	0.05	Set Aside	0.15
Forage	0.10	Silage	0.60
Hop	0.60	Summer Barley	0.50
Intensive Grassland	0.05	Sugar	0.55
Legumes	0.40	Summer Wheat	0.50
Maize	0.60	Wet Land	0.05
Natural Grassland	0.05	Winter Barley	0.50
Oat	0.60	Winter Wheat	0.50

#### 5.2.4. SOIL COVER AND DECOMPOSITION

The parameterisation of soil cover (as described in Section 4.5.4.2), differentiates between crop residue on agricultural areas (Section 4.5.6.2), and litter on natural areas.

Agricultural areas are parameterised under the assumption of conventional tillage systems, i.e. no mulching, minimal crop residue cover after harvest, and deep ploughing are implemented. For soil cover treatment, the three states *harvested*, *ploughed* and *sowed* (see Section 4.5.6.1) are used in the following manner:

- *harvested*: As no land use dependent information on crop residue remaining on the field after harvest is available for this study, a value of 15% residue cover is assumed for all arable crops. (This is by common definition the used upper threshold for conventional, intensive tillage systems. Reduced tillage leaves up to 30% cover on the field, whereas the cover amounts to over 30 % for conservation tillage). An exceptions of this assumption is forage, for which  $f_{cs}$  is set to 1.0 (i.e. 100% cover) after harvest.
- *ploughed*: The operation of ploughing buries the crop residue left on the field after harvest and destroys dead roots, which hold together soil aggregates. Therefore, after ploughing, the residue cover is reduced to 5% of its previous value, and additionally the dead root material in the soil (root length density, Section 4.5.5.3) is set to 50% of its previous value.
- *sowed*: The soil cover is set to 0%, as no mulching is done. Furthermore, it is assumed that for the subsequent state *emerged* (i.e. during plant growth) no dead plant material is produced, that covers the soil.

These rules apply to all *arable* crops, except for “set aside”, which always has a  $f_{cs}$  of 0.9.

Natural areas and grassland are parameterised with static values (Tab. 5.9), because vegetation there is perennial (like set aside), and thus continuously produces litter. It is assumed, that production and decomposition of litter are in an equilibrium state, thus no decomposition is modelled.

In contrast, on agricultural areas crop residue is left on the field, and for some cultivations, such as maize or potatoes, stays there over autumn and winter, by the time of the next



Tab. 5.9: Static soil cover values ( $f_{cs}$ ) for natural areas and non-arable grassland.

Land use	$f_{cs}$	Land use	$f_{cs}$
Alpine Vegetation	0.85	Intensive Grassland	0.90
Coniferous Forest	0.95	Natural Grassland	0.93
Deciduous Forest	0.97	Rock	0.85
Extensive Grassland	0.90	Wet Land	0.95

seedbed preparation. So after execution of harvest, the decay of organic crop residue as well as dead root material is initiated. This is approximated based on an approach used in the RUSLE (RENARD ET AL., 1996). The approach works on a daily time interval, and supposes that decomposition of organic material is determined by two limiting variables: temperature and moisture. This is expressed by the climatic factor

$$F_{cl} = \min(c_t, c_w) \quad (5.4)$$

which is the minimum of the temperature coefficient  $c_t$  and the moisture coefficient  $c_w$ . The temperature coefficient is calculated with:

$$c_t = \frac{2 \cdot (T_i - A)^2 \cdot (T_{opt} - A)^2 - (T_i - A)^4}{(T_{opt} - A)^4} \quad (5.5)$$

where  $T_i$  is the current daily mean air temperature [ $^{\circ}\text{C}$ ],  $T_{opt}$  is the optimum temperature for decomposition [ $^{\circ}\text{C}$ ] (and determines where  $c_t = 1$ ), and  $A$  [ $^{\circ}\text{C}$ ] indicates the lower limit for microbial activity ( $c_t = 0$ ).  $A$  is set to  $8^{\circ}\text{C}$ , which takes diurnal temperature variations into account.  $T_{opt}$  was calibrated against decomposition data to a value of  $32^{\circ}\text{C}$  (RENARD ET AL., 1996). If  $T_i$  falls below  $-10^{\circ}\text{C}$ ,  $c_t$  is set to 0.

The moisture coefficient  $c_w$  is calculated from the ratio of the current daily precipitation sum  $R_i$  [mm] to the optimum daily rainfall sum for decomposition  $R_{opt}$  [mm]:

$$c_w = \frac{R_i}{R_{opt}} \quad (5.6)$$

FOSTER (2004) calculated a value of 4.4 mm for  $R_{opt}$ , and the value of  $c_w$  is set to 1, if  $R_i$  exceeds  $R_{opt}$ .

Finally, for calculation of decomposition a first order exponential mass loss equation is used. Since in this study only the fraction of organic material covering the soil is available, the variable biomass is replaced by the fractional cover  $f_{cs}$ :

$$f_{cs,i} = f_{cs,(i-1)} \cdot e^{-k \cdot F_{cl}} \quad (5.7)$$

where  $f_{cs,i}$  represents the residue pool for the current time step,  $f_{cs,(i-1)}$  is the fractional cover from the previous time step, and  $k$  is a decomposition coefficient [ $1/d$ ]. The decomposition coefficients presented in Tab. 5.10 are estimated from literature values, based on FOSTER (2004) and STEINER ET AL. (1999).

The described process of decomposition starts with harvest, and ends with sowing, not only for crop residue, but also for root length density (see Section 4.5.5.3), which is stored after harvest and then reduced analogous to crop residue. (Technically this is realised by computing a cumulative fractional decay factor, which is applied to both crop residue and dead roots).

Tab. 5.10: Coefficients for decomposition of organic material.

Land use	$k$	Land use	$k$
Forage	0.02	Rye	0.02
Hop	0.02	Silage	0.02
Legumes	0.02	Sugar	0.02
Maize	0.02	Summer Barley	0.035
Oat	0.02	Summer Wheat	0.037
Oleaginous	0.02	Winter Barley	0.035
Potato	0.02	Winter Wheat	0.028

### 5.2.5. MANNING'S ROUGHNESS COEFFICIENT

Generally Manning's roughness coefficient  $n$  can be partitioned into different roughness elements, as e.g. proposed in MORGAN ET AL. (1998):

$$n = n_g + n_v + n_m \quad (5.8)$$

with  $n_g$ : grain roughness due to the soil particles,  $n_v$ : roughness imparted by vegetation and  $n_m$ : microtopographic roughness of the surface, particularly that associated with tillage practices and stoniness.

Although it is possible to calculate grain roughness  $n_g$  with the *Strickler* formula, no procedures for  $n_v$  and  $n_m$  have yet been developed, so it is necessary to refer to published tables of roughness values. From various literature sources SCHMIDT ET AL. (1996) compiled a table of Manning's  $n$  for a variety of different land cover conditions, cultivations and tillage practices. These are used as a guideline for parameterisation of the roughness values used in this study. In order to simulate the influence of vegetation during the growing season and microtopographic roughness (according to  $n_v$  and  $n_m$  in Eq. (5.8)), a linear interpolation of selected values depending on plant phenology is performed:

$$n = n_{min} + \frac{n_{max} - n_{min}}{\sum PS} \cdot PS \quad (5.9)$$

where  $n_{min}$  and  $n_{max}$  are minimum, respectively maximum values for  $n$  and  $PS$  is the phenological stage of the plant.

For  $n_{min}$  a value of 0.014 is used for all agricultural crops, as it is assumed, that tillage practices establish similar conditions before sowing, irrespective of crop type. The values for  $n_{max}$  are listed in Tab. 5.11. It should be noted, that these values are only used for crops of type "arable land", for all other types no interpolation is calculated, but  $n_{max}$  is set to a static value. The sum of phenological stages  $\sum PS$  is set to 7, as the influence of plant growth on  $n$  is assumed to begin with "emergence", and ends with "flowering" (see Tab. 4.3). Analogous  $PS$  also starts with "emergence" and ends with "flowering", denoting the current phenological phase of the plant. In summary, the roughness value is set to a static, land-use dependent  $n_{min}$  after sowing, increases incrementally during the growing season, and is again set to a static value of 0.044 after harvest.

### 5.2.6. PARAMETERISATION OF AGRICULTURAL MANAGEMENT

The parameterisation of the agricultural management component consists of:

Tab. 5.11: Maximum roughness values depending on land cover (top: maximum values for arable land use, except for hop, which is static; bottom: all static values depending on land cover).

Land cover	Manning's $n$	Land cover	Manning's $n$
Forage	0.25	Rye	0.2
Hop	0.115	Sugar beet	0.09
Legumes	0.09	Silage	0.115
Maize	0.115	Summer barley	0.2
Oat	0.2	Summer wheat	0.2
Oleaginous	0.1	Winter barley	0.2
Potato	0.09	Winter wheat	0.2
Alpine vegetation	0.023	Grassland extensive	0.3
Forest	0.8	Rock	0.011
Grassland intensive	0.3	Wetland	0.3

- Sowing and harvest dates: As described in Section 4.5.6.1, these are based on the long-term mean sowing and harvest dates of the Upper Danube Basin (compiled in Tab. 4.1). The threshold for earlier, respectively later harvest is set to 14 days (i.e. may be shifted depending on plant development by 14 days; cf. Section 4.5.6.1). Due to a lack of knowledge of the conditions needed for sowing (regarding minimum temperature or degree-days), the corresponding thresholds (concerning date, as well as temperature) are disabled.
- Ploughing: The date for ploughing was assumed to be 14 days after harvest for all arable crops.
- Residue management: The fraction of crop residue, left on the field after harvest, is specified in Section 5.2.4.



## 6. VALIDATION

### 6.1. VALIDATION OF THE CASCADE MODEL

Validation of the cascade model is split up in two parts: At first, performance of the model is evaluated with the aid of high resolution precipitation records at the point scale. In a second step, the model is introduced in the spatial interpolation routines of *AtmoStations* and results of the whole study area are presented. Spatial validation of disaggregated precipitation is impossible, as precipitation can only be measured at the point scale and is a discrete variable. Therefore only a comparison of the two disaggregation methods will be presented regarding especially extreme values, because precipitation totals remain constant, irrespective of the temporal disaggregation routine, as both are strictly mass conserving.

#### 6.1.1. VALIDATION AT THE POINT SCALE

Since the cascade model is based on statistical properties and disaggregation is executed based on random numbers, for validation at the point scale, an ensemble of 100 model runs with different random seeds is calculated. Statistical criteria of the ensemble are compared to the measured rainfall records. Due to the nature of the cascade model, the variations of the different runs can be summarised as follows:

- Theoretically it is possible, that two realisations differ completely, and that they also differ completely from the measured data (but only within the interval of a single *Mannheimer Stunde*).
- An extreme case which may occur, is for example a distribution of the whole rainfall volume of one *Mannheimer Stunde* to one hour (cf. Section 5.1.2).

But, since every model run is bound to the statistical properties of the generator (which was calculated based on measured data), these cases may only occur, with the same probability extracted from the empirical data, i.e. the statistical variations of the model runs are implicitly included in the properties of the generator (see Tab. 5.4 and Fig. 5.4).

Tab. 6.1 presents the specific statistics of the 100 runs of the ensemble. The values are averages of all stations belonging to their respective precipitation regimes (cf. Section 4.6.3.1). The re-aggregated values generally show the same behaviour as the evaluation experiments in Section 5.1.2. But comparing the disaggregated 10 min values to the measured data, it can be noticed, that intervals with volumes under the 50th percentiles are underestimated, whilst higher volumes are overestimated, especially the intervals above the 90th percentiles. Similar problems have been encountered by GÜNTNER ET AL. (2001), who reported an “inability of the model to reproduce a sharp decrease in maxima with increasing temporal resolution”. Since the simulation time stamp in this study is set to one hour, the re-aggregated values provide adequate results and the cascade model theoretically can be used within *AtmoStations*, which will be examined closer in the next section.

Tab. 6.1: Mean performances of the cascade disaggregation compared to measured values. Listed are statistics for regions (a): Low mountain ranges, (b): Forelands and (c): Alps. (no > 0: number of intervals with precipitation > 0, max: absolute maximum,  $\sigma$ : standard deviation, no >  $P_{XX}$ : number of intervals > XXth percentile of measured data)

(a) Reaggregation of 10 min intervals to 1 hour

Region	Data	no > 0	mean	$\sigma$	max	no > $P_{25}$	no > $P_{50}$	no > $P_{75}$	no > $P_{90}$
(a)	meas.	16819	0.72	1.26	39.10	11967	8160	4126	1650
	disagg.	19355	0.63	1.22	36.54	12818	8462	4261	1773
(b)	meas.	110011	0.81	1.32	39.90	81317	50424	24973	10702
	disagg.	120118	0.74	1.35	45.32	84703	50443	25668	12004
(c)	meas.	3022	1.03	1.91	31.20	2052	1395	753	293
	disagg.	2651	1.18	2.51	52.14	1780	1254	744	348

(b) 10 min intervals without re-aggregation. (\*)Note: The values of region (a) and (b) for  $P_{25}$  equals those for  $P_{50}$ , since the precipitation volume designating the percentiles equals for both. This results from the vast amount of very low disaggregated precipitation volumes at this temporal resolution.

Region	Data	no > 0	mean	$\sigma$	max	no > $P_{25}$	no > $P_{50}$	no > $P_{75}$	no > $P_{90}$
(a)	meas.	49111	0.25	0.42	26.30	22502(*)	22502(*)	8112	3850
	disagg.	52345	0.23	0.52	25.35	23240(*)	23240(*)	10969	6274
(b)	meas.	340515	0.26	0.43	22.30	165343(*)	165343(*)	60892	29201
	disagg.	327422	0.27	0.58	33.34	160109(*)	160109(*)	80189	47665
(c)	meas.	9883	0.32	0.57	16.00	5430	3298	2209	911
	disagg.	7642	0.41	1.01	32.52	4353	3194	2464	1323

### 6.1.2. PRACTICAL APPLICATION WITHIN *AtmoStations*

As the temporally disaggregated precipitation is subsequently interpolated spatially, the disaggregation method influences not only the resulting temporal, but also the spatial pattern of precipitation distribution in the catchment. In order to evaluate the impacts of the cascade model and to compare the two available disaggregation routines, a single model run over the whole catchment was carried out for the years 1995 – 2005.

Tab. 6.2 compares the modelled daily precipitation sums of the two different approaches, the advective-convective disaggregation (ACD) and the cascade disaggregation (CD). Values are extracted from all proxels where high resolution weather stations are located (see Fig. 4.4 and Tab. 5.1). Since disaggregation in *AtmoStations* is carried out down from the *Mannheimer Stunden*, it could be expected that statistical performances of daily sums would be perfect. But as daily aggregation is done at 00:00 CET and measured precipitation sums up from 21:00 to 07:00 CET, this results in a volume shift into the direction of the previous day, influencing the calculated statistics. Additionally, the spatial interpolation between the six adjacent stations (and the distance of the interpolated proxel to them) leads to deviances of the modelled precipitation to the validation data. At some stations, the deviations to the measured data are very high, e.g. at station *Wettlkam*, where the total precipitation sum is overestimated by approx. 100% (ca. 15500 mm vs. ca. 7600 mm). But without exact

Tab. 6.2: Mean performances of the different disaggregation methods compared to measured values. Listed are statistics of daily precipitation sums [mm] for all proxels with high resolution gauges. ( $\Delta x$  and  $\Delta h$ : horizontal respectively vertical distance to the next adjacent AtmoStations-station, used for precipitation interpolation.  $\Sigma$ : total precipitation sum [mm]. CME: coefficient of model efficiency (NASH & SUTCLIFFE, 1970). RMSE: Root Mean Square Error.)

Station	Method	$R^2$	CME	RMSE	$\Sigma$	$\Sigma$ (obs.)	$\Delta x$ [km]	$\Delta h$ [m]
Kühroint	ACD	0.86	0.74	5.93	1528.38	1683.4	5	791
	CD	0.78	0.61	7.26	1538.64			
Jenner	ACD	0.81	0.61	4.75	1255.35	1395	2	44
	CD	0.77	0.52	5.28	1267.47			
Reiteralm	ACD	0.39	0.07	14.22	1876.77	1425.9	9	1145
	CD	0.34	0.00	14.74	1893.19			
Untersberg	ACD	0.77	0.56	8.61	10616.91	15289.6	9	1356
	CD	0.69	0.45	9.55	10726.98			
Spitalhof	ACD	0.92	0.85	2.64	13612.69	12847	3	15
	CD	0.89	0.78	3.13	13731.95			
Wettkam	ACD	0.57	-1.00	5.97	15560.66	7636.4	5	10
	CD	0.58	-1.05	6.04	15697.64			
Nilling	ACD	0.72	0.40	3.87	10512.96	8180.1	20	97
	CD	0.71	0.36	3.99	10685.37			
Osterseeon	ACD	0.70	0.45	4.76	10820.85	11231.7	3	12
	CD	0.65	0.35	5.15	10904.74			
Reschenberg	ACD	0.65	0.38	4.83	10011.66	11569.2	5	40
	CD	0.58	0.28	5.21	10195.14			
Großberghofen	ACD	0.47	-0.29	4.73	9605.51	7349.5	9	8
	CD	0.45	-0.34	4.83	9778.98			
Engersdorf	ACD	0.75	0.50	3.33	8218.57	7448.1	8	12
	CD	0.71	0.42	3.60	8367.64			
Kringell	ACD	0.88	0.76	2.95	5246.68	4838.6	11	41
	CD	0.84	0.71	3.29	5326.03			
Neusling	ACD	0.87	0.74	2.41	9044.00	8269.4	18	32
	CD	0.83	0.68	2.72	9223.33			
Neuhof	ACD	0.71	0.48	3.39	8107.67	8365.7	3	2
	CD	0.65	0.36	3.75	8291.89			
Konnersreut	ACD	0.38	-0.08	5.34	9235.21	8862.8	10	25
	CD	0.39	-0.06	5.30	9453.96			
Schönau	ACD	0.91	0.83	3.38	4673.77	4632.7	0	0
	CD	0.85	0.70	4.48	4717.14			

knowledge of the site it is difficult to detect the causes for the overestimation, especially as the mean annual precipitation sum of the station is quantified by the LfL with approx. 1100 – 1400 mm as opposed to the total sum of 7636.4 mm in the recorded data from 1995 – 2005 (approx. 700 mm per year). Some deviations in the alpine regions are expected, as the altitudinal differences between interpolated proxel and weather station are very high. Deviations are also found by observing proxels which are far from the adjacent station proxels. Overall, the performances of both methods approximately show the same behaviour with respect of the daily precipitation sums.

Concerning extreme values, Tab. B3 (in appendix B) shows similar results as those presented in Section 5.1.2: rainfall intensities are higher in the CD approach than in ACD, which is indicated by the better reproduction of the number of intervals above the 75th and 90th percentiles. As already figured out in Section 5.1.2, the approach of ACD frequently produces a number of wet intervals twice as high as found in the measured datasets. Also the mean hourly precipitation volume of ACD only amounts to a maximum of the half of the observed intensities, and the standard deviations are too low, caused by the evenly redistribution of precipitation around the disaggregation intervals.

Fig. 6.1 and Fig. 6.2 show mean seasonal precipitation intensities [mm/h] (calculated from mean daily intensities, excluding days without precipitation). Noticeable are the circular areas distributed over the whole catchment, which do not represent locations of frequent thunderstorm cells, but result from spatial interpolation patterns. Big parts of the catchment are dominated by frequent convective conditions in the summer months, expressed by the increase of precipitation intensities in Fig. 6.1(c) and Fig. 6.2(c). During the winter months regions with orographic lift are emphasised, especially in the low mountain ranges and the proximate foothills of the Alps. Comparing the two illustrations from both disaggregation methods, one can notice, that the results from the ACD routine produces considerably lower intensities, especially in *JJA* with frequent thunderstorms.

The discrepancy between the two methods becomes clearer, when a more practical classification for storm rainfall is applied. Fig. 6.3 shows the mean number of days per year with heavy precipitation events for the period 1995 – 2005. For classification of those events the formula of the DWD (BAUMGARTNER & LIEBSCHER, 1996) was used:

$$P \geq \sqrt{5 \cdot t - \left(\frac{t}{24}\right)^2} \quad (6.1)$$

with  $P$ : threshold designating heavy precipitation events [mm] and  $t$ : event duration [min]. Applying this formula to 1 hour, respectively one day, this means that for the derivation of the number of heavy precipitation days, one of the two following criteria has to be fulfilled: either the threshold of 17.1 mm/h is exceeded during a day, or the total precipitation sum of a day is greater than 60 mm. The two criteria are chosen to take into account both short duration events with high intensities and long term events with large precipitation volumes.

Altogether, the pattern is smoother than those in Fig. 6.1 and Fig. 6.2, as longer-lasting events with lower intensities, but high volumes also contribute to the classification. Although the 60 mm/d threshold was included, i.e. not only short-term events influence the calculation, the ACD routine hardly produces any days with heavy precipitation. This means, that on the one hand, obviously the number of days exceeding a daily precipitation volume of 60 mm is



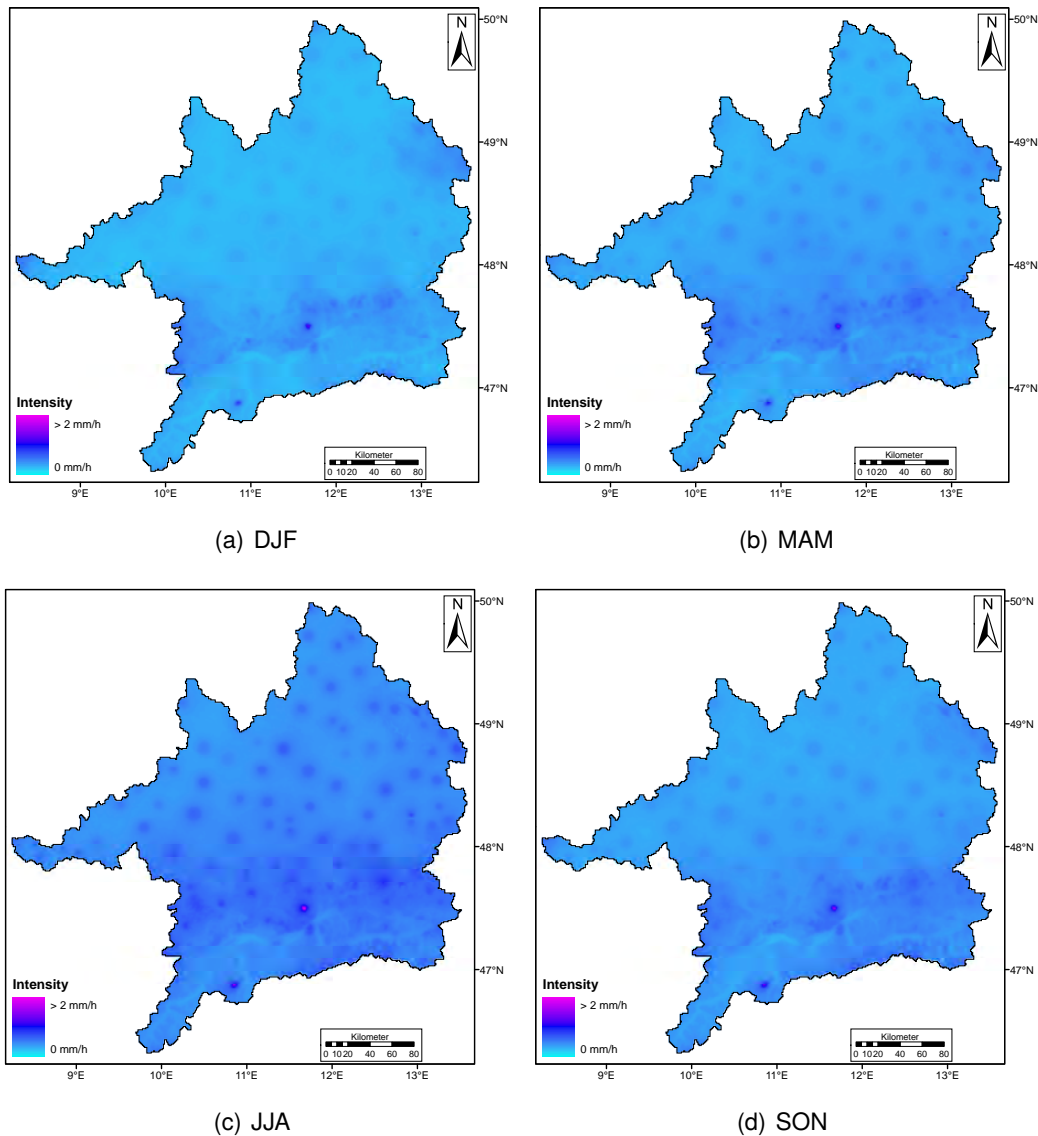


Fig. 6.1: Seasonal mean precipitation intensities [mm/h] calculated from precipitation data disaggregated with the ACD approach. (DJF: December, January, February; MAM: March, April, May; JJA: June, July, August; SON: September, October, November)

very low. On the other hand, the majority of storm rainfall events occurs during summer, which in turn means, that correct reproduction of intensities is particularly important in those months.

Case studies which rely on reproduction of extreme values concerning precipitation, as e.g. modelling soil erosion, are well advised to use a stochastic approach like the random cascade model presented here. Generally, statistical measures show a correct reproduction of intensities and maxima. Problems might arise, if correct temporal mapping is needed, as the temporal reproduction - especially within single events - is strongly influenced by the random component during disaggregation. However, for the purpose of this study the performance of the model is sufficient, because it is used to assess the long term impacts of global change at the meso- to large-scale.

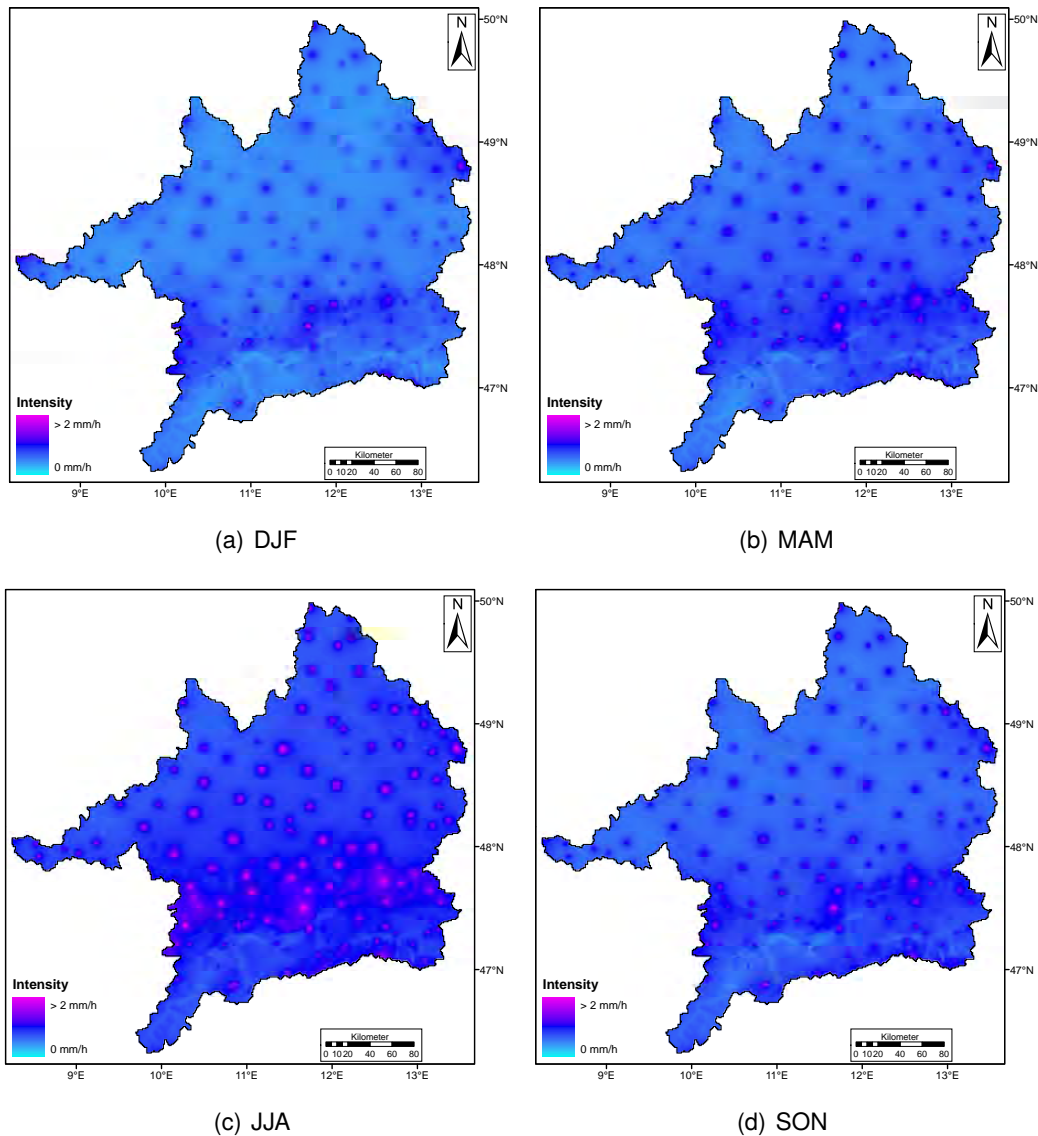


Fig. 6.2: Seasonal mean precipitation intensities [mm/h] calculated from precipitation data disaggregated with the CD approach. (DJF: December, January, February; MAM: March, April, May; JJA: June, July, August; SON: September, October, November)

## 6.2. VALIDATION OF THE EROSION MODEL

In natural sciences, especially in environmental modelling, usually a validation and/or an uncertainty analysis is carried out to assess the quality and reliability of the model, respectively its outputs. For a “classical” validation, measured data is needed, which is compared to the simulated model outputs. For the case of physically-based erosion modelling, this is achieved e.g. by setting up experimental test plots with defined/measured, detailed initial conditions (e.g. soil, slope, etc), which are exposed to well-defined runoff and/or rainfall conditions (e.g. rainfall simulator), and the resulting reactions of the observed system are recorded. The comparison to the modelled outputs allows for evaluation of the mathematical model. For the case of empirical erosion modelling, a similar procedure is applied, with the difference, that model development is based on the measured data. In order to provide reliable results (at

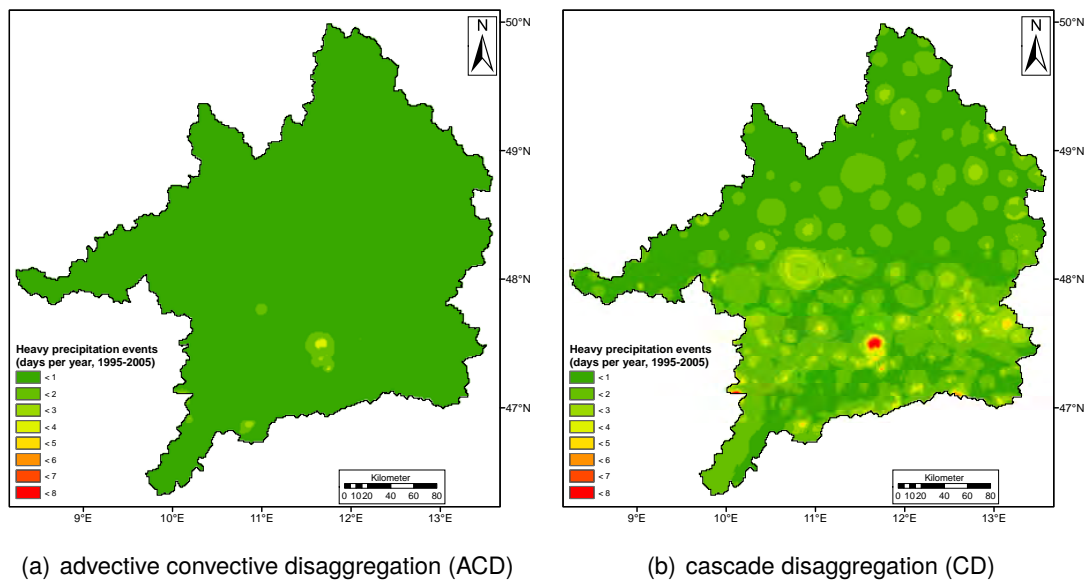


Fig. 6.3: Number of days per year classified as heavy precipitation events, calculated from the modelled period 1995 – 2005.

least within the boundaries of the measured data), for the derivation of an empirical model, a large amount of data is needed (e.g. the USLE uses experience of more than 2 decades (WISCHMEIER & SMITH, 1978)). For this study neither detailed measurements, nor long-term measurements of soil loss on the plot- or field-scale are available, which could be used for direct “point”-validation. Furthermore, it is virtually impossible to “point”-validate a model for the spatial extent of the Upper Danube Basin, as the conditions are way too heterogeneous, i.e. a vast amount of proxels had to be checked. Therefore, it seems to be more reasonable to check the model against measured specific sediment yield at the gauges of sub-catchments of the study area. These represent the mean response of erosion of the whole sub-catchment to the external input parameters and variables. So, the soil erosion module is only tested for sensitivity to input parameters within reasonable boundary conditions (Section 6.2.2) and for plausibility of its outputs with specific sediment yield measurements (Section 6.2.3).

### 6.2.1. THE SUBCATCHMENTS OF THE *Große Laber* AND *Ammer*

For validation of the erosion model two sub-catchments are chosen, the *Große Laber* and the *Ammer* (see Fig. 6.4), as they represent geographically very diverse regions. By analysing these two, a large part of the variability of the Upper Danube Basin can be explained. Whilst the *Große Laber* watershed is an agriculturally intensively used area with gentle slopes and soils susceptible to erosion, the *Ammer* is dominated by forests and grassland, has a steeper relief and very heterogeneous soils. The distribution of land use and soil classes are listed in Tab. 6.3 and Tab. 6.4, the distribution and statistics of the slope can be found in Fig. 6.5 and Tab. 6.5. Concerning the temporal variability of rainfall (and runoff), the *Ammer* watershed has more pronounced peaks in summer, due to thunderstorms, whereas the *Große Laber* catchment also shows such patterns, but higher amounts are usually expected in autumn.

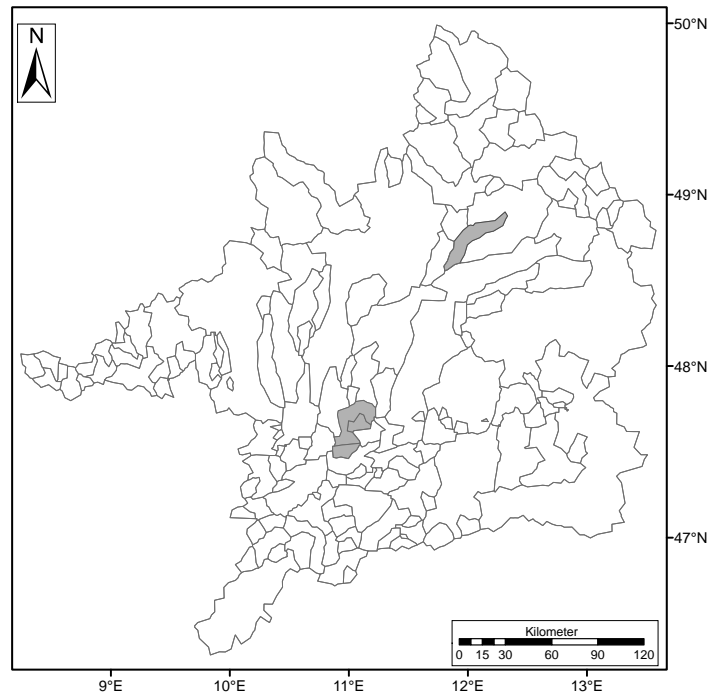


Fig. 6.4: Location of the subcatchments Große Laber and Ammer within the Upper Danube Basin. The sub-catchment of the Große Laber is located in the north-east, the Ammer lies in the south-west.

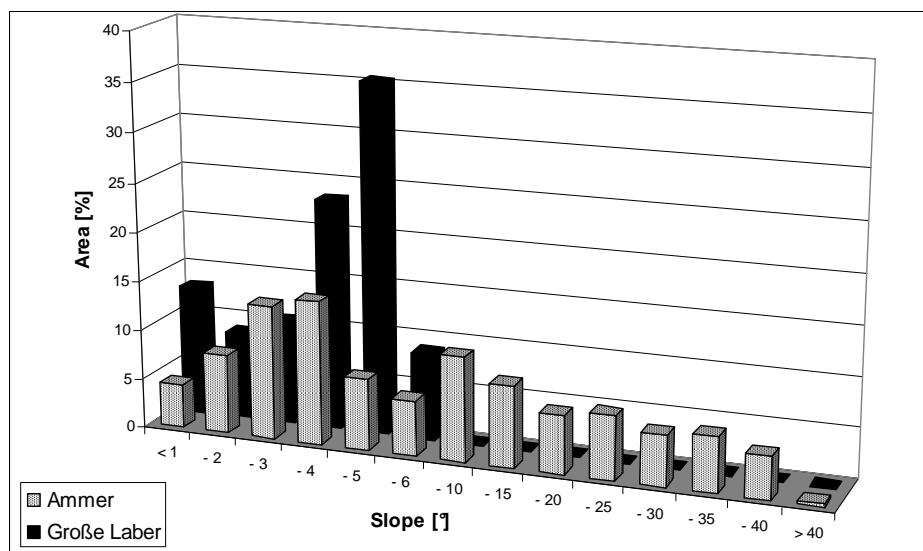


Fig. 6.5: Areal distribution of slope in the sub-catchments Große Laber and Ammer.

Tab. 6.3: Land use distribution of the sub-catchments Große Laber and Ammer.

Land use	<i>Große Laber</i>		<i>Ammer</i>	
	No. of proxels	Percentage	No. of proxels	Percentage
Grassland Extensive	13	3.3	108	17.8
Grassland Intensive	25	6.3	104	17.1
Silage	0	0.0	3	0.5
Forage	1	0.3	0	0.0
Hop	1	0.3	0	0.0
Maize	9	2.3	0	0.0
Oat	0	0.0	2	0.3
Oleaginous	47	11.8	0	0.0
Potato	16	4.0	0	0.0
Set aside	27	6.8	0	0.0
Sugar	11	2.8	0	0.0
Winter Barley	62	15.5	0	0.0
Winter Wheat	76	19.0	6	1.0
Built-up Industrial	0	0.0	1	0.2
Built-up Residential	10	2.5	17	2.8
Deciduous Forest	2	0.5	30	4.9
Coniferous Forest	99	24.8	266	43.8
Rock	0	0.0	5	0.8
Wetland	0	0.0	42	6.9
Alpine Vegetation	0	0.0	8	1.3
Natural Grassland	0	0.0	7	1.2
Water	0	0.0	8	1.3
Sum	399	100.0	607	100.0

Tab. 6.4: Soil class distribution of the sub-catchments Große Laber and Ammer.

Soil class	<i>Große Laber</i>		<i>Ammer</i>	
	No. of proxels	Percentage	No. of proxels	Percentage
Sandy Loam	0	0.0	209	34.4
Sandy Loam on Gravel	0	0.0	200	32.9
Clayey Silt	182	45.6	0	0.0
Silt Loam	217	54.4	0	0.0
Clay Loam	0	0.0	29	4.8
Peat	0	0.0	42	6.9
Soils on Calcareous Rock	0	0.0	116	19.1
High Alpine Soils	0	0.0	11	1.8
Sum	399	100.0	607	100.0

Tab. 6.5: Slope statistics of the sub-catchments *Große Laber* and *Ammer*.

	Slope [°]	
	<i>Große Laber</i>	<i>Ammer</i>
Minimum	0.1	0.2
Mean	3.4	10.8
Maximum	5.7	42.0

Tab. 6.6: Characteristics and default values of the proxel selected for sensitivity analysis.

Property	Value
Row/column	152/289
Land use	Maize
Soil class	Clayey Silt
Slope	4.2°
Elevation	434 m a.s.l
Grain sizes	0.4 µm/13.15 µm/100 µm (T/U/S)
$f_{cf}$	0.07
Soil cover	15% (after harvest)

### 6.2.2. SENSITIVITY ANALYSIS

For sensitivity analysis a single, “default” proxel is used. This means, that the proxel indeed exists, but it is not parameterised in the model with the corresponding parameters. “Default” conditions are defined, which are static for all model runs, and the most interesting parameters, i.e. those with the highest impacts, are varied. These variations range within reasonable, physically explainable boundaries for the respective parameters. The quality of the model outputs are assessed by comparison of temporal patterns of soil loss, and by total soil loss within the considered period.

The default proxel used for sensitivity analysis is located in the *Große Laber* watershed, as this area is much more endangered by erosion than the *Ammer* watershed due to its soils and land use. In principle, for sensitivity analysis it is irrelevant, if the proxel actually exists, merely the boundary conditions should be realistic. Yet, the influence of varying parameters on the temporal pattern of soil loss shall be visualised. Selecting a default proxel within an existing catchment allows for feeding the proxel with meteorological inputs of the selected location, and a comparison with a measured series of SSY. Anyway, one has to consider, that SSY only reflects a superposition of all variables of the whole catchment, and therefore cannot exactly resemble the temporal erosion pattern of a single proxel. Nevertheless, one can expect, that the impacts of the most important events, such as freeze-thaw cycles, harvest or heavy precipitation events, can be recognised by comparing soil loss to SSY. Since the simulated results are not really comparable to the measured outputs, it was decided to use merely a default proxel for sensitivity analysis. Tab. 6.6 shows the characteristics and default values of the selected proxel. The default values are held constant for sensitivity analysis, except for the one parameter which is analysed. Apart from these default values, the subroutines for cascade disaggregation (Section 4.6.2), soil freezing (Section 4.2.2.2) and FT-cycles (Sec-

tion 4.5.5.4), and dynamic agricultural management (Section 4.5.6.1) are enabled by default (whereas for some runs, these will be switched off) for the sensitivity analysis model runs. The selected year for simulation is 1995, as measured sediment yield is relatively high compared to other years, and the temporal distribution shows erosion events in summer, as well as winter, i.e. the full spectrum of influencing variables is available here.

The sensitivity analysis is split up in two parts: analysis of parameters, which directly (and some of them exclusively) influence the erosion model (in Section 6.2.2.1), and parameters integrated in subroutines, which indirectly control erosion and therefore cannot be assessed stand-alone, as the interaction between them is too complex to be analysed in detail (in Section 6.2.2.2).

### 6.2.2.1. DIRECT PARAMETER VARIATIONS

This section is intended to cover variations of direct parameters of the erosion model, i.e. changing the corresponding values shall result only in changes of soil loss, and should not impact any other sub-modules of PROMET. However, some variables indeed do influence other sub-modules, so the parameter variations were exclusively made in the erosion module (see annotations in the respective sections). The sensitivity of each variable is tested by simulating three model runs with the same boundary conditions, for which merely the variable to be tested is varied.

The sensitivity of the input parameters is presented in three different ways:

- Upper ( $v_u$ ) and lower ( $v_l$ ) boundaries and a mean value ( $v_m$ ) of the parameter dealt with, are used for illustration. These do not necessarily represent the absolute minimum, maximum and mean input values of this parameter, but are defined by reasonable limits. The total annual soil loss response to these parameters is calculated.
- For visualisation of the temporal context, the soil loss of each single event within the whole year is illustrated.
- With the aid of the upper and lower boundaries  $v_u$  and  $v_l$ , the sensitivity parameter  $S$  after NEARING ET AL. (1990) is used:

$$S = \frac{\frac{O_2 - O_1}{O_{12}}}{\frac{I_2 - I_1}{I_{12}}} \quad (6.2)$$

with  $I_1$  and  $I_2$ : the minimum, respectively maximum value of input used,  $I_{12}$ : the mean value of  $I_1$  and  $I_2$ ,  $O_1$  and  $O_2$ : the corresponding output values for the two input values and  $O_{12}$ : the mean value of the two outputs. Here  $I_1$  is represented by  $v_l$  and  $I_2$  by  $v_u$ . This allows for a dimensionless, relative inspection of the influence.

*Note on the illustration of the results: The input parameter variations  $v_u$ ,  $v_l$  and  $v_m$  and their effects are presented in the following sections in tabular form.  $v_m$  does not correspond to  $I_{12}$ , or respectively its output to  $O_{12}$ .  $I_{12}$  and  $O_{12}$  are calculated from  $v_u$  and  $v_l$ , but  $v_m$  represents only a typical mean value (e.g. the mean value of the slope in the Upper Danube Basin), selected independently. The additional figures illustrating the variations, also show  $v_u$ ,  $v_l$  and  $v_m$ , and not  $O_{12}$ . The red bars in the figures indicate the upper and lower boundaries,  $v_m$  is drawn with a black bar.*

Tab. 6.7: Sensitivity of the erosion model to variations concerning the grain size.

(a) Variations of the diameter of the clay grain size class			(b) Variations of the diameter of the silt grain size class		
Variable	Value [m]	Total Soil Loss [t/ha]	Variable	Value [m]	Total Soil Loss [t/ha]
$v_l$	$2.0 \cdot 10^{-6}$	43.09	$v_l$	$2.0 \cdot 10^{-6}$	55.83
$v_m$	$9.0 \cdot 10^{-7}$	43.09	$v_m$	$3.05 \cdot 10^{-5}$	12.35
$v_u$	$2.0 \cdot 10^{-7}$	43.09	$v_u$	$6.3 \cdot 10^{-5}$	9.50
S		0.00	S		-0.756

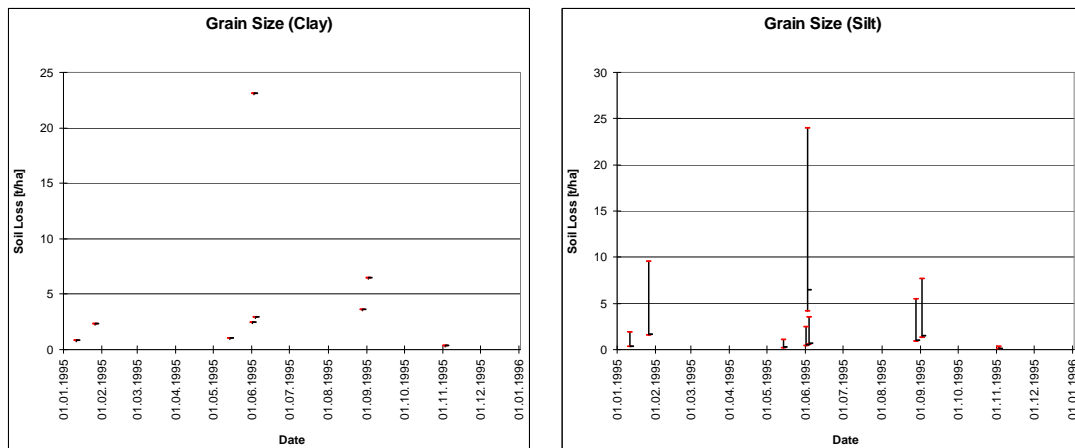
(c) Variations of the diameter of the sand grain size class			(d) Variations of the fraction of clay, silt and sand		
Variable	Value [m]	Total Soil Loss [t/ha]	Variable	Value [%]	Total Soil Loss [t/ha]
$v_l$	$6.3 \cdot 10^{-5}$	43.24	Clay	100	61.99
$v_m$	$9.69 \cdot 10^{-5}$	43.06	Silt	100	41.03
$v_u$	$2.0 \cdot 10^{-3}$	43.06	Sand	100	0.03
S		-0.002			

**GRAIN SIZES AND DISTRIBUTION** The effects of variations concerning the grain size solely affect the erosion module. Effects on other components, such as the soil module, are suppressed, by varying the grain size only *within* the erosion module. This means, that e.g. the soil module calculates matric suction based on other grain size distributions, than those which the erosion module uses for calculation of particle transport.

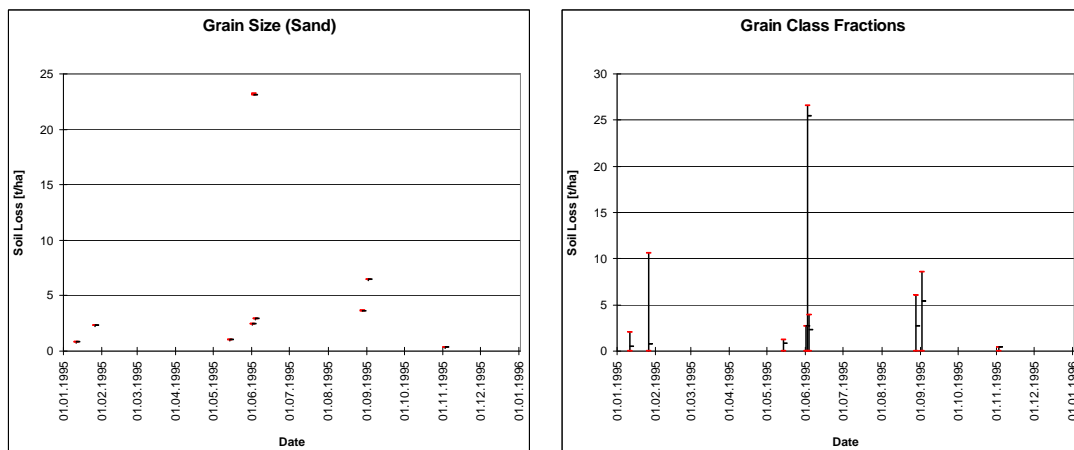
The variables modified for analysis are the mean particle diameters of the particle size classes and the fractional composition of the soil particle classes clay, silt and sand. Considering the grain size variations, one can see from Fig. 6.6 and Tab. 6.7, that only the silt class noticeable responds to the changes. The values applied range from the minimum over the mean value to the maximum of each grain size fraction (clay, silt and sand), as defined in AD-HOC-AG BODEN (2005). The absent reaction of the clay and sand class explains as follows: the grain size *only* plays a role in sediment transport (see Section 4.5.1.2). The equations used for transport modelling are obviously only sensitive within the range of the silt class, whereas variations in diameter of the sand and clay class do not result in changes of soil loss. For the case of clay this means, that *always* virtually all detached material is transported, whereas the transport of sand in any case is very low, and thus does not considerably account for the total amount of soil loss. This is confirmed by the results from the variations of the class fractions of the soil. These show, that generally the transport of sand is very low, whereas the transport of clay is very high. Since the fractional composition of the soil is given by the soil classification maps, and thus cannot be varied for areal model runs, the determining factor is the mean diameter of the silt class.

**SLOPE** Like in the previous section, the slope variations also influence other model components of PROMET, such as the radiation balance or runoff formation, and therefore are also varied only within the erosion module. As upper boundary  $v_u$  a value of  $45^\circ$  was selected, because due to the model equations, the total soil loss decreases at slope angles above  $45^\circ$ .





(a) Variations of the diameter of the clay grain size class (b) Variations of the diameter of the silt grain size class



(c) Variations of the diameter of the sand grain size class (d) Variations of the fraction of clay, silt and sand class

Fig. 6.6: Sensitivity of the erosion model to variations concerning the grain size.

Tab. 6.8: Variations of the slope.

Variable	Value [°]	Total Soil Loss [t/ha]
$v_l$	1	4.65
$v_m$	10	109.50
$v_u$	45	321.98
S		1.016

$v_m$  averages out to 10°, which is the mean value of the slope in the Upper Danube Basin. Finally the lower boundary is set to 1°, and not to zero, as then no soil loss would occur.

**FLOW CONCENTRATION FACTOR** The flow concentration factor  $f_{cf}$  exclusively affects the erosion module. For analysis, it is set to static values, which means that influences of agricultural management (as well as influences of the slope) are disabled.

An interesting aspect here is an increase in soil loss with an increase of the flow concen-

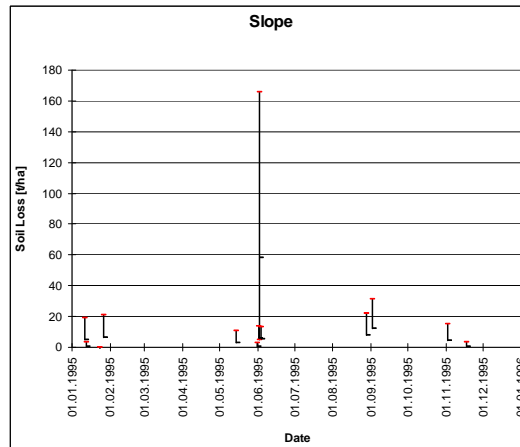


Fig. 6.7: Variations of the slope.

Tab. 6.9: Variations of the flow concentration factor. (The calculated value for  $S$  should be interpreted carefully, as the  $f_{cf}$  acts highly non-linear; further explanations in text).

Variable	Value [-]	Total Soil Loss [t/ha]
$v_l$	0.03	69.77
$v_m$	0.50	29.53
$v_u$	1.00	29.67
$S$	-0.428	

tration factor from  $v_m$  to  $v_u$ . As Fig. 6.8 shows, this is not a general trend, but only occurs occasionally (cf. e.g. the “large” event in June to the “small” events in September). Such seemingly “inverted” behaviour essentially results from the separation of the momentum fluxes of rainfall and runoff depending on rill area (i.e.  $f_{cf}$ , as described in Section 4.5.2.2)<sup>1</sup>.

<sup>1</sup>This behaviour is influenced by a multitude of factors. For example it may arise by reduction of the momentum flux of the raindrops by a thin water film. Considering a  $f_{cf}$ -value of 0.5, a water film may develop due to flow concentration, which is thick enough to reduce raindrop impact (on 50% of the affected area), whereas a value of 1.0 only leads to a thin water film, which does not reduce the raindrop energy.

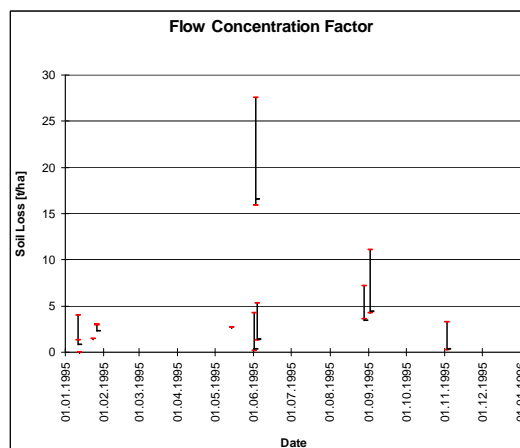


Fig. 6.8: Variations of the flow concentration factor.

Tab. 6.10: Variations of the soil cover.

Variable	Value [-]	Total Soil Loss [t/ha]
$v_l$	0.00	43.16
$v_m$	0.50	17.62
$v_u$	1.00	1.81
S	-0.920	

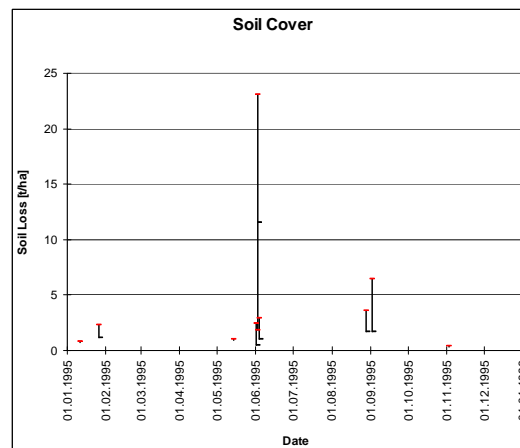


Fig. 6.9: Variations of the soil cover.

**SOIL COVER** Like the flow concentration factor the soil cover also affects the erosion module only. The selected variations are static, and agricultural management has no influences.

The result of 1.81 t/ha in Tab. 6.10 shows, that the influence of precipitation, respectively its momentum flux, is essential for erosion to occur. This can be seen in Fig. 6.9, too, where the red bars indicating the maximum value of soil cover are missing, except for one event.

**MANNING'S ROUGHNESS COEFFICIENT** For analysis of Manning's roughness coefficient, the same conditions apply, as for soil cover.

The selected values represent those of crusted soil ( $v_l$ ), an average developed, ripe crop field ( $v_m$ ), and forested areas ( $v_u$ ).

**SHEAR STRENGTH** As the definition of the shear strength uses a variety of different input parameters, here the testing is executed by changing the cohesion and the angle of internal

Tab. 6.11: Variations of Manning's roughness coefficient.

Variable	Value [-]	Total Soil Loss [t/ha]
$v_l$	0.006	73.14
$v_m$	0.2	33.11
$v_u$	0.8	24.61
S	-0.504	

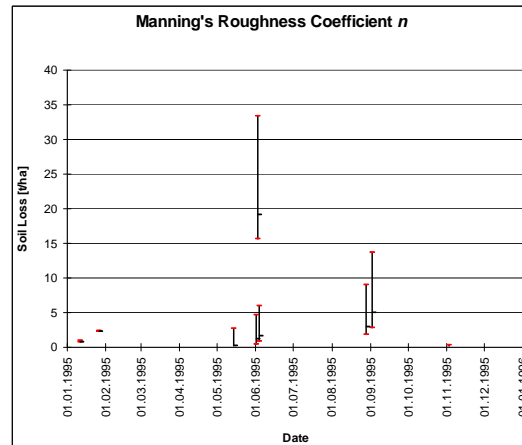


Fig. 6.10: Variations of Manning's roughness coefficient.

Tab. 6.12: Sensitivity of the erosion model to variations concerning the detachability of the soil.

(a) Variations of the cohesion. (angle of internal friction is fixed to 20°) (b) Variations of the angle of internal friction. (cohesion is fixed to 0.5 kPa)

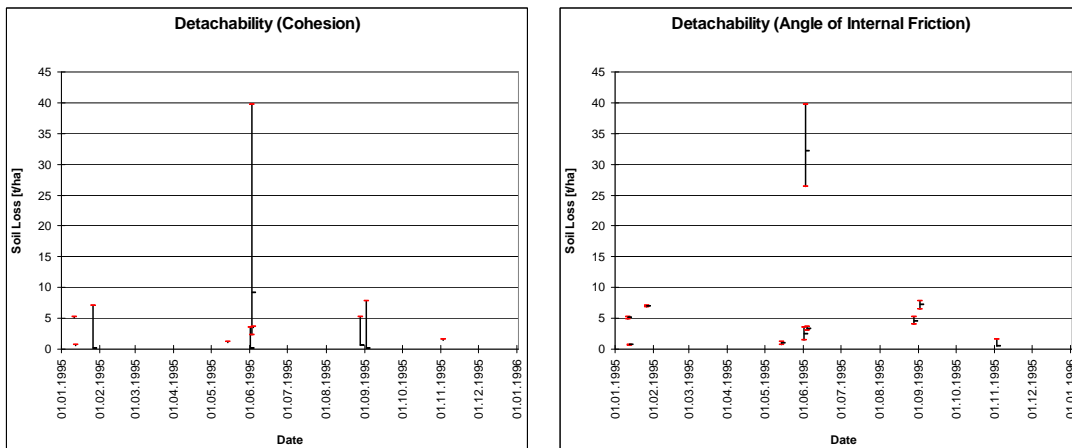
Variable	Value [kPa]	Total Soil Loss [t/ha]	Variable	Value [°]	Total Soil Loss [t/ha]
$v_l$	0.5	75.75	$v_l$	20.0	75.75
$v_m$	4.0	10.15	$v_m$	25.0	63.91
$v_u$	10.0	2.38	$v_u$	30.0	54.62
S		-1.038	S		-0.811

friction of the soil only. Similar to the tests of the erosion resistance, these two parameters are varied, disregarding the particle size distribution of the soil.

**EROSION RESISTANCE** This test represents an exception compared to the other parameter tests presented. Here, the erosion resistance as defined in the original EROSION 2D model is used for computation, instead of the redefined critical shear stress routine (Section 4.5.5). Erosion resistance is the central parameter in the original model, and therefore its sensitivity analysis allows to draw conclusions on the impacts of substituting the erosion resistance with the critical shear stress routine. That means, that if the sensitivities of the erosion resistance and the shear strength concept deviate strongly, the basic governing detachment equation of the model may be rendered invalid, respectively computes erroneous values of the detached sediment amount.

The values of the erosion resistance are taken from the parameter catalogue (SCHMIDT ET AL., 1996) for a soil, which is very susceptible to particle detachment, a silty sand (even though the particle size distribution is the one for the default soil, a "clayey silt"). They range from 0.00005 at seedbed preparation to 0.003 for maize cultivations in late summer. Values of  $v_u$  higher than 0.003 lead to zero soil loss with the default parameterisation.

**SENSITIVITY TO THE TESTED PARAMETERS** Fig. 6.13 summarises the sensitivity of the erosion model to all the parameters tested here. It has to be emphasised once more, that the



(a) Variations of the cohesion. (angle of internal friction is fixed to 20°) (b) Variations of the angle of internal friction. (cohesion is fixed to 0.5 kPa)

Fig. 6.11: Influence of cohesion and angle of internal friction on soil loss.

Tab. 6.13: Variations of the erosion resistance.

Variable	Value [-]	Total Soil Loss [t/ha]
$v_l$	0.00005	302.79
$v_m$	0.0005	50.76
$v_u$	0.003	1.46
S		-1.095

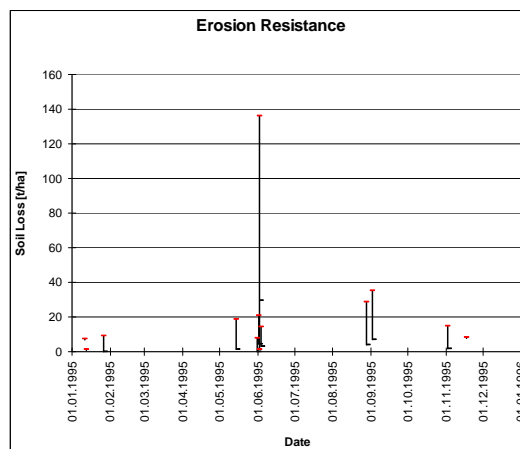


Fig. 6.12: Variations of the erosion resistance.

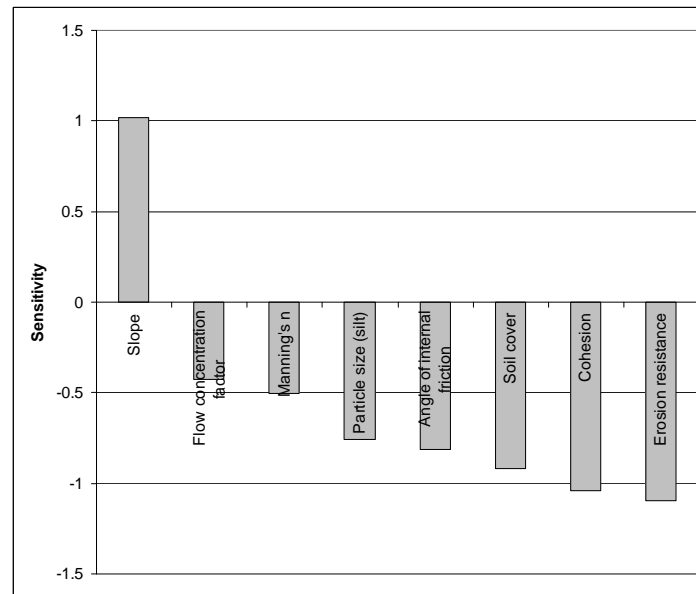


Fig. 6.13: Sensitivity of all tested parameters.

sensitivity parameter  $S$ , as used in this context, only represents a guideline, because of the non-linearity of the processes involved.

Nevertheless, comparing the sensitivity values with those calculated by SCHMIDT (1996) for the original EROSION 2D model, they range in the same order of magnitude. SCHMIDT (1996) specifies the highest sensitivity values for the initial soil moisture content (+2.72), organic matter content (-1.45) and precipitation intensity (+1.38), which all are not considered in this study. The value for the erosion resistance (-1.00) approximately equals the value found in this work, and the value for Manning's roughness coefficient (-0.84) differs slightly. But the slope deviates stronger (+0.33), which probably (because SCHMIDT's exact testing conditions are unknown to the author) is the result of the consideration of the slope length in the work of SCHMIDT (1996).

#### 6.2.2.2. INDIRECT PARAMETER VARIATIONS

In the following sections, the influence of whole parts (or subroutines) of the erosion model, respectively routines affecting the model, are analysed, as these consist of multiple parameters which cannot be analysed in detail, because the interactions are too complex. Therefore the subroutines are only switched off, in order to show their influence on the temporal pattern of soil loss. For this reason, the sensitivity parameter  $S$  here cannot be calculated.

**DISAGGREGATION OF PRECIPITATION** In order to compare the influence of the two available disaggregation methods (the cascade disaggregation (CD) described in Section 4.6.2 and the "default" model, ACD, from Section 4.2.1.2), both are applied to the default proxel. The soil loss of single events is not illustrated graphically, as the total soil loss occurs within a single day (03.06.1995) for the case of the ACD. Instead, the impacts on rainfall and runoff are shown in Fig. 6.14. Considering the runoff pattern, it becomes clear why soil loss is very low: only the rainfall event on 03.06.1995 induces surface runoff, which is required

Tab. 6.14: Influence of disaggregation method on total soil loss.

Sub-model	Total Soil Loss [t/ha]
Cascade disaggregation	41.4
"Default" disaggregation	0.4

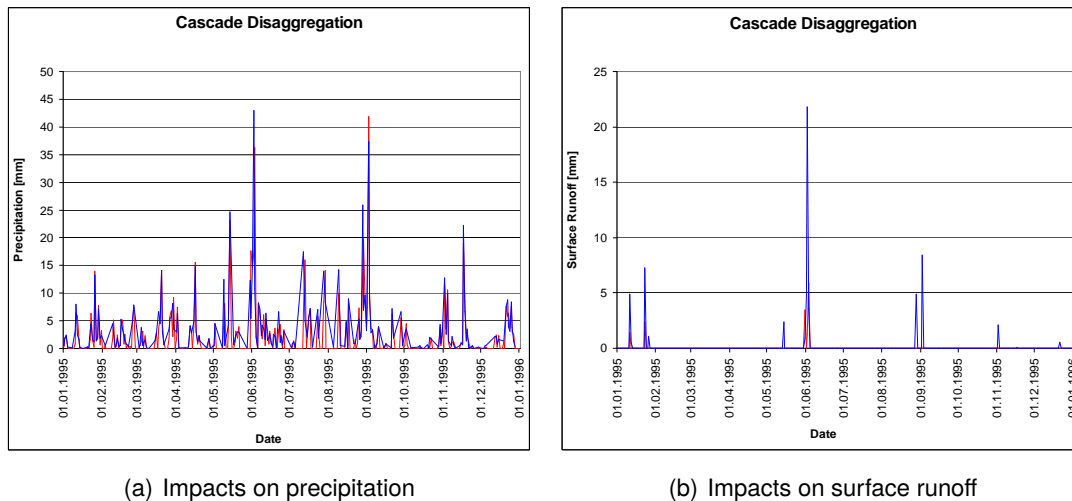


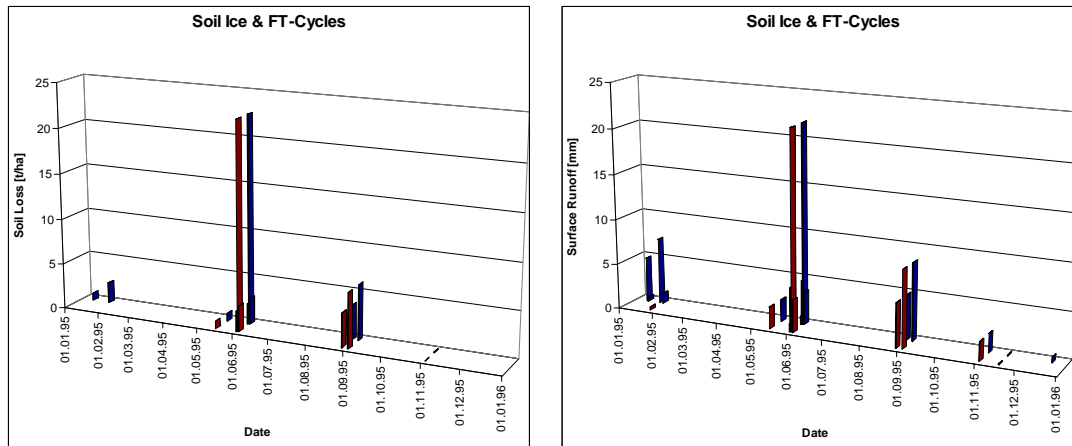
Fig. 6.14: Temporal course of rainfall and runoff formation induced by disaggregation methods. (The blue lines denote the series produced by the cascade disaggregation model, the red lines result from turning it off and using the "default" method.)

to transport detached soil particles. The temporal patterns of rainfall look very similar, but surprisingly the ACD does not produce runoff. The reason for this is the intra-diurnal course of precipitation intensities. As shown in Section 5.1.2, daily precipitation amounts disaggregated with both methods sum up to approximately the same value, but hourly precipitation intensities may differ strongly (which cannot be seen in this illustration, as the data is aggregated to 1 day). Intensities produced by CD are higher by trend than those from ACD, which means, that Hortonian overland flow more frequently occurs.

**SOIL FREEZING** Disabling the soil freezing routines (Section 4.2.2.2) means not only switching off the FT-cycles (Section 4.5.5.4), but also influences runoff formation in the colder seasons of the year. This can be seen in Fig. 6.15(a), where the difference in total soil loss of approx. 3 tons per hectare occurs only in January. Fig. 6.15(b) clarifies the influence on runoff formation. In late December 1995, the occurrence of surface runoff is observed, but no soil loss appears, which might be traced back to either totally frozen soil, or the conditions for a freeze-thaw-cycle are not fulfilled.

Tab. 6.15: Influence of soil freezing on total soil loss.

Sub-model	Total Soil Loss [t/ha]
Activated	41.4
Deactivated	38.4



(a) Impacts on soil loss (blue columns: with soil freezing and FT-cycles, red: w/o soil freezing and FT-cycles)  
 (b) Impacts on surface runoff (blue columns: with soil freezing and FT-cycles, red: w/o soil freezing and FT-cycles)

Fig. 6.15: Influence of soil freezing on runoff formation and soil loss.

Tab. 6.16: Influence of momentum flux partitioning on total soil loss.

Sub-models	Total Soil Loss [t/ha]
Activated	41.4
Deactivated	1.8

**MOMENTUM FLUX PARTITIONING** This paragraph covers the behaviour of sub-models, which affect the partitioning of the momentum fluxes into rill and interrill components and/or affect momentum flux (either by increase or decrease). Here, a number of sub-models is switched off, which results in a configuration similar to the original algorithms of EROSION 2D. The following implementations are affected:

- The calculation of canopy interception, including drip off and reduction of raindrop momentum flux by sheet flow (as described in Section 4.5.4) is switched off. Momentum flux of rainfall is only reduced by  $c_c$  in Eq. (4.12).
- Soil cover (as described in Section 4.5.4.2) is not modelled at all.
- The flow concentration factor (as described in Section 4.5.2) is switched off.

The results show, that without the modifications of the momentum flux treatment, the soil loss strongly decreases, respectively reacts only to a single event. As the influence of soil cover reduces soil loss, this means, that the effects of drip off and flow concentration factor considerably increase particle detachment and transport.

**PARTICLE SETTLING VELOCITY** For the testing of the influence of the particle settling velocity, the original Stokes equation for particle settling velocity (Eq. (4.16) in Section 4.5.1.2) and the one of CHENG (1997) are compared. The subroutine applying the approach of CHENG (1997) also uses the dynamic computation of the kinematic viscosity of the flow depending



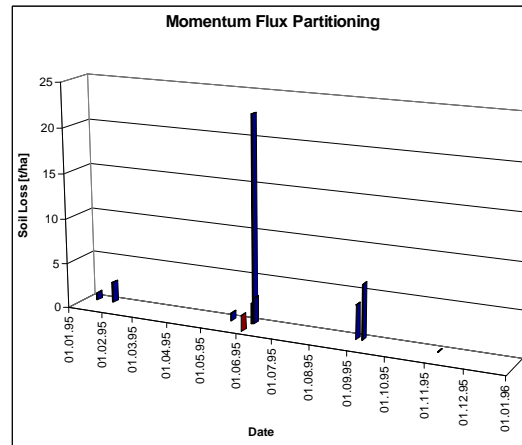


Fig. 6.16: Influence of momentum flux partitioning. (blue columns: with momentum flux partitioning, red: w/o partitioning)

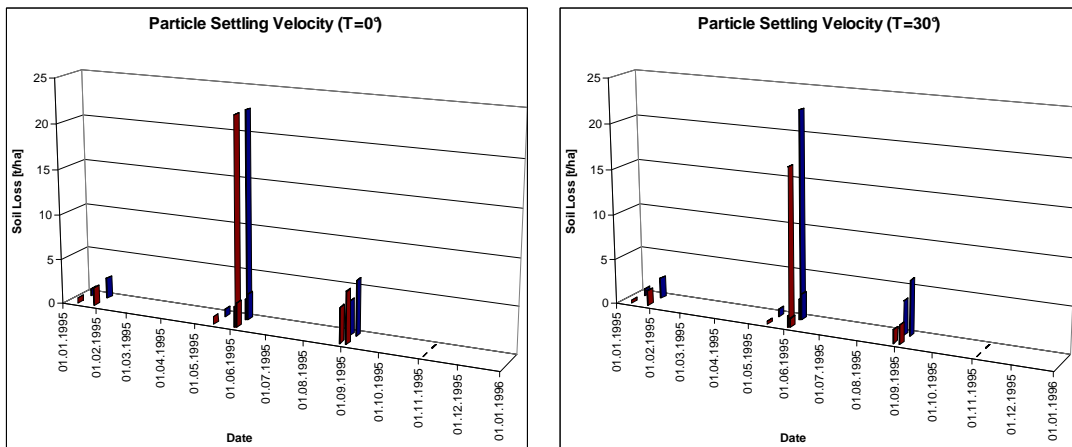
Tab. 6.17: Influence of the particle settling velocity depending on temperature on the total soil loss.

Sub-model	Total Soil Loss [t/ha]
CHENG (1997) with variable viscosity	41.4
Stokes with fixed viscosity (T = 0°C)	40.5
Stokes with fixed viscosity (T = 30°C)	25.4
CHENG (1997) with fixed viscosity (T = 0°C)	44.9
CHENG (1997) with fixed viscosity (T = 30°C)	33.4

on temperature (Section 4.5.3). For comparison, the Stokes version uses a static value for dynamic viscosity (0.001787 Pa·s for a temperature of 0°C and 0.000798 Pa·s for 30°C).

The results in Tab. 6.17 show, that the assumed temperature strongly influences the soil loss. The lower the temperature, the higher the viscosity becomes, and the fluid exhibits more resistance to the stresses of the sinking particles. This means, neglecting the influence of temperature and using a mean, static viscosity value very likely results in overestimations of soil loss in summer, and underestimations in winter. Generally, CHENG's equation leads to lower settling velocities, and thus to higher soil loss than the Stokes equation, which can be seen in Tab. 6.17.

**AGRICULTURAL MANAGEMENT** The agricultural management routines constitute the most complex sub-model influencing erosion, as the impacts of the numerous processes interfere with each other. Therefore, in order to demonstrate the effects of agricultural management, an arbitrary variation of the sowing and harvest is selected. Sowing is set to occur 30 days later (on 24.05.1995) and harvest is executed 40 days earlier (on 26.08.1995) than the corresponding mean dates for maize. Such a situation may be unlikely to occur, but is chosen, to show the influences of the dates. Fig. 6.18 illustrates the higher soil loss in June, due to weaker plant development, and the higher losses in autumn, which are caused mainly by the absence of the protecting vegetation cover.



(a) Particle settling velocity for a flow temperature of 0°C (b) Particle settling velocity for a flow temperature of 30°C

Fig. 6.17: Influence of the particle settling velocity. (blue columns: CHENG (1997) with variable viscosity, red: Stokes with fixed viscosity)

Tab. 6.18: Influence of agricultural management on total soil loss.

Sub-model	Total Soil Loss [t/ha]
Dynamic Management	41.4
Fixed harvest (-40 d) and sowing (+30 d) dates	51.5

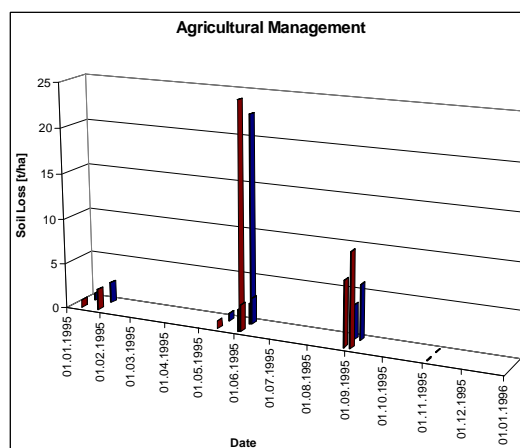


Fig. 6.18: Influence of agricultural management. (blue columns: dynamic agricultural management, red: fixed harvest and sowing dates)

Tab. 6.19: Influence of land use types on total soil loss.

Land Use	Total Soil Loss [t/ha]
Winter Wheat	19.6
Rapeseed	28.4
Maize	41.4

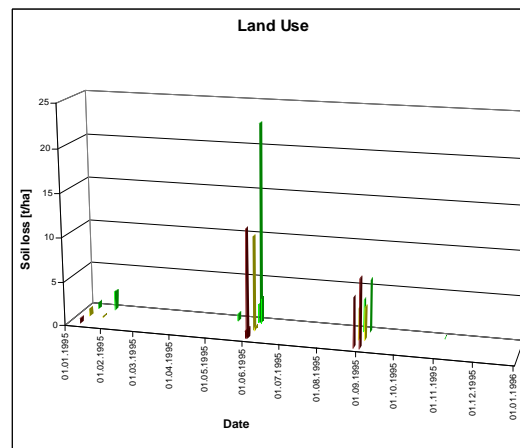


Fig. 6.19: Influence of land use types. (brown: rapeseed, yellow: winter wheat, green: maize)

**INFLUENCE OF LAND USE TYPE** The results of selected, different land use types on total soil loss are listed in Tab. 6.19. As expected, the highest soil loss occurs on maize cultivations, and the lowest on winter wheat. Natural land use types, such as grassland or forest, are not shown, as the parameters of the default proxel do not lead to erosion on these types. The most interesting aspects in the temporal pattern of soil loss in Fig. 6.19 are:

- The protecting influence of the winter crops (i.e. winter wheat and rapeseed) is observed in autumn and winter, where, in contrast to maize no soil loss or only reduced erosion occurs.
- The winter crops also protect the soil better in May, due to increased growth.
- The earlier harvest date of rapeseed leads to an increase of soil loss in late summer. Sowing occurs on 20.08.1995, thus the plants are not yet developed well, when the rainfall events on 28.08.1995 and 02.09.1995 occur.

**INFLUENCE OF SURFACE RUNOFF** In order to analyse the sensitivity of the erosion module to surface runoff, the amount of the actually modelled surface runoff is modified. For the analysis of the sensitivity of the erosion module to surface runoff, only the actual amount of surface runoff was modified, i.e. multiplied by a factor. This means, that runoff (and erosion) occur exactly on the same dates as presented above, and are modified only within the erosion module. Thereby, only the calculation of particle detachment and transport is influenced, but no additional erosion events are generated. The results in Fig. 6.20 and Tab. 6.20 are based on a percentage of 50% and 200% of the actual runoff, zero runoff is omitted, as the governing

Tab. 6.20: Influence of surface runoff on total soil loss.

Runoff	Total Soil Loss [t/ha]
50%	24.6
100%	41.4
200%	63.1

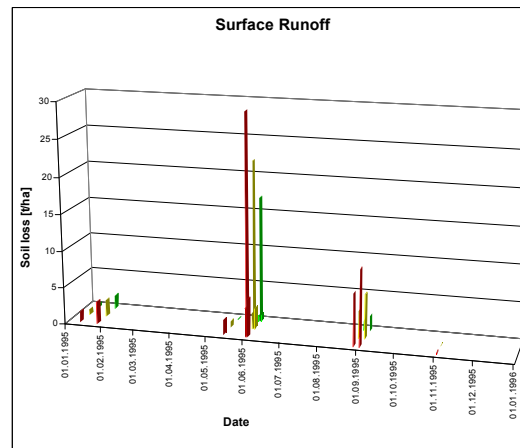


Fig. 6.20: Influence of surface runoff. (red: 200%, yellow: 100%, green: 50%)

equations of the model transport particles only via surface runoff, i.e. no soil loss would occur.

**SENSITIVITY OF THE MODEL COMPONENTS** As noted above, the sensitivity parameter  $S$  could not be calculated for the tests of this section, therefore here only a qualitative summary of the influence of the presented variations on soil erosion is discussed.

Whilst the soil loss responds adequately to the influence of the land use type and the surface runoff, the influence of the disaggregation of precipitation and the treatment of the momentum fluxes exhibit a much more extreme behaviour. Obviously they represent essential implementations for the erosion module, as without these nearly no soil loss is induced. For the case of disaggregation this is not surprising (as described above), but the influence of the momentum flux routine is considerable. It was stated above, that this depends mainly on drip off and the flow concentration factor (at least for the “default” proxel in the selected simulation year). Reviewing the moderate impact of the  $f_{cf}$  (cf. Section 6.2.2.1), this leads to the conclusion, that drip off contributes noticeably to soil erosion in the implementation of the erosion module.

The following implementations remarkably modify the temporal pattern of soil loss in the annual course:

- Soil Freezing may increase runoff formation in winter and spring, and FT-cycles simulate possibly weakened soil conditions in this period.
- The influence of the combined agricultural management routines affect soil erosion during the whole year by altering soil conditions and impacting momentum fluxes. The most crucial parameter here is the correct setting of the dates for tillage, sowing and harvest.

- The dynamic particle settling velocity also influences soil erosion during the whole year, by increasing soil loss in winter and decreasing it in summer (compared to static values).

All of these implementations essentially contribute to a realistic simulation of the annual course of soil erosion. Nevertheless, since their influence is relatively strong, it is indispensable that their parameterisation, respectively the inputs they gain, are reliable.

### 6.2.3. PLAUSIBILITY CHECK

The plausibility check is split up two essential parts. Section 6.2.3.2 and Section 6.2.3.3 deal with the analysis of temporal soil loss patterns within two selected sub-catchments of the Upper Danube Basin: the *Große Laber* and the *Ammer* watershed. Section 6.2.3.4 and Section 6.2.3.5 assess the long-term spatial patterns of soil loss within the whole Upper Danube Basin, and compare those to the results of other soil erosion studies.

For the first two sections of the plausibility check, data is available from two gauges of the LfU (Tab. 6.21), ranging from 1990 to 2005. At the gauges runoff  $Q$  [ $\text{m}^3/\text{s}$ ] and suspended

Tab. 6.21: Attributes of the LfU gauges for measurement of suspended sediment, which are used for the plausibility check. The data available ranges from 1990 to 2005. (RW and HW are easting, respectively northing of the Gauss-Krüger coordinate system)

	<i>Große Laber</i>	<i>Ammer</i>
Gauge	Schönach	Weilheim
Catchment area	406.69	607.39
RW	4531287	4435366
HW	5419875	5301350

sediment  $s_s$  [ $\text{g}/\text{m}^3$ ] is measured. Together with the catchment area  $A$  [ $\text{km}^2$ ], this can be converted to the specific sediment yield (SSY) [ $\text{t}/\text{km}^2$ ] of the catchment:

$$SSY = Q \cdot s_s \cdot A \quad (6.3)$$

Long-term measured annual mean SSY amounts to  $9.6 \text{ t}/\text{km}^2$  in the *Große Laber* catchment, and  $136.7 \text{ t}/\text{km}^2$  in the *Ammer* watershed. The long-term monthly mean values of discharge and SSY are listed in Tab. 6.22 and illustrated in Fig. 6.21.

Tab. 6.22: Measured SSY and MQ at the gauges Schönach (S) and Weilheim (W). The long-term mean discharge MQ [ $\text{m}^3/\text{s}$ ] is based on data from 1926–2005 for Weilheim, and from 1954–2005 for Schönach (LFW, 2005). The long-term mean specific sediment yield (SSY) [ $\text{t}/\text{km}^2$ ] is based on data from 1971–2002 for Weilheim, and from 1989–2002 for Schönach (LFW, 2002).

	J	F	M	A	M	J	J	A	S	O	N	D
MQ (S)	2.80	3.41	3.26	2.49	1.94	1.90	1.80	1.69	1.70	1.96	2.32	2.81
SSY (S)	0.89	1.14	0.89	0.66	0.65	1.03	0.62	0.59	0.42	0.72	0.85	1.18
MQ (W)	11.1	12.2	15.5	18.2	20.1	20.5	19.5	17.1	14.6	12.6	12.0	11.6
SSY (W)	1.46	3.46	7.37	6.65	24.26	23.15	31.35	18.40	7.28	3.41	4.89	5.08

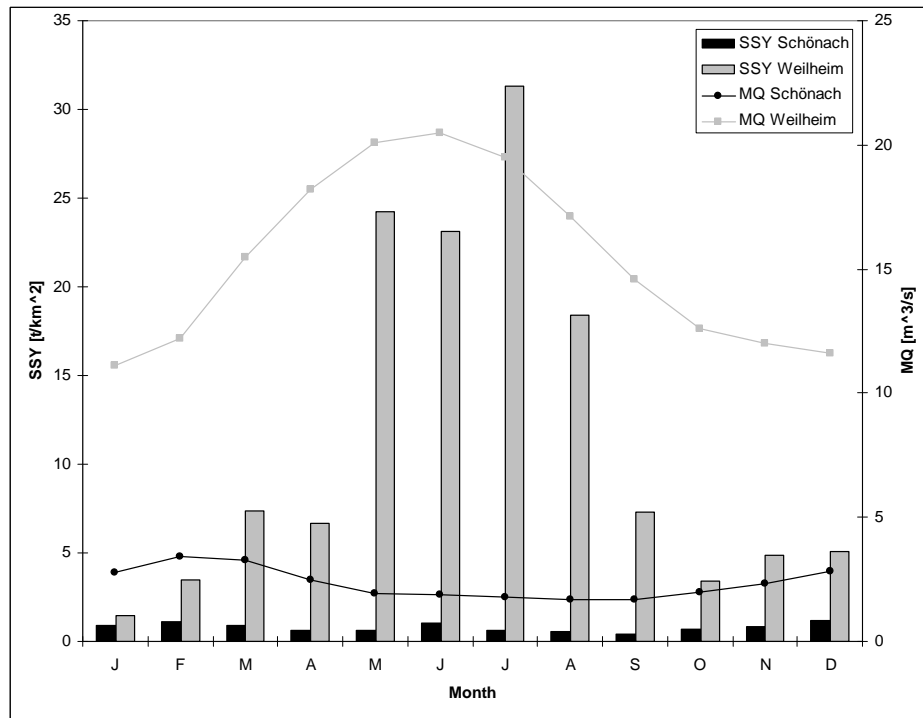
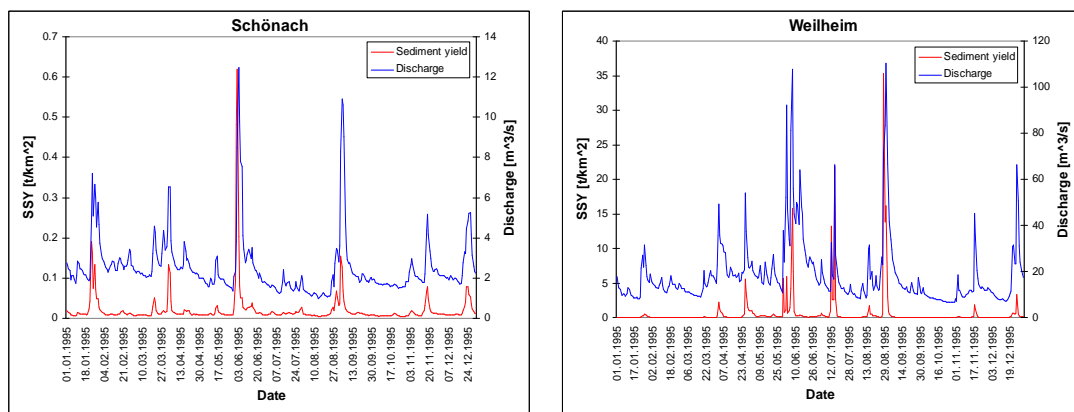


Fig. 6.21: Measured SSY and MQ at the gauges Schönach and Weilheim. (Base data: same as in Tab. 6.22)



(a) Schönach (Große Laber)

(b) Weilheim (Ammer)

Fig. 6.22: Measured specific sediment yield and discharge at the gauges Schönach and Weilheim for the year 1995.

### 6.2.3.1. PRELIMINARY CONSIDERATIONS

Fig. 6.22 shows the measured SSY at the gauges *Schönach* and *Weilheim* for the year 1995. The corresponding measured and modelled discharge is illustrated in Fig. 6.23. Comparing the SSY and the discharge in Fig. 6.23 exhibits, that the patterns resemble, but the level of the peaks do not necessarily range in the same magnitude. Nevertheless, an important conclusion from this observation is that transport of SSY only occurs in times of increased discharge. The same connection is relevant for evaluation of the erosion module, too, because it needs

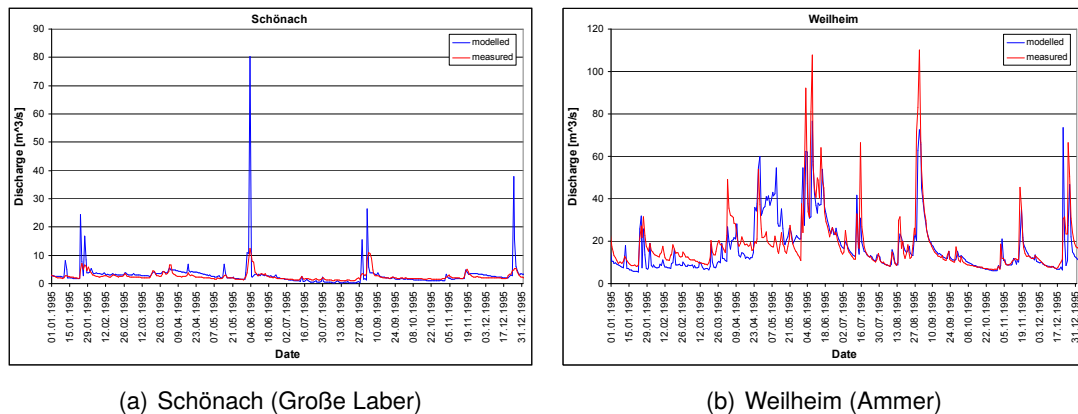


Fig. 6.23: Measured and modelled discharge for the Schönach and Weilheim for the year 1995.

surface runoff in order to transport particles, i.e. to cause erosion at all (see Section 6.2.2.2). The selected exemplary illustration in Fig. 6.23 shows, that the patterns of modelled discharge differ from the measured values in the year 1995. This implies, that the erosion module is likely to compute wrong soil loss values from deficient input data for the depicted year. But as the hydrographs only depict the total discharge (i.e. baseflow, interflow and overland flow) at the gauge, they cannot be directly linked to the spatial distribution of surface runoff (and therefore erosion) at the proxel level. Thus, in order to check the plausibility of the computed soil loss of the erosion module, it is more reasonable to observe the areal mean values of surface runoff, rather than total discharge at the gauge. The occurrence of surface runoff restricts erosion events to the dates illustrated in Fig. 6.24.

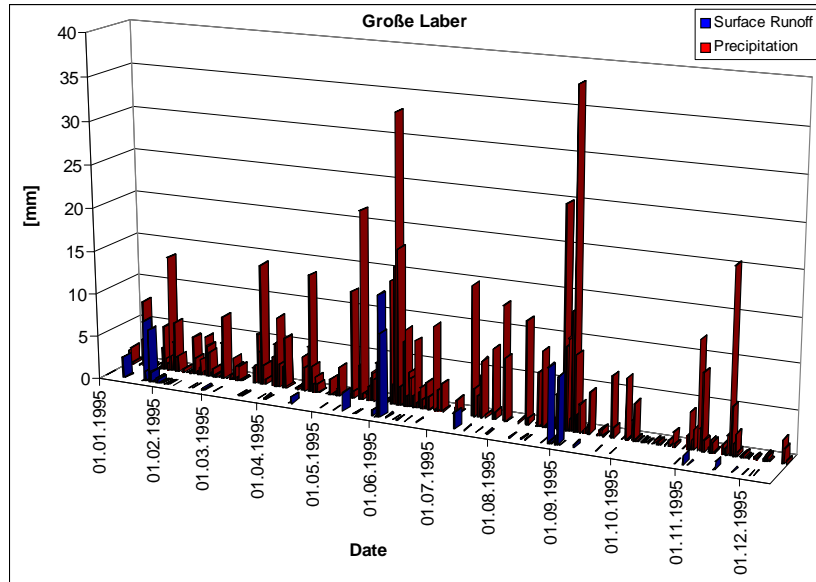
A comparison of this data to the measured discharge and the SSY shows, that it is impossible to model some erosion events, since for the latter simply no surface runoff is produced by the soil sub-model.

For the analysis of the modelled results and the comparison to measured values, all proxels with land use types which inhibit production of soil loss, i.e. water, built up areas and glacier (since glacial erosion cannot be simulated with the erosion module), are excluded.

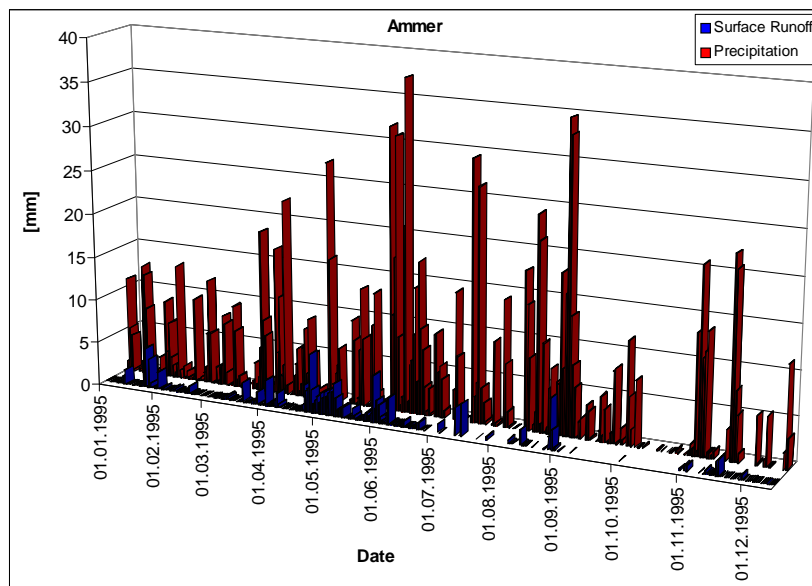
For the evaluation of the erosion module, model runs with the “standard” temporal and spatial resolution of PROMET, i.e. a time step of one hour on a proxel size of 1 km<sup>2</sup>, are executed. As already noted in Section 4.2.4, the Upper Danube Basin is carved by a dense channel network. Due to this high density, every proxel contains a channel if a scale of 1 km<sup>2</sup> is considered. This means, that eroded sediment will be delivered to this network by surface runoff. Thus it is very unlikely, that sediment will be transported downslope to the next proxel, where it might be deposited. Therefore it seems reasonable to switch off the computation of deposition, as described in Section 4.5.1.4.

All results from the erosion module, which are shown in this study, are not linked to the channel flow sub-model in PROMET. This means, if a modelled erosion event is compared to measured SSY at the gauge, the temporal patterns are shifted, since it usually takes some time for the sediment to be transported to the gauge.

In order to link on-site soil loss to specific sediment yield at the basin outlet, the sediment delivery ratio (SDR) is frequently used. “The SDR refers to the ratio between specific sediment yield and gross erosion” (DE VENTE ET AL., 2007), which means that specific sediment yield



(a) Große Laber watershed



(b) Ammer watershed

Fig. 6.24: Modelled areal mean precipitation and surface runoff for the watersheds of the Große Laber and Ammer for the year 1995.



can be calculated with:

$$SSY = SDR \cdot grossErosion \quad (6.4)$$

Of course the SSY in the rivers is determined by the gross erosion in the area, but also strongly modified by sediment sinks in the watershed and sedimentation and transport characteristics of the receiving water courses. Since the SDR usually is determined empirically, it accounts for these influences. Furthermore, for this study this means, that SSY and modelled soil losses cannot be compared directly. Many studies report a decrease of SSY, respectively SDR, with increasing drainage basin area, which is often explained by the fact that during transport through a river basin progressively more sediment is trapped in sinks (DE VENTE ET AL., 2007). Usually the SDR is calibrated by relating modelled soil loss to measured SSY at the gauge of a basin. Such a calibration is theoretically possible for the sub-catchments of the *Große Laber* and the *Ammer*, but it does not seem to be a reasonable method for evaluation in this context, as even totally wrong, modelled soil losses thus can be fitted to the measured SSY. Practically, this would inevitably lead to incorrect SDRs, as e.g. in the *Ammer* watershed other processes than soil erosion, such as bank erosion or mass movements, contribute to SSY, which currently definitely cannot be modelled by the erosion module. Therefore, the measured specific sediment yields are used in this work merely for the evaluation of temporal soil loss patterns.

*Note: For areal evaluation of model results in the following sections, a mask is applied before statistical values are calculated, which rejects built up areas and glacier and water proxels. This avoids the calculation of misleading results, as e.g. the surface runoff on built up areas may become very high.*

### 6.2.3.2. EVENT-BASED INSPECTION OF TEMPORAL SOIL LOSS PATTERNS

Prior to evaluating single erosion events, it is useful to interpret the intra-annual course of soil erosion, as this is differing for the catchments of the *Große Laber* and the *Ammer*. The annual course of sediment transport is shown in Fig. 6.21, which may be explained as follows:

- *Ammer* catchment: Generally, precipitation amounts are much higher in *Weilheim* (see Fig. 6.25) than in the *Große Laber* catchment: The clear maximum of precipitation in summer leads to high discharge volumes which may transport high amounts of sediment.
- *Große Laber* catchment: even if the maximum precipitation amounts occur in summer (Fig. 6.25), the annual course is much more balanced than in *Weilheim*. The discharge increases in winter (cf. Fig. 6.21), which also affects the amount of specific sediment yield. Nevertheless a secondary peak of SSY can be found in summer, when precipitation amounts are increased.

It should be noted here, that the absolute amounts of SSY are much higher in the *Ammer* catchment, than in the *Große Laber* catchment, although the percentage of agricultural area (i.e. area vulnerable to erosion) is much lower. The reason for this are the different processes acting in the sub-catchments, e.g. the transport within water courses and the sediment delivery into these, causing different SDRs (cf. Section 6.2.3.1). However this discrepancy does not matter for the analysis of patterns in this section, as here the temporal course is assessed

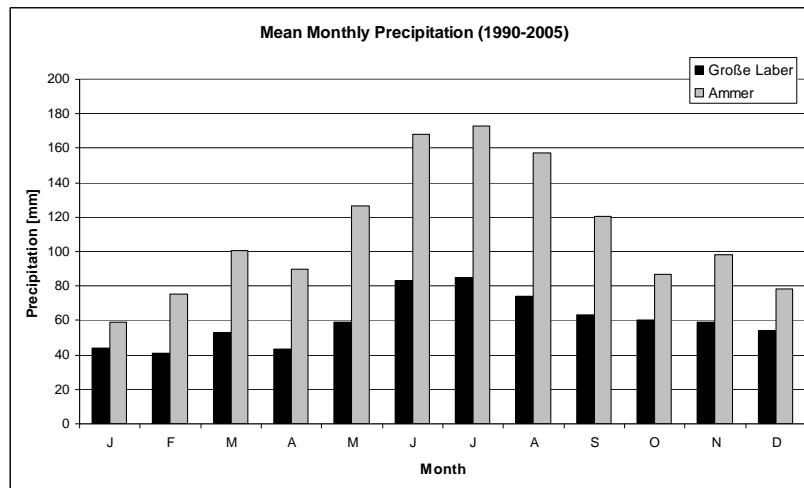
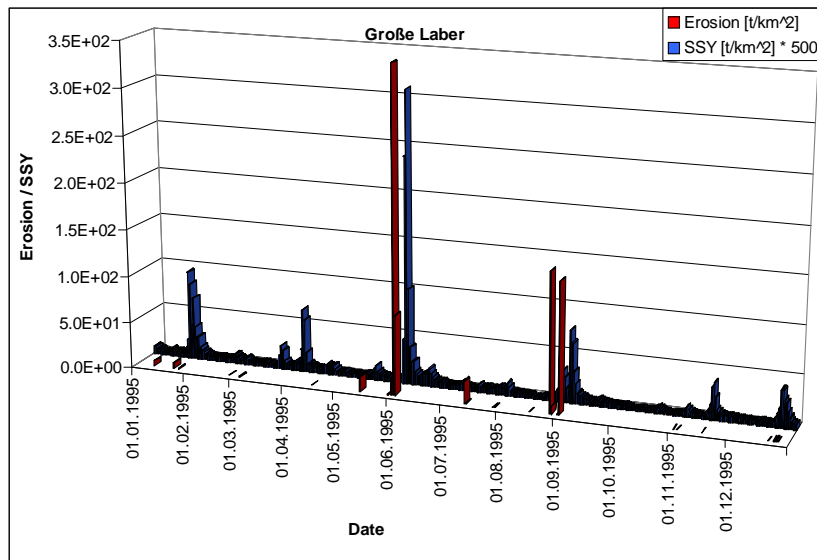


Fig. 6.25: Modelled long-term mean monthly precipitation amounts in the Große Laber and Ammer catchments. (Base data: DWD climate station measurements interpolated with AtmoStations from 1990 – 2005).

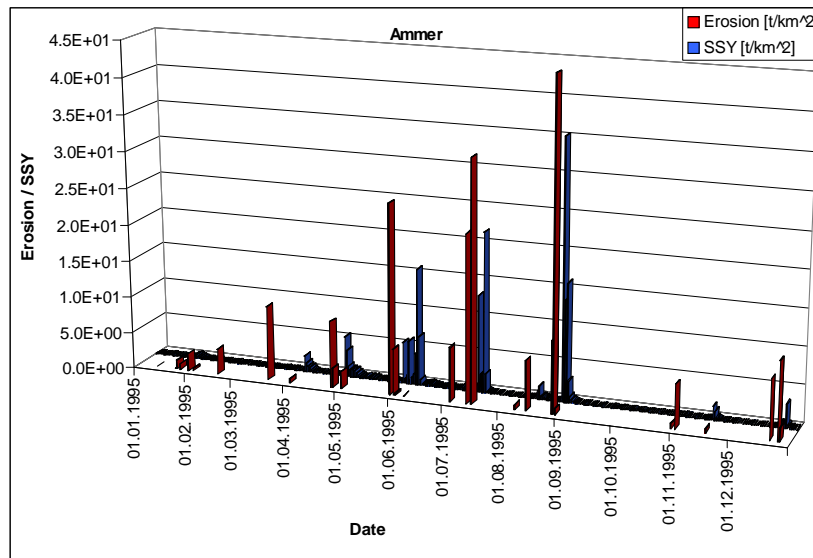
in a non-quantifying way only. In order to assess the ability of the erosion module to represent temporal patterns of soil loss, a single year is chosen for qualitative analysis, because it is beyond the scope of this work to discuss the occurrence of single erosion events over a period of 16 years. Fig. 6.26 shows the measured specific sediment yield and the modelled soil loss. Note, that the SSY in Fig. 6.26(a) is multiplied by an (arbitrary) factor of 500 for reasons of a better illustration only, as the differences on the ordinate between soil loss and SSY are much higher in the *Große Laber* than in the *Ammer* catchment. As mentioned above, this is a consequence of the fundamental prevailing erosion processes, and therefore specific sediment yield differs in magnitude in both catchments. This does *not* mean, that the magnitude of soil loss is miscalculated by a factor of 500 at the *Große Laber*, but simply that the two watersheds exhibit different sediment delivery ratios.

Overall the model seems to represent the temporal pattern of soil loss in the *Ammer* catchment better, than in the *Große Laber* catchment. The erosion events in summer are all represented well for the *Ammer* and exhibit the same variations in magnitude as the SSY. These events are strongly influenced by the precipitation events illustrated in Fig. 6.24(b). Even though the precipitation and runoff amounts are highest in June, the modelled soil loss pattern resembles the measured SSY pattern, which means that the descriptions of the other involved processes (such as protecting influence of vegetation) correctly take effect. Nevertheless, the model reacts very sensitive to precipitation, which becomes apparent in the (relative) overestimations of soil loss in March and November. These might be caused by erroneous information on the state of the vegetation.

The occurrence of erosion events in the *Große Laber* catchment is generally reproduced by the model, but the relative magnitudes are distorted. This means, that either the events in summer are overestimated or the events in autumn and winter are underestimated by the model. The events in late March and early April, which are not reproduced by the model at all, can be addressed mainly to surface runoff formation, which is either not present or very low (Fig. 6.24(a)). However these are expected to have occurred, as the discharge peaks at



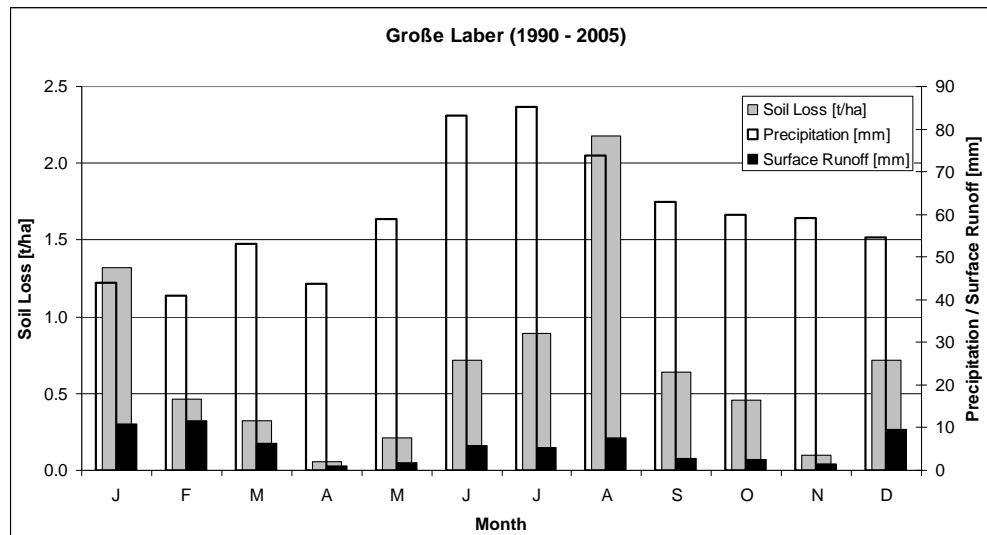
(a) Große Laber watershed



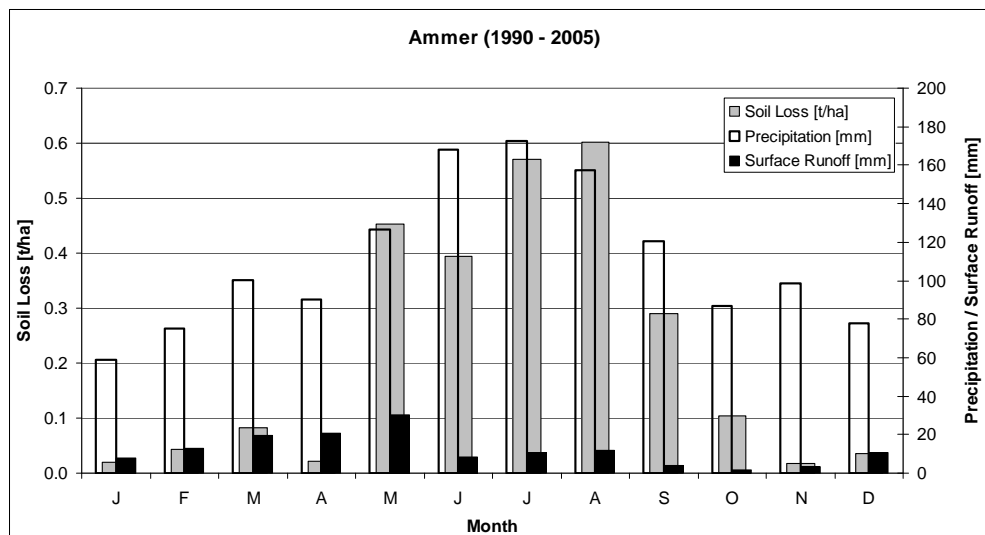
(b) Ammer watershed

Fig. 6.26: Measured ssy vs. modelled soil loss for the watersheds of the Große Laber and Ammer for the year 1995.

the gauge (Fig. 6.23(a)) suggest formation of surface runoff in the catchment. In contrast, the events in June and late August and early September presumably are overestimated, probably because the discharge at the gauge is overestimated, too. Critical appraisal of the soil properties supposes, that a better parameterisation of the silty soils of the *Große Laber* watershed can adjust the results produced by the erosion module, which generally delivers plausible patterns of soil loss.



(a) Große Laber watershed



(b) Ammer watershed

Fig. 6.27: Modelled long-term (1990–2005) monthly mean values of soil loss, precipitation and surface runoff of the Große Laber and Ammer watershed.

### 6.2.3.3. ANALYSIS OF LONG-TERM TEMPORAL SOIL LOSS PATTERNS

Tab. 6.23 and Fig. 6.27 show the long-term (1990 – 2005) modelled mean monthly soil losses from both watersheds.

In order to compare the patterns of modelled soil loss and measured SSY on a common basis, the values can be standardised with:

$$z = \frac{x - \mu}{\sigma} \quad (6.5)$$

where  $x$  is the raw score to be standardised,  $\mu$  is the mean value and  $\sigma$  is the standard deviation.

As in this section only the patterns of soil loss shall be evaluated, statistical measures are

Tab. 6.23: Modelled long-term (1990 – 2005) monthly mean values of soil loss [t/ha] of the Große Laber and Ammer watershed.

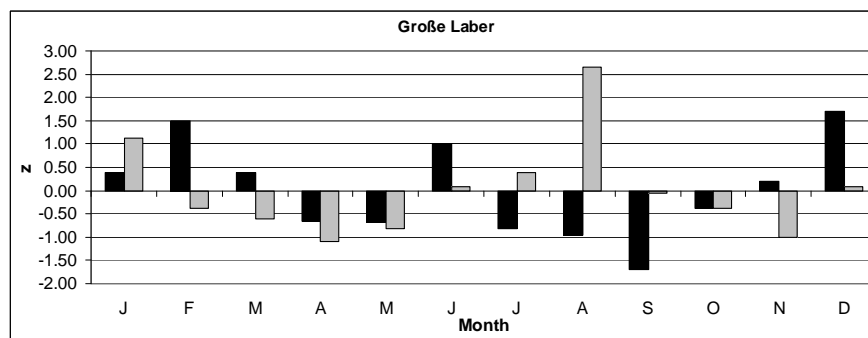
	J	F	M	A	M	J	J	A	S	O	N	D	$\Sigma$
Große Laber	1.3	0.5	0.3	0.1	0.2	0.7	0.9	2.2	0.6	0.5	0.1	0.7	8.1
Ammer	0.0	0.0	0.1	0.0	0.5	0.4	0.6	0.6	0.3	0.1	0.0	0.0	2.6

Tab. 6.24: Statistical criteria of standardised monthly model results. The presented values are averaged from 1990 – 2005 and aggregated to a monthly basis.

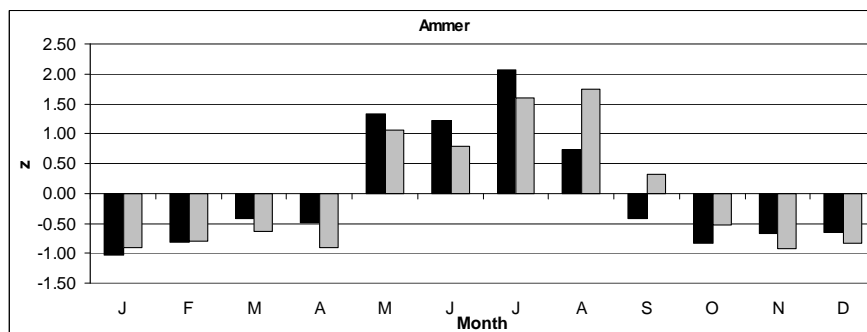
		CME	R <sup>2</sup>
Große Laber	MQ	0.88	0.88
	soil loss	-1.28	0.02
Ammer	MQ	0.77	0.78
	soil loss	0.79	0.80

calculated based on the *standardised* model results. The statistical criteria presented in Tab. 6.24 are the coefficient of model efficiency (CME) (NASH & SUTCLIFFE, 1970) and the coefficient of determination (R<sup>2</sup>). The considerable differences between the two catchments will be discussed in the following, with the aid of the standardised SSY and soil loss.

The illustration of the temporal course of the standardised SSY and soil loss in Fig. 6.28



(a) Große Laber watershed



(b) Ammer watershed

Fig. 6.28: Standardised long-term (1990 – 2005) monthly mean measured SSY (black bars) and modelled soil loss (grey bars) of the Große Laber and Ammer watershed.

Tab. 6.25: Ratios of soil loss [%] depending on agricultural management practices. The percentages are calculated from long-term monthly mean values from 1990 – 2005.

(a) Ratios of variable harvest dates and harvest dates forced to occur 21 days later than the parameterisation in Tab. 4.1.

	J	F	M	A	M	J	J	A	S	O	N	D	$\Sigma$
Große Laber	100	100	100	100	100	100	65	74	91	97	96	100	88
Ammer	100	99	99	100	100	101	100	93	92	98	100	101	98

(b) Ratios of conventional and conservative management practices. It is assumed, that conventional practices leave 15% crop residue on the field after harvest, whereas with conservative practices 30% residue remain on the field.

	J	F	M	A	M	J	J	A	S	O	N	D	$\Sigma$
Große Laber	86	87	82	82	100	100	99	63	57	79	92	90	80
Ammer	87	90	91	82	99	98	99	95	38	39	92	89	88

shows for both catchments overestimations of soil loss in late summer. The deviations of the standardised modelled soil loss to the standardised measured SSY are very high in August and September, when usually harvest of most cultivation occurs. This influence is much weaker in the *Ammer* watershed, since here grassland and forest dominate. Generally, the deviations are much higher in the *Große Laber* watershed, because arable land prevails there, which means that erosion rates are higher and thus the influence of anthropogenic measures, such as harvest and sowing becomes much stronger. Tab. 6.25 presents the influence of such measures on soil loss. Shifting the harvest dates to occur 21 days later than the estimated mean value in Tab. 4.1, causes a reduction of soil loss up to approx. 65%. The application of soil conservation practices even achieves a reduction to approx. 38% of its original value. Thus a better knowledge of the management practices applied in the Upper Danube Basin could significantly improve the modelled results. Nevertheless, as no data concerning such practices is available within this study, the results in the following sections are based on the assumptions of conventional management techniques.

Apart from the deviations during the harvest period, the temporal pattern of soil loss in the *Ammer* catchment fits reasonably well to the measured specific sediment yield at the gauge. The situation for the *Große Laber* catchment is more problematic, because here anthropogenic influences are much stronger, as noted above. But additionally discrepancies in the soil loss patterns in late autumn and late winter become apparent in Fig. 6.28(a). The event-based inspection in Section 6.2.3.2 already led to the assumption, that these shortcomings might be related to deficient modelling of runoff formation in this area. Fig. 6.29 presents the standardised long-term measured and modelled discharge of the *Große Laber* watershed (absolute, numerical values can be found in Tab. 6.22 and Tab. 6.26).

The illustration shows, that the discrepancies between measured and modelled discharge are highest in late autumn (November, December) and in late winter (February, March), where also the deviations between modelled soil loss and measured SSY (see Fig. 6.28(a)) are high. The discharge underestimations in February and March may explain the underestimated soil losses in these months, but surprisingly the overestimated modelled discharge in November

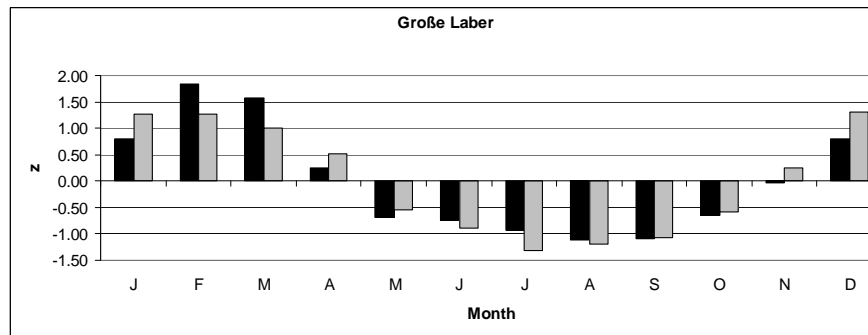


Fig. 6.29: Standardised long-term (1990 – 2005) monthly mean measured (black bars) and modelled (grey bars) MQ of the Große Laber watershed.

Tab. 6.26: Modelled long-term (1990 – 2005) monthly mean discharge [ $\text{m}^3/\text{s}$ ] at the gauges Schönach (S) and Weilheim (W).

	J	F	M	A	M	J	J	A	S	O	N	D
MQ (S)	4.6	4.6	4.2	3.6	2.2	1.7	1.2	1.3	1.5	2.1	3.2	4.6
MQ (W)	9.3	10.0	15.0	19.7	24.6	17.5	17.2	15.8	14.5	12.5	12.4	11.9

and December results in underestimations of soil loss. Since large parts of the *Große Laber* catchment are covered with winter crops (approx. 46%), which are sowed in (late) autumn, it seems likely that these are responsible for the deficiencies. The underestimated soil loss might be caused e.g. by too early sowing dates, or by a plant parameterisation which leads to a too rapid development in autumn, which both lead to an overestimation of the protecting soil cover, and thus reduce soil loss.

Finally, the simulated temporal pattern of soil loss in the whole Upper Danube Basin is presented in Fig. 6.30. Basically it is a superposition of the various precipitation and discharge regimes of the sub-catchments. On the one hand, the high peaks of soil loss in summer, which are found in alpine regions and the forelands (e.g. in the *Ammer* watershed) are attenuated. On the other hand, relatively high soil losses are observed in the winter months, which are caused by sub-catchments with high runoff amounts in winter, such as the *Große Laber*. The mean annual soil loss in the Upper Danube Basin averages out to 4.7 t/ha.

#### 6.2.3.4. ASSESSMENT OF LONG-TERM SPATIAL SOIL LOSS PATTERNS

*Note: In spite of the findings from the last section, i.e. the shortcomings of the model to represent the temporal soil loss patterns under certain conditions, the results presented in this section rely on the same model configuration, for reasons of comparability. It has to be pointed out, that the basic intention of this section is the analysis of the spatial distribution of soil loss patterns.*

Fig. 6.31 presents the modelled mean annual soil loss for the period 1961 – 2005. The image looks a bit “speckled”, which results from the variation of different land uses on neighbouring proxels. Considering a subscale land use map for modelling smoothens this effect, as presented for the ABAG in Fig. 6.32(a) (Section 6.2.3.5). The usage of an upscaled land use map for the simulation results in Fig. 6.31 thus is also responsible for the black coloured,

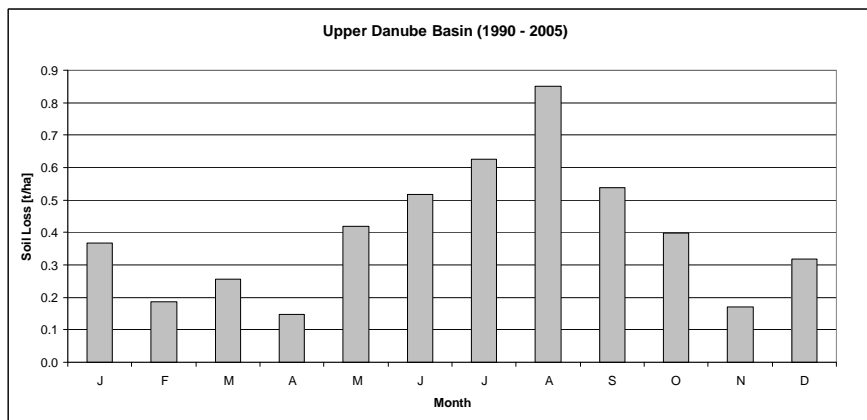


Fig. 6.30: Modelled long-term (1990–2005) monthly mean soil loss in the Upper Danube Basin.

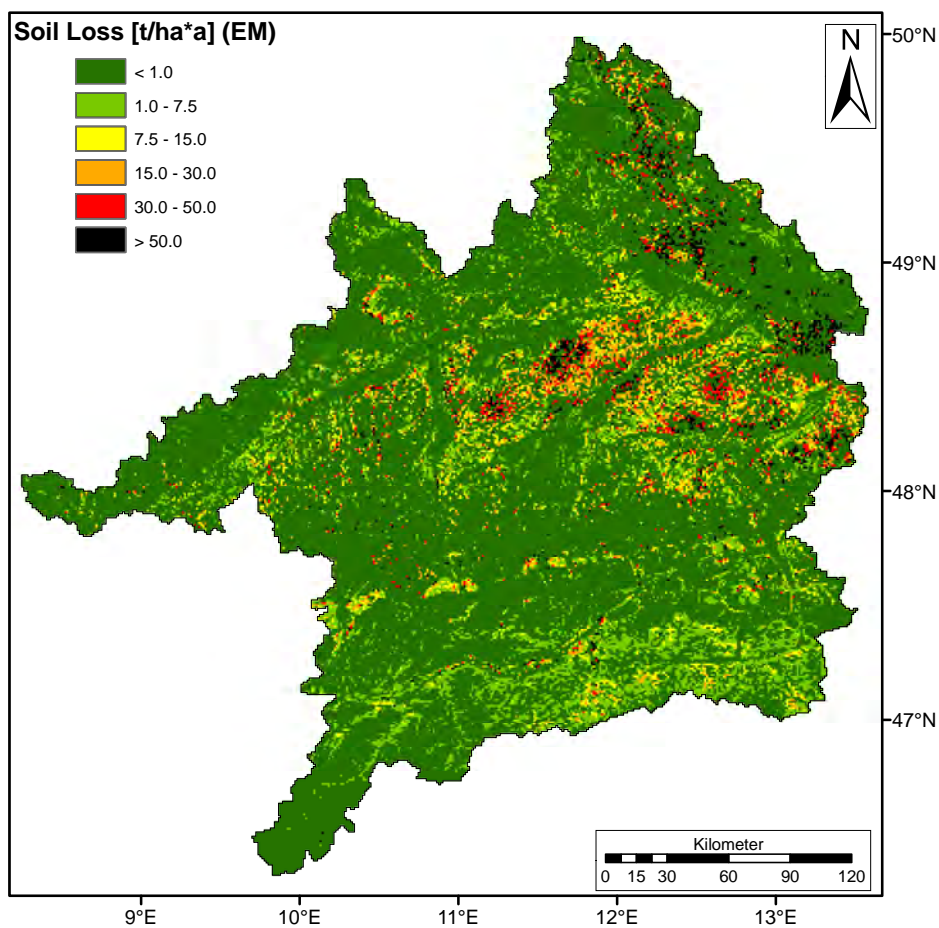


Fig. 6.31: Mean long-term annual soil loss (1961–2005) [t/ha] in the Upper Danube Basin, calculated with the erosion module (EM).



very high erosion rates. These would decrease by using subscale information, as generally in the Upper Danube Basin the parcel size of a single cultivation does not reach 1 km<sup>2</sup>. This means, that a subscale land use map does not necessarily change *areal mean values within a sub-catchment* (provided that the total fractions are the same), but the extreme values *per proxel* would be attenuated<sup>2</sup>. In order to suppress this effect, Fig. 6.34(a) shows the mean soil loss, aggregated to districts (here, the districts are used rather than sub-catchments, for reasons of comparability, since not all data sources are available in a high spatial resolution; see Section 6.2.3.5).

In both illustrations, the regions most vulnerable to erosion, the *Gäuboden* and the *Haller-tau*, are clearly recognisable in the spatial patterns. Both regions are agriculturally intensively used areas on soils susceptible to erosion (cf. Section 3.2.3.1 and Section 3.2.2.2).

In the south of the catchment, a belt following an east-west course in the forelands of the Alps can be recognised, which designates the areas, where due to the relief agricultural use is yet possible, but thus the steep slopes cause high soil losses. Towards the south, with increasingly steeper slopes, grassland and forests dominate, which protect the soil. As expected, the Inn valley exhibits high values of soil loss, but remarkable are the high soil losses extending from there far into the south-east. A closer look shows, that these occur mostly on very steep slopes covered with coniferous forest, where such high values are uncommon. But vast parts of the total area of coniferous forest in the Upper Danube Basin are located on steep relief, and considering the numerous spruce monocultures, or sparse mountain forests, the mean areal soil loss in coniferous forest in the whole catchment of 0.93 t/ha per year (Tab. 6.27) might be in a realistic order of magnitude. Such high soil losses might also contribute to the concentrations of suspended sediment in alpine rivers (cf. Section 3.3), which are much higher than those in the lowlands.

Another distinct pattern of high erosion rates occurs in the low mountain ranges of the Bavarian Forest. Here, high soil losses are observed on arable land, the maxima occurring typically on maize, respectively crop silage areas. Maize is generally vulnerable to erosion, and is sowed in spring, therefore the soil in those areas is not covered by vegetation during periods of high precipitation and runoff in winter. In combination with relatively steep slopes, these results seem to be plausible.

The above mentioned table of mean annual soil losses per land use (Tab. 6.27) features unexpected behaviour of some land use classes, which is explained in the following:

- Set Aside: The soil loss is very low, because set aside does not represent bare fallow. Set aside is parameterised in the biological sub-model as constantly covered with vegetation (like grassland). Since it is distributed mainly on gentle slopes, its soil loss is even lower than on other types of grassland.
- Forage: Forage has extremely high soil losses, because it is harvested and ploughed in autumn, i.e. the bare soil is exposed to the erosive forces of rainfall and runoff during winter and spring.

<sup>2</sup>Consider e.g. 2 proxels, each with 50% hop cultivation and 50% grassland versus 2 proxels, one with 100% hops and the other with 100% grassland. The first case would lead to equal soil losses on each proxel, whereas the latter case would produce very high soil loss rates on the hop area and very low values on the grassland. Altogether the areal mean of both cases would be the same, but the resulting spatial distribution of the first case would be smooth, whereas the second would be "speckled".

Tab. 6.27: Mean long-term (1961 – 2005) annual soil loss per land use, relative to the respective areal extent.

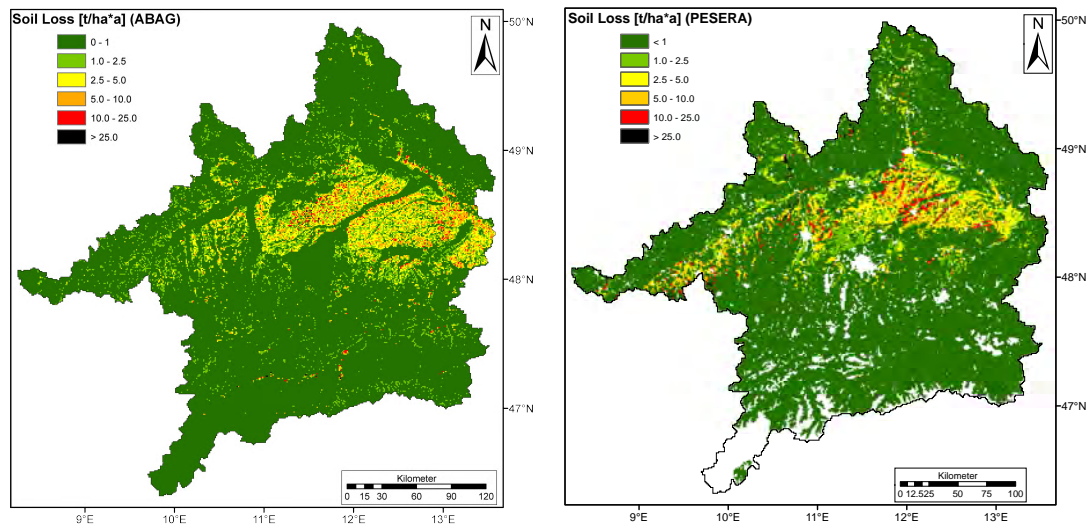
Land use	Soil loss [t/ha]	Land use	Soil loss [t/ha]
Hop	56.42	Summer Wheat	6.83
Silage	25.48	Sugar Beet	4.89
Oat	24.63	Rock	0.98
Forage	19.07	Coniferous Forest	0.93
Summer Barley	18.85	Alpine Vegetation	0.73
Maize	17.49	Deciduous Forest	0.25
Winter Wheat	14.85	Grassland Intensive	0.23
Winter Barley	13.25	Grassland Extensive	0.21
Legumes	12.32	Natural Grassland	0.18
Oleaginous	11.78	Set Aside	0.01
Rye	7.96	Wetland	0.00
Potato	7.72		

- Wetland: Wetland cannot (technically) produce any soil loss, as its parameterisation has no mineral soil, but only organic material.
- Alpine Vegetation: Like coniferous forest, alpine vegetation is found mainly on steep slopes, which increases soil loss rates. Additionally, it is regarded in the parameterisation (of the erosion module) as a kind of pasture.
- Silage and Maize: These technically represent the same cultivation, aside from minor differences. The difference in soil loss here results from the fact, that silage is cultivated on steeper slopes than maize.
- Oat and Summer Barley: Soil losses from both cultivations are very high, due to their sowing in spring, which leaves the field uncovered during winter. More knowledge about cover crops, crop residue or tillage practices could attenuate these high erosion rates.

#### 6.2.3.5. COMPARISON TO VARIOUS OTHER SOURCES

For comparison of the results from this study to the findings of other studies, various sources are available:

- The ABAG: With the data and equations presented in Section 3.2 soil loss is estimated based on the Universal Soil Loss Equation.
- The Pan-European Soil Erosion Risk Assessment (PESERA) project: PESERA (KIRKBY ET AL., 2004, 2008) is a process-based spatially distributed erosion model to quantify soil erosion by water and assess its risk across Europe. It is intended to replace existing models, such as the USLE, which are less suitable for European conditions (PESERA, 2009).
- The atlas of erosion risk in Bavaria: AUERSWALD & SCHMIDT (1986) computed maps of soil erosion for Bavaria based on the ABAG. (Since data from this source is only available based on districts, the results from the other studies are aggregated to districts, too).



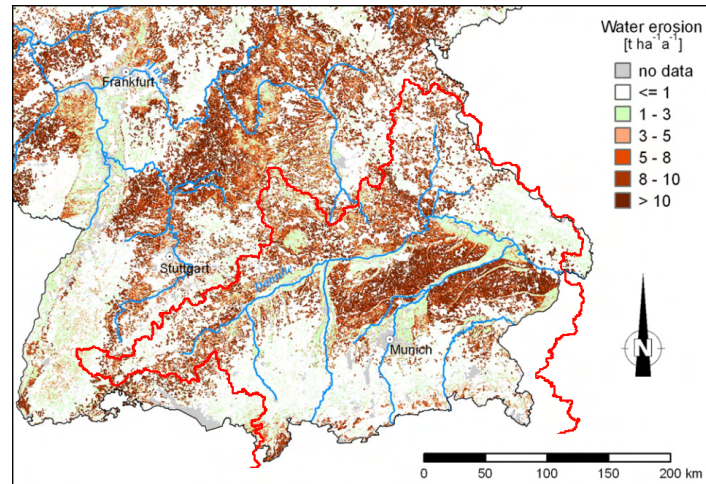
(a) Calculated with the ABAG, as described in Section 3.2  
 (b) Data from the PESERA project, available at (PESERA, 2009)

Fig. 6.32: Mean annual soil loss in the Upper Danube Basin (ABAG, PESERA).

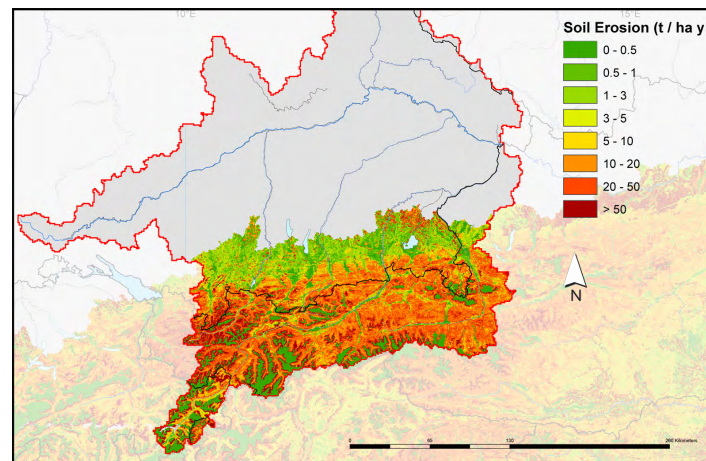
- AUERSWALD ET AL. (2009) compiled data from 27 studies covering 1076 plot years. They used modelling for a correction of different experimental settings and thus generated a soil erosion map of Germany, based on standardised soil erosion measurements.
- The Climate Change, Impacts and Adaptation Strategies in the Alpine Space (ClimChAlp) project (CLIMCHALP, 2009a): This project aims at developing “concrete transnational strategies and first measures how to react on the impacts of Climate Change in respect of spatial planning and risk prevention in the entire Alpine Space” (CLIMCHALP, 2009b). Soil erosion maps were calculated with the RUSLE.

Fig. 6.32 illustrates the computed soil loss values from the ABAG and PESERA, which are available numerically with a resolution of  $1 \text{ km}^2$  for the Upper Danube Basin. For the computations of AUERSWALD ET AL. (2009) and the ClimChAlp project only information partially covering the Upper Danube Basin is available, represented in Fig. 6.33. Generally all images show similar spatial patterns of soil losses, which also closely resemble those of the erosion module (Fig. 6.31). The regions featuring the most obvious patterns produced by the different methods shall be addressed briefly in the following:

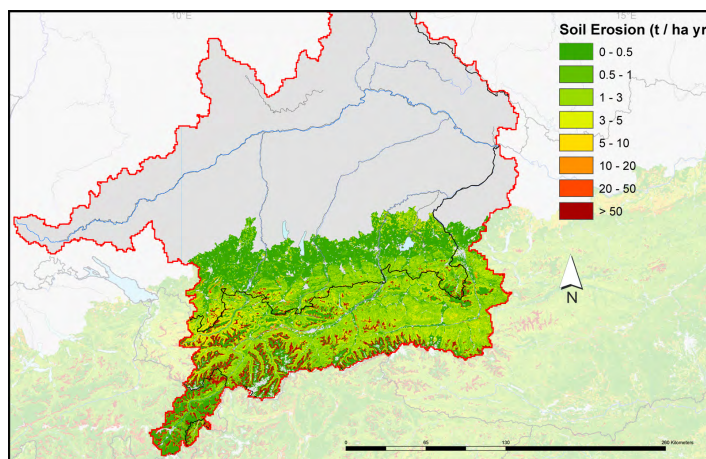
- The central regions of the *Gäuboden*, *Hallertau* and *Tertiärhügelland*: All of the presented methods clearly recognise the potential of soil erosion for these regions, which are particularly vulnerable to soil erosion due to the silty soils.
- The low mountain ranges in the north of the catchment around the Upper Palatinate Forest, down to the Bavarian Forest: All methods show an above-average erosion risk, the ABAG varies to soil losses which are relatively lower, whereas the erosion module delivers higher values.
- The Alps and the forelands: The two maps from the ClimChAlp project clearly show an increased erosion risk towards the south with steeper relief. The relative soil losses



(a) Soil erosion map for Germany based on standardised erosion measurements of different land use categories (modified after AUER-SWALD ET AL. (2009))



(b) ClimChAlp (R-factor calculated after ARNOLDUS (1980); illustration modified after CLIMCHALP (2009b))



(c) ClimChAlp (R-factor calculated after LO ET AL. (1985); illustration modified after CLIMCHALP (2009b))

Fig. 6.33: Maps of mean annual soil loss for regions overlapping the Upper Danube Basin.

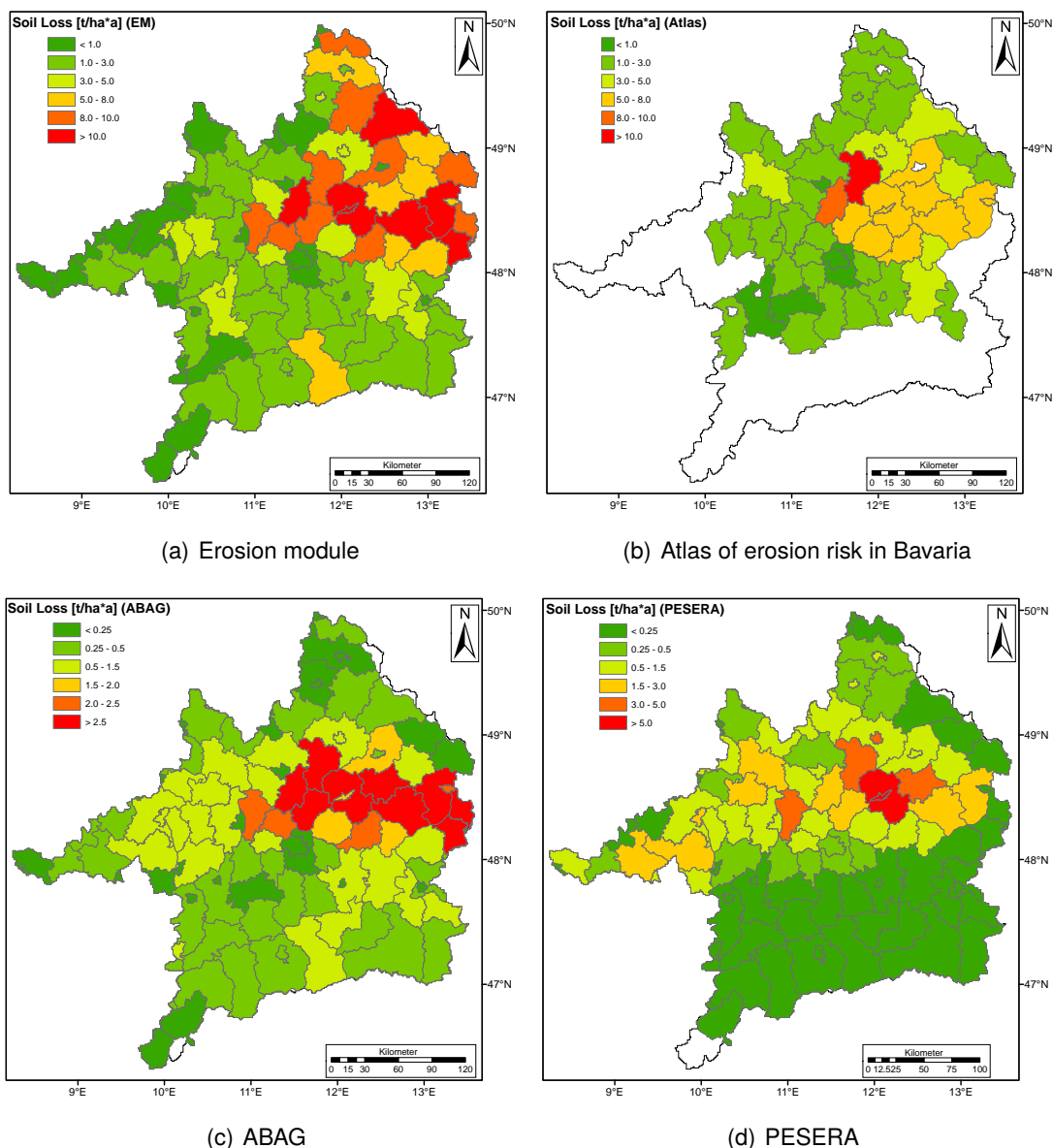


Fig. 6.34: Mean annual soil loss [t/ha] per district in the Upper Danube Basin.

amount up to the same values, as in the agriculturally intensively used areas of the *Tertiärhügelland*. Patterns, which are similar in relative magnitude can be found in the map produced by the erosion module.

In order to suppress the speckled patterns of the original resolution used for computation in the different approaches, the soil losses have been averaged to the area of the administrative districts in the catchment (see Fig. 6.34; for numerical values see Tab. D4). Comparing Fig. 6.34(a) to the other images, it seems that erosion might be overestimated by the erosion module in the north-eastern part of the catchment. These high values appear in the region of gneiss and granite rock only, where soils are classified as “soils on crystalline rock” (cf. Fig. 2.6 and Fig. 3.6). These shortcomings are expected to be caused by the parameterisation for this soil, which leads to an overestimation of surface runoff. (A preliminary appraisal of these potential deficiencies can be found in appendix E).

Tab. 6.28: Mean annual soil losses calculated by different approaches.

Source	Region	Mean annual soil loss [t/ha]
PESERA	Upper Danube Basin	0.79
ABAG	Upper Danube Basin	0.85
AUERSWALD & SCHMIDT (1986)	Bavaria	2.2
AUERSWALD ET AL. (2009)	Germany	2.7
Erosion module (1961 – 2005)	Upper Danube Basin	4.14

Tab. 6.28 lists mean annual soil losses averaged over different reference areas, calculated by some of the different approaches mentioned above.

The estimates from the PESERA project and from the ABAG are somewhat lower, than those from AUERSWALD & SCHMIDT (1986) and AUERSWALD ET AL. (2009). The most likely reason for this is the different reference area used for averaging soil losses. The Upper Danube Basin includes large parts of the Alps, which are underestimated by ABAG. For parameterisation of the ABAG the values of the C-factor are assumed to be too low. Grasslands and forests were parameterised with low values, and land covered by rock was even set to zero, which means, that there never occurs any erosion, which is very unlikely (e.g. AUERSWALD & SCHMIDT (1986) state, that denudation processes in the Alpine areas may exceed annual amounts of 2 t/ha, and BEHRENDT ET AL. (1999) assume a mean annual erosion rate of 2 t/ha for natural areas). By averaging over the whole Upper Danube Basin, these underestimations lower the areal mean value. Even though the parameterisation of the Alpine areas in the PESERA project is unknown to the author, it might be possible, that erosion is somewhat underestimated, as the Alps exhibit very low soil losses (cf. Fig. 6.32(b) and Fig. 6.34(d)).

The estimates of AUERSWALD & SCHMIDT (1986) for Bavaria are higher than the latter two, probably mainly because of the areal averaging over Bavaria, where large areas are used agriculturally, and the Alps are not included in the calculation. This might also be the reason for the again higher mean value calculated by AUERSWALD ET AL. (2009) for whole Germany, especially the inclusion of the highly erodible soils of Saxony.

The highest mean annual soil losses of 4.14 t/ha are computed by the erosion module for the Upper Danube Basin. Since all of the presented studies have their shortcomings in certain aspects (see below), it is difficult to evaluate the correctness of the results. Therefore, here merely an appraisal of the results from the erosion module can be conducted. It is most likely, that the computed soil loss is too high. Comparing the spatial patterns to those from the other studies, this results from the somewhat higher soil losses in the Alpine regions, which nevertheless are not considered to be implausible. Furthermore the high soil losses in the north-east of the catchment increase the areal mean value. These are likely to be overestimated due to a deficient soil parameterisation (as stated above, cf. also appendix E). The observation of the temporal patterns of soil loss in Section 6.2.3.3 leads to the conclusion, that soil loss is overestimated at the period of harvest. This may be addressed to an wrong computation of the exact harvest dates, but also to incorrect assumptions about crop residue after harvest. Altogether it seems obvious, that the computed value of soil erosion of 4.14 t/ha is overestimated, but further improvements in the parameterisation may overcome this problem.



In summary, it is difficult to evaluate which approach delivers the best results. The spatial patterns of soil loss of all approaches resemble, but the absolute amounts of soil loss differ. The lowest and highest soil loss values presented in Tab. 6.28 differ by a factor of approx. 5. As stated above, the lower values are probably underestimations, whereas the higher values seem to be overestimations. It is beyond the scope of this study, to assess the quality of the different approaches, thus the reader is referred to the original works mentioned above, to get an impression of those. Each work focuses on different objectives, and therefore has to accept drawbacks to a certain extent. For instance, AUERSWALD & SCHMIDT (1986) did not consider the influence of snow melt in their study, but (conservatively) estimate an increase in soil loss on agricultural areas by about 10% – 15 %. Other studies (e.g. BEHRENDT ET AL. (1999)) even neglect modelling mountainous areas and assume a constant soil loss there. Furthermore the applied methodology strongly influences the results, as e.g. in the ClimChAlp project, where the two different equations for computation of the R-factor produce results differing in magnitude by a factor of approx. 10 (cf. Fig. 6.33(b) and Fig. 6.33(c)). Even soil loss measurements on plots are to be viewed critically. In order to provide the reader a basis for critical appraisal of the results of this study, and to put these into perspective to other studies, Section 7.2 gives a review on (general) difficulties encountered in erosion modelling.





## 7. SUMMARY

### 7.1. ACHIEVEMENTS

In the course of this study, a soil erosion module for the land surface model PROMET was developed, which provides a basis for the assessment of environmental impacts of soil erosion by water resulting from Global Change conditions. It could be demonstrated, that the model is able to react on the relevant processes controlling soil erosion, and may simulate the soil loss over a sufficiently long period (1961 – 2005). The following requirements, postulated in Section 1.2, could be fulfilled:

- (a) Responsiveness on changing environmental conditions, as well as anthropogenic interventions: The evaluation of the erosion module in Section 6.2 has shown, that natural processes, which are likely to be altered by changing climate, could be represented adequately. Different arable land uses strongly influence the model results, and the model showed distinct reactions on anthropogenic measures, such as harvest dates and execution of ploughing. This means that assumptions about adaptation and/or mitigation strategies in future scenarios concerning such measures can be assessed, as well as reactions on changed natural drivers. Since the model structure does not rely on calibration, but on reasonable parameterisation, the model can be considered to react in a meaningful way on changing conditions.
- (b) Reliable process representation: The involved processes acting on the scale of DANUBIA have been identified and represented in the erosion module in an physically-based form. They interact in a plausible way and exchange, respectively receive input parameters from other sub-components within PROMET. The exchange of parameters relies on physical base units. Plausible reactions of the erosion module on changed input parameters have been observed.
- (c) Adequate process scaling: The soil erosion module was successfully applied to the Upper Danube Basin with a spatial resolution of 1 km<sup>2</sup> and a temporal resolution of 1 hour. The modifications made to the original erosion model, allowed for correct process representation at a scale, which the original model was not designed for. Computational efficiency and adequate complexity of parameterisation could also be reached.
- (d) Extensibility: The soil erosion module does not rely on spatially or temporally lumped parameters. Process descriptions are interchangeable, respectively some of these used in the original model already have been exchanged in this work successfully. New processes may easily be integrated into the module (see Section 7.3). The calculated soil losses and the distribution of the transported grain size classes are passed on a proxel-to-proxel basis to other sub-components of PROMET, respectively DANUBIA.

The achievements of this work allow for modelling of soil erosion by water on a temporal and spatial scale, which up to now (to the author's knowledge) has not yet been represented in a

physically-based way. The soil erosion module is able to simulate soil losses in a geographically very heterogeneous catchment on the regional scale.

The soil erosion module per se is considered a capable, powerful tool for assessing Global Change impacts on soil erosion, because the processes involved are represented correctly. The explicit process descriptions invoke direct, distinct reactions on the model inputs. Thus the validation of the model showed strong dependencies of the quality of the results on external sub-components and to the parameterisation used. Since a variety of processes is involved in erosion, every deficient input variable from an external sub-component directly passes its deviations to the erosion model. Since some of these inputs lead to a somewhat incorrect reproduction of the temporal and spatial patterns of soil erosion, it does not seem to be reliable to simulate a Climate Change scenario within this work and interpret the potential implications for the future development of soil erosion. A brief discussion of the shortcomings of the parameterisation and of external inputs is presented in Section 6.2 and potential improvements are addressed in Section 7.3.

However, these shortcomings clarify the advantages of process-oriented modelling, because thereby the main factors and processes influencing the spatiotemporal patterns of erosion could be revealed. Incorrect parameterisation of the model leads to distortions of these patterns and reveals the most important factors, which influence or control erosion. The knowledge about the impact of these factors may be used to identify potential future adaptation and mitigation strategies.

The next section presents a critical review of the achievements gained in this study, and addresses some problems encountered during the development of this work. This review is followed by an outlook, which depicts potential future applications and interesting questions, which the soil erosion module might answer.

## **7.2. CRITICAL REVIEW**

“Modellers tend to emphasize the successful part of the simulation only, while much more can be learned from difficulties encountered” (JETTEN ET AL., 1999). Therefore this section is intended to depict some general problems and difficulties, which are encountered in erosion modelling. Some of these are commonly known aspects, but some of them have been experienced gradually in a learning process during the integration of the erosion module into the framework of GLOWA-Danube. These experiences shall be addressed here too, and thus can also be perceived as the “lessons learned” during the development of this work. They hopefully provide some helpful information for future studies working on similar areas of interest. As erosion models frequently are used in a context, which they have not been designed for, this section also addresses the limitations of the erosion module and reviews the assumptions and results of this work critically.

As all erosion models rely on erosion measurements, either for model development, or for model calibration, the quality of the measurements has to be viewed critically. STROOSNIJDER (2005) summarises a variety of methods suitable for measurement of erosion. He points out, that different aims and areas of interest require different scales to be assessed, and therefore different measurement techniques. A lack of standardised methods makes it difficult to compare measured data reliably. Additionally, due to the high temporal and spatial variability

of erosion processes, a bias may be induced in erosion measurements, as their temporal duration and spatial coverage often are limited. So for extrapolation of measurements in space and time, erosion models are needed, which in turn depend on measurements. AUERSWALD ET AL. (2009) report on two comparable studies measuring soil loss on vineyards in Germany: whilst EMDE (1992) found a mean annual soil loss of 151 t/ha, averaged over 10 plot years<sup>1</sup>, RICHTER (1991) measured only 0.2 t/ha over 144 plot years. The differences can be explained by a large erosion event, which occurred in the study of EMDE (1992), whereas such an event was completely missing in the much larger data set of RICHTER (1991).

An indirect method for assessment of soil erosion is the comparison to suspended sediment load in rivers (cf. Section 3.3 and Section 6.2.3). The term “indirect” is used here, since the suspended sediment load cannot be compared to modelled soil erosion directly, as processes like sediment trapping in the watershed have to be considered. As already attributed in Section 6.2.3.1, for the evaluation of the results in this study, it was intentionally avoided to convert soil loss to absolute, suspended sediment loads. Instead a qualitative comparison based on relative measures was preferred. The reason for this is, that the sediment delivery ratio (SDR), which is usually used for mentioned conversion to suspended sediment load, has to be calibrated to the test site observed. Even though SDRs are readily available in literature sources, these cannot be used for an arbitrary erosion model, as they have been calibrated to the model, with which they have been developed. As the SDR is calibrated to the erosion model, it is theoretically also possible, that even if the erosion model does not compute correct soil losses, the modelled SSY fits the measured data at the gauge. BEHRENDT ET AL. (1999) experienced this problem, when they computed the SSY from soil losses calculated with the ABAG. They used an empirical relationship for the SDR found by AUERSWALD (1992) for Bavarian river systems. The application in the northeast of Germany showed that, if a threshold for soil loss was undercut, the equation calculated values for SSYs even greater than the input soil loss. Therefore BEHRENDT ET AL. (1999) question the usual approach used for determining the SDR (as e.g. by AUERSWALD (1992)), as it only relates calculated soil loss to total suspended sediment load. But in fact, the transported sediment consists of a considerable amount of autochthonous material, which means, that deriving such a relationship overestimates the sediment yield due to soil erosion. BEHRENDT ET AL. (1999) derived a new, spatially transferable empirical relationship, but as it also was fitted to soil losses of the ABAG, it did not seem to be reasonable to use the equation in conjunction with the erosion module developed in this study.

Nevertheless, physically-based models, which claim to be independent of such an empirical correction procedure as described in the previous paragraph, also have their disadvantages, when applied in a new setting. JETTEN ET AL. (1999) compared the performance of 11 soil erosion models (most of these physically-based or process-oriented) on 10 storm events in the same catchment. They concluded, that “the test results of the field scale and catchment scale models are not very encouraging”. They designate one of the problems causing these weak results as a “hidden calibration”. Great effort goes into the construction of the input data sets, i.e. variables have to be derived from the “raw” data sets. This way, the constructed input data sets are calibrated for the model. In the mentioned study, for each model at least one model variable was adjusted in order to reflect the hydrograph of the training set. Some

---

<sup>1</sup>A plot year designates data representative for one year of measurement on a specific plot of land.

models even had to be calibrated for each event analysed (including the test set). This renders many models unusable for Global Change studies, as future conditions are not available for calibration. The problems of model calibration also have been encountered within this study, but nevertheless it was attempted to rather parameterise the model, instead of “tuning” it by adjusting one or more variables until the model output fits the measured data. The most useful advice of JETTEN ET AL. (1999) was the following guideline for parameterisation: “Visual calibration by means of comparing observed and simulated runoff and erosion/sedimentation patterns is very valuable and should be done more often. Modellers are too much focused on the water and sediment leaving the study area”. During parameterisation, this led to the development of most of the model modifications presented in Section 4.5. A calibration to correct the output data might have been possible in some cases, but the identification of important processes and the inclusion of these additional process descriptions significantly improved the temporal patterns of soil loss. In this way, for example the soil loss in winter could not be represented adequately prior to considering the FT-cycles. Similar features could also be observed in the agricultural management routines, which obviously have deficits in modelling the correct harvest dates, which led to overestimation of soil loss in late summer and autumn.

So, if conclusions regarding Global Change shall be made, above mentioned processes are essential features, which neither may be neglected nor should be represented in a lumped parameter, as e.g. the P-factor or the C-factor of the USLE. This was for example recognised by RENARD ET AL. (1996), who split up the individual factors of the USLE into sub-factors taking into account various involved processes. Starting as a simplistic equation for estimation of mean soil loss, the USLE (respectively its derivatives) developed to a complex, process-oriented (although empirical) model. Increasing demand for the assessment of Climate Change scenarios led to the derivation of future rainfall erosivities (i.e. R-factors), which is a labour-intensive task. A common proceeding is the calculation of the Fournier index (e.g. SAUERBORN ET AL., 1999; NEARING ET AL., 2004; CLIMCHALP, 2009b), which for example was also used by SAUERBORN ET AL. (1999). They summarised the “combination of well established methods” as “applicable for the prediction of future climatic developments”, but also correctly identified the need for an adaptation of the soil and plant factors, as these are influenced by Climate Change conditions, too. Such an adaptation requires further expert knowledge and/or empirical data to derive the factors for altered conditions. Summarising this paragraph, one has to keep in mind, that using lumped factors in empirical models requires correct interpretation and adaptation, as processes are not modelled explicitly, but are included implicitly in the factors. Furthermore some processes are not incorporated at all, such as the influence of snow melt in the USLE. It is up to the modeller to decide, whether such processes are relevant in the case study, and should be considered, or whether they can be neglected.

“Due to their high data demand and the chronic lack of good data erosion prediction models often use input data which are estimated or derived from (empirical) pedotransfer functions. Hence, although many erosion models are classified as deterministic they may be called empirical as well” (STROOSNIJDER, 2005). It is surely true, that deterministic or physically-based erosion models utilise empirical equations for the description of some processes they model (cf. e.g. Eq. (4.10), or Eq. (4.15) in Section 4.5.1.1), or for derivation

of variables (cf. e.g. Section 4.2.3). Anyhow, due to the physical process representation, these models allow for the replacement of such equations, if e.g. better descriptions are found by research. Such changes very likely would influence the results, but it can be expected, that these will improve. As already mentioned above, similar experiences have been made in this study, by learning from the model. The inclusion of additional process descriptions led to improvements in the modelling results. Reflections about unexpected behaviour of the model in certain circumstances helped to understand the relevance and interdependencies of diverse processes, such as particle detachment by drip-off counteracting the protection of soil by canopy cover.

These mentioned replacements inherently ask for a critical review of the assumptions made, and potential limitations arising from these.

A crucial point in erosion modelling is the fact, that erosion is strongly influenced by lateral flows. This involves a strong dependence on the spatial and temporal scale used in modelling, and the processes, which reasonably can or must be represented on these scales. The scales used in this work are relatively coarse for a physically-based soil erosion model, therefore it is not to be taken for granted, that scaling successfully works. Since the processes considered during development of EROSION 2D act on a much finer scale, the scaling in this study could only be achieved by representing these in a different way. In this regard, the introduction of the flow concentration factor is the most important modification to the original model. It adjusts the routing of surface runoff, which is accumulated in the original model over each internal computation unit of 1 m per 10 min, i.e. on a much finer scale. Without such a correction, the momentum flux of the runoff would be way too low, but yet the implementation is physically consistent. Interestingly, the testing of the model EROSION 3D (VON WERNER (1995), cf. Section 4.5.2.1) at various spatial scales led to an optimum spatial resolution (depending on the test site) for operating the model, whereupon higher or lower resolutions over- or underrated the calculated soil loss, due to the concentration of runoff within flow paths. Obviously, the flow concentration factor overcomes this problem reasonably well. Nevertheless, it has to be noted that by modelling on a higher spatial resolution, the usage of this factor will be insufficient since the process of deposition then becomes most important. This also applies to the treatment of sediment transport, which currently assumes, that every proxel is drawn through by a drainage channel, which discharges the detached particles to the channel network. For the scale applied in this study, this is absolutely plausible, since VON WERNER (1995) already addressed the sediment discharge via drainage channels on a much smaller scale (cf. Section 4.5.2.1). Anyway, in summary this means that the model in its current state is limited its current spatial scale. It would require further adaptation, should the scale of application be changed in other studies.

Another assumption to be reviewed, is the substitution of the erosion resistance with the critical shear stress, in particular the dimensioning of the critical shear stress to the erosion resistance with the factor of 0.0005 (cf. Section 5.2.1). This factor has neither been validated with, nor was derived from measured data. However, since the resulting computed values range in the same order of magnitude as the values presented by SCHMIDT ET AL. (1996), both should be interchangeable. Moreover, as already noted in Section 4.5.5, in some studies the erosion resistance seems to be misused as a calibration parameter. If this is true, it would be better to substitute it by a dependent variable (such as the shear strength, which is dependent

of matric suction), instead of fitting it. Furthermore, sensitivity analysis has shown that the sensitivity parameter  $S$  of the erosion resistance and the critical shear stress both constitute about the same range. Thus one may expect, that the influences of substituting the erosion resistance on the modelling results are not implausible or unrealistic.

### 7.3. OUTLOOK

This section discusses potential future applications of the soil erosion module. Even though the objectives of this study are successfully fulfilled, some aspects have to be pointed out, which are relevant for future operation of the model.

An important preliminary achievement for the modelling of soil erosion on the scale applied within this study was the temporal disaggregation of precipitation. It has to be emphasised here, that without using the disaggregation, rainfall intensities are modelled way too low (cf. Section 6.1.2), and rarely induce any particle detachment (cf. Section 6.2.2.2). The main reason for this is the attenuation of hourly rainfall intensities by the advective-convective disaggregation, which leads to reduced momentum fluxes. Moreover, it has to be considered, that mathematical abstractions of processes inherently incorporate simplifications on the temporal scale of these processes. Such simplifications are necessary since the processes cannot be modelled on an infinitesimal time step. So each process must be described on a temporal scale adequate for a physically consistent representation of the respective process. This way, for example, the soil heat transfer modelled within the soil component of PROMET is overclocked, in order to avoid heat oscillations which would result from the geometrical setup of the soil layers in conjunction with a time step of one hour MURTH (2008). MAUSER & BACH (2009) proved, that the temporal resolution of the components interacting in PROMET delivers sound results, i.e. the model has an appropriate design within the temporal (and spatial) scales applied in DANUBIA. This means, that the disaggregation of precipitation, as presented in this study, is applicable. Nevertheless, comparing the different available disaggregation approaches, the non-linear interaction of the sub-components of PROMET may lead to somewhat different results regarding the (surface) runoff behaviour. Therefore, a future investigation should assess the influences of temporal disaggregation techniques on the water cycle, since not only runoff formation is affected, but also evapotranspiration, due to the temporal redistribution of rainfall volumes (i.e. less wet intervals).

Likewise concerning precipitation, it should be a topic of future works to evaluate the representation of precipitation intensity within climate change scenarios. The latter may either be computed by RCMs, or can be compiled by a synthetic climate generator. Since precipitation intensity is a variable which strongly influences erosion, it has to be verified whether these methods are suitable for this purpose. A first step, prior to simulating Climate Change scenarios, should be an evaluation of the capability to reproduce statistics of historical rainfall intensities with the mentioned two resources.

As noted in Section 7.1, it was intentionally avoided in this study to simulate Climate Change scenarios, due to the deficient quality of some input variables for the erosion module. The main determining parameters are surface runoff formation (soil sub-component), plant development (i.e. dynamic harvest dates from the biological sub-component) and agricultural management practices (agricultural management sub-component). Future work should aim at

improving the parameterisation of these sub-components. Concerning the agricultural management practices, the results of the erosion module should noticeably improve by coupling to the farming component of DANUBIA with its extensive knowledge in this sector (see below). Furthermore, first results of a revised soil parameterisation show improvements of the surface runoff formation in the *Naab* sub-catchment appendix E. In summary, it is highly advisable to rectify these parameterisation issues before modelling Climate Change scenarios, respectively drawing conclusions on potential future impacts without considering these would lack a serious scientific basis.

The model results presented in the evaluation overestimated soil loss due to problems in the correct reproduction of agricultural measures. These shortcomings most likely result from deficient sowing and harvest dates, respectively inaccurate dynamic modelling of harvest dates, and missing information about agricultural management techniques per se, such as tillage practices or crop residue remaining on the field after harvest. Also, information about the adoption of rules in the course of the *cross compliance*<sup>2</sup> was not available. Hence, before analysing future scenarios, the soil erosion module should be coupled to the farming component of DANUBIA. The farming component is modelled as a *DeepActor* (cf. Section 1.1.1) in DANUBIA coupled to the Agro-economic model for agricultural production on regional level (ACRE) (further information on the *DeepActor* concept and ACRE can be found e.g. in BARTHEL ET AL. (2008), respectively HENSELER ET AL. (2009)). In short, this stands for the ability of the farming model to decide on agricultural actions to be executed, depending on the currently prevailing conditions on each proxel. The farming model is able to estimate the impacts of Climate Change and weather variability on the vegetation period of various cultivations, on the crop rotation and on the crop yield, considering a potential temporal shift of agricultural management practices KRIMLY ET AL. (2008). In the context of this study, this essentially means that expert knowledge, incorporated in the farming model, can be queried and used for erosion modelling, which promises a noticeable improvement of the calculated soil loss results. Interesting agro-economic aspects in Global Change scenarios, which influence erosion, can be modelled by reasonable reactions of the farming component on:

- potential future options for action, such as the cross compliance, which might encourage farmers to cultivate cover crops or mulch fields over winter.
- the potential of a longer vegetation period. This could imply e.g. more than one harvest per season, or a shift of cultivations (i.e. dynamic land use changes), depending on the preferences and requirements of the cultivations, and the feasibilities of irrigation.

Such mentioned land use changes are not only interesting on arable land, but also as a general option for action in Global Change scenarios. An interesting investigation in the GLOWA-Danube project is, for instance, the option for action of a clearing of all forests until 2060, in order to reduce evapotranspiration and thus provide more base flow for rivers. As the forest protects the soil very well from erosion, this could be an interesting scenario to simulate. Even if such extreme scenarios probably will never occur, the erosion module can give hints on potential impacts, which might not have been considered during definition of an option for action.

---

<sup>2</sup>Since the 1980s, the *cross compliance* (cf. GROSSCOMPLIANCE, 2009; STMELF, 2009) defines European guidelines for soil conservation in agriculture.

As already mentioned in Section 1.1.2, since the implementation of the EU Water Framework Directive (WFD), the interest for assessment of water quality has grown. Since the erosion module simulates soil loss differentiated by grain size classes, and phosphorus (P) transport into water bodies occurs bound to clay particles, the module is capable of modelling this process. The farming component of DANUBIA dynamically applies P-fertilisation to the fields according to the need of the plants. These applications can be used to simulate the particulate phosphorus (PP) transport into aquatic ecosystems via the channel flow component. Further extensions in the channel flow component may simulate the transport through rivers and sedimentation in lakes or hydraulic structures, and thus allow the assessment of water quality regarding the WFD.

Analyses of scenario results within the project GLOWA-Danube indicate drier conditions in summer in the future, therefore current efforts in the development of PROMET deal with a module for the simulation of forest fires. Forest fires represent intense interferences in the water cycle, and also heavily affect soil erosion. Increased erosion rates are caused mainly by an increase of runoff rates due to the burnt vegetation cover, but also by changes in soil properties, mostly water repellency (INBAR ET AL., 1998). Since the most important processes, which result from forest fires, are already considered in the erosion module, it should be possible to assess the impacts without implementing further extensions in the erosion module.

The still existing problem of modelling (soil erosion) on different (spatial) scales was repeatedly addressed in the course of this work. One of the conclusions of this work is, that the processes relevant for soil erosion were adequately scaled to the temporal and spatial resolution of DANUBIA. The implementation of the erosion module is capable of subscale modelling, as well as modelling on (theoretically) arbitrary spatial resolutions. Thus, a direct comparison of model results of different spatial resolutions and results of subscale model runs may give information on the scalability and the relative influence of the processes on different scales.



## BIBLIOGRAPHY

- AD-HOC-AG BODEN (2005). *Bodenkundliche Kartieranleitung*. 5 edn. Bundesanstalt für Geowissenschaften und Rohstoffe, 438 pp.
- ARNOLDUS, H.M.J. (1980). An approximation of the rainfall factor in the Universal Soil Loss Equation. In: M. DE BOODT & D. GABRIELS (Eds.) *Assessment of erosion*. John Wiley & Sons, Chichester, pp. 127 – 132.
- AUERSWALD, K. (1992). Predicted and measured sediment loads of large watersheds in bavaria. In: *5th International Symposium on River Sedimentation*. Karlsruhe.
- AUERSWALD, K. (1993). *Bodeneigenschaften und Bodenerosion. Wirkungswege bei unterschiedlichen Betrachtungsmaßstäben*. Gebrüder Borntraeger, Berlin, Stuttgart.
- AUERSWALD, K., FIENER, P., & DIKAU, R. (2009). Rates of sheet and rill erosion in Germany – A meta-analysis. *Geomorphology*, 111, pp. 182 – 193.
- AUERSWALD, K. & SCHMIDT, F. (1986). Atlas der Erosionsgefährdung in Bayern. Karten zum flächenhaften Bodenabtrag durch Regen. GLA-Fachbericht 1, Bayerisches Geologisches Landesamt, München.
- BALDOCCHI, D.D., HICKS, B.B., & CAMARA, P. (1987). A canopy stomatal resistance model for gaseous deposition to vegetated surfaces. *Atmospheric Environment*, 21(1), pp. 91 – 101.
- BARTH, M., HENNICKER, R., KRAUS, A., & LUDWIG, M. (2004). DANUBIA: An Integrative Simulation System for Global Change Research in the Upper Danube Basin. *Cybernetics and Systems*, 35(7 – 8), pp. 639 – 666.
- BARTHEL, R., BRAUN, J., ROJANSCHI, V., & WOLF, J. (2006). Hydrogeologie. In: GLOWA-DANUBE-PROJEKT (Ed.) *Global Change Atlas, Einzugsgebiet Obere Donau*, 1 edn., chap. 1.5. Universität München (LMU), Dept. für Geo- und Umweltwissenschaften. ISBN: 978-3-00-026548-8.
- BARTHEL, R., JANISCH, S., SCHWARZ, N., TRIFKOVIC, A., NICKEL, D., SCHULZ, C., & MAUSER, W. (2008). An integrated modelling framework for simulating regional-scale actor responses to global change in the water domain. *Environmental Modelling and Software*, 23, pp. 1095 – 1121.
- BARTHEL, R., ROJANSCHI, V., WOLF, J., & BRAUN, J. (2005). Large-scale water resources management within the framework of GLOWA-Danube. Part A: The groundwater model. *Physics and Chemistry of the Earth*, 30(6-7), pp. 372–382.
- BAUMGARTNER, A. & LIEBSCHER, H.J. (1996). *Allgemeine Hydrologie Quantitative Hydrologie*, vol. 1 of *Lehrbuch der Hydrologie*. Gebrüder Borntraeger, Berlin Stuttgart.

- BAYFORKLIM (Ed.) (1996). *Klimaatlas von Bayern*. Bayerischer Klimaforschungsverbund, München.
- BECKER, A. & LAHMER, W. (Eds.) (2004). *Wasser- und Nährstoffhaushalt im Elbegebiet und Möglichkeiten zur Stoffeintragsminderung*, vol. 1 of *Konzepte für die nachhaltige Entwicklung einer Flusslandschaft*. Weißensee Verlag, Berlin.
- BEHRENDT, H., HUBER, P., OPITZ, D., SCHMOLL, O., SCHOLZ, G., & UEBE, R. (1999). Nährstoffbilanzierung der Flussgebiete Deutschlands. p. 288.
- BEHRENDT, H., VENOHR, M., HIRT, U., HOFMANN, J., OPITZ, D., & GERICKE, A. (2007). *The model system MONERIS Version 2.0 User's Manual*. Leibniz Institute of Freshwater Ecology and Inland Fisheries, Berlin.
- BLA-GEO (2003). Methodenkatalog zur Bewertung natürlicher Bodenfunktionen, der Archivfunktion des Bodens, der Gefahr der Entstehung schädlicher Bodenveränderungen sowie der Nutzungsfunktion "Rohstofflagerstätte" nach BBodSchG. In: A. HOC-AG BODEN DES BUND/LÄNDER-AUSSCHUSSES BODENFORSCHUNG (Ed.) *Arbeitshefte - Boden*, vol. 2. E. Schweizerbart.
- BLUME, H.P. (1990). *Handbuch des Bodenschutzes: Bodenökologie und Bodenbelastung*. ecomed Verlagsgesellschaft mbH, Landsberg/Lech.
- BMU (Ed.) (2001). *Hydrologischer Atlas von Deutschland*. Bundesministerium für Umwelt, Naturschutz und Reaktorsicherheit, Bonn.
- BRANDT, C.J. (1989). The size distribution of throughfall drops under vegetation canopies. *Catena*, 16, pp. 507 – 524.
- BROOKS, R.H. & COREY, A.T. (1964). Hydraulic properties of porous media. *Hydrology Paper*, 3.
- CAMPBELL, G.S. & NORMAN, J.M. (1998). *An Introduction To Environmental Biophysics*. Second edn. Springer New York Berlin Heidelberg.
- CARSON, M.A. (1971). *The mechanics of erosion*. Pion.
- CERDÀ, A. (1997). Rainfall drop size distribution in the Western Mediterranean basin, València, Spain. *Catena*, 30, pp. 169 – 182.
- CHENG, N.S. (1997). A simplified settling velocity formula for sediment particle. *Journal of Hydraulic Engineering*, 123(2), pp. 149 – 152.
- CHRISTENSEN, J.H., HEWITSON, B., BUSUIOC, A., CHEN, A., GAO, X., HELD, I., JONES, R., KOLLI, R.K., KWON, W.T., LAPRISE, R., MAGAÑA RUEDA, V., MEARN, L., MENÉNDEZ, C.G., RÄISÄNEN, J., RINKE, A., SARR, A., & WHETTON, P. (2007). Regional Climate Projections. In: S. SOLOMON, D. QIN, M. MANNING, Z. CHEN, M. MARQUIS, K.B. AVERYT, M. TIGNOR, & H.L. MILLER (Eds.) *Climate Change 2007: The Physical Science Basis. Contribution of Working Group I to the Fourth Assessment Report of the Intergovernmental Panel on Climate Change*, chap. 11. Cambridge University Press, Cambridge.

- CLIMCHALP (2009a). ClimChAlp: Climate Change, Impacts and Adaptation Strategies in the Alpine Space. <http://www.climchalp.org/>. Visited 02.11.2009.
- CLIMCHALP (2009b). ClimChAlp: Climate Change, Impacts and Adaptation Strategies in the Alpine Space. <http://eusoiils.jrc.ec.europa.eu/library/themes/erosion/ClimChalp/>. Visited 30.10.2009.
- COLGAN, A. & WEIDINGER, R. (2006). Klimastationen. In: GLOWA-DANUBE-PROJEKT (Ed.) *Global Change Atlas, Einzugsgebiet Obere Donau*, 1 edn., chap. 1.4. Universität München (LMU), Dept. für Geo- und Umweltwissenschaften. ISBN: 978-3-00-026548-8.
- CONNOLLY, R.D., SCHIRMER, J., & DUNN, P.K. (1998). A daily rainfall disaggregation model. *Agricultural and Forest Meteorology*, 92(2), pp. 105–117.
- COWPERTWAIT, P.S.P. (1991). Further Developments of the Neyman-Scott Clustered Point Process for Modeling Rainfall. *Water Resources Research*, 27(7).
- COWPERTWAIT, P.S.P., O'CONNELL, P.E., METCALFE, A.V., & MAWDSLEY, J.A. (1996a). Stochastic point process modelling of rainfall. I. Single-site fitting and validation. *Journal of Hydrology*, 175(1-4), pp. 17–46.
- COWPERTWAIT, P.S.P., O'CONNELL, P.E., METCALFE, A.V., & MAWDSLEY, J.A. (1996b). Stochastic point process modelling of rainfall. II. Regionalisation and disaggregation. *Journal of Hydrology*, 175(1-4), pp. 47–65.
- CROSSCOMPLIANCE (2009). COUNCIL REGULATION (EC) No 73/2009 of 19 January 2009 establishing common rules for direct support schemes for farmers under the common agricultural policy and establishing certain support schemes for farmers, amending Regulations (EC) No 1290/2005, (EC) No 247/2006, (EC) No 378/2007 and repealing Regulation (EC) No 1782/2003. *Official Journal of the European Union*, 73/2009.
- CUNGE, J.A. (1969). On the subject of a flood propagation method (Muskingum Method). *Journal of Hydraulic Research*, 7(2), pp. 205–230.
- DE BAETS, S., TORRI, D., POESEN, J., SALVADOR, M.P., & MEERSMANS, J. (2008). Modelling increased soil cohesion due to roots with EUROSEM. *Earth Surface Processes and Landforms*, 33, pp. 1948 – 1963.
- DE VENTE, J., POESEN, J., ARABKHEDRI, M., & VERSTRAETEN, G. (2007). The sediment delivery problem revisited. *Progress in Physical Geography*, 31(2), pp. 155 – 178.
- DEINLEIN, R. & BÖHM, A. (2000). *Soil Erosion*, chap. 9. Springer, p. 315.
- DESMET, P.J.J., POESEN, J., GOVERS, G., & VANDAELE, K. (1999). Importance of slope gradient and contributing area for optimal prediction of the initiation and trajectory of ephemeral gullies. *Catena*, 37, pp. 377– 392.
- DESTATIS (Ed.) (2007). *Statistisches Jahrbuch 2007 für die Bundesrepublik Deutschland*. Statistisches Bundesamt, Wiesbaden.

- DIKAU, R. (1986). Experimentelle Untersuchungen zu Oberflächenabfluß und Bodenabtrag von Meßparzellen und landwirtschaftlichen Nutzflächen. In: *Heidelberger Geographische Arbeiten*. Geographisches Institut der Universität Heidelberg.
- DIN19708 (2005). Bodenbeschaffenheit - Ermittlung der Erosionsgefährdung von Böden durch Wasser mit Hilfe der ABAG.
- DUBBER, H.J. (1967). Untersuchungen über den Bodenabtrag auf Tonmergel- und Kalksteinverwitterungsböden der Schwäbischen Alb und ihres Vorlandes. *Zeitschrift für Kulturtechnik und Flurbereinigung*, 8, pp. 85 – 101.
- DVWK (Ed.) (1986). *Schwebstoffmessungen*, vol. 125/1986. DVWK, Paul Parey, Hamburg, Berlin.
- DVWK (Ed.) (1995). *Gefügestabilität ackerbaulich genutzter Minderalböden Teil I: Mechanische Belastbarkeit*, vol. 234/1995. DVWK, DVWK, Bonn.
- DWD (2008). Wetterlexikon. URL <http://www.deutscher-wetterdienst.de/lexikon/download.php?file=Foehn.pdf>. Visited 03.10.2008.
- EAGLESON, P.S. (1978). Climate, soil, and vegetation 3. A simplified model of soil moisture movement in the liquid phase. *Water Resources Research*, 14(5), pp. 722 – 730.
- ECONOPOULY, T.W., DAVIS, D.R., & WOOLHISER, D.A. (1990). Parameter transferability for a daily rainfall disaggregation model. *Journal of Hydrology*, 118, pp. 209–228.
- EMDE, K. (1992). Experimentelle Untersuchungen zu Oberflächenabfluß und Bodenaus-trag in Verbindung mit Starkregen bei verschiedenen Bewirtschaftungssystemen in Weinbergsarealen des oberen Rheingaus. In: *Geisenheimer Berichte*. Gesellschaft zur Förderung der Forschungsanstalt Geisenheim, Geisenheim.
- ERHARD, M., EVERINK, C., JULIUS, C., KREINS, P., SIETZ, D., & MEYER, J. (2002). Bundesweite Betrachtung der Zusammenhänge zwischen Agrarstatistikdaten und aktuellen Daten zur Bodennutzung. Tech. rep., Bundesministerium für Umwelt, Naturschutz und Reaktorsicherheit.
- FAO (Ed.) (2006). *World reference base for soil resources 2006*, no. 103 in World Soil Resources Reports. Food and Agriculture Organization of the United Nations, Rome.
- FAO (2009). Conservation Agriculture. <http://www.fao.org/ag/ca/index.html>. Visited 14.05.2009.
- FARQUHAR, G.D., VON CAEMMERER, S., & BERRY, J.A. (1980). A biochemical model of photosynthetic CO<sub>2</sub> assimilation in leaves of C<sub>3</sub> species. *Planta*, 149, pp. 78–90.
- FAVIS-MORTLOCK, D.T., QUINTON, J.N., & DICKINSON, W.T. (1996). The GCTE validation of soil erosion models for global change studies. *Journal of Soil and Water Conservation*, 51(5), pp. 397 – 403.

- FERRARIS, L., GABELLANI, S., REBORA, N., & PROVENZALE, A. (2003). A comparison of stochastic models for spatial rainfall downscaling. *Water Resources Research*, 39(12), p. 1368.
- FLANAGAN, D.C. & NEARING, M.A. (1995). USDA-Water Erosion Prediction Project (WEPP) Technical Documentation. Tech. rep., USDA.
- FOLLY, A., QUINTON, J.N., & SMITH, R.E. (1999). Evaluation of the EUROSEM model using data from the Catsop watershed, The Netherlands. *Catena*, 37, pp. 507 – 519.
- FOSTER, G.R. (2004). *User's Reference Guide Revised Universal Soil Loss Equation Version 2 RUSLE2*. USDA-ARS, Washington, D.C.
- FREDLUND, D.G., MORGENSTERN, N.R., & WIDGER, R.A. (1978). The shear strength of unsaturated soils. *Canadian Geotechnical Journal*, 15(3), pp. 313 – 321.
- FREDLUND, D.G. & RAHARDJO, H. (1993). An overview of unsaturated soil behaviour. In: *Proceedings of the American Society of Civil Engineers. Specialty Series on Unsaturated Soil Properties*. Dallas, Texas, pp. 1 – 31.
- FREDLUND, D.G., XING, A., FREDLUND, M.D., & BARBOUR, S.L. (1996). The relationship of the unsaturated soil shear strength to the soil-water characteristic curve. *Canadian Geotechnical Journal*, 33, pp. 440 – 448.
- FRÜH, B., SCHIPPER, J.W., PFEIFFER, A., & WIRTH, V. (2006). A pragmatic approach for downscaling precipitation in alpine-scale complex terrain. *Meteorologische Zeitschrift*, 15(6), pp. 631–646.
- FUCHS, S., BUTZ, J., & BECHTEL, A. (2004). Stoffstromanalysen für kleine bis mittlere Flussgebiete als Grundlage für die Planung und Umsetzung von Gewässerschutzmaßnahmen. Forschungsbericht fzka-bwplus, University Karlsruhe.
- GASH, J.H.C. (1979). An analytical model of rainfall interception in forests. *Quarterly Journal of the Royal Meteorological Society*, 105(443), pp. 43 –55.
- GATTO, L.W., HALVORSON, J.J., MCCOOL, D.K., & PALAZZO, A.J. (2002). *Landscape Erosion and Evolution Modeling*, chap. 3. Effects Of Freeze-Thaw Cycling On Soil Erosion. Springer, pp. 29 – 55.
- GERLINGER, K. (1996). Spatial and temporal analysis of the erosion resistance for calibrating a soil erosion model. *Géomorphologie : relief, processus, environnement*, 2(2 – 2), pp. 69 –82.
- GERLINGER, K. (2000). *Soil Erosion*, chap. 2. Springer, p. 315.
- GLA (Ed.) (1996). *Erläuterungen zur Geologischen Karte von Bayern 1:500000*. Bayerisches Geologisches Landesamt, München.
- GLOWA-DANUBE (Ed.) (2007). *GLOWA - Danube Integrative Techniken, Szenarien und Strategien zur Zukunft des Wassersim Einzugsgebiet der Oberen Donau Jahresbericht 2006*. GLOWA-Danube, Universität München (LMU), Dept. für Geo- und Umweltwissenschaften.

- GÜNTNER, A. (2002). Large-scale hydrological modelling in the semi-arid north-east of Brazil. Ph.D. thesis, Mathematisch-Naturwissenschaftliche Fakultät der Universität Potsdam.
- GÜNTNER, A., OLSSON, J., CALVER, A., & GANNON, B. (2001). Cascade-based disaggregation of continuous rainfall time series - the influence of climate. *Hydrology and Earth System Sciences*, 5(2), pp. 145 – 164.
- GORDON, N.D., FINLAYSON, B.L., McMAHON, T.A., & GIPPEL, C.J. (2004). *Stream hydrology: an introduction for ecologists*. John Wiley & Sons.
- GRAY, D.H. & LEISER, A. (1982). *Biotechnical slope protection and erosion control*. Van Nostrand Reinhold, New York.
- GYSSELS, G., POESEN, J., BOCHET, E., & LI, Y. (2005). Impact of plant roots on the resistance of soils to erosion by water: a review. *Progress in Physical Geography*, 29(2), pp. 189 – 217.
- HANK, T. (2008). A Biophysically Based Coupled Model Approach for the Assessment of Canopy Processes under Climate Change Conditions. Ph.D. thesis, Ludwig-Maximilians University, Department of Geography, München.
- HENNINGS, V. (2000). *Methodendokumentation Bodenkunde*. Sonderhefte Reihe G - Geol. Jahrb., Heft 1. E. Schweizerbart.
- HENSELER, M., WIRSIG, A., HERRMANN, S., KRIMLY, T., & DABBERT, S. (2009). Modeling the impact of global change on regional agricultural land use through an activity-based non-linear programming approach. *Agricultural Systems*, 100, pp. 31 – 42.
- HERSHENHORN, J. & WOOLHISER, D.A. (1987). Disaggregation of daily rainfall. *Journal of Hydrology*, 95(3–4), pp. 299–322.
- HINGRAY, B. & BEN HABA, M. (2005). Statistical performances of various deterministic and stochastic models for rainfall series disaggregation. *Atmospheric Research*, 77(1 – 4), pp. 152 – 175.
- HJULSTRÖM, F. (1939). *Recent marine sediments: a symposium*, chap. Transportation of detritus by moving water. American Association of Petroleum Geologists, Tulsa, Oklahoma, pp. 5 – 31.
- HOBBS, P.V. & RANGNO, A.L. (2004). Super-large raindrops. *Geophysical Research Letters*, 31, p. L13102.
- HUDSON, N. (1981). *Soil Conservation*. Batsford Academic and Educational, London.
- ICPDR (Ed.) (2005). *The Danube River Basin District Part A - Basin-wide overview*. International Commission for the Protection of the Danube River, Vienna.
- INBAR, M., TAMIR, M., & WITTENBERG, L. (1998). Runoff and erosion processes after a forest fire in Mount Carmel, a Mediterranean area. *Geomorphology*, 24, pp. 17 – 33.

- IPCC (2007). Summary for Policymakers. In: S. SOLOMON, D. QIN, M. MANNING, Z. CHEN, M. MARQUIS, K.B. AVERYT, M. TIGNOR, & H.L. MILLER (Eds.) *Climate Change 2007: The Physical Science Basis. Contribution of Working Group I to the Fourth Assessment Report of the Intergovernmental Panel on Climate Change: Contribution of Working Group I to the Fourth Assessment Report of the Intergovernmental Panel on Climate Change*. Cambridge University Press, Cambridge.
- JARVIS, P.G. & MORISON, J.I.L. (1981). The control of transpiration and photosynthesis by the stomata. *Stomatal Physiology*, pp. 247 – 279.
- JETTEN, V., DE ROO, A., & FAVIS-MORTLOCK, D. (1999). Evaluation of field-scale and catchment-scale soil erosion models. *Catena*, 37, pp. 521 – 541.
- KAY, B.D. & ANGERS, D.A. (2002). *Soil Physics Companion*, chap. 6. CRC Press, pp. 189 – 295.
- KHALIQ, M.N. & CUNNANE, C. (1996). Modelling point rainfall occurrences with the modified Bartlett-Lewis rectangular pulses model. *Journal of Hydrology*, 180(1 – 4), pp. 109 – 138.
- KINNELL, P.I.A. (1980). Rainfall intensity - kinetic energy relationships for soil loss prediction. *Soil Science Society of America Proceedings*, 45, pp. 153 – 155.
- KINNELL, P.I.A. (2005). Raindrop-impact-induced erosion processes and prediction: a review. *Hydrological Processes*, 19, pp. 2815 – 2844.
- KINSEL, W.G. (1980). *CREAMS: A Field Scale Model for Chemicals, Runoff, and Erosion for Agricultural Management Systems*. USDA.
- KIRKBY, M.J., IRVINE, B.J., JONES, R.J.A., GOVERS, G., BOER, M., CERDAN, O., DAROUSSIN, J., GOBIN, A., GRIMM, M., LE BISSONNAIS, Y., KOSMAS, C., MANTEL, S., PUIGDEFABREGAS, J., & VAN LYNDEN, G. (2008). The PESERA coarse scale erosion model for Europe. I. - Model rationale and implementation. *European Journal of Soil Science*, 59, pp. 1293 – 1306.
- KIRKBY, M.J., JONES, R.J.A., IRVINE, B., GOBIN, A., GOVERS, G., CERDAN, O., VAN ROMPAEY, A.J.J., LE BISSONNAIS, Y., , DAROUSSIN, J., KING, D., MONTANARELLA, L., GRIMM, M., VIEILLEFONT, V., PUIGDEFABREGAS, J., BOER, M., KOSMAS, C., YASSOGLU, N., TSARA, M., MANTEL, S., VAN LYNDEN, G.J., & HUTING, J. (2004). Pan-European Soil Erosion Risk Assessment: The PESERA Map, Version 1 October 2003. Explanation of Special Publication Ispra 2004 No.73 (S.P.I.04.73). Research Report 16, European Soil Bureau, Luxembourg.
- KLISCH, A. (2003). Ableitung von Blattflächenindex und Bedeckungsgrad aus Fernerkundungsdaten für das Erosionsmodell EROSION 3D. Ph.D. thesis, Mathematisch-Naturwissenschaftliche Fakultät der Universität Potsdam. URL <http://opus.kobv.de/ubp/volltexte/2005/104/>.
- KÖPPEN, W., GEIGER, R., MILANKOVITCH, M., CONRAD, V., BORCHARDT, W., WEGENER, K., & WAGNER, A. (1936). *Handbuch der Klimatologie*. Borntraeger.

- KRESSER, W. (1964). Gedanken zur Geschiebe- und Schwebstoffführung der Gewässer. *ÖWW*, 16(1), pp. 6 – 11.
- KRIMLY, T., APFELBECK, J., HUIGEN, M., & DABBERT, S. (2008). Teilprojekt Agrarökonomie - Entscheidungsmodell zur Land- und Wassernutzung landwirtschaftlicher Betriebe - Das Modell DeepFarming. In: GLOWA-DANUBE-PROJEKT (Ed.) *Global Change Atlas, Einzugsgebiet Obere Donau*, 2 edn., chap. 2.9.2. Universität München (LMU), Dept. für Geo- und Umweltwissenschaften. ISBN: 978-3-00-026548-8.
- KURON, H. (1948). Veränderung unserer Ackerböden unter dem Einfluß der Bodenerosion. *Zeitschrift für Pflanzenernährung, Düngung und Bodenkunde*, 41(3), pp. 245 – 258.
- LAL, R. (2005). *Encyclopedia of Soil Science Volume 1*. 2 edn. Marcel Dekker.
- LAWS, J.D. (1941). Measurements of the fall velocity of water drops and raindrops. *Transactions American Geophysical Union*, 22, pp. 709 – 721.
- LAWS, J.D. & PARSONS, D.A. (1943). The relation of raindrop-size to intensity. *Transactions American Geophysical Union*, 24, pp. 452 – 460.
- LE BISSONNAIS, Y. (1996). Aggregate stability and assessment of soil crustability and erodibility: I. Theory and methodology. *European Journal of Soil Science*, 47(4), pp. 425 – 437.
- LEAVESLEY, G.H. (1994). Modelling the effects of climate change on water resources - a review. *Climatic Change*, 28, pp. 159 – 177.
- LEBERT, M. (2008). Herleitung und Darstellung der potenziellen, mechanischen Verdichtungsempfindlichkeit für Unterböden von Ackerflächen der Bundesrepublik Deutschland. Zwischenergebnisse aus dem UBA-Vorhaben: "Entwicklung eines Prüfkonzepes zur Erfassung der tatsächlichen Verdichtungsgefährdung landwirtschaftlich genutzter Böden" FKZ 3707 71 202, Umweltbundesamt.
- LEHRSCHE, G.A., SOJKA, R.E., CARTER, D.L., & JOLLEY, P.M. (1991). Freezing effects on aggregate stability affected by texture, mineralogy, and organic matter. *Soil Science Society of America Journal*, 55(5), pp. 1401 – 1406.
- LFL, B. (2005). Wie stark ist die Bodenerosion auf meinen Feldern?
- LFU (2009). Schwebstoffdaten. [http://www.lfu.bayern.de/wasser/fachinformationen/fließgewaesser\\_schwebstoffmessung/schwebstoffdaten/index.htm](http://www.lfu.bayern.de/wasser/fachinformationen/fließgewaesser_schwebstoffmessung/schwebstoffdaten/index.htm). Visited 29.04.2009.
- LFULG (Ed.) (2005). *Bodendruck und Bodenbelastbarkeit*, vol. 15 of *Schriftenreihe der Sächsischen Landesanstalt für Landwirtschaft*. Sächsisches Landesamt für Umwelt, Landwirtschaft und Geologie.
- LFW (Ed.) (2002). *Deutsches Gewässerkundliches Jahrbuch Donauegebiet 2002*. Bayerisches Landesamt für Wasserwirtschaft, München.
- LFW (Ed.) (2005). *Deutsches Gewässerkundliches Jahrbuch Donauegebiet 2005*. Bayerisches Landesamt für Umwelt, München.



- LIU, G., XU, M., & RITSEMA, C. (2003). A study of soil surface characteristics in a small watershed in the hilly, gullied area on the Chinese Loess Plateau. *Catena*, 54, pp. 31 – 44.
- LO, A., EL-SWAIFY, S.A., DANGLER, E.W., & SHINSHIRO, L. (1985). Effectiveness of EI30 as an erosivity index in Hawaii. In: S.A. EL-SWAIFY, W.C. MOLDENHAUER, & A. LO (Eds.) *Soil Erosion and Conservation*. Soil Conservation Society of America, pp. 384 – 392.
- LÉONARD, J. & RICHARD, G. (2004). Estimation of runoff critical shear stress for soil erosion from soil shear strength. *Catena*, 57, pp. 233 – 249.
- LOW, T.B. & LIST, R. (1982). Collision, coalescence and breakup of raindrops, Part 1: Experimentally established coalescence efficiencies and fragment size distributions in breakup. *Journal of the Atmospheric Sciences*, 39, pp. 1591 – 1606.
- LUDWIG, R., MAUSER, W., NIEMEYER, S., COLGAN, A., STOLZ, R., ESCHER-VETTER, H., KUHN, M., REICHSTEIN, M., TENHUNEN, J., KRAUS, A., LUDWIG, M., BARTH, M., & HENNICKER, R. (2003). Web-based modelling of energy, water and matter fluxes to support decision making in mesoscale catchments - the integrative perspective of GLOWA-Danube. *Physics and Chemistry of the Earth*, 28(14 – 15), pp. 621 – 634.
- LUDWIG, R. & MUERTH, M. (2006). Bodenarten. In: GLOWA-DANUBE-PROJEKT (Ed.) *Global Change Atlas, Einzugsgebiet Obere Donau*, 1 edn., chap. 1.2. Universität München (LMU), Dept. für Geo- und Umweltwissenschaften. ISBN: 978-3-00-026548-8.
- MANDELBROT, B.B. (1974). Intermittent turbulence in self-similar cascades: divergence of high moments and dimension of the carrier. *Journal of Fluid Mechanics*, 62(2).
- MANGELSDORF, J. & SCHEURMANN, K. (1980). *Flußmorphologie*. Oldenbourg.
- MARKE, T. (2008). Development and Application of a Model Interface to couple Land Surface Models with Regional Climate Models for Climate Change Risk Assessment in the Upper Danube Watershed. Ph.D. thesis, Ludwig-Maximilians University, Department of Geography, München.
- MARKE, T. & MAUSER, W. (2008). SCALMET - A tool for bidirectional coupling of climate models with physically-based simulations of land surface processes. In: A. BORSORF, J. STÖTTER, & E. VEULLIET (Eds.) *Managing Alpine Future Proceedings of the Innsbruck Conference October 15 - 17, 2007*. Innsbruck.
- MAUSER, W. (2002). GLOWA-Danube Papers Technical Release No. 3 (MeteoStationsData), Software-Release-No.: 0.9, Documentation Version: 0.9\_01, Release Date: Jan 2002. Tech. rep., GLOWA-Danube Project.
- MAUSER, W. & BACH, H. (2009). PROMET - Large scale distributed hydrological modelling to study the impact of climate change on the water flows of mountain watersheds. *Journal of Hydrology*, 376(3 – 4), pp. 362 – 377.
- MAUSER, W. & MUERTH, M. (2008). The Decision Support System DANUBIA. In: A. BORSORF, J. STÖTTER, & E. VEULLIET (Eds.) *Managing Alpine Future Proceedings of the Innsbruck Conference October 15 - 17, 2007*. Innsbruck.

- MAUSER, W., PRASCH, M., & STRASSER, U. (2006). Physically based Modelling of Climate Change Impact on Snow Cover Dynamics in Alpine Regions using a Stochastic Weather Generator. In: L. OXLEY & D. KULASIRI (Eds.) *MODSIM 2007 International Congress on Modelling and Simulation*. Modelling and Simulation Society of Australia and New Zealand, pp. 2138–2145.
- MAUSER, W. & SCHÄDLICH, S. (1998). Modelling the spatial distribution of evapotranspiration using remote sensing data and PROMET. *Journal of Hydrology*, 212, pp. 250 – 267.
- MERRITT, W.S., LETCHER, R.A., & JAKEMAN, A.J. (2003). A review of erosion and sediment transport models. *Environmental Modelling and Software*, 18, pp. 761 – 799.
- MOLNAR, P. & BURLANDO, P. (2005). Preservation of rainfall properties in stochastic disaggregation by a simple random cascade model. *Atmospheric Research*, 77(1 – 4), pp. 137 – 151.
- MONTEITH, J. (1965). Evaporation and environment. In: *Symp. Soc. Exp. Biol. 19*. Swansea, pp. 205 – 234.
- MORGAN, R.P.C., QUINTON, J.N., SMITH, R.E., GOVERS, G., POESEN, J.W.A., AUERSWALD, K., CHISCI, G., TORRI, D., STYCZEN, M., & FOLLY, A.J.V. (1998). The European Soil Erosion Model (EUROSEM): documentation and user guide. Tech. rep., Cranfield University.
- MORGAN, R. (2001). A simple approach to soil loss prediction: a revised Morgan-Morgan-Finney model. *Catena*, 44(4), pp. 305 – 322.
- MUERTH, M. (2008). A Soil Temperature and Energy Balance Model for Integrated Assessment of Global Change Impacts at the Regional Scale. Ph.D. thesis, Ludwig-Maximilians University, Department of Geography, München.
- MUERTH, M. & MAUSER, W. (2008). Implications of a regional scale soil temperature and freezing model in the Upper Danube Basin for climate change scenarios. In: A. BORSDORF, J. STÖTTER, & E. VEULLIET (Eds.) *Managing Alpine Future Proceedings of the Innsbruck Conference October 15 - 17, 2007*. Innsbruck.
- MULQUEEN, J., RODGERS, M., & SCALLY, P. (2004). Phosphorus transfer from soil to surface waters. *Agricultural Water Management*, 68, pp. 91 – 105.
- MUTCHLER, C.K. & YOUNG, R.A. (1975). Soil detachment by raindrops. In: *Present and perspective technology for predicting sediment yields and sources.*, vol. ARS-S-40. U.S.D.A. Agricultural Research Service, pp. 113 – 117.
- NACHTNEBEL, H. (1998). Herkunft und Zusammensetzung der Schwebstoffe in der Donau und ihren wichtigsten Zubringern. In: *Schriftenreihe des Verbund*, vol. 45. Verbundgesellschaft.
- NANKO, K., HOTTA, N., & SUZUKI, M. (2006). Evaluating the influence of canopy species and meteorological factors on throughfall drop size distribution. *Journal of Hydrology*, 329, pp. 422 – 431.
- NASH, J.E. & SUTCLIFFE, I.V. (1970). River flow forecasting through conceptual models part I – A discussion of principles. *Journal of Hydrology*, 10, pp. 282 – 290.

- NEARING, M.A., DEER-ASCOUGH, L., & LAFLEN, J.M. (1990). Sensitivity Analysis of the WEPP Hillslope Profile Erosion Model. *Transactions of the American Society of Agricultural Engineers*, 33(3), pp. 839 – 849.
- NEARING, M.A., JETTEN, V., BAFFAUT, C., CERDAN, O., COUTURIER, A., HERNANDEZ, M., LE BISSONNAIS, Y., NICHOLS, M.H., NUNES, J.P., RENSCHLER, C.S., SOUCHÈRE, V.H., & VAN OOST, K. (2005). Modeling response of soil erosion and runoff to changes in precipitation and cover. *Catena*, 61(2 – 3), pp. 131 – 154.
- NEARING, M.A., PRUSKI, F.F., & O'NEAL, M.R. (2004). Expected climate change impacts on soil erosion rates: a review. *Journal of Soil and Water Conservation*, 59(1), pp. 43 – 50.
- OLSSON, J. (1995). Limits and characteristics of the multifractal behavior of a high-resolution rainfall time series. *Nonlinear Processes in Geophysics*, 2(1), pp. 23 – 29.
- OLSSON, J. (1998). Evaluation of a scaling cascade model for temporal rainfall disaggregation. *Hydrology and Earth System Sciences*, 2(1), pp. 19 – 30.
- OLSSON, J. & BURLANDO, P. (2002). Reproduction of temporal scaling by a rectangular pulses rainfall model. *Hydrological Processes*, 16, pp. 611 – 630.
- OLSSON, J., NIEMCZYNOWIZ, J., & BERNDTSSON, R. (1993). Fractal analysis of high-resolution rainfall time series. *Journal of Geophysical Research. D. Atmospheres*, 98, pp. 23265 – 23274.
- OZTAS, T. & FAYETORBAY, F. (2003). Effect of freezing and thawing processes on soil aggregate stability. *Catena*, 52, pp. 1 – 8.
- PESERA (2009). PESERA: Pan-European Soil Risk Assessment. [http://eussoils.jrc.ec.europa.eu/ESDB\\_Archive/pesera/pesera\\_download.html](http://eussoils.jrc.ec.europa.eu/ESDB_Archive/pesera/pesera_download.html). Visited 02.11.2009.
- PHILIP, J.R. (1957). The theory of infiltration: 1. The infiltration equation and its solution. *Soil Science*, 83(5), pp. 345 – 357.
- PIERZYNSKI, G.M., SIMS, J.T., & VANCE, G.F. (2005). *Soils and environmental quality*. CRC Press.
- PROBECK, M., COLGAN, A., KRIMLY, T., ZÁRATE, M., & SCHNEIDER, K. (2006). Landbedeckung und Landnutzung. In: GLOWA-DANUBE-PROJEKT (Ed.) *Global Change Atlas, Einzugsgebiet Obere Donau*, 1 edn., chap. 1.3. Universität München (LMU), Dept. für Geo- und Umweltwissenschaften. ISBN: 978-3-00-026548-8.
- PRUPPACHER, H.R. & PITTER, R.L. (1971). A semi-empirical determination of the shape of cloud and rain drops. *Journal of the Atmospheric Sciences*, 28, pp. 86 – 94.
- RENARD, K.G., FOSTER, G.R., WEESIES, G.A., MCCOOL, D.A., & YODER, D.C. (1996). Predicting soil erosion by water: A guide to conservation planning with the Revised Universal Soil Loss Equation (RUSLE). Agriculture Handbook 703, USDA-ARS.

- RICHTER, G. (1991). The soil erosion measurement station and its program. In: G. RICHTER (Ed.) *Combating Soil Erosion in Vineyards of the Mosel-Region*. Forschungsstelle Bodenerosion der Universität Trier.
- RICHTER, G. (1998). *Bodenerosion Analyse und Bilanz eines Umweltproblems*. Wissenschaftliche Buchgesellschaft, Darmstadt.
- RODRIGUEZ-ITURBE, I., COX, D.R., & ISHAM, V. (1987). Some Models for Rainfall Based on Stochastic Point Processes. *Proceedings of the Royal Society of London. Series A, Mathematical and Physical Sciences (1934-1990)*, 410(1839), pp. 269 – 288.
- ROGLER, H. & SCHWERTMANN, U. (1981). Erosivität der Niederschläge und Isoerodentkarte von Bayern. *Zeitschrift für Kulturtechnik und Flurbereinigung*, 22, pp. 99 – 112.
- SAAVEDRA, C. (2005). Estimating spatial patterns of soil erosion and deposition in the Andean region using geo-information techniques. Ph.D. thesis, Wageningen University.
- SAUERBORN, P., KLEIN, A., BOTSCHEK, J., & SKOWRONEK, A. (1999). Future rainfall erosivity derived from large-scale climate models – methods and scenarios for a humid region. *Geoderma*, 93, pp. 269 – 276.
- SCHEFFER, F. & SCHACHTSCHABEL, P. (2002). *Lehrbuch der Bodenkunde*. 15 edn. Spektrum Akademischer Verlag, Heidelberg.
- SCHERTZER, D. & LOVEJOY, S. (1987). Physical modeling and analysis of rain and clouds by anisotropic scaling multiplicative processes. *Journal of Geophysical Research*, 92(D8).
- SCHMIDT, J. (1996). *Entwicklung und Anwendung eines physikalisch begründeten Simulationsmodells für die Erosion geneigter landwirtschaftlicher Nutzflächen*, vol. 61. Berliner Geographische Abhandlungen, Berlin.
- SCHMIDT, J., MICHAEL, A., SCHMIDT, W., & VON WERNER, M. (1996). *EROSION 2D/3D Ein Computermmodell zur Simulation der Bodenerosion durch Wasser*. Sächsisches Landesamt für Umwelt und Geologie, Sächsische Landesanstalt für Landwirtschaft, Freiberg.
- SCHMIDT, J., VON WERNER, M., & MICHAEL, A. (1997). Application of the EROSION 3D model to the CATSOP watershed, The Netherlands. *Catena*, 37, pp. 449 – 456.
- SCHMIDT, R.G. (1979). *Probleme der Erfassung und Quantifizierung von Ausmass und Prozessen der aktuellen Bodenerosion (Abspülung) auf Ackerflächen*. Physiogeographica, Basler Beiträge zur Physiogeographie.
- SCHULTZE, J.H. (1952). *Die Bodenerosion in Thüringen*. Perthes.
- SCHWERTMANN, U. (1981). Die Vorausschätzung des Bodenabtrages durch Wasser in Bayern. Tech. rep., Bayerisches Staatsministerium für Ernährung, Landwirtschaft und Forsten.
- SIEGRIST, S. (2004). Aktuelle Erodierbarkeit von Böden in verschiedenen Landschaftstypen der Schweiz - Methoden und Modelle. Ph.D. thesis, University Basel.

- SRIKANTHAN, R. & McMAHON, T.A. (1985). Stochastic generation of rainfall and evaporation data. *Australian Water Resources Council Technical Paper*, p. 301 pp.
- STEINER, J., SCHOMBERG, H., UNGER, P., & CRESAP, J. (1999). Crop Residue Decomposition in No-Tillage Small-Grain Fields. *Soil Science Society of America Journal*, 63(6), pp. 1817 – 1824.
- STMELF (2009). Cross Compliance 2009 Einhaltung der anderweitigen Verpflichtungen. <http://www.stmelf.bayern.de/agrarpolitik/11030/>. Visited 12.01.2010.
- STROOSNIJDER, L. (2005). Measurement of erosion: Is it possible? *Catena*, 64, pp. 162 – 173.
- SUKHANOVSKI, Y.P., OLLESCH, G., KHAN, K.Y., & MEINER, R. (2002). A new index for rainfall erosivity on a physical basis. *Journal of Plant Nutrition and Soil Science*, 165(1), pp. 51 – 57.
- SVERDRUP, H.U., JOHNSON, M.W., & FLEMING, R.H. (1942). *The Oceans Their Physics, Chemistry, And General Biology*. Prentice-Hall.
- TENGBEH, G.T. (1993). The effect of grass roots on shear strength variations with moisture content. *Soil Technology*, 6, pp. 287 – 295.
- THIES, B., NAUSS, T., REUDENBACH, C., CERMAK, J., & BENDIX, J. (2006). Teilprojekt Niederschlag/Fernerkundung. In: GLOWA-DANUBE-PROJEKT (Ed.) *Global Change Atlas, Einzugsgebiet Obere Donau*, 1 edn., chap. 2.6.1. Universität München (LMU), Dept. für Geo- und Umweltwissenschaften. ISBN: 978-3-00-026548-8.
- TODINI, E. (2007). A mass conservative and water storage consistent variable parameter Muskingum-Cunge approach. *Hydrology and Earth System Sciences*, 11(5), pp. 1645 – 1659.
- ULÉN, B.M. & KALISKY, T. (2005). Water erosion and phosphorus problems in an agricultural catchment - Need for natural research for implementation of the EU Water Framework Directive. *Environmental Science and Policy*, 8, pp. 477 – 484.
- USGS (2008). MODFLOW and related programs. <http://water.usgs.gov/nrp/gwsoftware/modflow.html>. Visited 07.07.2008.
- VAN DIJK, A.I.J.M., BRUIJNZEEL, L.A., & ROSEWELL, C.J. (2002). Rainfall intensity - kinetic energy relationships: a critical literature appraisal. *Journal of Hydrology*, 261, pp. 1 – 23.
- VANAPALLI, S.K., FREDLUND, D.G., PUF AHL, & W., C.A. (1996). Model for the prediction of shear strength with respect to soil suction. *Canadian Geotechnical Journal*, 33, pp. 379 – 392.
- VICENTE-SERRANO, S., SAZ-SANCHEZ, M., & CUADRAT, J. (2003). Comparative analysis of interpolation methods in the middle Ebro Valley (Spain): application to annual precipitation and temperature. *Climate Research*, 24(2), pp. 161 – 180.

- VON WERNER, M. (1995). GIS-orientierte Methoden der digitalen Reliefanalyse zur Modellierung von Bodenerosion in kleinen Einzugsgebieten. Ph.D. thesis, Freie Universität Berlin.
- WFD (2000). Directive 2000/60/EC of the European Parliament and of the Council of 23 October 2000 establishing a framework for Community action in the field of water policy. *Official Journal of the European Communities*, 372.
- WICKS, J.M. & BATHURST, J.C. (1996). SHESED: a physically based, distributed erosion and sediment yield component for the SHE hydrological modeling system. *Journal of Hydrology*, 175, pp. 213 – 238.
- WILLIAMS, J.R., DYKE, P.T., & JONES, C.A. (1983). *State-of-the-Art in Ecological Modeling*, chap. EPIC: a model for assessing the effects of erosion on soil productivity. In *Analysis of Ecological Systems*. Elsevier, Amsterdam, pp. 553 – 572.
- WIRSIG, A., KRIMLY, T., STOLL, M., & DABBERT, S. (2006). Landwirtschaft. In: GLOWA-DANUBE-PROJEKT (Ed.) *Global Change Atlas, Einzugsgebiet Obere Donau*, 1 edn., chap. 1.15. Universität München (LMU), Dept. für Geo- und Umweltwissenschaften. ISBN: 978-3-00-026548-8.
- WISCHMEIER, W. & SMITH, D.D. (1978). Predicting rainfall erosion losses. A guide to conservation planning. Agriculture Handbook 537, USDA-ARS.
- WISCHMEIER, W.H. & SMITH, D.D. (1958). Rainfall energy and its relation to soil loss. *Transactions of the American Geophysical Union*, 39, pp. 285 – 291.
- WISCHMEIER, W.H. & SMITH, D.D. (1965). Predicting rainfall-erosion losses from cropland east of the Rocky Mountains. Tech. rep., USDA-ARS.
- WOOLHISER, D.A., SMITH, R.E., & GOODRICH, D.C. (1990). *KINEROS, A Kinematic Runoff and Erosion Model*. USDA-ARS.
- WU, T.H., MCKINNELL, W.P., & SWANSTON, D.N. (1979). Strength of tree roots and landslides on Prince of Wales Island, Alaska. *Canadian Geotechnical Journal*, 16, pp. 19 – 33.
- YAO, C., LEI, T., ELLIOT, W.J., MCCOOL, D.K., ZHAO, J., & CHEN, S. (2008). Critical conditions for rill initiation. *Transactions of the American Society of Agricultural and Biological Engineers*, 51(1), pp. 107 – 114.
- ZHANG, B., ZHAO, Q.G., HORN, R., & BAUMGARTL, T. (2001). Shear strength of surface soil as affected by soil bulk density and soil water content. *Soil and Tillage Research*, 59, pp. 97 – 106.

# Appendix





## A. CASCADE PARAMETERISATION

Tab. A1: Empirically fitted parameters for Eq. (5.2) for calculation of the volume class thresholds of regions (a): Low mountain ranges, (b): Forelands and (c): Alps.

Region	Position class	a	b	R <sup>2</sup>
(a)	starting	1.3655	0.7273	0.9967
	enclosed	1.5776	0.7741	0.9986
	ending	0.9107	0.7101	0.9977
	isolated	0.5499	0.8925	0.9943
(b)	starting	1.5809	0.7560	0.9973
	enclosed	1.6963	0.7705	0.9988
	ending	1.0151	0.7282	0.9990
	isolated	0.5933	0.9153	0.9917
(c)	starting	1.7728	0.8558	0.9946
	enclosed	1.9110	0.7701	0.9885
	ending	1.2011	0.7558	0.9817
	isolated	0.9436	0.9200	0.9495

Tab. A2: Empirically determined  $W_{x/x}$ -distributions of the generator (numerical values).

Volume	Position	$W_1$						
		0.07	0.21	0.36	0.50	0.64	0.79	0.93
below	starting	0.08	0.17	0.21	0.35	0.11	0.06	0.02
	enclosed	0.02	0.07	0.21	0.39	0.21	0.08	0.02
	ending	0.01	0.04	0.09	0.41	0.21	0.18	0.06
	isolated	0.02	0.05	0.09	0.64	0.10	0.07	0.03
above	starting	0.23	0.19	0.18	0.14	0.11	0.08	0.07
	enclosed	0.05	0.10	0.17	0.27	0.22	0.13	0.06
	ending	0.03	0.04	0.07	0.12	0.22	0.27	0.25
	isolated	0.08	0.11	0.16	0.12	0.20	0.18	0.15

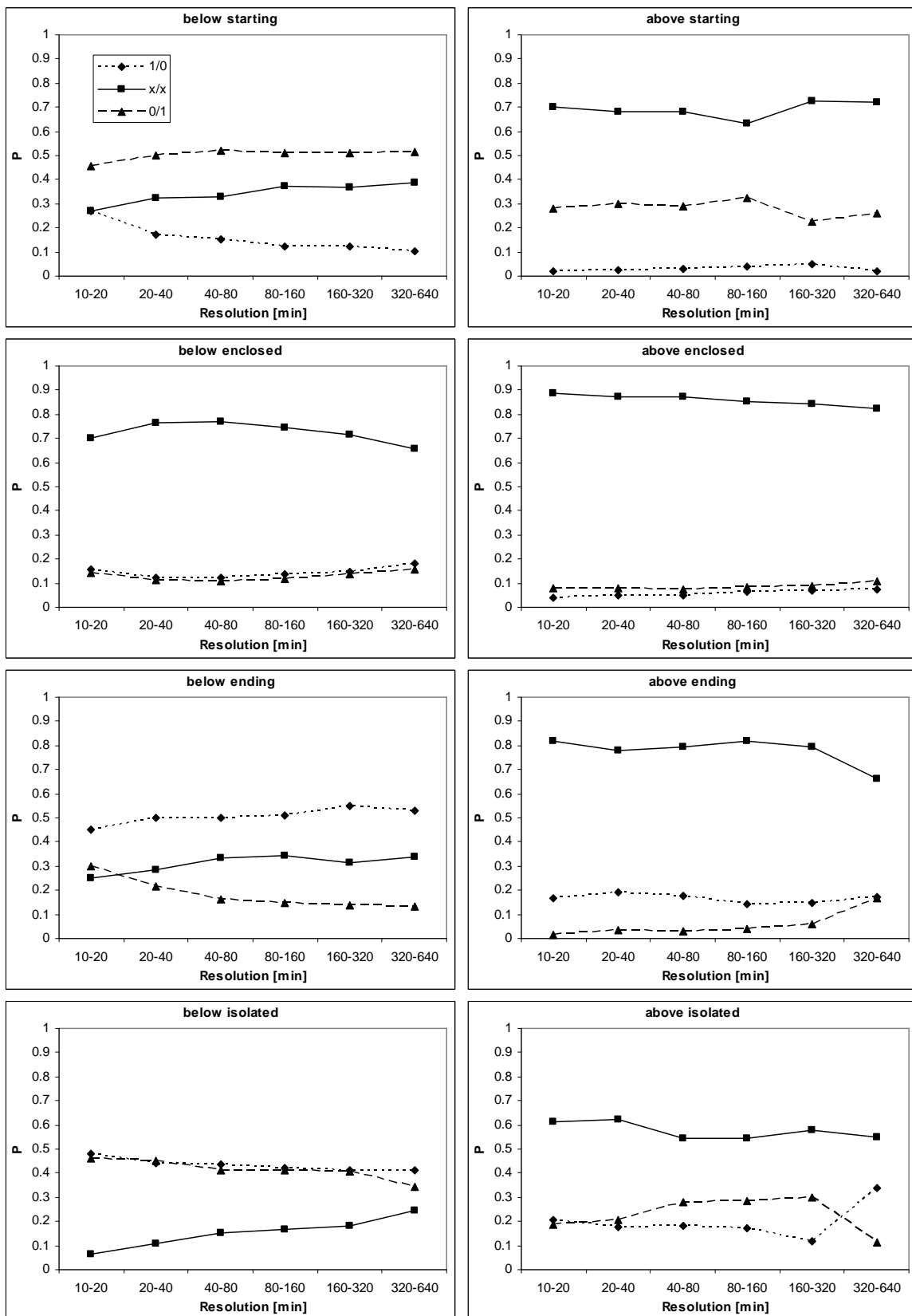


Fig. A1: Probabilities  $P(1/0)$ ,  $P(0/1)$  and  $P(x/x)$  of all levels for all position and volume classes. Probabilities are averaged from all stations, except Untersberg, and no weighting is included.

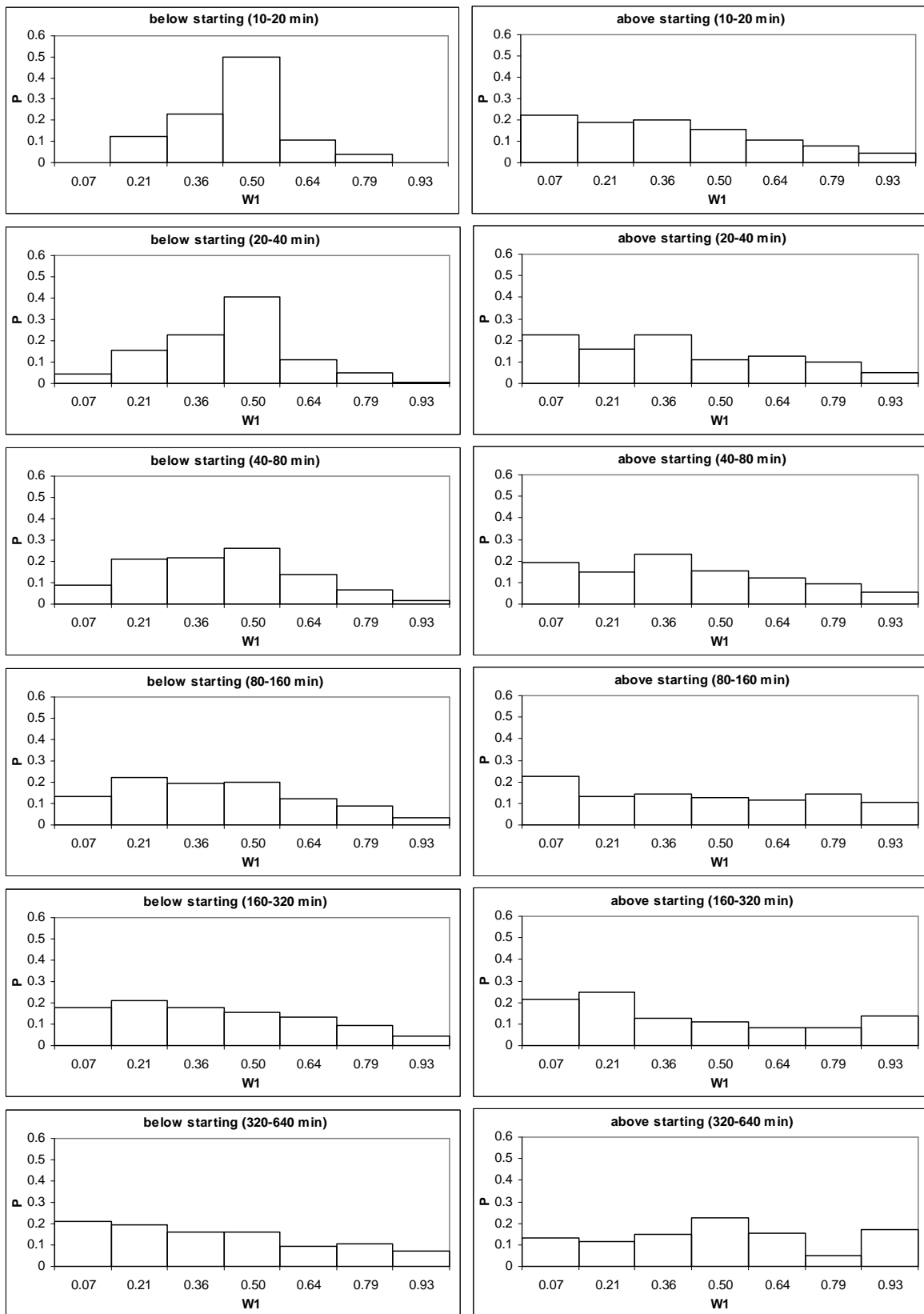


Fig. A2:  $W_{x/x}$ -distributions of all levels for starting boxes. Probabilities are averaged from all stations, except Untersberg, and no weighting is included.

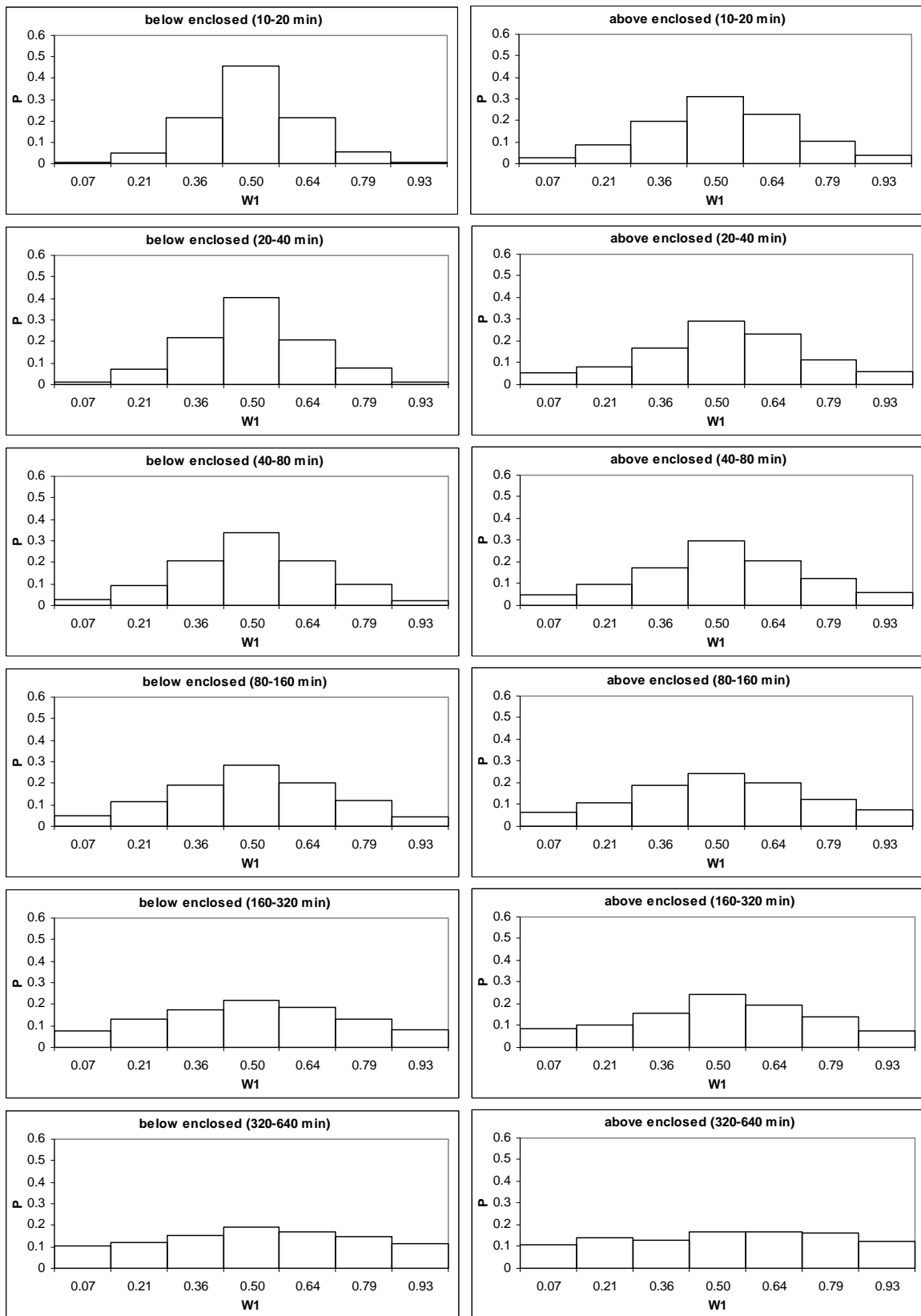


Fig. A3:  $W_{x/x}$ -distributions of all levels for enclosed boxes. Probabilities are averaged from all stations, except Untersberg, and no weighting is included.

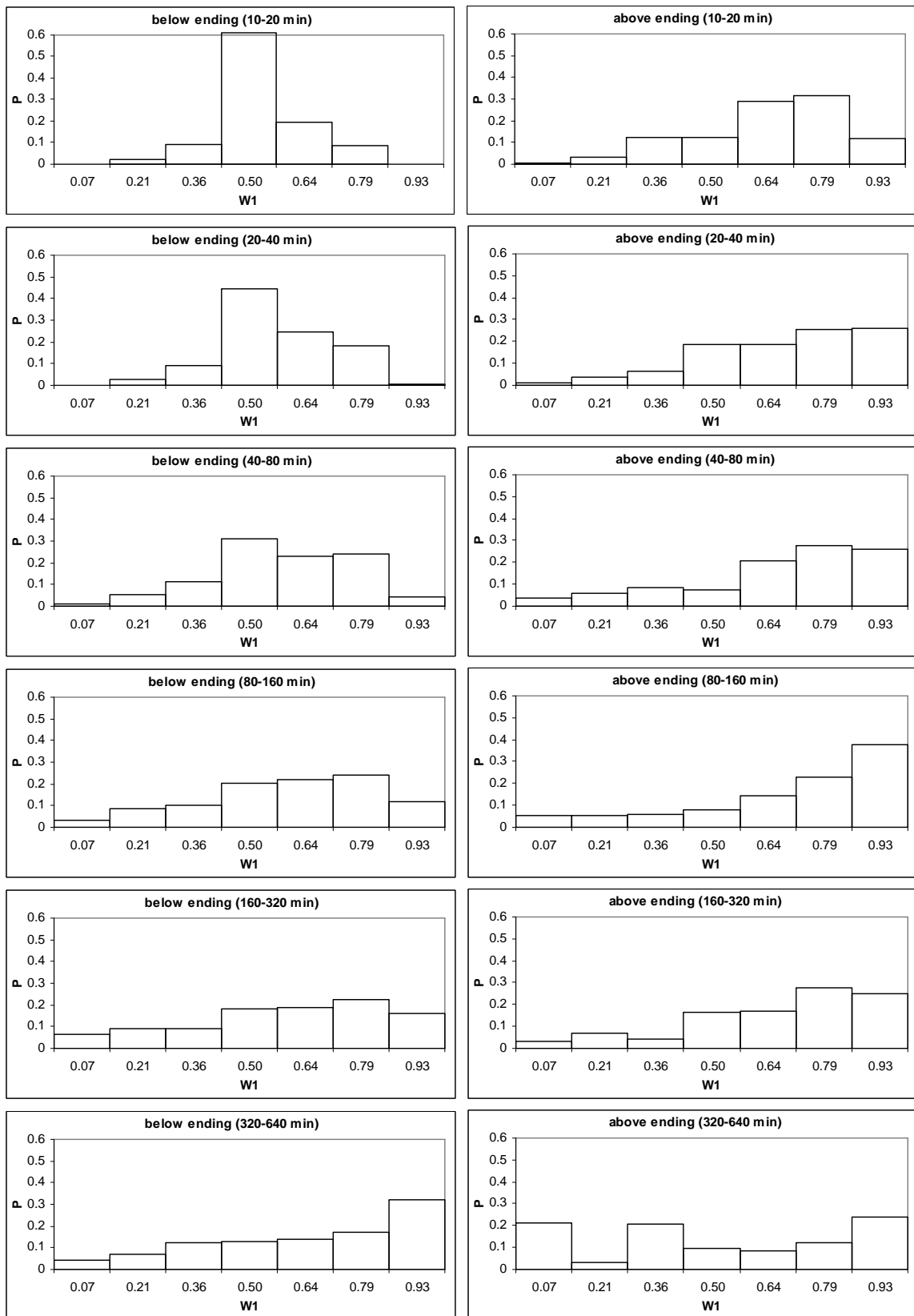


Fig. A4:  $W_{x/x}$ -distributions of all levels for ending boxes. Probabilities are averaged from all stations, except Untersberg, and no weighting is included.

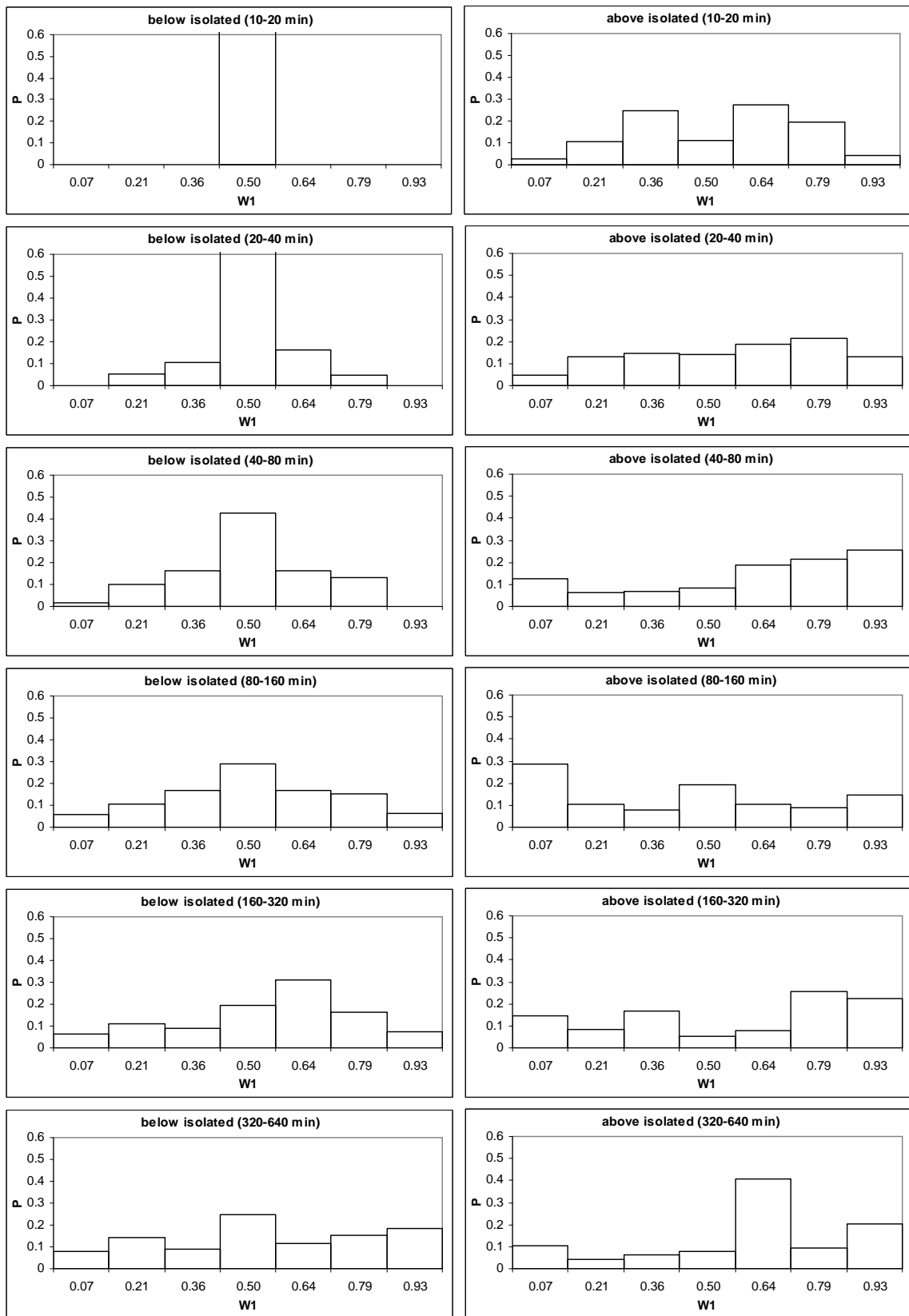


Fig. A5:  $W_{x/x}$ -distributions of all levels for isolated boxes. Probabilities are averaged from all stations, except Untersberg, and no weighting is included.

**B. DISAGGREGATION PERFORMANCE**

Tab. B3: Mean performances of the different disaggregation methods compared to measured values. Listed are statistics of hourly precipitation sums [mm] for all proxels with high resolution gauges. Note that precipitation for these proxels is interpolated spatially, as the proxels do not coincide with station proxels. (no > 0: number of intervals with precipitation > 0,  $\sigma$ : standard deviation, no >  $P_{XX}$ : number of intervals > XXth percentile of measured data)

Station	Method	no > 0	mean	$\sigma$	no > $P_{25}$	no > $P_{50}$	no > $P_{75}$	no > $P_{90}$
Kühroint	measured	1727	0.97	1.53	1119	781	394	161
	ACD	2640	0.58	0.69	1773	944	310	98
	CD	1376	1.12	1.68	981	698	369	183
Jenner	measured	2002	0.70	1.21	1413	944	469	193
	ACD	2454	0.52	0.58	2079	1242	455	133
	CD	1262	1.01	1.45	1084	779	447	221
Reiteralms	measured	1283	1.11	2.31	929	619	318	127
	ACD	3067	0.61	0.72	2110	1163	463	131
	CD	1631	1.16	1.84	1147	794	502	234
Untersberg	measured	13365	1.14	1.59	8999	6554	3173	1320
	ACD	19028	0.56	0.70	12198	6718	1414	263
	CD	10128	1.06	1.72	6968	4771	2110	903
Spitalhof	measured	14416	0.89	1.37	9329	7135	3403	1428
	ACD	24271	0.56	0.65	16201	10747	3194	839
	CD	8975	1.53	2.28	7092	5804	3519	1954
Wettkam	measured	10746	0.71	1.14	7633	5232	2600	997
	ACD	30082	0.52	0.59	24572	15349	5994	1359
	CD	13725	1.14	1.80	11573	8233	5176	2756
Nilling	measured	10827	0.76	1.21	7860	4784	2587	1037
	ACD	26896	0.39	0.44	21297	8623	2649	393
	CD	13926	0.77	1.10	11659	6666	3575	1542
Osterseeon	measured	12725	0.88	1.40	8232	6309	2956	1209
	ACD	21645	0.50	0.61	13321	8411	2349	526
	CD	9046	1.21	1.95	6269	5027	2835	1477
Reschenberg	measured	13579	0.85	1.44	10136	6318	3140	1305
	ACD	23632	0.42	0.53	18368	7540	2250	485
	CD	12087	0.84	1.50	9590	5250	2862	1325
Großberghofen	measured	10769	0.68	1.19	7511	5021	2479	1045
	ACD	23598	0.41	0.50	18142	9576	3214	724
	CD	12378	0.79	1.25	10116	6530	3463	1661
Engersdorf	measured	9620	0.77	1.30	7036	4286	2310	923
	ACD	20146	0.41	0.50	15488	6564	2104	474
	CD	10082	0.83	1.42	8080	4476	2600	1241
Kringell	measured	6055	0.80	1.40	4455	2697	1501	605
	ACD	12433	0.42	0.48	10017	4083	1414	302

continued on next page

Tab. B3 – continued from previous page

Station	Method	no > 0	mean	$\sigma$	no > $P_{25}$	no > $P_{50}$	no > $P_{75}$	no > $P_{90}$
	CD	6385	0.83	1.22	5364	3182	1761	775
Neusling	measured	10624	0.78	1.22	7947	4929	2594	1016
	ACD	23999	0.38	0.42	18688	7342	2104	367
	CD	12806	0.72	1.05	10404	5846	3079	1246
Neuhof	measured	11321	0.74	1.23	8048	5588	2567	1120
	ACD	21586	0.38	0.45	16431	8292	2017	461
	CD	9270	0.89	1.39	7765	5283	2663	1359
Konnersreut	measured	11158	0.79	1.38	8010	4849	2615	1034
	ACD	26859	0.34	0.42	19987	6978	2141	373
	CD	13576	0.70	1.09	11009	5831	2953	1135
Schönau	measured	4902	0.95	1.47	3276	2196	1170	464
	ACD	8866	0.53	0.68	5642	2912	1038	185
	CD	4568	1.03	1.68	3211	2156	1238	552



### **C. CONFIGURATION OF THE MODEL RUNS**

The PROMET simulation runs have been executed with a “standard” parameterisation, which was also used e.g. by MUERTH (2008), HANK (2008), or MAUSER & BACH (2009). Here, only the most important parameters, respectively parameter modifications, concerning the erosion module are listed.

The saturated hydraulic conductivities of the soil classes “clay silt” and “silt loam” have been increased, since runoff formation was very low on those soils.

The parameterisation of oleaginous, potato and sugarbeet has been improved, since plant growth and phenological stages were unrealistic.

The sowing and harvest dates have been corrected with empirical data, since they did not seem to fit for some cultivations. The threshold for earlier and later harvest was set to 14 days. Sowing was not allowed to be shifted.

The slope of the DTM was derived from a 50 m · 50 m DTM.

The modifications described in this study have been used for all model runs. These are the temporal disaggregation of precipitation and a modified canopy interception. Furthermore the soil freezing routines have been used.

## D. MEAN SOIL LOSSES PER DISTRICT

Tab. D4: Mean long term annual soil losses [t/ha] per district, calculated with the erosion module (EM) and the ABAG, and results of the study of AUERSWALD & SCHMIDT (1986) (Atlas) and the PESERA project (PESERA). (Districts with small areal coverage in the catchment have been removed.)

District	EM	ABAG	Atlas	PESERA
Aichach-Friedberg	8.10	2.10	2.51	3.69
Alb-Donau-Kreis	0.95	0.50	N/A	0.73
Altötting	6.86	1.96	4.40	0.65
Amberg	4.30	0.09	2.57	0.79
Amberg-Sulzbach	1.56	0.21	2.57	0.49
Ansbach L.	0.49	0.29	1.70	0.39
Ansbach S.	4.11	0.52	1.70	0.15
Augsburg L.	2.35	0.96	1.64	1.18
Augsburg S.	0.24	0.17	1.64	0.81
Bad Tölz-Wolfratshausen	2.41	0.28	1.64	0.01
Berchtesgadener Land	4.39	0.69	1.50	0.00
Biberach	2.12	0.68	N/A	2.25
Bludenz	0.67	0.43	N/A	0.02
Braunau am Inn	7.21	1.46	N/A	0.04
Bregenz	0.65	0.52	N/A	0.02
Breisgau-Hochschwarzwald	0.12	0.08	N/A	0.01
Cham	11.89	0.37	3.61	0.07
Dachau	9.60	2.09	2.95	1.24
Deggendorf	6.66	1.47	4.38	0.72
Dillingen	2.76	1.04	2.20	2.22
Dingolfing-Landau	7.64	3.08	7.40	3.50
Donau-Ries	2.39	0.94	3.43	2.05
Ebersberg	1.74	0.40	2.70	0.49
Eichstätt	1.32	0.55	2.34	0.45
Erding	3.71	1.80	6.47	0.64
Freising	9.48	2.63	6.51	1.90
Freyung-Grafenau	9.96	0.19	2.20	0.00
Fürstenfeldbruck	3.46	0.67	1.80	1.08
Garmisch-Partenkirchen	1.63	0.29	1.28	0.00
Günzburg	4.24	1.31	2.62	1.01
Hallein	1.61	0.51	N/A	0.00
Heidenheim	0.94	0.58	N/A	0.27
Imst	1.22	0.31	N/A	0.00
Ingolstadt	0.43	0.18	0.68	0.52
Inn	0.19	0.18	N/A	0.00
Innsbruck-Land	1.61	0.48	N/A	0.02
Innsbruck-Stadt	1.93	0.37	N/A	0.00
Kaufbeuren	3.43	0.20	N/A	0.00
Kelheim	8.96	2.51	11.37	3.38
Kempten	0.03	0.10	N/A	0.00
Kitzbühel	2.06	0.39	N/A	0.00

continued on next page

Tab. D4 – continued from previous page

District	EM	ABAG	Atlas	PESERA
Kufstein	1.93	0.57	N/A	0.00
Landeck	1.90	0.33	N/A	0.00
Landsberg	2.59	0.40	1.50	0.39
Landshut L.	11.81	3.44	7.60	5.17
Landshut S.	13.14	1.87	7.60	7.00
Maloja	0.04	0.18	N/A	N/A
Memmingen	1.17	0.23	N/A	0.18
Miesbach	1.43	0.32	1.03	0.03
Mühldorf	8.58	2.15	7.77	0.92
München L.	0.52	0.13	0.22	0.48
München S.	0.03	0.04		0.38
Neuburg-Schrobenhausen	3.21	1.07	1.42	0.79
Neumarkt	0.69	0.31	2.94	1.38
Neustadt an der Waldnaab	6.78	0.24	2.29	0.38
Neu-Ulm	3.02	0.87	1.62	1.19
Oberallgäu	2.44	0.33	1.11	0.03
Ostalbkreis	2.19	0.47	N/A	0.61
Ostallgäu	3.02	0.36	0.82	0.07
Passau L.	15.37	3.10	6.29	1.69
Passau S.	7.07	2.18	6.29	0.08
Pfaffenhofen	11.24	3.83	9.69	2.07
Ravensburg	0.39	0.19	N/A	1.01
Regen	6.26	0.14	2.00	0.00
Regensburg L.	4.07	0.78	4.77	1.32
Regensburg S.	3.31	0.89		3.79
Reutlingen	0.19	0.36	N/A	0.03
Reutte	0.27	0.32	N/A	0.01
Ried im Innkreis	14.26	2.84	N/A	0.23
Rosenheim L.	2.69	0.51	2.11	0.03
Rosenheim S.	0.19	0.06	2.11	0.00
Roth	0.44	0.02	1.12	0.77
Rottal-Inn	11.26	3.19	5.93	2.63
Salzburg(Stadt)	0.99	0.13	N/A	0.00
Salzburg-Umgebung	1.68	0.47	N/A	0.00
Sankt Johann im Pongau	1.70	0.36	N/A	0.00
Schärding	8.73	3.50	N/A	0.20
Schwandorf	9.47	0.29	2.17	0.37
Schwarzwald-Baar-Kreis	0.94	0.20	N/A	1.19
Schwaz	7.98	0.52	N/A	0.00
Sigmaringen	1.27	0.39	N/A	2.25
Starnberg	1.61	0.32	1.59	0.46
Straubing	0.77	0.46	N/A	0.73
Straubing-Bogen	8.91	1.75	6.50	1.41
Tirschenreuth	8.69	0.33	2.47	0.23
Traunstein	3.26	0.61	3.55	0.17
Tuttlingen	0.72	0.30	N/A	0.30
Ulm	4.49	0.67	N/A	1.69

continued on next page

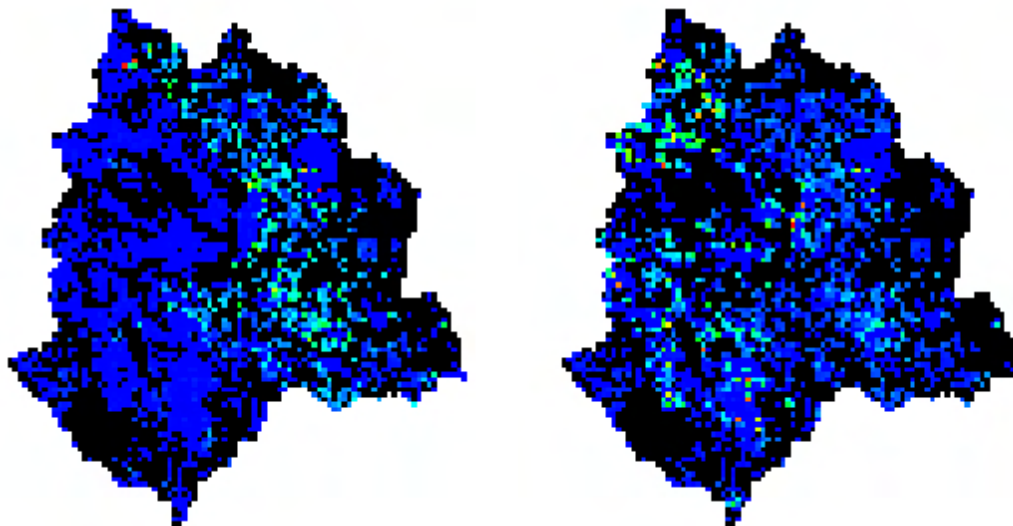
*Tab. D4 – continued from previous page*

District	EM	ABAG	Atlas	PESERA
Unteralpgäu	1.72	0.57	N/A	0.26
Weiden	2.38	0.15	N/A	0.85
Weilheim-Schongau	1.31	0.23	0.88	0.01
Weißenburg-Gunzenhausen	1.09	0.38	1.99	0.82
Zell am See	1.92	0.39	N/A	0.00
Zollernalbkreis	0.26	0.35	N/A	0.06

## E. INFLUENCE OF SOIL PARAMETERISATION IN THE NAAB SUB-CATCHMENT

*Note: The parameters used for the simulation results presented in this section differ from those used in the validation (Section 6.2.3). They are intended to demonstrate the effects of a better soil parameterisation on the modelled soil loss, but the results presented have not been analysed in detail.*

The parameterisation of soils used within this study has some shortcomings in some regions of the Upper Danube Basin. This results from weak information in the data bases, which were used for soil parameterisation. The mainly affected features are formation of runoff and discharge, which in turn affect soil erosion. Section 6.2.3.5 addressed the insufficient representation of soil loss in the regions of the Bavarian Forest. As a revised soil map and parameterisation was made available to this work, here are some first results presented, which have been modelled with the revised parameterisation of the soils in the watershed of the *Naab*. The *Naab* lies in the northernmost part of the Upper Danube catchment, and covers parts of the Bavarian Forest. Fig. E6 qualitatively shows the mean annual soil loss (1990 – 2005) resulting from both parameterisations. The mean annual soil loss in the *Naab* watershed averaged from 1990 – 2005 is reduced to 91 %, from 6.8 t/ha to 6.2 t/ha, if the new soil map and parameterisation is used. As results in Fig. E6 are only shown qualitatively, it has to be noted, that the new parameterisation results in an relative increase of soil loss in the western part of the *Naab* watershed, and a relative decrease in the eastern part. As the new parameterisation affects the soil classes in the Bavarian Forest, a decrease in soil loss over the whole area of this low mountain range can be expected, which corrects the weak results presented in Section 6.2.3.5.



(a) Standard soil parameterisation (used within the whole study)

(b) New soil parameterisation (used only for the results of this section)

*Fig. E6: Qualitative comparison of soil losses induced by usage of different parameterisations for modelling in the Naab subcatchment. (Red: high soil losses, blue: low soil losses)*



# **CURRICULUM VITAE**

## **PERSONAL**

Name Daniel Marc Georg Waldmann  
Date of Birth 02.07.1978  
Place of Birth Munich  
Nationality German

## **EDUCATION**

1985 – 1989 Primary School, Poing  
1989 – 1998 High School, Franz-Marc-Gymnasium Markt Schwaben  
1999 – 2004 Study of Physical Geography, LMU Munich  
Subsidiary subjects: Computer Sciences, Remote Sensing  
Diploma thesis: Entwicklung und Anwendung eines  
Klassifikators hyperspektraler Daten mit Hilfe  
eines Strahlungstransfermodells (GeoSAIL)  
Graduate degree: Diplom-Geograph (Univ.)  
Naturwissenschaftliche Richtung  
2005 – 2010 PhD studies at the Department for Geography, LMU Munich

## **EMPLOYMENT**

1998 – 1999 Alternative civilian service, Regenbogen e.V. Haar  
2000 – 2001 Student research assistant at the Department for Geography,  
LMU Munich  
Since 2004 Research associate at the Department for Geography,  
LMU Munich  
Since 2004 Collaboration in the “Hydrology and Remote Sensing”  
working group of the BMBF project GLOWA-Danube  
2005 – 2006 Freelance collaborator at Vista Geowissenschaftliche  
Fernerkundung GmbH  
2006 – 2008 Lecturer at the Department of Geography, LMU Munich